Studies on the aqueous film coating of tablets using model systems.

Prater, D. A.

Award date:
1982

Awarding institution:
University of Bath

STUDIES ON THE AQUEOUS FILM COATING OF TABLETS USING MODEL SYSTEMS

Thesis

Submitted by D.A. Prater, B. Pharm.,

for the degree of Doctor of Philosophy

of the University of Bath

1982

This research has been carried out in the School of Pharmacy and Pharmacology of the University of Bath under the supervision of B.J. Meakin, B. Pharm., F.P.S.

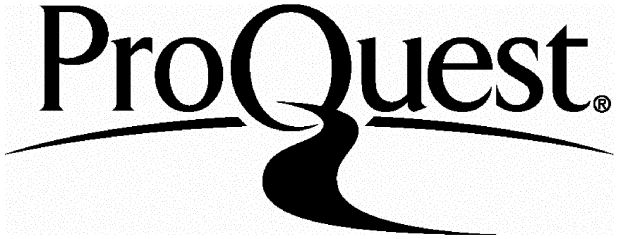

ACKNOWLEDGEMENTS

The author wishes to thank Mr. B.J. Meakin and Mr. J.S. Wilde for their encouragement and advice throughout the project. His thanks are also due to Prof. D.A. Norton for providing the facilities for the research and to the other members of this school for their participation in helpful discussions and occasional practical assistance.

The author wishes to acknowledge the advice and interest shown by Mr. G. Cole and other staff of Merck Sharp and Dohme Research Laboratories and to thank Dr. A. Covell for providing additional facilities for research within the Development Laboratories at Hoddesdon.

The author's thanks are also due to Mr. C. Arnold of the School of Material Sciences for help in use of the Instron Tensile Tester; Mr. A. Carter of the School of Mechanical Engineering for helpful discussions and advice on relocation surface profilometry; Mr. P. Barlow for help with the design and construction of electronic circuits; and Mr. J. Fosdyke of the Electron Optics Centre for much theoretical and practical assistance in the field of electron microscopy.

This work was carried out with the aid of a grant from the Science Research Council to whom the author wishes to express his gratitude.

Finally the author wishes to thank his wife for her patience and encouragement throughout this work.

SUMMARY

In this thesis the film coating of tablets is reviewed with reference to the coating materials and processes which are available. The effects of formulation and processing variables are discussed together with techniques for the evaluation of film properties. The discrepancies observed in the literature between the properties of free films and those applied to tablets in commercial coating equipment formed the basis for one section of the work, in which a more realistic model coating system was developed. The coating parameters used successfully in a 24" Accela-Cota for the aqueous coating of tablets were isolated and then reproduced on a model system. The water vapour permeability of coatings produced on the model system and in the Accela-Cota were not significantly different.

The viscosity and thermal behaviour of aqueous solutions of film coating polymers were investigated to compare the film formers and to gain an understanding of the process of film formation on tablets; in particular to evaluate the possibility that thermal gelation of the polymer may play a role in the transition from a sol to a gel state during film formation on the tablets.

A mass spectrometry permeability technique was developed and evaluated in order to follow the low level transfer of gas across a small area of film coating. Techniques were also developed to measure the tensile properties and water vapour

permeability of films and to follow the changes in surface roughness of a tablet during deposition of a coating on the model system.

The effects of film preparation technique, substrate and titanium dioxide content on the oxygen permeability, water vapour permeability and mechanical properties of hydroxypropylmethyl cellulose (HPMC) films were investigated. The changes in oxygen permeability of HPMC films with increasing relative humidity were also demonstrated.

CONTENTS

Page No.

RESULTS AND DISCUSSION

INTRODUCTION

1. INTRODUCTION AND LITERATURE REVIEW

For many years tablets and pills have been sugar coated to improve their aesthetic appearance and organoleptic properties. This process, involving the deposition of a thick layer of sugar around the tablet core can take several days to complete, is labour intensive and results in a product with greatly increased weight and volume. During the 1950's the demand for a more rapid process led to the development of film coating, in which a thin layer of a film forming polymer is applied to the tablets. The polymer usually causes a 2 to 5% increase in the weight and volume of the tablet cores and therefore does not materially increase the cost of packaging and transport. The variability of drug release, sometimes produced by a thick sugar coating, is minimised whilst the use of coating polymers which are insoluble in all or part of the gastrointestinal tract can delay or prolong the release of the active ingredient if desired.

1.1 Aims and Objectives of the Project

The rationale for film coating tablets, described in section 1.2, necessitates the production of a film with good mechanical properties which, if required, will also provide a barrier to the ingress of atmospheric gas and vapour and the egress of the active ingredient. To study such properties, polymer films may be produced and detached from the substrate on which they are deposited. Frequently these substrates are smooth, non porous materials such as glass or mercury, which bear little relation to the surface of a tablet. The properties of such free films may also

be different from those of films produced on tablets in industrial equipment due to discrepancies in the production conditions of the former.

Thus it was proposed to design, construct and evaluate a model coating system to mimic the aqueous film coating of tablets in industrial equipment. The properties of films applied to model compacts using this system were to be compared with those of films sprayed and cast on to non-porous substrates such as glass or teflon. Film evaluation techniques including gas and moisture permeability evaluation, tensile testing, surface roughness measurements and electron microscopy were to be developed. Using the model system and film evaluation techniques, the effect of formulation and processing variables on the properties of aqueous film coatings could be studied.

1.2 Film Coating Materials

Tablets are film coated for numerous reasons including[1-9]:

a) modification of drug release to prevent gastric irritation, drug degradation in the stomach, or to provide a sustained therapeutic action.

b) protection of the active components from light, moisture, or atmospheric gases

c) to mask unpleasant taste and/or odour and to aid ingestion of the tablets

d) increased abrasion resistance and reduced dust formation, to promote tablet flow during packaging.

e) increased elegance and easier product identification.

In the past film coatings have been applied from organic solvent systems, but recent legislation in the areas of Health and Safety and Environmental Protection has highlighted the advantages of using aqueous-based systems[3,8,9-14], which may be listed as:

a) decreased solvent costs although the increased energy input required to evaporate water makes the overall savings marginal

b) absence of toxicity problems, including those of solvent residues in the final product

c) absence of environmental pollution or the need for extensive solvent recovery systems

d) absence of a fire risk eliminates the need to flameproof coating equipment and areas

e) minimal explosion risk, although this cannot be eliminated due to the production of dust through attrition of the tablets.

Data has been published[10,13,15,16] to show that even moisture sensitive materials such as acetyl salicylic acid and ascorbic acid can be coated with aqueous formulations without a detrimental effect on their stability.

The wide range of film forming materials reviewed in the literature[1-65] are of limited use in aqueous coating and are therefore a subject beyond the scope of this project. Consequently,

only a brief survey of the groups of materials most commonly used will be given. The characteristics of an ideal film forming material have been defined as follows[5]:

a) soluble in suitable solvents

b) soluble or permeable in all or at least some of the pH conditions found in the gastrointestinal tract

c) capable of producing a strong continuous film which is smooth, elegant and provides adequate protection from light, moisture, atmospheric gases, drug odour, taste or sublimation.

d) stable in the presence of heat, light, atmospheric gas and moisture and most drug entities.

e) non-toxic, inert, tack-free and whilst requiring no unusual additives or coating procedures, it should be capable of supporting pigments, fillers and other conventional adjuvants.

Few if any coating materials fulfil all of these criteria; for example, hydroxypropyl cellulose produces films with good mechanical properties, which tend to be tacky, whilst ethyl cellulose films are somewhat brittle. Those materials commonly used as film formers can be classified according to their solubility in the gastrointestinal tract.

a) Soluble: these materials include hydroxypropyl cellulose (HPC), hydroxypropylmethyl cellulose (HPMC), methyl cellulose (MC), sodium carboxymethyl cellulose (CMC), polyvinylpyrollidone (PVP), polyvinyl alcohol (PVA), acrylic resins (e.g. Eudragit E) and polyethylene glycol (PEG, molecular weight grades 1,000 to 6,000).

b) Enteric Resistant: these materials include cellulose acetate phthalate (CAP), polyvinyl acetate phthalate (PVAP), hydroxypropylmethyl cellulose phthalate (HPMCP), acrylic resins (e.g. Eudragit L/S) and styrene-maleic acid co-polymer.

c) Insoluble: these include ethyl cellulose, polyvinyl acetate and acrylic resins (e.g. Eudragit R.S. - low permeability and Eudragit R.L. - high permeability). With such coating materials drug release is by diffusion through the intact coating or coating erosion in the gastrointestinal tract, although soluble additives can be included to increase the permeability[10,22,61,66-71].

The properties of the film former can be modified by internal plasticization, although plasticization procedures which involve the creation of a co-polymer are more related to the initial choice of coating material.

External plasticizers are essentially high boiling point solvents for the film former which, by decreasing polymer chain interactions, allow a greater degree of film flexibility. Commonly used materials include PEG (grades 200 to 600), propylene glycol, castor oil, glycerin and phthalates, although the use of the latter is somewhat limited by their bitter taste.

Opacifiers and fillers are used to decrease the amount of film former required, to increase the solids loading of the formulation without raising the viscosity and to provide an opaque

base to which colourants can be added. Titanium dioxide is the material of choice due to its pure white colour, chemical stability and good hiding power, although talc, silicates, carbonates and oxides can also be used.

Colourants are included in coating formulations to aid product identification and improve its aesthetic appearance. In general,dyes are unsuitable colouring materials for film coatings since colour migration during drying and tablet to tablet film weight variations cause considerable intra- and inter-batch colour variation. Furthermore, these materials have been shown[36] to adversely affect the disintegration characteristics of the coating. These problems are minimized by the use of pigment colouring systems, often based on insoluble aluminium lakes, which allow superior colour density and uniformity to be attained.

To offset problems of foam production during preparation of the coating suspension, silicone emulsions may be added, whilst the inclusion of wetting agents such as Tween 80 facilitates the rapid coverage of the tablet surface and improves adhesion. Gloss inducers such as PEG 6000 improve the elegance of the product and additives such as lactose accelerate the disintegration of the film.

Organic solvents commonly used in film coating include methanol, ethanol, acetone, methylene chloride, chloroform and isopropanol. To obtain the most appropriate solvent system for the

chosen film former, these may be used singly, in combination with each other, or with water. In contrast, it is the polymer and adjuvants which must be selected for their solubility in water when film coating from an aqueous vehicle, the exception being dispersions of acrylic resins or ethyl cellulose. To prevent microbial attack of aqueous coating suspensions, preservatives such as methyl and propyl para-hydroxybenzoates can be included in the formulation although in polymeric systems their potentiation[34] or inactivation[29] should always be evaluated.

1.3 Film Coating Processes

The film coating equipment which is available commercially aims to distribute the coating liquid over all the tablets whilst preventing them from sticking together. Thus the coating formulation is applied to a moving bed of tablets and the solvent rapidly removed by the application of drying air.

The wide variety of equipment available for film coating tablets has been reviewed in the literature[72,73] and consequently individual techniques will not be discussed in detail. Table 1.1 lists the main types of coating equipment which are commercially available. Conventional panning equipment used for sugar coating can be modified to allow even aqueous film coating, despite the poor air exchange inherent in its design. Upgrading and redistribution of the inlet air flows and temperature combined with a powerful exhaust can aid solvent removal and the introduction of baffles improves tablet mixing[17,74,75]. To further improve the drying efficiency and reduce material losses, an immersion-tube

Table 1.1. The main types of tablet film coating equipment which are available commercially

	Coating equipment	Manufacturer or supplier
Equipment for use with conventional coating pans	Strunck immersion tube	H. Strunck and Co., Cologne, W. Germany
	Glatt immersion sword	Glatt Air Techniques Inc., Ramsey, New Jersey, U.S.A.
	Driamat	Driam Metall produkt, GmbH
Modified coating pans	Pellegrini pans	Franco-Nigris and Co. Milan, Italy.
	Accela-Cota	Manesty Machines, Liverpool
	Freund Hi-Coater	Vector Corp., Marion, Iowa
	Driacoater	Driam Metall produkt, GmbH.
	Damoulin I.D.A.	Damoulin, La Varenne, France
Fluidized Bed Coaters	Wurster Coater	Glatt Air Techniques Inc., Ramsey, New Jersey, U.S.A.
	Aeromatic Coater	Aeromatic Inc., Bernardiville, New Jersey, U.S.A.
	Flo-Coater	Vector Corp., Marion, Iowa.

system[21,72,73] can be adopted by which drying air and sometimes the coating suspension are applied from a duct which opens within the tablet bed.

Details of modified coating pans are common in the literature[4,6,9,11,17,21,72,73,76,77], but all aim to improve drying efficiency and mixing and reduce coating times. These range from drum- and

doughnut-shaped pans to the less conventional Pelligrini pan and Accela-Cota. Until recently the latter has been unequalled with respect to optimal air flow within the pan, although its pre-eminence in the field of aqueous film coating may be challenged by developments such as the Freund Hi-Coater and the Driacoater[73]. The operation of the Accela-Cota is described in detail in section 4.3 with respect to the design of a model coating system.

Fluidized bed coating maximizes the mixing and drying efficiency, since the coating suspension is sprayed on to tablets which are suspended in a moving column of drying air. However, due to the abrasive nature of the tablet movements this technique is only applicable to cores of low friability.

Less conventional techniques, which as yet are not widely available, include dip-coating[5,78], brush coating[79], electrostatic spraying[80], conveyor belt coating systems[81-84], vacuum coating[85] and a specially designed air suspension coater for use with friable cores[86]. Automation of the coating process by use of punch tapes[74], timers[87,88], temperature sensors[89,90] and moisture sensors[72] can improve product quality and uniformity and reduce coating times.

Whatever system is chosen, the coating suspension is applied as an atomized spray, since the pouring techniques used in sugar coating cannot be successfully used for film coating[87]. The main alternatives are hydraulic or pneumatic spraying systems,

although spinning disc[92] and ultra-sonic[72] atomizers have been considered. The relative advantages and disadvantages[4,5,17,21,72,92] of hydraulic and pneumatic atomization are listed in Table 1.2, although the latter is generally preferred for aqueous coating.

1.4 The Evaluation of Film Properties

1.4.1 Preparation of Free Films

Tablet film coatings are often evaluated by reference to the properties of free films, but in many cases the preparation conditions have been chosen for convenience rather than their realism in simulating the application of coatings to tablets. For instance Zatz et al.[93,94] believed that only the gross properties of polymers could be evaluated using free films and advocated the use of surface pressure-area data, at the air-liquid interface, obtained from monolayers of the film former, for the study of subtle changes in polymer interactions. However, the relevance of such measurements to the development of useful coating formulations was not established. Due to the elimination of variation caused by the coating technique or dosage form, Kanig and Goodman[95] regarded the study of free films as useful, although differences in the properties of free and applied films[41,96-102] have led other workers[99] to conclude that film formers should not be evaluated solely on the basis of free film performance. However the undoubted advantages of using free films has led several workers[41,98,103-107] to attempt their preparation under conditions which more realistically simulate tablet coating.

Table 1.2 The relative advantages and disadvantages of pneumatic and hydraulic atomization of coating suspensions for the film coating of tablets

Atomization system	Advantages	Disadvantages
Hydraulic (airless)	Atomization more uniform and droplet size often smaller Higher viscosity solutions can be sprayed Little blow-back of spray from pan Spray pattern is easier to control, leading to less overspray and material loss	Controlled variation of the spray rate is difficult as atomization becomes poor if pressure is reduced Equipment is expensive High atomization pressure 1.7×10^6 - 2.1×10^7 Pa Nozzle blocking and orifice erosion
Pneumatic (air)	Fine spray, even at low spray rates Low atomization pressures, 6.9×10^4 - 6.9×10^5 Pa Rapid drying due to solvent flash is especially good for aqueous coating	Blow back of spray from pan Spray drying of the coating suspension Large volume of atomizing air can cool the tablet bed. Nozzle blocking and orifice erosion

The substrates on which free films can be successfully prepared are governed by the spreading coefficient of the coating formulation and the extent of polymer adhesion. Due to a low resistance to the spreading of the coating suspension, highly polished chromium plated steel has been used[95,108-111] although shellac[111] and vinyl acetate[110] polymers show a high level of adhesion to this surface. To decrease film adhesion glass substrates are either highly polished[10,22,41,67-69,96,97,100] [102,104,109,111-115] or coated with a silicone release agent[116,117], although use of a mercury substrate[26,41,68,69,96,104,110,111,118-120] can avoid this problem and also create a perfectly plane surface provided the coating formulation exhibits a positive spreading coefficient and mercury droplets do not adhere to the underside of the film[111]. Other substrates such as teflon (PTFE)[41,98,103,109,121-124] aclar[103], aluminium foil[103,125], celluloid[109,111], Formica[109,111] and silicone impregnated paper[111] have been used with varying degrees of success.

The differences observed in the water vapour permeability and mechanical properties of cellulose acetate free films sprayed on to teflon, aclar and aluminium substrates were not significant[103], although several workers[61,96] have changed substrates for different coating formulations without regard to the possibility of a substrate effect.

The coating solution or suspension is commonly applied to the levelled substrate by a casting or pouring technique, in which the spread of liquid is controlled by metal or perspex strips cemented

to the substrate[96,109,116,125], circular glass or aluminium rings placed on the substrate[10,68,100], a well machined in the substrate[121,122] or the walls of a petri dish in which the substrate has been placed[26,96,110,119,120]. Thus the film thickness is controlled by the volume and concentration of the coating solution. Alternatively an applicator knife/Doctor blade can be used[95,108-113,126] to spread a liquid film of known thickness on the substrate, although Munden et al.[110] found that the uniformity of dry film thickness is inferior to that achieved with a pouring technique.

The conditions under which the films are dried vary widely, from room temperature in a solvent laden atmosphere[109,115,118,119] to forced drying at elevated temperatures in an oven[67,95,121,125]. Some workers[95] have ignored the effect of drying conditions on the film properties despite evidence that rapid drying produces a heterogenous film with a dense surface layer[67,121,125].

Since film coatings are applied to tablets from an atomized spray, several workers[97,98,100,103,106,117,124,126,127] have compared the properties of free films produced by casting and spraying techniques, although the atomization conditions used have sometimes been poor when compared with those used industrially[97,100,103]. In general both the mechanical and barrier properties of sprayed films have been inferior due to partial spray drying of the coating suspension during their production, although the extent of these changes was dependent upon both the nature of the polymer[98] and concentration of plasticizer[106] present in the formulation.

Whichever way the free films are produced, when dry, they are removed from the substrate and stored before testing. The choice of storage conditions appears arbitrary and varies from room temperature at 0%[97,116,118] or 50%[10] relative humidity to vacuum drying in an oven[115]. The film thickness is usually measured with a micrometer, but the surface roughness of sprayed films can introduce errors[103,106,117]. Pickard[106,117] overcame this problem by use of cyclohexane pycnometry, although the technique was too tedious for routine use and only produced a mean thickness for the whole area of film. By sectioning the film and measuring its thickness microscopically Lindberg[118] was able to evaluate the film thickness in different areas of the coating, although the technique was destructive and could only be carried out after the film properties had been evaluated. Alternative techniques, used for the measurement of the thickness of paint films, which could be applied to tablet coatings include X - ray fluorescence measurements of titanium dioxide[128], or u/v fluorescence measurements of compounds specially added to the coating formulation[129].

1.4.2 Measurement of Gas and Vapour Permeability

The transfer of a permeant across a membrane can be described by Fick's first law of diffusion[243,269].

$$\frac{dm}{dt} = - D A \frac{dc}{dx} \qquad \text{.....(equation 1.1)}$$

where $\frac{dm}{dt}$ = mass transfer per unit time

D = diffusion or mass transfer coefficient

A = film area

$\frac{dc}{dx}$ = concentration gradient of permeant in the film

Assuming that a linear concentration gradient exists across the film and Henry's law is obeyed for the distribution of the permeant between the film matrix and bulk phases, equation 1.1 can be re-written:-

$$\frac{dm}{dt} = \frac{PA\Delta c}{L} \qquad \text{...(equation 1.2)}$$

where P = permeability coefficient

Δc = permeant concentration difference between the donor and receptor sides of the film

L = film thickness

However, the concentration gradient of permeant in a membrane of finite thickness is not usually linear and demands the use of Fick's second law of diffusion[243] to describe the transfer process:-

$$\frac{dc}{dt} = D\left[\frac{d^2c}{dx^2}\right] \qquad \text{...(equation 1.3)}$$

where $\frac{dc}{dt}$ = permeant concentration change in the film per unit time

D = diffusion coefficient

$\frac{d^2c}{dx^2}$ = change in concentration gradient of permeant in the film.

Equation 1.3 can be solved by treating the membrane as a series of thin parallel sheets, in each of which $\frac{dc}{dt}$ is constant (equation 1.4)[243]

$$M_t = \frac{D\ A\ C_1^p}{L}\left[t - \frac{L^2}{6D}\right] \quad \text{...(equation 1.4)}$$

where M_t = cumulative mass transfer across membrane in time t

L = membrane thickness

A = membrane area

C_1^p = permeant concentration at the donor surface of membrane

D = diffusion coefficient.

If Henry's law is obeyed, if the mass of permant adsorbed in the membrane is very small in comparison with the mass appearing in the receptor compartment and if the concentration difference across the film is constant (mass transfer under 1%), equation 1.4 can be re-written to yield the Barrer equation[243,269] (equation 1.5):-

$$C_2^s = \frac{P\ A\ C_1^s}{LV_2}\left[t - \frac{L^2}{6D}\right] \quad \text{...(equation 1.5)}$$

where C_2^s =permeant concentration in the receptor compartment

P = permeability coefficient

C_1^s = permeant concentration in the donor compartment

V_2 = volume of receptor compartment

Alternatively the permeability coefficient (P) can be calculated from sorption - desorption measurements by use of equation 1.6:-

$$P = D\ K \quad \text{...(equation 1.6)}$$

where the diffusion coefficient (D) is related to the rate of sorption and the Henry's law solubility coefficient (K) to the amount of permeant sorped. However, these latter methods of measuring permeability are inappropriate for use with thin films and permanent gases and very inaccurate with water vapour and many polymers[130,131]. In many types of polymer water molecules tend to form immobile clusters[130,132,133], leading to a decrease in D with increasing vapour pressure unless the degree of clustering can be accurately determined and the effective concentration of monomeric water calculated. Further errors can arise if these clusters inhibit the movement of monomeric water, or heat is liberated on sorption of water by hydrophilic polymers[131]. Thus transmission methods which follow the volume, pressure or concentration rise on the distal side of a film are preferred for the determination of permeability coefficients for thin films, especially as they more closely approximate to the in-use conditions of tablet coatings.

The transmission techniques available have been extensively reviewed in the literature[130,134-137] and consequently only the general principles and advantages of those which are applicable to free tablet film coatings are described here. The water vapour permeability of film coatings has commonly been investigated by methods akin to that of ASTM E96-53T, for the determination of the water vapour transmission of packaging media. The film is sealed over a cup containing either desiccant[22,95,109,110,112,113,130] or a saturated salt solution[26,96,108,115-119,134,138] and the respective weight gain or loss determined. However, due to errors

in film sealing, the development of vapour pressure gradients and estimation of the film area exposed to the permeant, the results obtained using these techniques are only comparable when determined under identical conditions within a given system[130,131,134,139]. Additional errors introduced by removing the cups from a constant temperature and humidity environment for weighing can be eliminated by installation of a quartz micro-balance within the humidity cabinet[130].

The gas permeability of tablet film coatings although receiving little attention has been reported to be essentially zero[109]. However, the equipment used in this study was designed to measure the permeation of paper, a process known to occur by rapid capillary or conventional flow rather than slow activated diffusion as in polymers[130]. The permeation of oxygen has also been studied by sealing the films across alkaline pyrogallol solutions and following the rate of darkening spectroscopically[110,140]. This technique is tedious and suffers from the complication that water vapour from the pyrogallol solution may plasticize the film and modify the oxygen permeability in an unknown way[134,141].

Other techniques available are derived from the fields of engineering, polymer and packaging sciences and can be classified according to the method of detecting the permeating gas. Volumetric and pressure techniques apply an absolute pressure difference across the film and follow the respective volume[130,142,143] or pressure[130,133,134,144,145] rise on the distal side, the latter

generally being more sensitive[142]. The pressure difference across the membrane is achieved by applying either a positive pressure to the proximal side[130] (superatmospheric technique) or a vacuum to the distal side[133,144] (subatmospheric or vacuum technique); the latter enables the lag time to be determined more accurately since the film is initially devoid of permeant[130]. As these techniques are not specific for one gas, only single component systems can be studied unless an elaborate system for selectively trapping gases is used. The use of liquid nitrogen traps has allowed their application to the permeation of condensable vapours[130,132,146-148], although large errors can occur in the measured lag time for water vapour due to its high cohesive energy density and hydrogen bonding capacity causing significant adsorption on to the walls of the receiving compartment[131]. Such errors are minimized by having a large volume:surface area ratio in the receiving side of the apparatus and pre-wetting all surfaces[131]. To maintain steady state permeation, transfer across the membrane must occur under sink conditions, but in order to measure this transfer the volume or pressure in the receiver chamber must rise significantly. These contradictory requirements have been overcome by isolating the distal side of the film from the receiver chamber by use of diffusion pumps[131] or liquid nitrogen traps[132,146,148].

The absolute pressure difference across the film can be eliminated by use of techniques which measure the concentration of permeant on the distal side of the film. Additionally the

use of specific detectors allows the transfer of individual species from a multicomponent gaseous mixture to be studied. Procedures utilizing tritiated water[130,134,149], reaction with cinnamic acid chloride[130,150] or naphthalene phosphonyl chloride[130] have enabled the study of water vapour permeability, whilst Verdin[151] and Funke et al.[152] have reviewed the various methods of oxygen analysis. The errors and problems associated with the analysis of oxygen by mass spectrometer systems have been discussed by Nobbs[153], although their application to the measurement of film permeability has required either a substantial film support[154] or a trapping system[155] since the films could not be subjected to the high vacuum required for mass spectrometer operation.

The permeability coefficient of permanent gases is independent of the partial pressure gradient across the film[143,144] (equation 1.5) and the presence of other permanent gases[130,134,141], provided mixing is adequate to prevent the formation of concentration gradients and neither gas interacts with the polymer. The gas permeability of hydrophobic films is unaffected by the presence of water vapour, whilst that of hydrophilic films is increased due to plasticization by water increasing the diffusion coefficient[134,141]; measurement at different temperatures indicating that the magnitude of the effect is dependent on the relative humidity rather than the absolute water content of the gas.

The water vapour permeability coefficient of hydrophobic films is unaffected by the water vapour pressure or the presence

of water vapour on the distal side of the film[97,132,134,148]. However, the diffusion coefficient, measured from the lag time[148], increases with increasing vapour pressure due to adsorption of water vapour onto the walls of the receiver compartment, unless these have been pre-wetted[132]. Due to the plasticizing action of water within hydrophilic films the water vapour permeability coefficient increases with increasing vapour pressure[97,134,135] and with the presence of water vapour on the distal side of the film[97,121,138], causing non-Fickian behaviour of many polymers below the glass-transition temperature[156] (T_G); T_G being defined as the temperature at which a sharp increase in polymer chain motion occurs. The water vapour permeability of both hydrophobic and hydrophilic films is unaffected by the presence of non-interactive gases[134,141].

The effect of temperature on the permeability and diffusion coefficients of permanent gases in polymers follows an Arrhenius-type relationship[133,134,142-144,157]:-

$$P = P_o e^{-E_a/RT} \quad \text{...(equation 1.7)}$$

where P = permeability coefficient

P_o = constant

E_a = activation energy for permeation

R = gas constant

T = absolute temperature

or

$$\log P = \log P_o - \frac{E_a}{2.303R} \cdot \frac{1}{T} \quad \text{...(equation 1.8)}$$

Thus plots of log P versus $^{1}/_{T}$ are linear, although the effects around the glass transition temperature are dependent on both the permeant and polymer. Often the slope changes abruptly at the glass transition temperature[134,157], although the inflexion can be absent[133,157] if the free volume occupied by the gas molecules is very small and the diffusion coefficient therefore not significantly affected by the increase in total free volume at the glass transition. The diffusion coefficient has been shown to be proportional to the molecular diameter of the permeant[133-135,144], whilst the solubility coefficient followed the ease of condensation of the gas[134,144].

The effect of temperature on the water vapour permeability coefficient is dependent on the nature of the film[97,119,138,158]. Permeation in hydrophobic films follows an Arrhenius type relationship, increasing with increasing temperature due to enhanced diffusion and solubility coefficients. However, that in hydrophilic films can decrease with increasing temperature as hydrogen bonds between the polymer and moisture are broken, reducing the solubility of the permeant and/or its diffusion rate. An alternative explanation for this phenomenon[133] is that polymer crystallinity increases with temperature, leading to a greater diffusion path length and reduced polymer segmental motion.

1.4.3 Measurement of Mechanical Properties

Micro-identation testing is widely used to characterize the mechanical properties of tablets and tablet coatings[107,114,159-163],

although some caution should be exercised when correlating these surface properties with the bulk properties of elasticity and hardness. The instruments described[162,164,165] in the literature record the depth of penetration of a spherical-end indenter on application of a known load, as a function of time. The derivation of the equations for hardness and elasticity parameters and their relationship to the trace produced by the indenter, have been presented by Ridgway et al.[163] and Aulton[161]. Being small, the apparatus can be enclosed in a glove box of controlled temperature and humidity, allowing evaluation of film properties under specific atmospheric conditions. Provided the indentation is small relative to the film thickness, the results obtained are independent[114,164] of the film substrate, enabling the comparison of free and applied films.

Tensile testing of free films is used to characterize their mechanical properties[105-107,109,159,166] and it has been claimed that at similar rates of deformation such measurements correlate well with indentation testing, pencil hardness and abrasion resistance[166]. In these tests, a strip of film coating is elongated at a constant rate until failure, whilst recording the stress strain profile. From this curve, the mechanical properties can be characterized in terms of the elastic modulus, elongation and tensile stress at the elastic limit, elongation and tensile stress at failure and work of failure. The definition and calculation of these parameters is described

in section 6.3.

Other tests which have been applied to film coatings include measurement of the pendular hardness[109,167], bursting strength[109,167] and diametrical crushing strength; results from the latter mirror those of tensile testing[105,107,168].

1.4.4 Measurement of Adhesion and Related Parameters

The measurement of film adhesion can be a useful parameter in helping to predict the resistance of a film to mechanical damage, since detachment from the substrate will render it more susceptible to impact damage during subsequent handling. In addition, poor film adhesion can result in the bridging or loss of clarity of intagliations on the tablet surface.

There are thought to be four complementary mechanisms of adhesion[169-171]:-

a) mechanical interlocking of the surfaces, which may be important for rough surfaces.

b) diffusion of polymer and substrate molecules and their subsequent entanglement, which may play a role in the autohesion of polymers, although the limited mobility of the substrate will prevent any gross effects.

c) electrostatic interaction between the substrate and the coating may occur if an exchange of electrons takes place between the surfaces.

d) adsorption, which is probably the main mechanism of

interaction, with van der Waals forces and hydrogen bonding providing the main adhesive force between the film and substrate, although this may occasionally be supplemented by chemisorption.

The adhesion of film coatings can be measured by peel testing[169,172,173] which detaches the film at 90 degrees to the substrate, or tensile testing[105,107,174-179], in which the film is removed normal to the substrate. The forces measured with the former may be enhanced by deformation of the test material[169], thus creating additional problems when comparing the adhesion of coatings of different elasticity[175]. To minimize such effects the peel angle is maintained at 90° by moving the crosshead of the tester[173,181], although other workers[172] have maintained that the distances involved in most peel tests are too small to significantly affect the peel angle. Peel tests can also be regarded as a measure of the cohesive strength of the film[181] since failure is generally cohesive rather than adhesive[169], cohesive failure occurring if even a monolayer of film remains on the substrate or vice versa.

To avoid these problems, Fisher and Rowe[175] have designed a tensile adhesion tester, although an Instron Tester can also be used[179]. In such tests the tablet is held in a collet and double-sided adhesive tape, attached to the moving crosshead, brought into contact with the tablet under a fixed pressure sufficient to ensure good adhesion of the tape and coating. The crosshead is withdrawn at a constant rate and the force necessary to remove the

coating recorded. Jacobsson[180] has emphasized the importance of obtaining a uniform bond between the tester and film, since faults may concentrate or relieve the applied stresses so altering the measured adhesion. Similarly it has been shown[179] that the padding material between the crosshead and the adhesive tape and the speed of pull-off can affect the measured adhesion. Fung and Parrott[182] also found that the atmospheric relative humidity affects the adhesion measured by tensile tests.

The adhesion of film coatings is known to be affected by the surface roughness[172,174,175,183,184] and porosity[174,178] of the substrate and the speed and extent to which it is wetted by the coating formulation[172,173,183,185].

Surface roughness can be evaluated qualitatively by visual comparison of scanning electron micrographs[121,184,186] or by the use of Y-modulation[187] to enhance the vertical deviations of the surface. The applications of the electron microprobe have been reviewed[188,189], with respect to the analysis of the elemental distribution in the surface and the use of detectors placed 180° apart to enable the surface topography to be studied by back scattered electrons. A stylus instrument is used to obtain a quantitative estimate of the surface roughness by recording the vertical deviations of a fine stylus as it is moved across the surface[184,190,191]. The specifications of such instruments, their use and the calculation of basic surface roughness parameters are detailed in British Standard 1134[191], although alternative parameters may be more suitable for the detailed characterization of surfaces[192,193].

Mercury intrusion porosimetry[194] has been used to evaluate the porosity of tablet substrates[195,196]; a pore volume-size distribution is obtained by recording the penetration of mercury into the sample at several known intrusion pressures. Helium-air pycnometry[198,199] can also be applied to measure the absolute volume of a tablet, which when compared with the bulk volume obtained by dimensional analysis, allows calculation of the porosity.

The critical surface tension, γ_c, can be used to evaluate spreading and wetting on a substrate, where γ_c represents the liquid surface tension at which liquids will spread over the solid surface. γ_c has been determined by measuring the contact angles of a homologous series of liquids of increasing surface tension and extrapolating to zero contact angle[169,172,173,200-202]. Such measurements have demonstrated a correlation between coating adhesion and tablet critical surface tension, but not the surface tension of the coating solution[172,173,201,203]. The critical surface tension appears to be controlled by the most poorly wetted species present in the surface, even when it represents a small proportion of the total available surface[204]. As the measured values for critical surface tension depend upon the ambient temperature[202] and polarity of the homologous series of liquids used in the determination[200,203], it has been proposed[203] that the surface free energy, which is a measure of the operative cohesional forces in the tablet surface in the presence of the coating liquid, would be a more appropriate parameter from which to predict the adhesion of film coatings to tablets.

1.5 The Effects of Formulation and Processing Variables

The effects of formulation and processing variables reported in the literature largely refer to solvent-based systems. However, the general trends and principles which have been observed are useful when considering aqueous film coating.

1.5.1 Formulation Variables

The reported effects of formulation parameters vary widely and contradictory findings can often be attributed to differences in the techniques of film preparation, storage or testing.

a) Film Former

The polymer structure can affect the rate of gas permeation via either the diffusion coefficient or the solubility coefficient[134,144,205]; the former being decreased by cross-linkage and crystallinity whilst the latter is affected only by crystallinity until a very high degree of cross-linking has occurred. Several guidelines[108] can be followed to select a polymer with low moisture permeability. Those materials which are non-hydrophilic, with a low degree of chain branching and high degree of lateral symmetry are generally crystalline and impermeable to moisture, although increasing the hydrophilic nature by addition of amide, ester or acetal groups to the polymer backbone, or ester, acetal, nitrile or hydroxyl substituents as side groupings can outweight the effects of crystallinity. Decreasing the polymer symmetry by the introduction of large substituents will increase the moisture permeability, as

seen when changing from poly methyl to poly butyl methacrylate. Thus any changes in structure which increase the hydrophobicity or crystallinity[26,68,69,96,97,118,119,121,122,147,144,181,206] of the polymer will decrease the moisture permeability, although the disintegration time and dissolution rate of subsequent film coatings may be adversely affected[66,68,69].

The polarity of the polymer and adjuvants is important with respect to the adhesion of the film to the substrate, since this is thought to occur by the interaction of polar groupings. Film adhesion has been shown by Brantley et al.[207] to increase as the proportion of polar groups in the film increases and other workers have demonstrated that the adhesion of polymers containing carboxyl groupings can be increased by displacing short chain fatty acid surface contaminants with low molecular weight polar molecules[208]. The higher adhesion of HPMC compared to MC films has been attributed to the hydroxypropoxy grouping possessing a greater hydrogen bonding capacity than the methoxy grouping[186].

The molecular weight of a film former governs the viscosity of the coating solution and hence the polymer content which can be attained without adversely affecting the atomization conditions. Thus for aqueous film coating low molecular weight polymers are used to enable a reduction in the water content of the coating suspension and aid drying. The water vapour permeability of cast films has been shown to be unaffected by the molecular weight of HPMC[59,109,118], although use of high molecular weight

polymer yields films which are more continuous, elastic and resistant to attrition[8,10,109,186,209,210]. This improvement in mechanical properties can be attributed to increased polymer chain interaction as the molecular weight increases. Rowe[186] has also demonstrated that the disintegration time of coated tablets increases linearly with the molecular weight of HPMC used as the film former.

The effect of polymer molecular weight on film adhesion is complex due to several opposing factors. The use of low molecular weight polymers delays gelation of the coating until a greater proportion of the solvent has been removed, so minimizing shrinkage stresses on drying[208]. In addition, the lower solution viscosity enhances spreading on and wetting of the substrate, increasing the contact area and improving the adhesion[169,183]. Rowe[186] demonstrated that the decrease in adhesion of HPMC films with increasing molecular weight is related to a decrease in penetration of the substrate caused by increases in solution viscosity and polymer chain hindrance. Further work confirmed this finding[174] since the adhesion at zero substrate porosity is independent of polymer molecular weight. However, in the field of polymer technology, other authors have found that adhesion is independent of[211] or increased to a maximum with[212] increasing molecular weight.

As the polymer molecular weight increases, the surface roughness of coated tablets first decreases then increases again[213]. A similar profile is seen with increasing polymer concentration and

both effects may be attributed to the increasing viscosity of the solution first decreasing the tendency for spray drying and then retarding spreading over the substrate.

The use of mixtures of polymers to modify the solubility characteristics of film coatings in the gastrointestinal tract is widespread[28,117,122,123] and the use of HPC in combination with PEG[53] or HPMC[54] has been reported to improve the taste masking capability of the coating.

b) Solvent

Solvation of the polymer is very important and any reduction brought about by the addition of adjuvants or a change in solvent mixture has been shown to adversely affect the permeability of solutes[214,215], adhesion[182], cohesion and integrity[109,214] of the resulting film coating. The reported effects of solvent on the properties of cellulosic films are variable. HPMC films produced from aqueous-based systems are more elastic and have a lower water vapour permeability than similar films prepared from organic solvents. The latter effect is more pronounced with low molecular weight grades of polymer[10,125]. In contrast Lindberg[118] found that the moisture permeability of HPC films is not significantly affected by the choice of either aqueous or organic casting solvents; an explanation for this unexpected behaviour was not given. Good polymer solvation and hence chain extension has[172,216] a greater influence on film adhesion than the effect of low surface tension in enhancing spreading and wetting[172,173]. The choice of

solvent can affect the dissolution rate and ageing characteristics of Eudragit[218] and HPMC[219] films; the dissolution rate of the latter being lower for films prepared from solutions containing isopropyl alcohol and decreasing further on storage. The extent of solvent residues in the film coating, a factor of increasing concern to the Food and Drugs Administration, is also affected by the choice of solvent system[217,218].

Film coating solvents can be chosen by matching the solubility parameters of the polymer and solvent[181,216], since optimal solvation will occur when inter- and intra- molecular forces in the system are equal. Solvent mixtures should be used with some caution however, since the formation of azeotropes during drying can alter the proportions of each solvent, possibly leading to premature precipitation of the polymer and negating the advantages gained by rationally choosing the solvent[101,107].

The volatility of the solvent, characterized by reference to its latent heat of vaporization, is important with respect to the application of film coatings to tablets. It has been shown that continuous CAP films could not be produced by spraying a solution in acetone ,which has a low latent heat (520 kJ kg^{-1}), due to almost complete spray drying of the coating suspension[126]. In contrast, one of the main problems associated with aqueous film coating, involving a very large latent heat (2,260 k J kg^{-1}) is to increase the drying efficiency enough to allow the rapid evaporation of an aqueous solvent[76,77,177].

c) Plasticizers

Plasticizers are included in a formulation to produce a softer, more flexible[102,105,109,114,221] film coating with an increased abrasion resistance[17,24]. The efficiency with which a plasticizer decreases intra- and inter-molecular forces within a polymer matrix depends primarily on its functional groups; carboxylic and ester groups are most effective and ether linkages and aryl groups least effective[222]. Plasticizers can be evaluated by reference to solubility parameter data and intrinsic viscosity measurements of dilute solutions of polymer in the plasticizer[216,223,224].PEG 200 interacts maximally with HPMC[223], resulting in increased film elasticity[114,224] and decreased bridging of intagliations[225]. Although the functional groups associated with plasticization are also those involved in the adhesion of the film to the substrate,plasticizers such as PEG, glycerol and propylene glycol do not affect the adhesion of HPMC films[105,175]. However, the reduction in residual stress in the film caused by plasticization may have masked any interference with the forces responsible for adhesion.

The moisture permeability of film coatings is affected by the concentration and type of plasticizer. Hydrophilic plasticizers first decrease then increase the permeability of films as their concentration is increased[109,112,113,119,120,126,206,226,227], a phenomenon which can be attributed to low levels of plasticizer either slightly increasing chain mobility and allowing a better packing of the polymer chains, or plasticizer filling the interstices in the polymer matrix and blocking the passage of water

vapour. At higher plasticizer concentrations the decrease in chain interactions becomes much greater allowing easier diffusion of moisture within the film. In contrast, the water vapour permeability is decreased by increasing concentrations of hydrophobic plasticizers[109,228] until the film integrity is lost. Other works however found that a wide concentration range of different plasticizers had no effect on the water vapour permeability of HPC[118] or methacrylate films[129].

The permeability of CAP films to caffeine and hydrochloric acid is unaffected by plasticization with diethyl phthalate and acetyltriethyl citrate, but is increased greatly by PEG 400 due to the latter being leached from the film and thus creating channels[230].

Pickard[106] has reported that the plasticizer, propylene glycol, was completely lost during the production and storage of ethyl cellulose/HPMC films, leading to a significant change in their mechanical properties and water vapour permeability. The mechanism of such losses was unclear, although the formation of azeotropic mixtures of propylene glycol with the components of the solvent system was shown to be unlikely to occur.

d). Fillers, Opacifiers and Pigments

The mode of action of colouring and opacifying agents has been discussed by Zorll[231] with respect to the optimum particle size and concentration for both the scattering and absorption of

light. By decreasing the particle size, the scattering of light is increased, leading to more opaque films of increased strength; the latter resulting from the disorder created in the polymer matrix by the particles being reduced[232]. The optimization of coating suspension stability has been investigated by Bayer[41] with reference to filler particle size and the addition of surface active agents and co-solvents to alter respectively the zeta potential and dielectric constant of the system.

By increasing the solids loading of the coating suspension, fillers reduce the problems of tack and picking during the coating process[5,17] and may also increase the film strength and decrease tablet friability[17,98]. However, the strength and elasticity of films are more commonly unaffected[102,233] or decreased[105,221]. A 45% decrease in the adhesion of HPMC films on addition of 10% w/w titanium dioxide has been attributed to the filler interfering with hydrogen bonding between the film and substrate[175], although other workers[105] found that adhesion is unaffected by the presence of titanium dioxide. The surface roughness of film coated tablets is affected by the particle size and concentration of filler[234], although the size ranges studied were much larger than the optimum of 0.2 μm suggested by Zorll[231].

The water vapour permeability of HPMC films has been shown[102,105,116,221] to first decrease then increase with increasing titanium dioxide concentration; an effect which was explained by postulating that the filler increased the effective length of the diffusion pathway,thus

decreasing permeability until there was insufficient polymer to bind the filler particles together, resulting in a rise in permeability. A similar explanation has been used to describe the permeation of oxygen through soft gelatin films containing titanium dioxide[140]. In contrast, Kummins[156] has postulated that a decrease in polymer chain mobility resulting from adsorption on to the filler is responsible for the initial reduction in permeability. Other workers[118] have shown that the water vapour permeability of HPC films was unaffected by the addition of large quantities of either amorphous silica or titanium dioxide.

The addition of talc to HPMC films decreases the water vapour permeability[116,221], by increasing the hydrophobic nature of the film, although this rises again when the film is overloaded with filler.

1.5.2 Processing variables

The effect of processing variables on the properties of film coatings has not been the subject of intensive study, although recent developments[235] have attempted to isolate some of the more fundamental parameters.

a) Air Temperature and Flow Rate

The adhesion and cohesion of film coatings are increased by the application of a warm coating suspension to warm tablets, due to the increased thermal motion and diffusion of the polymer chains allowing better interaction between the polymer and the

substrate and between contiguous layers of polymer[17,181]. However, the increased rate of solvent removal at higher temperatures can counteract this effect, by decreasing the time available for polymer molecules to orientate with respect to each other and the substrate prior to gelation of the film. Increasing the temperature of the coating liquid has been shown[236] to decrease the release rate of salicylic acid from coated micro-granules, an effect attributed to the production of a more coherent coating.

The drying conditions have been shown to affect the solvent residues in organic based film coatings[217] and the stability of active ingredients when coated with aqueous-based formulations[13]. In the latter case inadequate drying air temperatures allow the penetration of moisture and subsequent hydrolytic degradation of the active compound, whilst excessive heat leads to thermal degradation. The drying conditions during fluidized bed coating[13] are governed by the temperature, volume and humidity of the processing air, whilst in a conventional pan[91] the volume of air is the major factor. The upper limit of the processing temperature is often set by the stability of the active compound. However, in the absence of such problems excessive temperatures can lead to spray drying of the coating suspension, slipping and peeling of the coating as it approaches its softening point or a glass transition temperature, or the development of pinholes by evaporation of the solvent through a case-hardened surface[181]. In addition thermal stresses may be generated on cooling which can adversely affect the adhesion and mechanical properties of the coating[237].

b) Atomization Conditions

The moisture permeability of films prepared by pneumatic atomization of a coating solution is greater than that of films prepared using a hydraulic spray system due to the increased tendency for spray drying creating a less coherent coating[117]. The inferior properties of films produced from low molecular weight grades of HPMC can, in part, be attributed to the reduced solution viscosity allowing the production of smaller droplets on atomization with a consequent increase in spray drying[186]. Changes in the atomizing air pressure, liquid feed rate and distance between the spray gun and substrate which minimize spray drying also reduce the permeability and increase the mechanical strength of the resulting films[103,236].

The published work on the factors affecting the spray rate for hydraulic atomization are conflicting since Heyd[238] has shown the flow rate to be linearly related to the nozzle orifice diameter, whilst Stern[239] found the relationship to exist for the square of the orifice diameter. In addition, Stern[239] showed that the the delivery rate is dependent upon the density and not viscosity of the coating suspension whilst Heyd[238] found it essentially independent of suspension density.

c) Film Substrate and Film Thickness

The properties of film coatings are affected by the size, nature and surface roughness of the tablet cores to which they are applied. The increase in coating adhesion with increasing surface

roughness[172,174,175,183,184] can be explained by either an increase in contact area between the film and substrate[172,184] or enhanced penetration of the porous surface of the tablet by the coating suspension[174,175,178]. The presence of hydrophobic groups in the surface of the substrate decreases film adhesion, whilst hydrophilic groups such as hydroxyl and carboxyl substituents increase adhesion by hydrogen bonding. Thus the addition of magnesium stearate as a lubricant decreases adhesion whilst stearic acid increases it[178].

The adhesion of coatings to flat-faced tablets is proportional to their surface area demonstrating the presence of a uniform bond to the substrate[175]. However, at any one diameter the measured film adhesion to convex tablets is lower than that to flat-faced tablets, possibly due to the development of additional shear stresses during testing of the former[177]. Due to attrition in the coating pan, films applied to large tablets tend to be discontinuous, an effect which is more pronounced with low molecular weight film formers due to their lower elasticity[186,197].

The film thickness is determined by the concentration and delivery rate of the coating suspension and the time for which coating is continued. Whilst the permeability coefficients for non-interactive gases[143] and liquids[240] are independent of film thickness, other properties such as adhesion[169,174] and enteric resistance[19,241] are strongly dependent on it. The adhesion, as measured by peel testing, increases as a zero order function of

film thickness until a maximum occurs, beyond which thickness has no further effect[181]. However, the adhesion measured by tensile testing decreases with increasing film thickness[174], a discrepancy which can be attributed to the residual stress within the film increasing with film thickness and augmenting the applied forces in tensile testing and opposing them in peel testing. To avoid confusion arising from changes in the residual stress, the measured adhesion can be extrapolated to a theoretical adhesion at zero film thickness[174]. The increase in the incidence of bridging of intagliations with increasing film thickness is also due to the build-up of residual stresses as the film becomes thicker[242].

As predicted from classical diffusion theory[243], the rate of water vapour transmission decreases with increasing film thickness (equation 1.2), although the extent of this decrease depends upon the nature of the film[95,96,99,229]. The majority of moisture permeability studies are based on Fick's first law of diffusion (equation 1.1) and examination of equation 1.2 shows that if Fickian diffusion is occurring the logarithm of the mass transfer rate will be linearly related to the logarithm of the film thickness.

Banker et al.[96,99] found that although cast free films exhibit the predicted log-log relationship, the moisture transfer rate across films applied to calcium chloride compacts is linearly related to the film thickness. Swarbrick et al.[158] whilst observing the expected log-log relationship for hydrophobic films noted that

the gradient obtained with hydrophilic films could be as low as -0.4, rather than -1.0 as predicted from equation 1.2. This deviation from expected behaviour can be attributed to hydrogen bonding between the polymer and the permeating water, a theory supported by the permeability of hydrophobic films increasing with temperature whilst that for hydrophilic films decreases due to a reduction in hydrogen bonding at higher temperatures.

EXPERIMENTAL

2. SPECIFICATIONS OF RAW MATERIALS

2.1 General Materials

All chemicals used were of Analytical Reagent grade unless otherwise stated. Distilled water was produced by an all glass still and used immediately on collection for the preparation of coating solutions and after cooling in a glass aspirator (Pyrex) for other solutions.

2.2 Hydroxypropylmethyl cellulose

This material has the following chemical structure:-

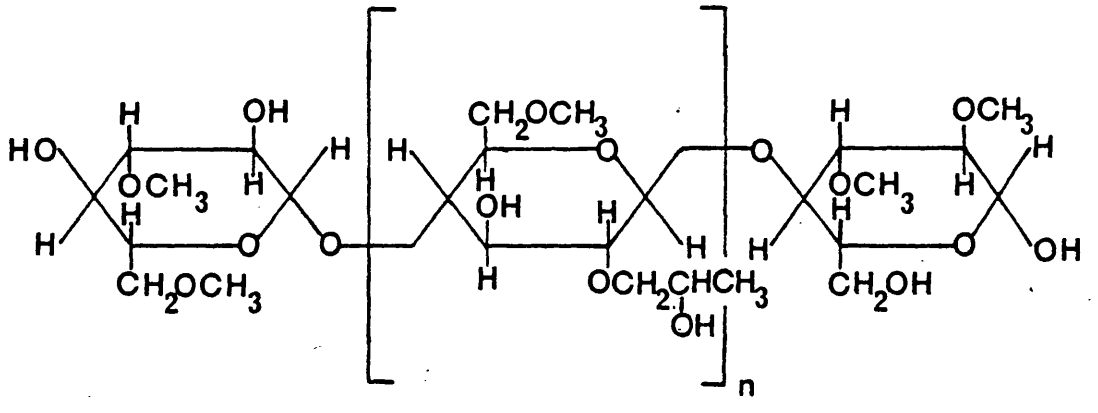

The molecular weight grades used for aqueous film coating usually have values of n in the range 45 to 90.

It is produced by the degradation of cellulose fibres with potassium hydroxide, followed by treatment with methylene chloride and propylene oxide. The number and ratio of methoxy to propoxy substituents is variable and affects the organic solubility and thermal gelation temperatures of aqueous solutions.

a) Pharmacoat 606 (Shinetsu Chemical Co. Ltd.)

A single batch of Pharmacoat 606 was used throughout the work and conformed to the following specification, determined by the Analytical Department, Merck Sharp and Dohme Ltd.:-

Supplier	Stancourt Sons and Muir Ltd.
Suppliers Number	54-056
M.S.D. Batch Number	8355K

Test	Limits	Result
Identity	I.R. Spectra	Pass
Appearance	white	Pass
Loss on Drying	<5%	0.9%
Ignition Residue	<1.5%	0.8%
Hydroxy propoxy groups (dried basis)	7-12%	9.5%
Methoxy groups (dried basis)	28-30%	28.4%
Viscosity of 2% w/v aqueous solution at 20°C (Ubbelohde Viscometer - ASTM D2363-72)	4.8-7.2 cps	5.8 cps
pH aqueous solution (2%)	6-8	6.3
Arsenic	<3 ppm	Pass
Heavy metals	<20 ppm	<10 ppm

The equilibrium moisture content at different relative humidities was also determined. A sample of Pharmacoat 606 was

dried at 60°C in a vacuum oven (Townson and Mercer Ltd.) over phosphorous pentoxide (B.D.H. Ltd.) for 48 hours. The moisture content of the dried sample was determined using a Gallia Thermo-balance (The Northern Media Supply) and found to be under 0.2% w/w. Approximately 2g was accurately weighed into each of 5 beakers and the beakers placed in a desiccator containing an appropriate saturated salt slush at 30°C. The weight increase due to adsorption or absorption of water vapour was measured at regular intervals until an equilibrium weight was obtained, from which the mean percentage moisture gain, on a dry basis, was calculated.

Table 2.1 lists the saturated salt slushes used to obtain different relative humidities[244] and Figure 2.1 shows the equilibrium moisture content at 30°C versus relative humidity.

Table 2.1 The equilibrium relative humidity of air above aqueous saturated salt solutions at 30°C[244].

Relative humidity at 30°C %	Saturated Salt Slush
100	water
91	potassium nitrate
80	potassium bromide
75	sodium chloride
63	sodium nitrite
52	sodium dichromate
43	potassium carbonate
33	magnesium chloride
22	potassium acetate

Figure 2.1 The equilibrium moisture content versus relative humidity, for samples of Pharmacoat 606 at 30 °C.

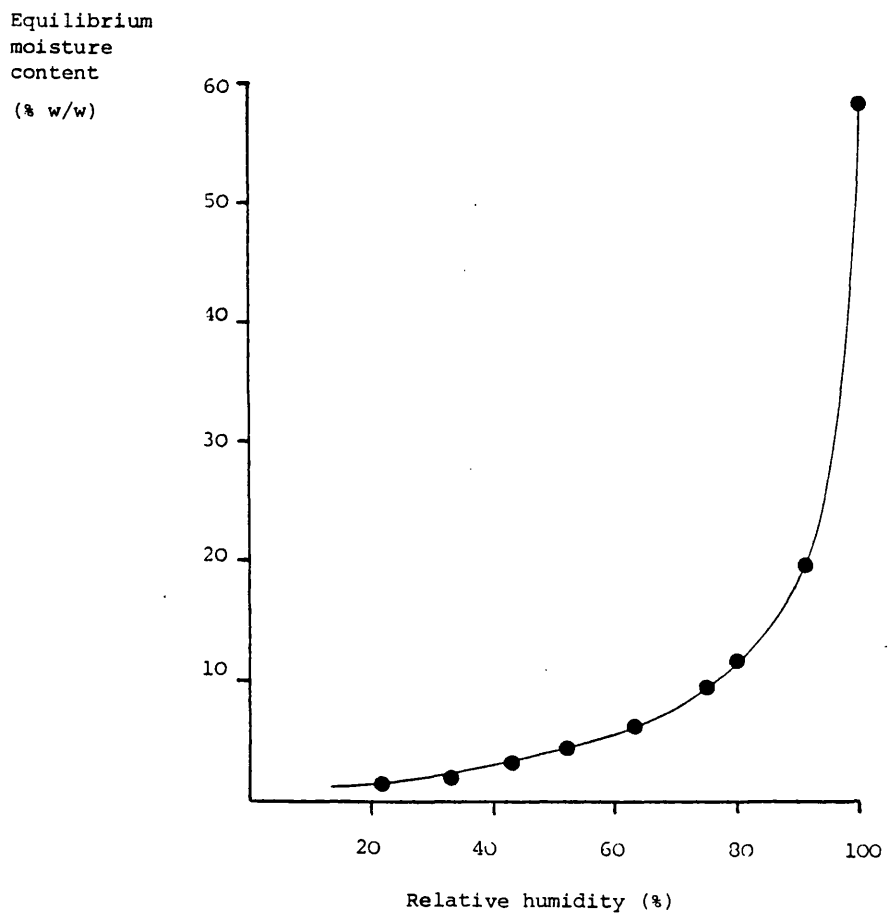

b) Pharmacoat 603 (Batch Number 46-032)

The specification was as for Pharmacoat 606, except the viscosity of a 2% w/v aqueous solution lay in the range 2.4 to 3.6 cps.

c) Methocel E5 Premium (Batch Number 5759 - Colorcon Ltd.)

The specification was similar to Pharmacoat 606, except the viscosity of a 2% w/v aqueous solution lay in the range 4 to 6 cps.

2.3 Hydroxypropyl cellulose

Klucel L.F. (Hercules Powder Company Ltd., Batch 5411) was included in some coating formulations. The material was used as supplied by the manufacturer, without further characterization of its properties.

2.4 Titanium Dioxide

A single batch of titanium dioxide was used and conformed to the following specification, determined by the Analytical Department, Merck Sharp and Dohme Ltd.:-

Supplier	Colorcon Ltd.
Suppliers Number	JB 42
M.S.D. Batch Number	9026K

Test	Limits	Result
Colour	White	Pass
Form	Amorphous powder	Pass
Solubility	Insoluble in water and dilute mineral acids; soluble in hot sulphuric acid	Pass
Identity	Conforms to test A,B and C of B.P.	Pass
Acidity or alkalinity	<1 ml 0.01N NaOH or HCl	0.4 ml 0.01 HCl
Loss on drying	<0.5%	0.21%
Loss on ignition	<0.5%	<0.01%
Arsenic	<5 ppm	<2 ppm
Barium	<5 ppm	<5 ppm
Heavy metals	<10 ppm	<5 ppm
Iron	<200 ppm	<100 ppm
Antimony	<100 ppm	<100 ppm
Water-soluble substances	<0.25%	<0.04%
Acid-soluble substances	<0.35%	0.09%
Organic impurities	No charing on ignition	Pass
Mesh	100% passes 100 mesh sieve	100.1% passes

The mean particle size and particle size distribution were determined by laser light scattering and scanning electron microscopy respectively.

a) Laser Light Scattering

A Nano-Sizer (Coulter Electronics Ltd.) was used to give a mean hydrodynamic diameter for titanium dioxide in dilute suspension, by measuring the rate of change of laser light scattered by the particles whilst in Brownian Motion[245]. This diameter, being dependent upon the particle volume, is closely related to the weight average particle size. The instrument also computes a polydispersity index, or ratio of largest to smallest particles present in the distribution and for a log-normal size distribution to be assumed, this must not exceed four.

Distilled water, 0.1% w/v, 0.2% w/v sodium pyrophosphate (B.D.H. Ltd.), 0.001% w/v or 0.01% w/v Tween 80 (Atlas Chemical Industries) were used as dispersion media after filtration through a 0.05 μm Millipore filter (V.A. Howe & Co. Ltd.) held in a 25 mm diameter 'Swinnex' holder (V.A. Howe & Co. Ltd.). A small quantity of titanium dioxide was added to the dispersion media and placed in an ultrasonic bath (MEL Equipment Co. Ltd.) for 15 minutes to break up aggregates. The suspension was serially diluted with freshly filtered dispersion medium resonicating between each dilution, until a slightly turbid but translucent suspension was obtained. Five replicate measurements were made on the final suspension and the mean hydrodynamic diameter and polydispersity

index calculated (Table 2.2).

When dispersed in distilled water the indicated size and degree of polydispersity were beyond the range of the instrument due to the presence of aggregates, which broke down when a wetting agent was present. The mean particle diameter and polydispersity index (548 nm and 7.15 respectively) were not significantly affected by the nature and quantity of wetting agent present, indicating that either titanium dioxide did not possess a log-normal size distribution, or that agglomerates were present which were very strongly bound together.

b) Scanning Electron Microscopy

Double sided tape (3M Ltd.) was applied to the sample stub, dipped in titanium dioxide powder and the excess shaken off. The sample was sputter coated with gold and examined using a Joel 35C Scanning Electron Microscope (Section 5.1a). Photomicrographs taken at a magnification of 1500 were enlarged to 200 mm x 273 mm and the individual particles classified according to their projected area diameters (Figure 2.2 and Table 2.3).

Figure 2.2 demonstrates that the particles were largely spherical with a narrow size distribution, although agglomerates (A) up to 0.7 μm in diameter could be seen. Figure 2.3 shows the particle size distribution plotted on a number and weight basis and confirms the uniformity of size observed in Figure 2.2. The mean and median projected area diameters are listed in Table 2.4.

Table 2.2 The effect of dispersion medium on the hydrodynamic diameter and polydispersity index of titanium dioxide measured by laser light scattering.

Dispersion Fluid	Hydrodynamic Diameter			Polydispersity Index		
	Mean nm	S.D.	C.V. %	Mean	S.D.	C.V. %
Distilled water	>3000	-	-	> 9	-	-
0.1% w/v sodium pyrophosphate	581.2	38.7	6.66	7.2	0.5	6.94
0.2% w/v sodium pyrophosphate	494.8	36.8	7.44	7.2	0.5	6.94
0.001% w/v Tween 80	553.4	30.0	5.42	7.0	0	0
0.01% w/v Tween 80	562.4	31.3	5.57	7.2	0.5	6.94

S.D. = Standard Deviation

C.V. = Coefficient of Variation

Mean Diameter = 547.95

S.D. = 37.3

C.V. = 6.8

Mean Index = 7.15

S.D. = 0.1

C.V. = 1.4%

χ^2 Diameter = 3.52

χ^2 Index = 0.20

χ^2_{tab} (P=0.05) = 7.82

Figure 2.2 Scanning electron micrograph of a sample of titanium dioxide powder.

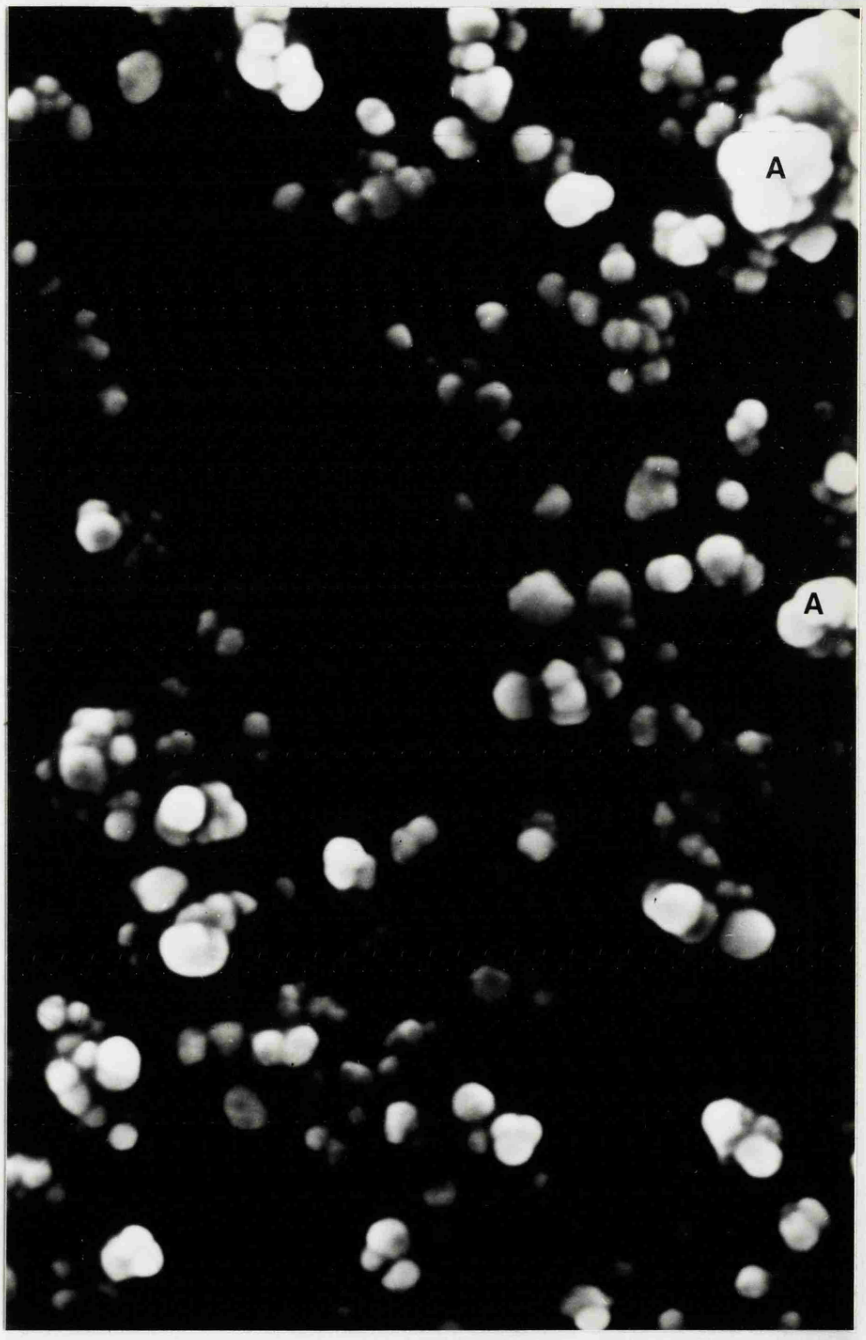

Table 2.3. Particle size distribution of titanium dioxide determined by scanning electron microscopy

Size Range (μm)	Mean Projected Area diameter (d) (μm)	Number Distribution			Weight Distribution			
		Number of particles counted (N)	Frequency (%)	Cumulative frequency undersize (%)	d^3 (μm^3)	$d^3 N$	Frequency (%)	Cumulative frequency undersize (%)
0 - 0.1	0.05	376	35.74	0	1.25×10^{-4}	0.047	0.99	0.01
0.1 - 0.2	0.15	537	51.05	35.73	3.38×10^{-3}	1.812	38.28	1.0
0.2 - 0.3	0.25	115	10.93	86.78	1.56×10^{-2}	1.797	37.97	39.28
0.3 - 0.4	0.35	23	2.19	97.71	4.29×10^{-2}	0.986	20.83	77.25
0.4 - 0.5	0.45	1	0.10	99.90	9.11×10^{-2}	0.091	1.92	98.08
0.5 - 0.6	0.55	0	0	100	1.66×10^{-1}	0	0	100

Figure 2.3 Number and weight distribution of the particle size of titanium dioxide determined by scanning electron microscopy.

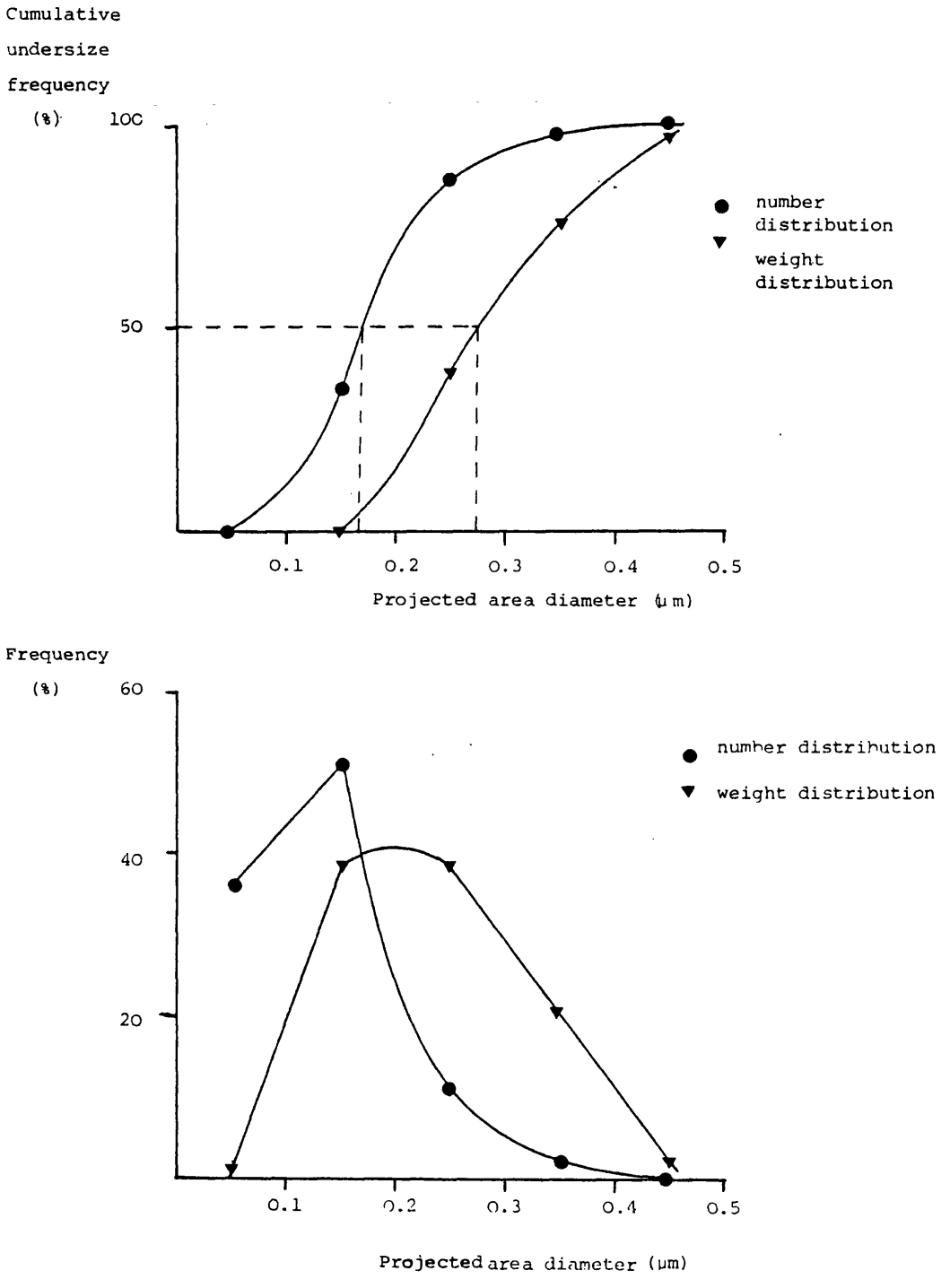

Table 2.4 The mean and median projected area diameters of the number and weight distributions of titanium dioxide

	Projected Area Diameter	
	Arithmetic mean (μm)	Median (μm)
Number Distribution	0.15	0.17
Weight Distribution	0.20	0.27

These data therefore confirm that the hydrodynamic diameter measured by laser light scattering was influenced by agglomerates, since the mean weight average particle size, determined by SEM was 0.2 μm, compared to a value of 0.55 μm determined by laser light scattering. Furthermore the narrow size distribution observed by S.E.M. could not have given rise to a polydispersity index of 7.15 unless agglomerates were present. However, since titanium dioxide was used in coating suspensions without ensuring that aggregates were broken down, the aggregate size may be of more significance to the spray characteristics and film properties than the absolute size of individual particles.

3. PREPARATION, HANDLING AND PROPERTIES OF COATING SOLUTIONS AND SUSPENSIONS

3.1 Introduction

To help understand the process of film formation, the properties of aqueous polymer solutions were investigated. Viscosity parameters allow the evaluation of the extent of polymer solvation, the polymer molecular weight and the maximum polymer concentration which can be adequately atomized. Aqueous solutions of some substituted cellulose ethers undergo thermal gelation and clouding, thus affecting the physical state of the polymer during film deposition. Consequently the temperatures at which such changes occurred were measured and compared with those attained in a 24" Accela-Cota during the coating process.

3.2 Preparation of Solutions

a) Cleaning of Glassware

All glassware, with the exception of that used to prepare bulk volumes of coating solution, was cleaned with chromic acid before use. The items were immersed in chromic acid for between 30 and 90 minutes, rinsed 6 times with tap water, twice with distilled water and dried at 100°C.

b) Small Volume Preparation (up to 500 ml)

The small volumes of polymer solution required for the viscosity, gelation and clouding studies and for the development of the coating assay, were prepared by placing the polymer in a volumetric flask, adding 70% of the distilled water heated to 80°C

and shaking vigorously to ensure complete dispersion. Shaking was continued intermittently until the solution reached room temperature when other components such as propylene glycol or tartrazine were added and the flask made up to volume. Adequate hydration of the polymer during cooling of the solution has been demonstrated by other workers[246], even if a system of forced cooling was employed.

c) Large volume Preparation (0.5 - 5 litres)

Approximately 75% of the distilled water was heated to 65°C in a beaker and the polymer added whilst mixing with a high shear mixer (Laboratory Mixer-Emulsifier fitted with the cutting head, Silverson Machines Ltd.). When dissolution was complete and the solution had cooled to room temperature, it was transferred to a volumetric flask, the beaker repeatedly rinsed with distilled water, the rinsings added to the flask, made up to volume and thoroughly shaken. If solids were to be included in the coating formulation, the polymer was initially dissolved in 50% of the water and the pigment dispersed separately in 20% of the water using the high shear mixer. The pigment suspension was homogenized by passage through a colloid mill fitted with stainless steel stator and rotor (gap 0.127 mm, 3" Multipurpose Mill, Premier-Colloid Mills Ltd.) and added to the polymer solution. The colloid mill was rinsed and the rinsings added to the beaker and thoroughly mixed prior to transfer to the volumetric flask and making up to volume.

To minimize microbial contamination, the solutions were covered

with cling film (Snap-wrap, Gillette Industries Ltd.) whenever possible during their preparation.

3.3 Viscosity Measurements

a) Dilute Solution Viscometry

The relative viscosity of a solution can be obtained from equation 3.1:-

$$\frac{t_1 \rho_1}{t_o \rho_o} = \frac{\eta_1}{\eta_o} = \eta_{rel} \qquad \text{...(equation 3.1)}$$

t_1, ρ_1 and η_1 are respectively the flow time, density and viscosity of the solution

t_o, ρ_o and η_o are respectively the flow time, density and viscosity of the pure solvent

η_{rel} is the relative viscosity

For dilute solutions $\rho_1 = \rho_o$

Hence

$$\frac{t_1}{t_o} = \eta_{rel} \qquad \text{...(equation 3.2)}$$

Einstein derived a hydrodynamic equation (equation 3.3) relating to the disturbance of the flow lines when identical, non-interacting rigid spherical particles were dispersed in a liquid:-

$$\eta_{rel} = 1 + a\phi \qquad \text{...(equation 3.3)}$$

a is a constant

ϕ is the volume fraction

Einstein assumed:-

a) The motion of the spherical particles was extremely slow.

b) The liquid medium extended an infinite distance from the particle .

c) The liquid medium was continuous compared with the dimensions of the particles.

Under such conditions equation 3.3 is valid, the constant having a value of 2.5.

In practice however, deviations arise from an overlapping of the disturbed regions of flow around the particles, particle/particle and particle/solvent interactions and particle asymmetry. Thus the Einstein equation has to be modified, leading to a power series in ϕ:-

$$\eta_{rel} = 1 + a\phi + b\phi^2 + c\phi^3 \quad \ldots z\,\phi^i \quad \ldots \text{(equation 3.4)}$$

considering the first three terms:-

$$(\eta_{rel} - 1) = a\phi + b\phi^2 \quad \ldots \text{(equation 3.5)}$$

$(\eta_{rel} - 1) = \eta_{sp}$, the specific viscosity

Dividing by ϕ :-

$$\frac{\eta_{sp}}{\phi} = a + b\phi \quad \ldots \text{(equation 3.6)}$$

$\frac{\eta_{sp}}{\phi}$ is the reduced specific viscosity

a is the volume intrinsic viscosity

For macromolecular solutions, the true value of the volume fraction can be calculated from the concentration, but is tedious to obtain, involving a knowledge of the partial specific volume which assumes the polymer molecule has a spherical configuration.

Thus equation 3.6 is generally used in the form:-

$$\frac{\eta_{sp}}{c} = [\eta] + b'c \qquad \text{...(equation 3.7)}$$

c is the polymer concentration

$[\eta]$ is the concentration intrinsic viscosity, representing the reduced specific viscosity at the limiting value $c \rightarrow 0$

Equation 3.7 can be re-written to yield the Huggins equation:-

$$\frac{\eta_{sp}}{c} = [\eta] + k_H [\eta]^2 c \qquad \text{...(equation 3.8)}$$

The Huggins constant k_H, is specific for each polymer/solvent system at a given temperature and is an indication of the polymer configuration. A value around 2.0 indicating solid spheres, up to 0.8, rods and 0.4, random coils[247].

The intrinsic viscosity is related to the polymer molecular weight by the empirical Mark-Houwink equation:-

$$[\eta] = K_m M^{\alpha} \qquad \text{...(equation 3.9)}$$

K_m and α are constants for a particular polymer-solvent system and temperature.

For HPMC, Rowe[209] has determined these values as 9.94×10^{-4} and 1.096 respectively from intrinsic viscosity data at 20° in aqueous solution, this in turn derived from single point viscosities measured for 2% polymer solutions and peak molecular weights determined by gel permeation chromatography (G.P.C.) in dimethyl-

acetamide, using polystyrene standards at an unspecified temperature. However, these values should be treated with caution as they refer to peak rather than viscosity or weight average molecular weight and the degree of solvation, chain coiling and hence the hydrodynamic radius of the polymer may alter substantially with changes in solvent and temperature. Furthermore, the polystyrene standards used in the calibration of the G.P.C. may not have exhibited a molecular orientation and configuration similar to HPMC in dimethylacetamide, leading to retention times which were not strictly comparable.

A suspended level dilution viscometer (catalogue number 1710, Poulten Selfe and Lee Ltd.) was placed in a viscometer bath (Laboratory Thermal Equipment Ltd.) at 20°C and the viscosities of a serial dilution of each polymer measured according to British Standard 188[248]. 5 ml of distilled water were added to the viscometer, the mean flow time recorded (3 replicates within 0.2%) and 5 ml of a 4% w/v polymer solution added. After mixing, the mean flow time was measured and the solution diluted with four successive 5 ml volumes of distilled water. A kinetic energy correction was not applied since the flow times in the presence of polymer were always in excess of 300 seconds[248]. The results are shown in Figure 8.1 and Tables 8.1 and 8.2.

b) Continuous Shear Viscometry

A Ferranti-Shirley cone and plate viscometer (Ferranti Ltd.),with automatic flow curve recorder unit, was employed to determine the viscosities of polymer solutions in the concentration

range 0.25 to 20% % w/v. The plate temperature was $29^{o} \pm 1^{o}C$. A sweep time of 120 seconds was used and the shear rate varied from 0 to 1745 sec^{-1}. As the concentration of the polymer increased,the solution became more viscous, necessitating successive reductions in cone size to obtain a measurable shear stress.

For Newtonian solutions the viscosity was obtained from the slope of the rheogram plotted by the instrument. At higher polymer concentrations, the rheological behaviour became pseudo-plastic and the Power Law[249] (equation 3.10) was applied to obtain the viscosity:-

$$\tau = \eta_N D^N \qquad \text{...(equation 3.10)}$$

τ is Shear Stress (Pa)

D is Shear Rate (sec^{-1})

η_N is Apparent Newtonian Viscosity (Pas)

N is Index of Non-Newtonian Behaviour

hence;

$$\log \tau = \log \eta_N + N \log D \qquad \text{...(equation 3.11)}$$

Thus a plot of log shear stress versus log shear rate yielded a slope equal to the index of non-Newtonian behaviour and an intercept equal to the log of the apparent Newtonian viscosity. An index of non-Newtonian behaviour less than 1 indicates pseudoplastic (shear thinning) behaviour, whilst a value above 1 indicates dilatancy (shear thickening). The results are shown in Figures 8.2, and 8.3 and Table 8.3.

c) Creep Rheometry

Using a Deer Rheometer (Modified MK II, K. Luckie Eng. Ltd.) the viscoelastic properties of a 20% w/v aqueous solution of each polymer were evaluated at 29°C. The instrument was fitted with a 4° cone and the gap set at 0.18 mm since the cone had a flat circle at its apex. The instrument allowed a constant shear stress to be applied instantaneously to the cone and its angular deformation (strain) to be recorded as a function of time. Experiments were carried out using shear stress values of between 0.01 and 0.77 Pa. The resulting creep curves were analysed by reading the displacement at various times from the trace and feeding this data into a computer, programmed to generate the appropriate creep parameters[250].

Figure 3.1 is a diagrammatic representation of a creep curve. The instantaneous compliance (J_o) represents polymer molecules which are folded and when subjected to an applied stress can extend instantaneously and recover as soon as the stress is removed. The retarded compliance (J_R) is due to the stretching of bonds being hampered by the entanglement of other polymer chains. The degree of entanglement can vary, giving a series of retardation times and compliances which, for a linear viscoelastic system, can be summed to give the total retarded compliance (J_R):-

$$J_R = \sum_{1}^{i} J_i \left(1-e^{\frac{-t}{\tau_i}}\right) \qquad \text{...(equation 3.12)}$$

J_i = compliance; τ_i = retardation time

t = Time

Figure 3.1 Typical Creep Curve.

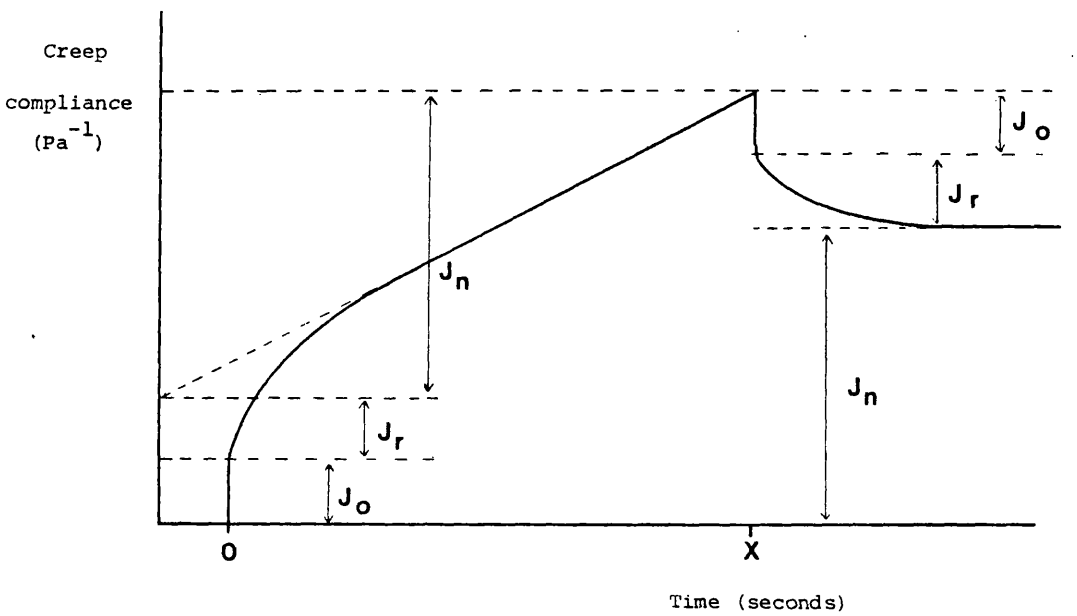

Stress applied t = 0

Stress removed t = x

Creep compliance = $\frac{\text{strain}}{\text{stress}}$

J_o = Instantaneous or elastic compliance

J_R = Retarded compliance

J_N = Viscous or Newtonian compliance

Similarly, on relaxation of the stress, the recovery of this deformation is retarded due to the entanglement of chains.

The viscous compliance (J_N) represents bonds being broken and is the non-recoverable part of the deformation

$$J_N = \frac{t}{\eta_N} \qquad \text{...(equation 3.13)}$$

t = time

η_N = Newtonian viscosity.

Thus the slope of the linear region of the creep curve will represent the reciprocal of the Newtonian viscosity. The total creep compliance at any time t is therefore the sum of these components (equations 3.14 and 3.15).

$$J_T = J_o + J_{R(t)} + J_{N(t)} \qquad \text{...(equation 3.14)}$$

or

$$J_T = J_o + \sum_{1}^{i} J_i \, (1 - e^{\frac{-t}{\tau_i}}) + \frac{t}{\eta_N} \qquad \text{...(equation 3.15)}$$

The computer programme, given values of J_T and t re-constructs the creep curve and solves equation 3.15 to give values of:-

J_o = Instantaneous compliance

η_N = Newtonian viscosity

$J_{1 \text{ to } 3}$ = Retarded compliances

$\eta_{1 \text{ to } 3} = \frac{J_i}{\tau_i}$

$\tau_{1 \text{ to } 3}$ = Retardation times.

The results are shown in Figure 8.4 and Tables 8.4 and 8.5.

3.4 Thermal Properties

Certain substituted cellulose ethers exhibit inverse temperature solubility relationships, leading to the hazing and gelation of solutions as the temperature is raised. The significance of these changes was evaluated with respect to the temperatures attained during coating in a 24" Accela-Cota.

a) Clouding Behaviour

A series of eight aqueous solutions of each polymer, concentration 0.25 - 20% w/v, were placed in a glass spectrophotometer cuvette and the lid sealed with silicone grease. At 65°C the weight loss, due to evaporation of water, was under 2% w/w per 24 hours indicating that adequate sealing occurred. The cuvette was placed in the heated cell carrier of a spectrophotometer (S.P. 1800, Pye Unicam Ltd.) and the absorbance at 450 nm measured against a distilled water reference. The polymer solutions equilibrated to each temperature within 5 minutes, but the clouding phenomenon was time dependent, taking up to 40 minutes to stabilise for large temperature rises. Consequently the absorbances at 450 nm were recorded after the solutions had equilibrated for 1 hour at each temperature and the data presented as plots of absorbance versus temperature (Figures 8.5 and 8.6).

The effect of sodium chloride, a known impurity of HPMC (< 1% w/w), on the clouding behaviour was evaluated for a solution

containing 10% w/v polymer and 0.1% w/v sodium chloride (i.e. 1% w/pw NaCl). Similarly the effect of propylene glycol (Evans Medical Ltd.) , a commonly used plasticizer, was evaluated for a solution containing 5% w/v HPMC and 1% w/v propylene glycol (i.e. 20% w/pw plasticizer). The results are shown in Figure 8.7.

b) Thermal Gelation

Thermal gelation was studied with the aid of a Brookfield Synchro-lectric viscometer (Model RTV, Brookfield Instruments Ltd.). Thermal gelation was defined as the point at which the viscosity of a polymer solution rapidly increased as the temperature was raised. Each solution to be studied was placed in a water-jacketed glass beaker and the lid sealed with a rubber bung to prevent evaporation (Figure 3.2). Two holes were cut in the bung into which plastic inserts were fixed enabling the thermometer and viscometer spindle to pass into the solution and rotate freely, whilst minimizing evaporation of the solvent. To reduce the problem of shear thinning, the viscometer was attached to a helipath stand, allowing fresh samples of polymer solution to be sheared as the spindle was drawn upwards in a helical path. Despite the use of the largest spindle (T-A) the viscosity behaviour prior to gelation could only be quantified for solutions of concentration 10% w/v and above; below this level no deflection of the viscometer scale was observed until gelation had occurred.

The viscosity change at each temperature was found to be time dependent, but stabilized after 1 hour. To measure the viscosity,

Figure 3.2. The arrangement used to determine the thermal gelation temperature of polymer solutions using a Brookfield viscometer.

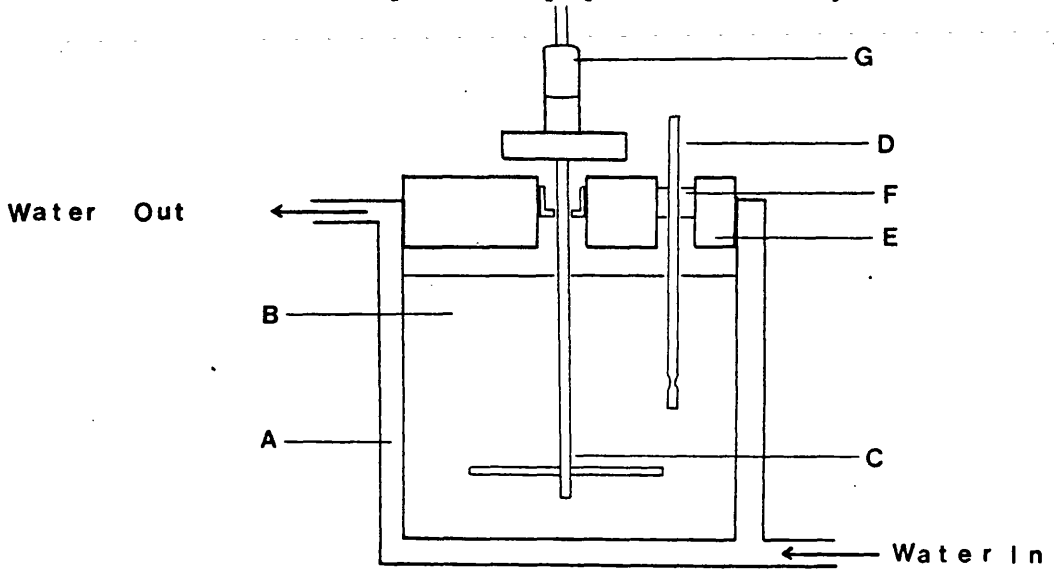

Key: A = water-jacketed glass beaker

B = polymer solution

C = T-A spindle

D = thermometer

E = rubber bung

F = plastic insert

G = chuck of Brookfield viscometer.

rotation of the spindle was started near the bottom of the beaker for 15 seconds before the helipath stand was switched on, thus allowing the spindle to attain the correct speed and any thixotropic behaviour to be noted by a fall in the instrument reading. At the end of each measurement, the spindle was carefully lowered to the bottom of the beaker, the temperature raised a further increment and gelation allowed to take place for 1 hour. The data was presented as plots of log viscosity versus temperature. The results are shown in Figures 8.8 to 8.10 and Table 8 6.

The effects of 1% w/pw sodium chloride and 20% w/pw propylene glycol were also evaluated. The results are shown in Figure 8.11.

c) Temperatures Attained in the 24" Accela-Cota

The temperature in the spray zone was measured whilst coating 8 kg of 10.32 mm diameter normal convex tablets with a formulation containing 5.16% w/v Pharmacoat 606; 0.9% w/v propylene glycol and 1% w/v filler. The following process conditions were used:-

Liquid nozzle	2050
Air Cap	120
Atomizing Air Pressure	2.76×10^5 Pa
Liquid Pressure	6.9×10^4 Pa
Liquid Feed Rate	Variable
Inlet Air Temperature	$90^{\circ}C$
Exhaust Temperature	variable upon liquid Feed

The solution feed rate was adjusted by a needle valve and measured by the decrease in weight of the pressure pot (Platform Balance, Avery Ltd.) as a function of time. Spray rates from 1 to 143 g min^{-1} were used and the exhaust temperature allowed to reach equilibrium at each rate prior to measurement of the temperature in the spray. The temperatures in the spray, at various distances from the nozzle, were recorded using a Comark 3001 digital thermometer fitted with a KM 1510/MPK probe (Comark Electronics Ltd.). This was calibrated against a mercury in glass thermometer graduated at 0.1^{o}C intervals and carrying NPL certificates (Figure 3.3) and all recorded temperatures corrected accordingly. The results are shown in Figures 8.12 and 8.13 and Table 8.7.

Figure 3.3 Calibration plot for the temperature indicated by a digital thermocouple against the temperature recorded by a mercury in glass thermometer .

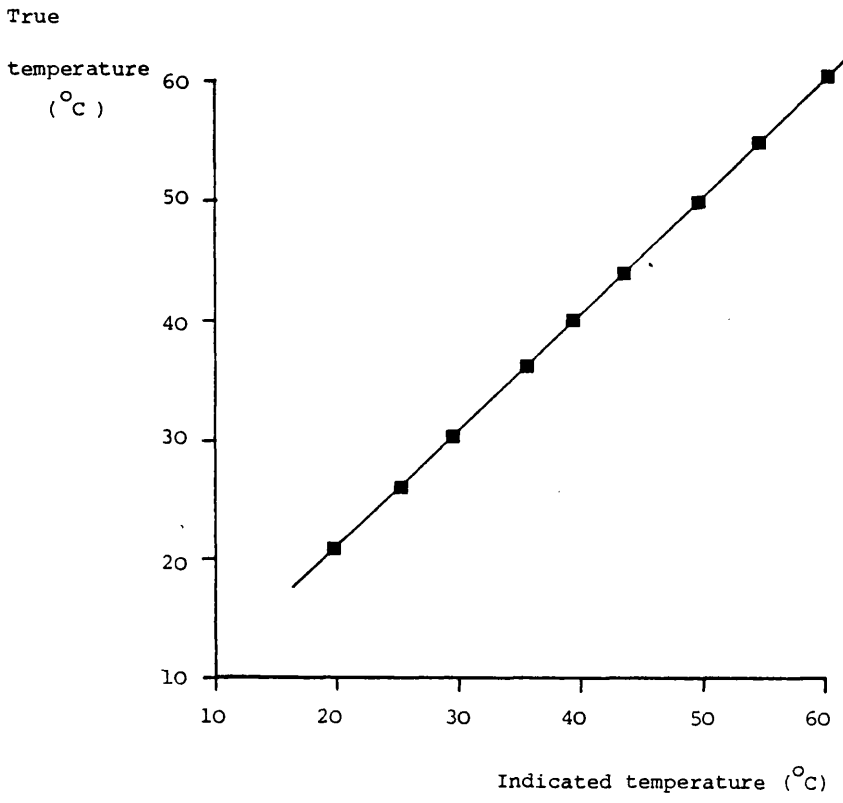

Slope	= 0.968
S.D. slope	= 0.003
Rel S.D.	= 0.29%
Intercept	= 1.906
S.D. Intercept	= 0.118%
Correlation coefficient	= 0.999

4. PREPARATION OF FILM COATINGS

4.1 Introduction

To allow the accurate determination of the properties of film coatings, a large plane test area was needed on which measurements could be carried out. However, flat-faced compacts whose diameter exceeded 10 to 15 mm were very difficult to coat in commercial equipment unless special conditions were employed, which effectively limited the formulation and processing variables which could be studied. Techniques involving the addition of a few large compacts to a charge of normal tablets could produce misleading results, since their tumbling characteristics were often totally different, leading to changes in the degree and frequency with which the test surfaces were exposed to the sprayed coating solution. To overcome such problems many workers have employed cast or sprayed free films, although it has been shown that their properties often do not correspond to those applied to tablets in industrial equipment[41,98,102,106]. One explanation for this may be in the fact that the coating conditions used in the production of coated tablets were inadequately mimiced, in particular the frequency with which a core was presented to the spray and its dwell time within the spray area. Consequently techniques were developed to enable the production of films by casting (section 4.2) and by use of a realistic model spray coating system (section 4.3).

4.2 Cast Films

A free film preparation technique was developed for use with both simple polymer solutions and suspensions enabling a single

technique to be employed for all formulations.

Casting onto a mercury substrate was unsatisfactory due to problems of poor spreading of the coating solution and disturbance of the substrate surface by vibration and draughts. The latter could not be readily overcome, as the cumulative toxicity of mercury vapour demanded that it be used in a fume cupboard. Cast films exhibited a high level of adhesion to siliconized paper (Phase Separating Paper, Whatman Ltd.), PTFE sheet (F.R. Warren & Co. Ltd.) and aluminium foil (Bacofoil); in the latter case adhesion was great enough to tear the foil when removal of the film was attempted.

Glass plates, 101.6 mm square (4") provided a good substrate although thorough cleaning was required to avoid adhesion of the resulting films. Chromic acid appeared to be a better cleaning agent than RBS 25 (Chemical Concentrates (R.B.S.) Ltd.), yielding films with virtually no adhesion to the substrate. Contact angle measurements tended to confirm that HPMC bound to glass cleaned with RBS 25 more than to that cleaned with chromic acid (Table 4.1). Using a glass micrometer syringe ('Agla', Burroughs Wellcome and Co. Ltd.) 25 µl of a 5% w/v solution of Pharmacoat 606 were placed onto a cleaned glass slide placed between the lamp and objective lens of a projector (Tutor 500, Rank Aldis). The contact angle of the projected drop was measured from a screen using a protractor. The contact angles of four replicate drops were measured, the glass slide rinsed with

Table 4.1 The mean contact angles (4 replicates) for 25 µl of a 5% w/v solution of Pharmacoat 606 on glass cleaned with chromic acid or RBS 25.

Glass cleaned with chromic acid				Glass cleaned with RBS 25			
Initial contact angle		Contact angle after polymer washed off		Initial contact angle		Contact angle after polymer washed off	
Mean (S.D.) (degrees)	CV (%)	Mean (S.D.) (degrees)	CV %	Mean (S.D.) (degrees)	CV (%)	Mean (S.D.) (degrees)	CV (%)
33.55 (1.24)	3.70	33.19 (1.10)	3.31	32.82 (0.67)	2.04	38.23 (1.04)	2.72
t_{calc} = 0.43				t_{calc} = 8.75			
t_{tab} (P = 0.05) = 2.45							

S.D. = standard deviation

C.V. = coefficient of variation.

distilled water, dried at 100°C and the contact angles re-measured. Table 4.1 demonstrates that the contact angle was unchanged when the solution was washed from the glass cleaned with chromic acid whereas the second value of the contact angle rose by 5° on glass cleaned with RBS 25.

The spread of polymer solution on the glass was controlled by glass rings (66 mm i.d. 14 mm high) whose lower edge had been ground flat and lightly greased (Silicone Stopcock Grease, Dow Corning Ltd.). To eliminate the meniscus of the coating solution at the edge of the glass ring and thus prevent film thickness variations, a very light coating of silicone grease was applied to their inside edges.

The glass plates could not be adequately levelled on a solid surface, leading to 10 to 30 μm variations in film thickness across the width of the substrate. This was overcome by placing four glass plates of equal weight in a perspex trough floating in an oil bath (Shell Voluta 71 Oil) (Figure 4.1). The high viscosity of the oil ensured that minor movements of the bench were damped, whilst allowing the inner trough and hence glass plates to remain perfectly horizontal. The high boiling point of the oil ensured that little or no vaporization could occur to modify the evaporation of the aqueous solvent. The film thickness was determined by the volume of solution poured onto the glass plates, although a minimum of approximately 2 ml was necessary to ensure complete coverage of the substrate area. The

Figure 4.1 Diagrammatic representation of the film casting arrangement

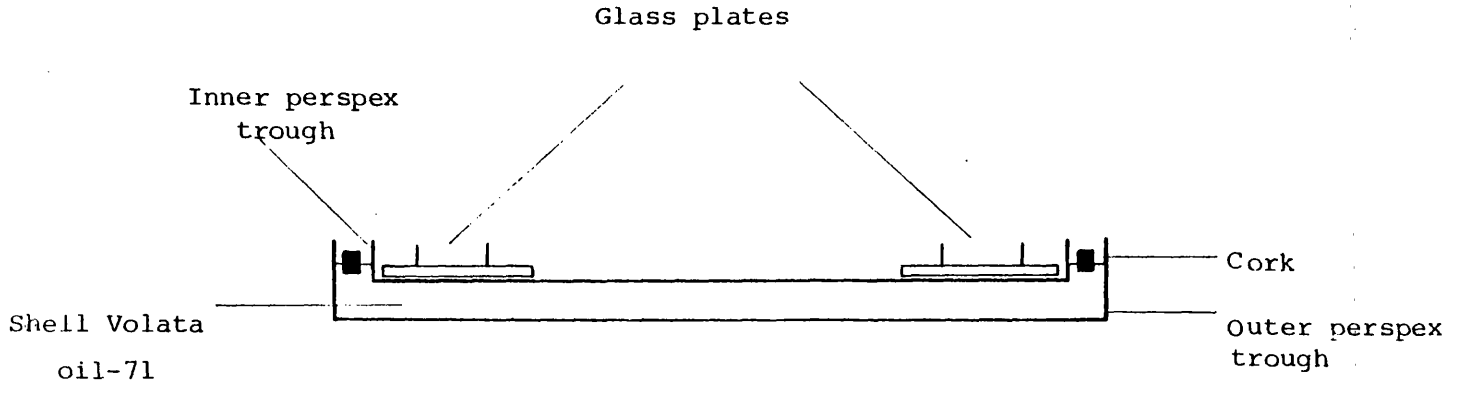

concentration of polymer in the solution did not affect the ability to produce cast films, but low viscosity solutions did allow any filler present to sediment during drying.

Formulations containing solids could not be dried at temperatures in excess of 35 to 40°C since uneven patches of filler and pigment developed. Two possible explanations for this behaviour were:-

a) At higher temperatures the increased kinetic energy of the pigment particles allowed them to overcome the repulsive forces between them and so interact and aggregate.[251]

b) At higher temperatures the lower viscosity of the suspension no longer kept the filler particles homogenously suspended.

The possibility that coacervation or separation of a solute rich layer led to sedimentation of filler in a solvent rich layer was eliminated since the results in Section 8 demonstrate that the properties of aqueous solutions of Pharmacoat 606 did not alter until much higher temperatures were achieved.

Thus films were cast on to glass plates and allowed to dry for 24 hours at 30°C in an oven (Townson & Mercer Ltd.) away from draughts and vibration. The resulting films, of uniform thickness ($\pm$ 1 µm in the range 17 to 100 µm), were lifted off the substrate and stored between cartridge paper in a desiccator until use.

4.3 The Development of a Model System for the Production of Film Coatings

Of the commercial instruments used for aqueous film coating, the Accela-Cota (Manesty Machines Ltd.) is probably the most versatile and widely used. Therefore a model coating system was designed around the coating parameters used successfully for aqueous film coating in a 24" Accela-Cota, although sufficient flexibility was built in to allow data obtained from other commercial coating equipment to be substituted if required. In addition to allowing relatively large areas of coating to be produced under more realistic conditions, this model should also enable process and formulation variables to be studied in isolation from production equipment and without the need to commit large quantities of either active or non-active materials.

4.3.1 Development of the Experimental Technique

4.3.1.1 Substrate

To enable the properties of cast and sprayed films to be compared, glass substrates cleaned with chromic acid (Section 3.1a) were used. 25.4 mm squares of glass were cut from microscope slides to provide a substrate of similar size to the compacts described below.

To study the effects of the substrate on the properties of film coatings, several existing formulations were developed for the production of a 25.4 mm diameter compact with similar surface appearance and characteristics to tablets of conventional size.

Ordinary tablets have been shown to have porosities in the range 10 to 20% and an arithmetic mean surface roughness of 0.5 to 2.0 μm.[192,213] Table 4.2 gives details of the formulations and preparation techniques used. The formulations were compressed on either a single stroke Manesty F3 machine fitted with a 22.23 mm diameter die and flat-faced punches, a Manesty D3RY rotary machine fitted with eight 25.4 mm diameter dies and flat-bevelled-edge punches, or a hydraulic press (25 ton Ring Press, Research and Industrial Instruments Co.) using the 22.23 mm diameter die and punches. The maximum compaction pressures available, with this tooling, were 102 MPa, 197 MPa and 200 MPa respectively (representing loads of 4,064 kg, 10,160 kg and 8,000 kg).

The properties of each powder were characterized, using a Hosokawa Powder tester (Type PT-D, Hosokawa Micromeritics), to give the flowability and floodability indices[252,253] shown in Table 4.4.

The compacts were characterized by their porosity, surface roughness and diametrical breaking strength. The porosity of the compacts was determined using equation 4.1:-

$$\text{percentage porosity} = 100 \left[1 - \frac{V_T}{V_B} \right] \quad \text{...(equation 4.1)}$$

V_T = true volume

V_B = bulk volume

The true volume (V_T) was calculated from the weight (w) and particle density (ρ) of each material present in the compact according to

Table 4.2 Formulations and preparation techniques used in the production of a 25.4 mm diameter compact

Ingredient Number	Ingredient Concentration % w/w	Formulation Number I	IA	II	IIA	II_B	III	III_A	IV	V	VI
1	Dibasic calcium phosphate	20.0	20.0							20.0	88.3
2	Lactose 80 mesh	61.5	59.0						62.5	61.5	
3	Maize starch	15.4	15.4						31.3	17.9	
4	Polyvinyl pyrrolidone	2.5	5.0								
5	Magnesium stearate	0.6	0.6				0.5	1.0	1.0	0.6	0.3
6	Asagran			75.0	75.0	72.0					
7	Avicel PH101			18.6	18.6	18.0	49.5	49.25			
8	Sta Rx 1500			6.4	6.3	6.2					
9	Aerosil OT				0.1		0.5	0.5			0.4
10	Talc B.P.					3.8					
11	Lactose 70/100 mesh						49.5	49.25			
12	Acacia B.P.								5.2		
13	Ethyl cellulose N 100										5.6
14	Guar Gum										3.0
15	Solka Floc										2.4
Preparation Technique		A	B	C	C	C	D	D	E	F	G

Key to Table 4.2: Preparation Techniques

A) Pass 1, 2 and 2/3 of 3 through a 40 mesh screen and mix for 5 minutes. Granulate with a solution of 4(1.25% w/v in IMS:water 1:1). Press mass through a 12 mesh screen, dry at 50°C to under 3% w/w moisture and pass through a 16 mesh screen. Add 5 and 1/3 of 3 through a 60 mesh screen and mix for 5 minutes.

B) As A but granulate with 2.5% w/v solution of 4.

C) Mix ingredients for 5 minutes

D) Mix 5, 7, 9 and 11 for 5 minutes, pass through a 30 mesh screen and remix for 5 minutes

E) Pass 2 and 3 through a 40 mesh screen and mix for 5 minutes. Granulate with a solution of 12 (25% w/v in IMS:water 1:1). Press through a 12 mesh screen, dry at 50°C to under 3% w/w moisture and pass through a 16 mesh screen. Add 5 through a 60 mesh screen and mix for 5 minutes.

F) Pass 1, 2 and 60% of 3 through a 40 mesh screen and mix for 5 minutes. Granulate with a solution of 15% of 3 (10% w/v mucilage in water). Press mass through a 12 mesh screen, dry at 50°C to under 3% w/w moisture and pass through a 16 mesh screen. Add 5 and 25% of 3 through a 60 mesh screen and mix for 5 minutes.

G) Pass 1 and 70% of 13 through a 40 mesh screen and mix for 5 minutes. Granulate with a solution of 30% of 13 (6% w/v in IMS). Pass through a 12 mesh screen, dry at 50°C to under 3% w/w moisture and pass through a 12 mesh screen. Add 5, 9, 14 and 15 through a 60 mesh screen and mix for 5 minutes.

The equipment used varied with the batch size and included:-

i Hobart Mixer Model N-50G (Hobart Corporation)

ii Bear Varimixer (Wodschow & Co.)

iii Glen Mixer Model 74-57 (American Machine and Foundry Co., Bakery Division)

iv Sieve Shaker Model 1557 (Russell Constructions Ltd.)

v Moisture Balance Model 26680-8 (Cenco Instrumentation.)

equation 4.2.

$$V_T = \frac{w_1}{\rho_1} + \frac{w_2}{\rho_2} + \ldots\ldots \frac{w_i}{\rho_i} \quad \ldots(\text{equation 4.2})$$

The values of particle density, determined by helium pycnometry (Model 1302, Micromeritics Instrument Co.), are listed in Table 4.3.

The bulk volume of the compacts was obtained by dimensional analysis:- For cylindrical compacts

$$V_B = \Pi \left(\frac{D}{2}\right)^2 L \quad \ldots(\text{equation 4.3})$$

V_B = bulk volume

D = compact diameter

L = compact thickness

For flat bevelled edge compacts

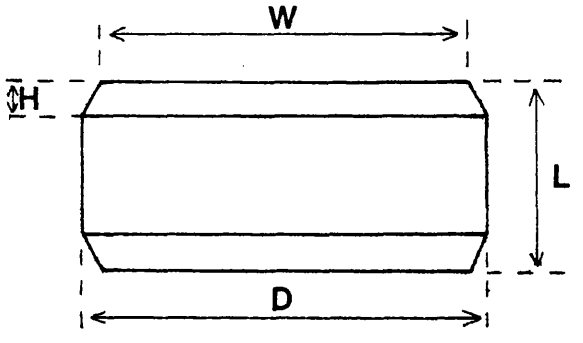

The top and bottom bevelled edge portions each have the volume of the frustum of a cone with parallel ends (V_f) (equation 4.4)

$$V_f = \frac{1}{3} H \left[B + b + (B.b)^{\frac{1}{2}}\right] \quad \ldots(\text{equation 4.4})$$

where B = area of base

b = area of top

H = perpendicular height

Table 4.3 Particle density of compact ingredients as determined by helium pycnometry.

Ingredient Number	Identification	Particle density g cm^{-3}
1	Dibasic Calcium Phosphate	2.31
2	Lactose 80 mesh	1.51
3	Maize Starch	1.47
4	Polyvinyl Pyrrolidone	1.06
5	Magnesium Stearate	1.07
6	Asagran	1.40
7	Avicel PH 101	1.53
8	Sta Rx 1500	1.49
9	Aerosil OT	3.60
10	Talc B.P. (Purified)	2.98
11	Lactose 70/100 mesh	1.52
12	Acacia B.P.	1.54
13	Ethyl Cellulose N100	1.27
14	Guar Gum	1.48
15	Solka Floc	1.55

Thus:

$$V_f = \frac{1}{3} H \left[\Pi \left(\frac{D}{2}\right)^2 + \Pi \left(\frac{W}{2}\right)^2 + \left(\Pi^2 \left(\frac{D}{2}\right)^2 \left(\frac{W}{2}\right)^2\right)^{\frac{1}{2}} \right]$$

...(equation 4.5)

The volume of the centre cylindrical portion V_c is given by equation 4.6 :

$$V_c = \Pi \left(\frac{D}{2}\right)^2 (L-2H) \quad \text{...(equation 4.6)}$$

D = diameter of compact

L = thickness of compact

H = depth of bevel

Thus

$$V_B = V_c + 2V_f \quad \text{...(equation 4.7)}$$

The values of D and T were measured with a micrometer (L.S. Starrett and Co. Ltd.) and those of W and H obtained from punch drawings supplied by the tooling manufacturer.

The surface roughness parameter, R_a was measured using a Talysurf 3 surface measuring instrument, three replicate profiles on each of five compacts being recorded (see also section 7).

The diametrical breaking strength was recorded using a Schleuniger Tablet tester (model 2E/205) and for compacts of such large diameter, a hardness value below 20 kp was regarded as unsatisfactory.

The 'feel' and general appearance of the compacts, with reference to tablets of conventional size were also recorded.

The data are presented in Table 4.4. Despite all the formulations having 'normal' to 'good' powder flow properties, as classified by Carr[252,253], marked differences were observed in the ability to flow evenly into a die. For example formulation II

Table 4.4 The properties of the compact formulations developed.

Formulation number	Compression instrument	Powder Properties			Compact Properties				Comments
		Flowability Index	Floodability Index	Die Feed	Diametrical breaking strength kp	Porosity %	Surface roughness Ra µm (S.D.)	Surface Appearance	
I	F3	76.5	63.0	Good	5-7	26.4	stylus ploughs surface	Soft/ friable	
	Hydraulic press				19-20	12.9	1.1 (0.2)	Good	
I_A	F3	74.0	67.0	Good	10-12	24.0	2.8 (0.7)	Rough	
	Hydraulic press				> 20	12.5	1.1 (0.2)	Very Good	
	D3 RY			Good	> 20	13.4	2.1 (0.4)	Good	Useful with model system
II	F3	74.5	71.5	Very poor	> 20	12.4	2.1 (0.3)	Atypical	
II_A	F3	72.0	71.5	Good	> 20	13.2	2.4 (0.3)	Atypical	Useful formulation, but atypical mottled surface made its use limited
	Hydraulic press				> 20	8.2	1.3 (0.2)	Atypical	
II_B	F3	67.0	69.0	Good	12-14	15.7	3.2 (0.7)	Rough	
	Hydraulic press				> 20	15.2	1.5 (0.2)	Rough	
III	F3	72.3	74.0	Good	14-16	25.0	2.6 (0.5)	Friable	
	Hydraulic press				>20	9.1	0.9 (0.1)	Good	Tended to stick in die and laminate
III_A	F3	69.0	69.5	Very Good	9-11	25.4	3.0 (0.6)	Friable	
	Hydraulic press				> 20	9.0	0.9 (0.1)	Good	
	D3 RY			Good	> 20	18.1	1.9 (0.4)	Good	Useful with model system
IV	F3			Poor	< 1	-	-	soft/ friable	
V	F3			Good	4-5	25.6	3.1 (0.8)	Soft/ friable	
	D3 RY			Adequate	11-12	21.7	2.7 (1.0)	Friable	
VI	F3			Good	8-10	39.2	2.3 (0.4)	Friable	
	D3 RY			Good	> 20	23.7	1.5 (0.4)	Good	

had a high flowability index (74.5), yet failed to flow into the die on the F3 tablet machine, whilst formulation II_A exhibited a lower index yet produced a very good die feed.

The inability to produce satisfactory compacts on the single stroke machine, with the exception of formulation II_A, was attributed to the low compaction pressure (maximum 102 MPa) when fitted with 22.23 mm diameter punches. The excellent compaction and consolidation properties of aspirin (Asagran) and microcrystalline cellulose (Avicel PH101) contained in formulation II_A enabled good compacts to be obtained despite the low compression force used.

Formulations which exhibited good flow properties but did not compact well on the F3 machine, were evaluated at a pressure of 200 MPa using the hydraulic press, prior to larger scale trials on the rotary tablet machine. Good compacts were produced with formulations I_A, II_A III_A and VI. The high porosity of VI, combined with the tedious granulation technique, resulted in this formulation being abandoned. Despite having a low porosity and surface roughness and high hardness, II_A was rejected since it possessed an atypical surface appearance which was dull and mottled.

Both I_A and III_A were selected for use with the model system since they exhibited good surface appearance and their porosity and roughness values lay within the range found for

tablets of conventional size. A sieve analysis was carried out to characterize the particle size distributions of the powder blends used to produce these compacts (Figure 4.2).

4.3.1.2 The Isolation of Important Coating Parameters

As described earlier, the Accela-Cota is possibly the most versatile and widely used commercial instrument for aqueous film coating. Figure 4.3 is a diagrammatic representation of the 24" model, which having a working capacity of 18 kg is ideally suited for development studies and small batch production. The periphery of the coating pan is peforated allowing an even distribution of hot drying air with minimal disturbance of the spray pattern. The exhaust plenum, being located outside the pan, enables drying air to be drawn through the tablet bed thereby minimizing dead spaces and maintaining a rapid drying rate throughout the bed. In addition dust produced by abrasion of the tablets is rapidly removed.

As the pan rotates tablets are carried upwards starting a tumbling action, which can be modified by altering the speed of rotation. To promote tablet mixing the two sides of the pan have different angles, although the addition of baffles is usually necessary to achieve a satisfactory action.

The coating solution is applied to the tablets as an atomized spray. A pneumatic spray system is most suitable for aqueous coating and directing the spray at the upper third of the tablet

Figure 4.2. Particle size analysis of formulations I_A and III_A which were successfully used for 25.4 mm diameter compacts.

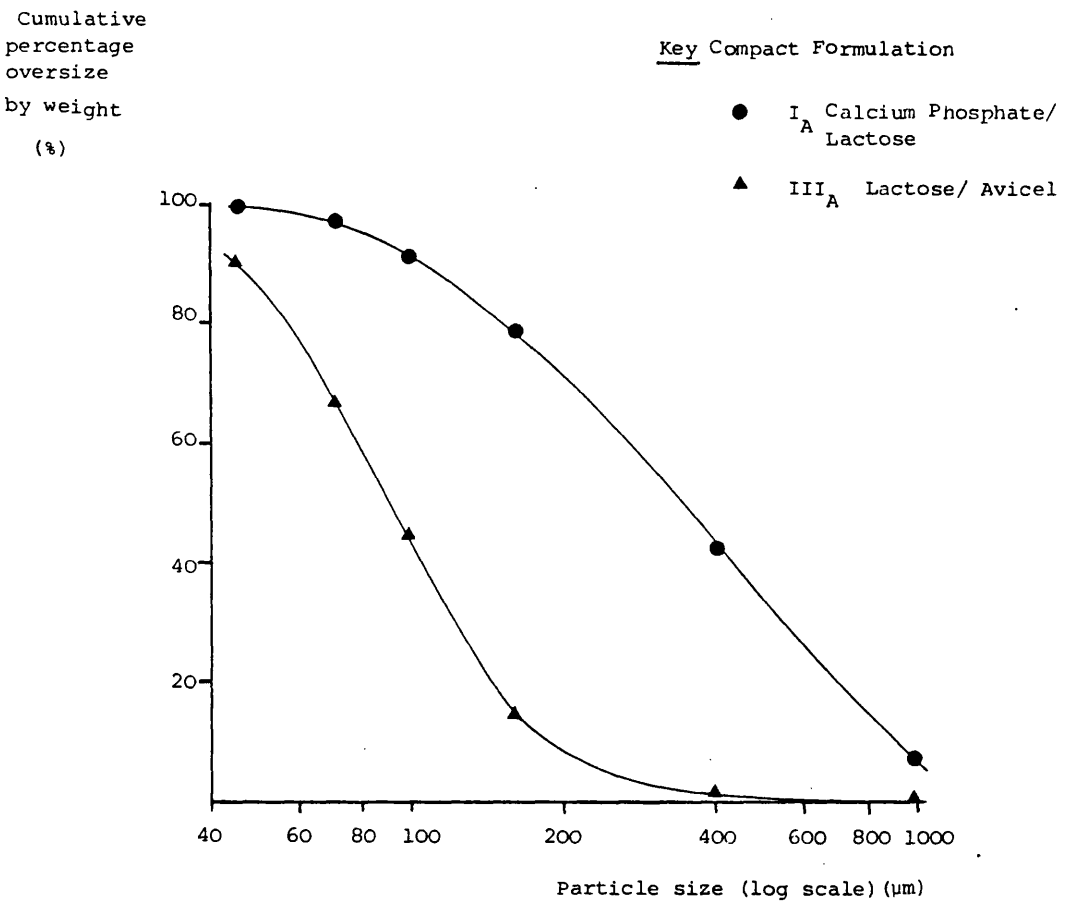

Figure 4.3 Diagrammatic representation of a 24" Accela-Cota

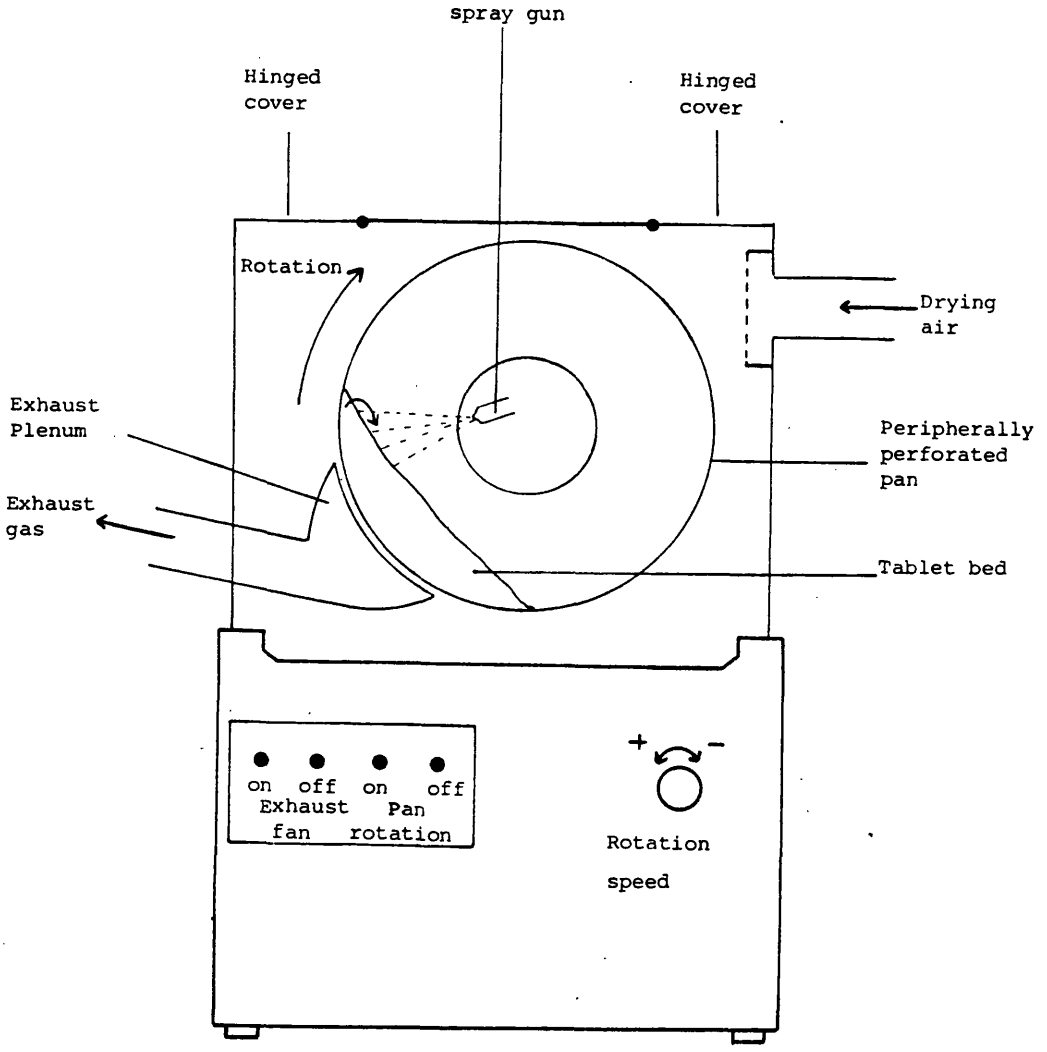

bed, maximises the drying time before the tablets are re-submerged in the bed.

The factors which affect the production of film coatings in a 24" Accela-Cota include the volume and temperature of drying air, the exhaust capacity and temperature, the characteristics of the spray system, the pan speed and tumbling action and the spray time parameters which are defined below. The values of these parameters were therefore recorded for a 24" Accela-Cota which was routinely used for the aqueous film coating of tablets.

a) Drying Air Volume and Temperature

Using a velometer (Tube Pattern Type 3002, Associated Electrical Industries) the air velocity in the articulated input conduit (i.d. 101.6 mm) was found to be 487.7 m min^{-1} at 90°C (Metal Rototherm Temperature Gauge Model 35, British Rototherm Co. Ltd.) giving an input air volume of 3.95 m^3 min^{-1}.

b) Exhaust Capacity and Temperature

The exhaust capacity was stated by the manufacturer[76] as 10.61 m^3 min^{-1}, but measurement with the velometer gave an air velocity of 1252.7 m min^{-1}, corresponding to an exhaust volume of 10.16 m^3 min^{-1} (cross-sectional area of exhaust 8.11×10^{-3} m^2). The temperature in the exhaust plenum (Metal Rototherm Temperature Gauge Model 35) was maintained between 40 and 45°C during aqueous film coating. Previous work[254] had shown this to closely reflect the temperature of the tablet bed.

c) Spraying System

Initially a pneumatic spray gun (¼ JCO, Spraying Systems Co.) fitted with a 2850 fluid nozzle and 120 air cap was used in the Accela-Cota, at a gun to bed distance of 200 mm. Liquid was fed at a rate of 20 to 25 g min^{-1} from a pressure pot at 6.9×10^4 Pa and compressed air at 2.76×10^5 Pa was used for atomization. Comparison of this system with the Walther Pilot spray gun (WAXV, Manesty Machines Ltd.) indicated that the latter could be used at higher liquid feed rates (30 to 35 g min^{-1}) despite being situated 50 mm closer to the tablet bed. Observation of the spray pattern produced on a flat surface by both systems indicated that the Walther gun produced a fairly uniform flat or oval spray, whilst the 2850/120 nozzle combination gave a round spray with a very dense centre region, which tended to overwet a small area of the tablet bed unless a low liquid feed rate was used. Consequently the spray pattern and deposition characteristics of several nozzle combinations were evaluated by measuring the change in deposition across the spray area of a marker dye, tartrazine, added to the coating solution.

A thin layer of high density polyurethane foam was stuck to a glass plate, 100 mm square, with double-sided sellotape (Dickinson Robinson Group Ltd.). This target was placed 200 mm from the spray nozzle and intermittently sprayed with a stock coating solution containing 5% w/v Pharmacoat 606 and 0.3% w/v tartrazine (B.D.H. Ltd.) until a reasonable thickness of coating had been applied. The foam and applied film were cut into

10 mm squares or vertical strips 5 mm or 10 mm wide and 100 mm long (Figure 4.4) and the amount of tartrazine deposited on each portion determined spectroscopically. Each section of foam and the associated coating was placed in a separate test-tube containing 5 ml of distilled water, the tubes mechanically shaken for 30 minutes and the absorbance of the supernatant measured after further dilution where necessary.

The wavelength of maximum absorption for tartrazine was found to be 425 nm (S.P. 500, Pye Unicam). Two separately prepared solutions containing 5% w/v Pharmacoat 606 and 0.3% w/v tartrazine were serially diluted with water to maintain a constant ratio of polymer to dye. The absorbance, measured at 425 nm in 10 mm glass cuvettes, was recorded for these dilutions over the concentration range 4.8×10^{-4} to 2.4×10^{-3} % w/v tartrazine. A Beer-Lambert plot of absorbance versus tartrazine concentration was linear; the data from both solutions being coincident were subjected to a single least squares regression analysis (Table 4.5). The plot passed through the origin within $\pm$ two standard deviations and the slope gave a percentage extinction coefficient of 338.70 $\%^{-1}\ cm^{-1}$.

The tartrazine concentration of the stock coating solution was determined by measuring the absorbance of a 1 in 250 dilution since the loss of dye during the preparation of large volumes of solution (section 3.2c) would have produced deviations from the nominal content. Three replicate determinations gave

Figure 4.4 Diagrammatic representation of the target used for determining the spray deposition characteristics of spray nozzle combinations

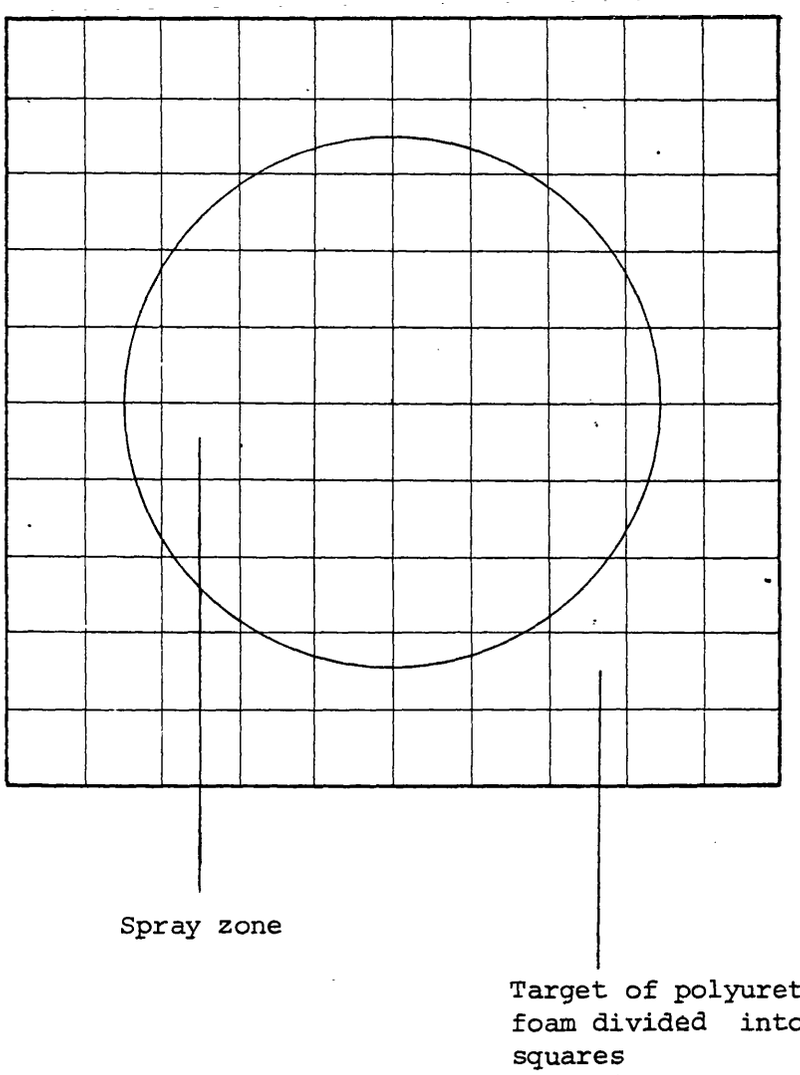

Table 4.5 Least squares regression data for the absorbance at 425 nm versus tartrazine concentration (0.00048 to 0.00240% w/v) in the presence of Pharmacoat 606 (0.008 to 0.040% w/v).

Slope	$338.70\%^{-1}\ cm^{-1}$
S.D. slope	4.97
Rel. S.D. Slope	1.47%
Intercept	-0.010
S.D. Intercept	0.007
Correlation coefficient	0.9997

S.D. = Standard Deviation

Rel. S.D. = Relative Standard Deviation

an absorbance of 0.387 (S.D. 5.0×10^{-4}), leading to a calculated tartrazine concentration of:-

$$\% \text{ w/v tartrazine} = \frac{0.387}{338.70} \cdot \frac{250}{1}$$

$$= 0.286 \% \text{ w/v}$$

Thus tartrazine comprised $\frac{0.286}{5.286} \cdot 100 = 5.405\%$ w/w of the solids deposited on the substrate.

The weight of solids deposited on each section of polyurethane foam could thus be calculated from the absorbance of the supernatant, using equation 4.8 :

$$\text{Tartrazine concentration (\% w/v)} = \frac{A_{425}}{E^{1\%}_{1cm}} \cdot \text{Dilution Factor (DF)}$$

Thus

$$\text{Solids deposited (mg)} = \frac{A_{425}}{338.7} \cdot DF \cdot \frac{5}{100} \cdot \frac{100}{5.405} \cdot 1000$$

$$\text{Solids (mg)} = A_{425} \cdot DF \cdot 2.731 \qquad \text{...(equation 4.8).}$$

To ensure that the foam did not affect the detected tartrazine concentration, 5 ml of a 1 in 250 dilution of the stock coating solution were added to 500 mm^2 pieces of foam, shaken for 30 minutes and the absorbance of the supernatent measured. Ten replicates gave a mean absorbance of 0.388 (S.D. 8.8×10^{-4}) which was not significantly different from that in the absence of the foam ($t_{calc} = 1.84$, t_{tab} (P=0.05) = 2.20).

Table 4.6 shows the weight of solids deposited on each 10 mm square of the foam substrate by the 2850/120 nozzle combination. The majority of the coating was deposited in a circle approximately 70 mm in diameter, although some overspray was evident and there was a sharp variation in the amount of material deposited in each region within the main spray cone. Figure 4.5 shows the data for 10 mm wide strips and the summation vertically of the 10 mm squares from Table 4.6, plotted as the percentage of total material deposited in each strip versus the distance from the centre of the spray pattern. The two sets of data shown in this plot demonstrate the reproducibility of the measurements and confirm the sharp

Table 4.6 The weight of coating (mg) deposited on each 10 mm square of substrate, placed 200 mm from the 2850/120 nozzle combination, with an atomizing air pressure of 0.28 MPa.

0.02	0.03	0.03	0.05	0.05	0.04	0.04	0.03	0.02	0.02
0.02	0.04	0.05	0.07	0.11	0.12	0.10	0.06	0.04	0.03
0.02	0.05	0.09	0.16	0.28	0.37	0.26	0.13	0.06	0.03
0.04	0.06	0.15	0.38	0.82	1.18	0.79	0.26	0.11	0.03
0.04	0.07	0.20	0.58	1.61	2.05	1.62	0.41	0.14	0.05
0.04	0.08	0.23	0.56	1.55	2.90	1.56	0.41	0.15	0.06
0.05	0.07	0.15	0.34	0.64	1.44	0.65	0.26	0.13	0.06
0.04	0.06	0.09	0.16	0.23	0.30	0.25	0.14	0.08	0.05
0.04	0.05	0.07	0.09	0.11	0.11	0.14	0.08	0.06	0.05
0.03	0.04	0.05	0.05	0.05	0.06	0.06	0.04	0.03	0.02

Figure 4.5 Percentage of total solids deposited in each 10 mm wide vertical strip versus distance from the centre of the spray pattern produced by the 2850/120 nozzle combination at a distance of 200 mm with an atomizing air pressure of 0.28 MPa.

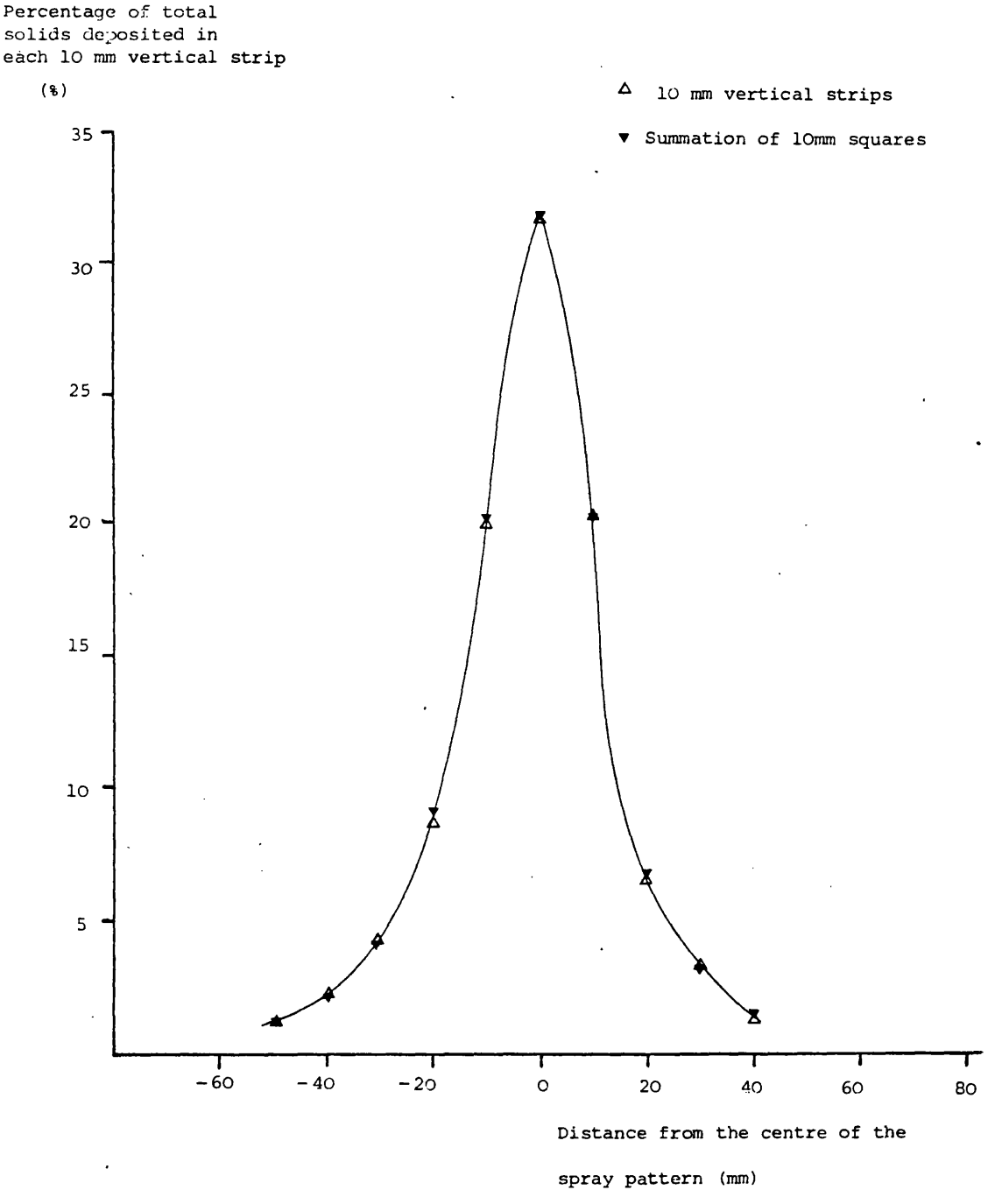

increase in the amount of material deposited towards the centre of the spray pattern. If used to coat 25.4 mm diameter substrates on a model system, the resulting thickness variation across the films would create problems in the evaluation of film properties. Consequently other nozzle combinations were evaluated for their ability to produce an even spray coverage.

Fluid nozzle-air cap combinations of 2850/70, 2050/70, 1650/120 and 1650/70 were eliminated on visual comparison of the spray coverage since they were inferior to the 2850/120 combination. Neither increasing the atomizing air pressure to 0.41 MPa or decreasing it to 0.14 MPa had a beneficial effect with any of these combinations. The combination of a 2050 liquid nozzle and 120 air cap gave a more even spray pattern and was evaluated in detail using the technique described earlier.

Table 4.7 shows that coating material sprayed by the 2050/120 nozzle combination was deposited in a circular pattern of similar diameter to that produced with the 2850/120 combination, although the variation in the quantity deposited in each region was much lower. Figure 4.6 shows the data for 10 mm and 5 mm wide strips, plotted as the percentage of the total material deposited in each strip versus the distance from the centre of the spray pattern. As found with the 2850/120 nozzle combination, the data presented in Table 4.7 for the 2050/120 combination, when summed vertically lay very close to that for the 10 mm wide strips, although for clarity these points have been ommitted from Figure 4.6. The reproducibility was further demonstrated

Table 4.7 The weight of coating deposited on each 10 mm square of substrate, placed 200 mm from the 2050/120 nozzle combination with an atomizing air pressure of 0.28 MPa.

0.05	0.06	0.92	0.11	0.12	0.11	0.09	0.07	0.05	0.04
0.09	0.13	0.19	0.26	0.32	0.27	0.20	0.12	0.07	0.04
0.13	0.26	0.46	0.64	0.68	0.58	0.45	0.24	0.10	0.05
0.27	0.58	1.02	1.26	1.21	1.04	0.85	0.41	0.14	0.06
0.34	0.84	1.25	1.28	1.23	1.26	1.32	0.61	0.20	0.08
0.32	0.82	1.22	1.18	1.20	1.22	1.10	0.61	0.18	0.06
0.28	0.56	1.06	1.26	1.16	1.06	0.87	0.55	0.12	0.05
0.16	0.27	0.47	0.64	0.71	0.57	0.52	0.18	0.08	0.04
0.10	0.14	0.20	0.27	0.32	0.27	0.22	0.11	0.07	0.04
0.05	0.08	0.09	0.11	0.12	0.11	0.09	0.06	0.05	0.03

Figure 4.6 Percentage of total solids deposited on each 5 or 10 mm wide vertical strip versus distance from the centre of the spray pattern produced by the 2050/120 spray nozzle combination at a distance of 200 mm with an atomizing air pressure of 0.28 MPa.

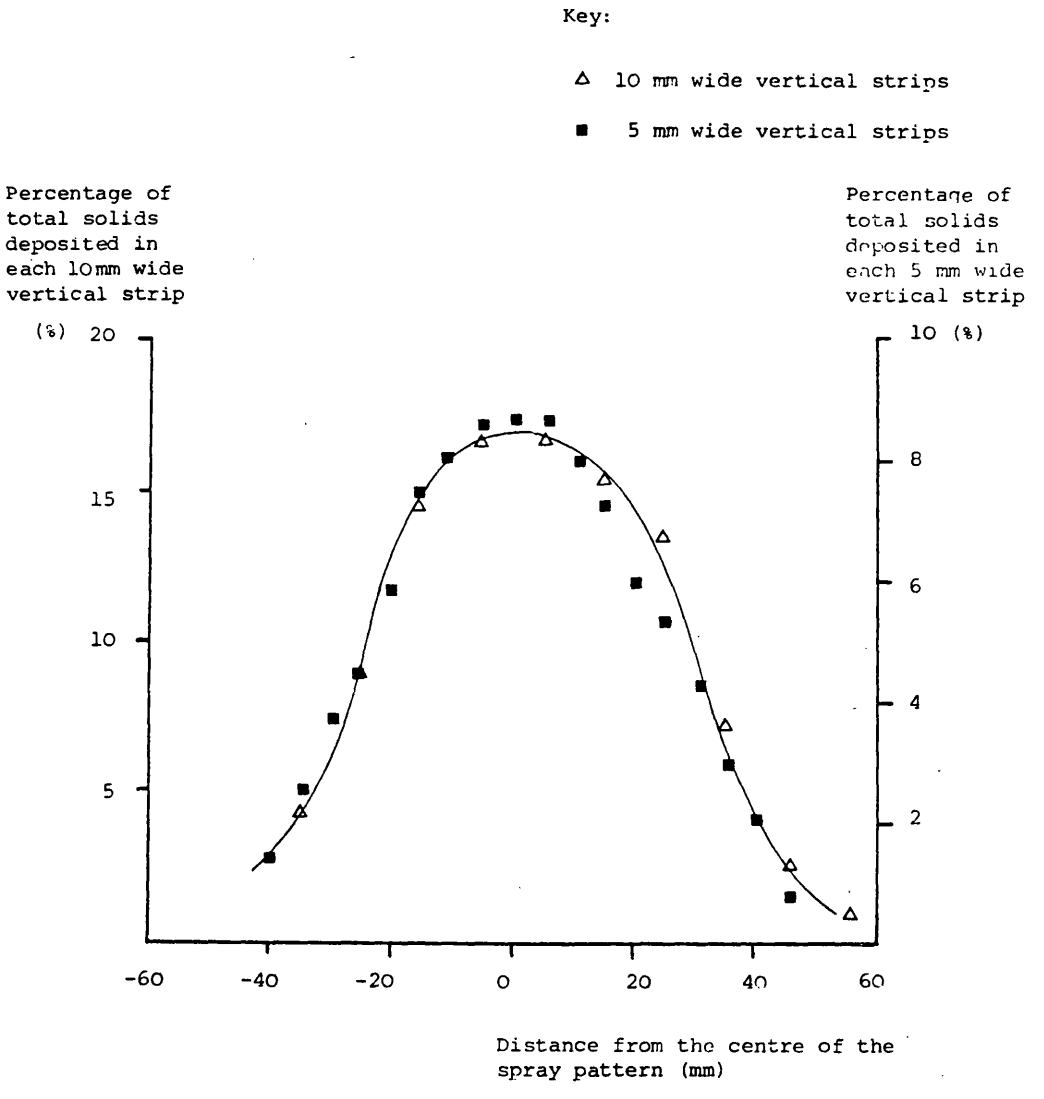

by the data from 5 mm wide vertical strips showing a very similar profile to that for the 10 mm wide strips (Figure 4.6). It can be seen therefore that the spray pattern of the 2050/120 nozzle combination was more even than that of the 2850/120 combination, with less than 7% variation in the amount deposited over the centre 25 mm.

To enable the flat spray of the Walther gun to be evaluated, the target used previously was enlarged to 150 mm by 250 mm. Figure 4.7 shows the percentage of total solids deposited on each 10 mm wide vertical strip versus the distance from the centre of the spray pattern. Although the width of the spray was greater, the deposition at the centre was similar to that produced with the 2050/120 nozzle combination. The relative differences between the spray patterns of the three systems evaluated were highlighted by plotting the weight of coating deposited in each 10 mm wide vertical strip, equalized to 10 mg deposited at the centre, versus the distance from the centre of the spray pattern (Figure 4.8). Clearly decreasing the fluid nozzle size , for the Spraying Systems Co. guns, produced a more even spray coverage which, at the centre, was similar to that obtained with the Walther spray gun.

Since the operation of the Walther gun required an air supply of 0.48 m^3 min^{-1} at 0.55 MPa it would have been necessary to employ a compressor, whilst the 2050/120 combination could be used in conjunction with compressed air cylinders. Therefore the 2050/120 nozzle combination was used for all subsequent work

Figure 4.7 Percentage of total solids deposited in each 10 mm wide vertical strip versus distance from the centre of the spray pattern produced by the Walther spray gun at a distance of 200 mm with an atomizing air pressure of 0.55 MPa.

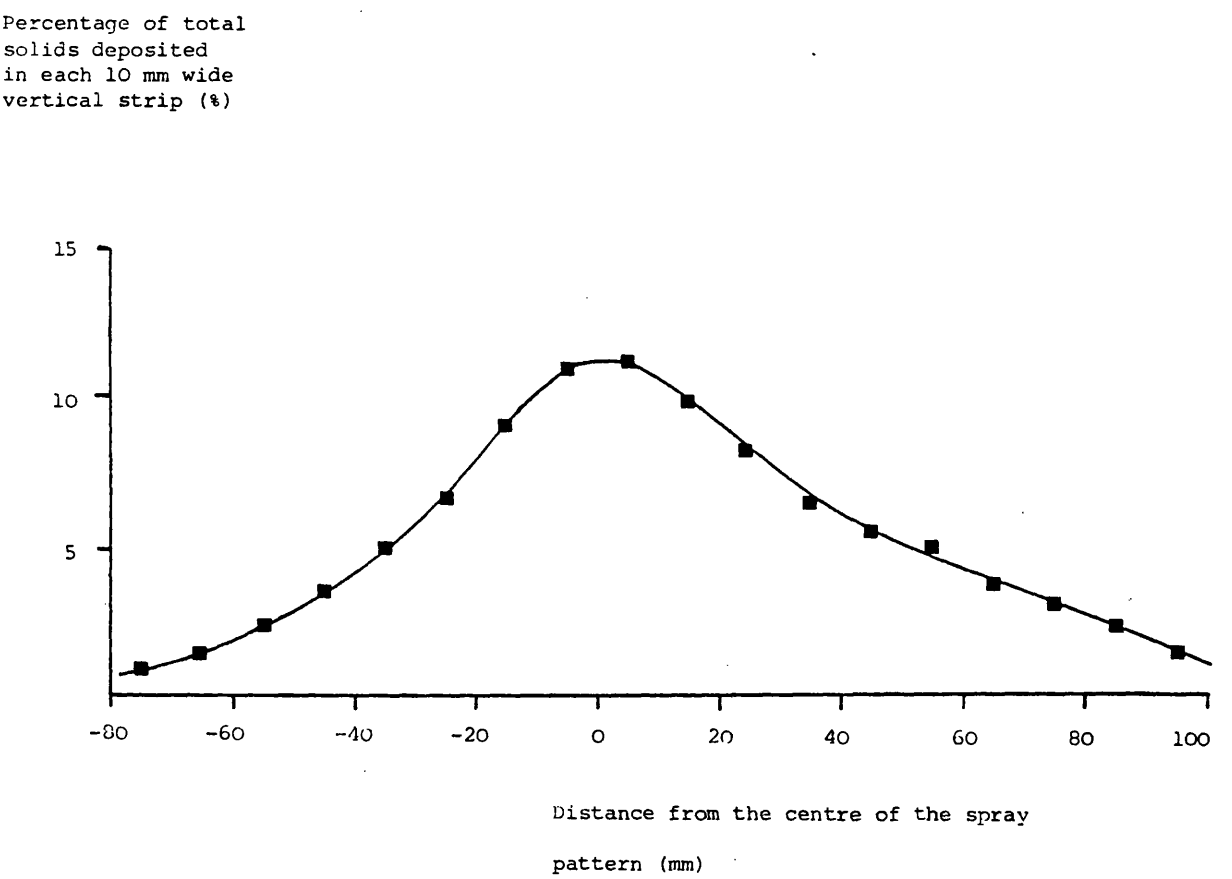

Figure 4.8 Comparison of the weight of material deposited in each 10 mm wide vertical strip versus distance across the spray area, for each spray gun evaluated.

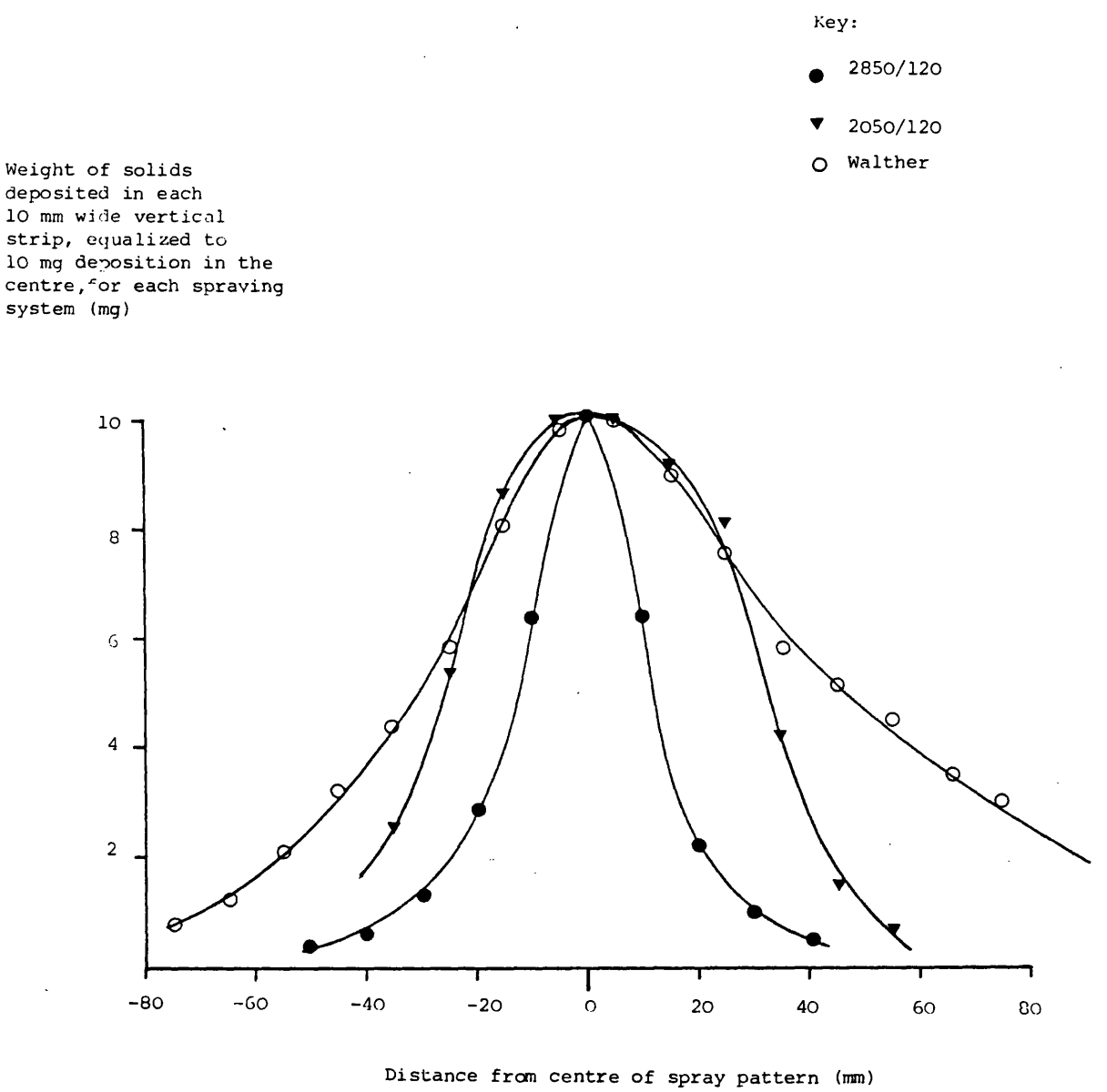

in the Accela-Cota and with the model system. This modified spray system also enabled spray rates of 30 to 35 g min^{-1}, previously attainable only with the Walther Spray gun, to be used successfully in the Accela-Cota.

d) Pan Speed and Tumbling Action

For aqueous film coating the Accela-Cota was routinely used at the lowest pan speed (approximately 12 rpm), with all eight baffles installed. This produced a good tumbling action of the tablets, although mixing within the bed was shown to be very poor (Sections 4.3.1.2e and 4.3.2.1).

e) Spray Time Parameters

The length of time any tablet spent within or outside the spray area were regarded as critical factors in the production of a film coating. With a fixed set of drying conditions, these parameters determine the degree of tablet wetting and time available for solvent removal prior to further wetting. Consequently they would be expected to affect:-

a) the proximity and extent of contact between the core and coating and hence adhesion and surface roughness.

b) the ability of the film to relieve stresses which develop during drying and hence mechanical properties[210,225,242,255].

c) the interaction between contiguous layers of coating to produce a uniform film.

To observe the passage of individual tablets through the spray

area of the Accela-Cota, coloured marker compacts were added to 8 kg loads of 10.32 mm diameter normal convex tablets and coated with a 5% w/v solution of Pharmacoat 606 using the conditions described earlier.

The conventional tablets were produced from the direct compression mix shown below:

	% w/w
Avicel PH 101	49.5
Lactose 70/100 mesh	49.5
Aerosil OT	0.5
Magnesium stearate	0.5

The blend was compressed on a rotary tablet machine (D3RY, Delta Press or Express, Manesty Machines Ltd.) fitted with 10.32 mm dies and normal concave plain punches, to the following specifications:

Weight	375 mg $\pm$ 5 mg
Thickness	4.45 mm $\pm$ 0.05 mm
Hardness	11 - 12 kp

The coloured compacts were produced from a similar formulation:

	100 g
Avicel PH 101	48 g
Lactose 70/100 mesh	48 g
Water soluble dye (as a 5% w/v aqueous solution)	4 g
Powder from above	98 g
Aerosil OT	1 g
Magnesium stearate	1 g

The lactose and Avicel were mixed for 10 minutes (Kenwood Chef, Thorn Domestic Appliances (Electrical) Ltd.) whilst a 5% w/v solution of the dye was slowly added. The moist mass was passed through a 15 mesh sieve, spread onto trays and dried at 45°C to under 3% w/w moisture. (Cenco Moisture Balance Model 26680-8). The dried powder was passed through a 30 mesh screen, the lubricant and glidant added through a 30 mesh screen and mixed for 5 minutes. The resulting powder was compressed on a Manesty F3 machine, fitted with 10.32 mm diameter die and normal concave plain punches, to the same specifications as the conventional tablets. The increased lubricant and glidant concentration were necessary to prevent sticking in the die and lamination of the coloured compacts. Several dyes were evaluated, but tablets containing F.D. and C. red number 2 (amaranth, B.D.H. Ltd.) or F.D. and C. blue number 2 (indigo carmine, B.D.H. Ltd.) were most easily distinguished from a bed of white tablets rotating in the Accela-Cota.

Spray Dwell Time

The passage through the spray area of 25 blue compacts, added to an 8 kg load of white tablets, was observed through the open mouth of the coating pan; the spray area being recognised by the surface depression in the tablet bed caused by the atomizing air. Neither black and white nor colour video recordings were able to 'freeze' the motion of tablets tumbling in the spray area and it was necessary to resort to high speed cine photography. To enable a fast film speed to be used, the Accela-Cota was floodlit by removing the top panel of the casing (Figure 4.9). Despite this, the temperature within the coating drum remained constant due to the heat produced by the flood-lights counteracting any loss through the open top of the instrument, thus enabling a 5% w/v aqueous solution of Pharmacoat 606 to be applied at a rate of 30 to 35 g min^{-1} using a 2050/120 nozzle combination. Thus all the coating parameters were reproduced during measurement of the dwell time by high speed cine photography. 30.5 m of 16 mm cine film were exposed at both 64 frames per second (fps) (Kodak 7246 video news film, Bolex camera) and 400 fps (2498 RAR film, Hycam camera); the latter camera possesses a stroboscope facility which allowed the edge of the film to be marked at precise time intervals (0.01 seconds)

The films were replayed at 16 fps (Specto Analyser, Ampro Ltd.) and the spray area marked on the projection screen from the depression observed in the tablet bed. Frame by frame

Figure 4.9 Floodlighting of the Accela-Cota during a coating run, to allow the use of high speed cine photography for the determination of dwell times of compacts in the spray area.

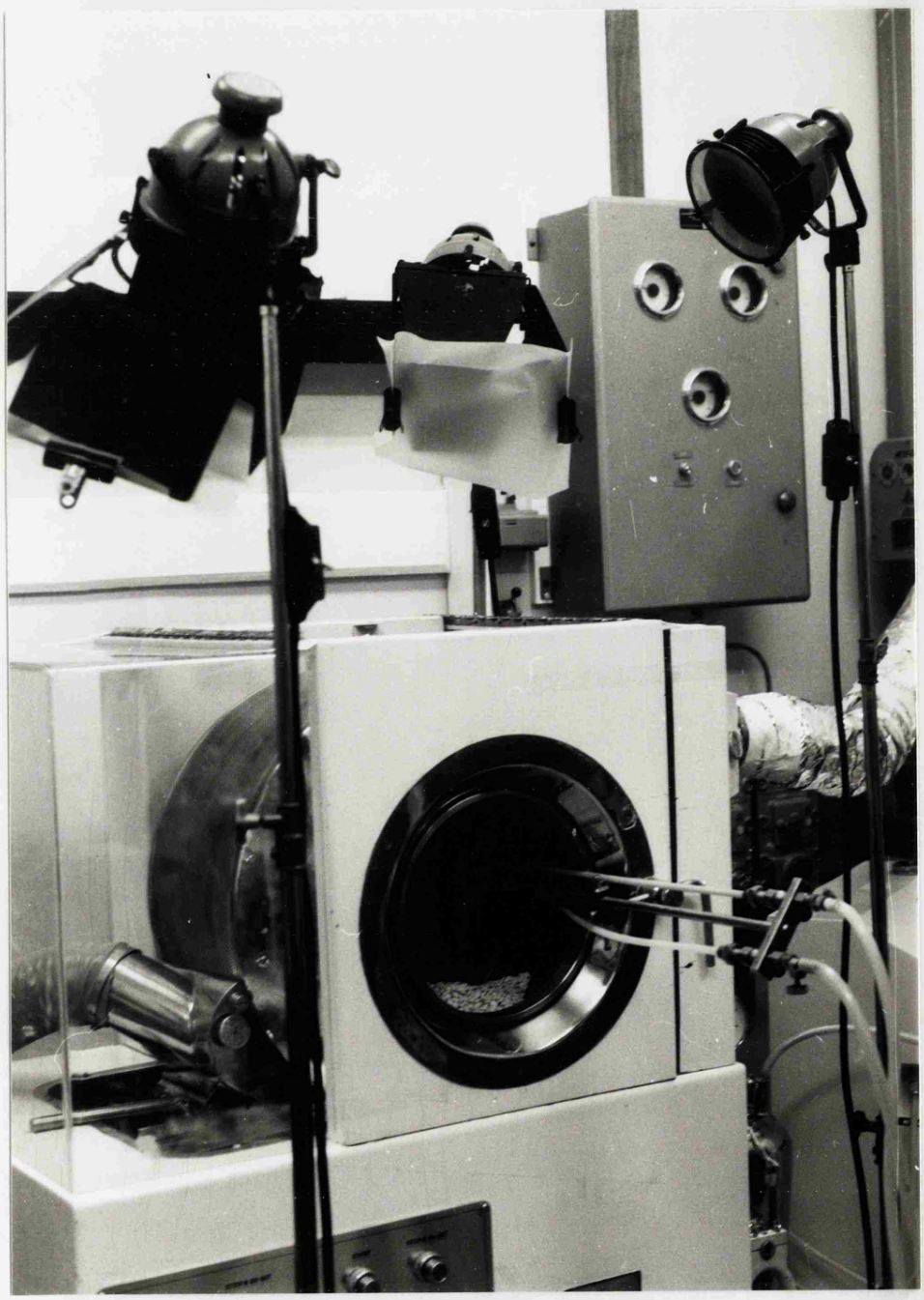

analysis then allowed the time each coloured compact spent in the spray area to be calculated from the number of frames and the film speed. The first 15 metres of the black and white film were disregarded since the stroboscope markings indicated that during this time the film speed had been increasing up to 400 fps (1 mark per 4 frames or 0.01 seconds = 400 fps) after which it remained constant. Figure 4.10 shows a single frame from the black and white high speed cine film with a blue compact in the spray area (arrowed). 39 passages through the spray area were recorded on the colour film and 8 on the black and white film, giving mean dwell times of 0.091 secs and 0.121 secs respectively. A 't' test (Table 4.8) showed these values to be significantly different at the 5% level. This discrepancy between the dwell time values was most probably due to an error in the film speed of the Bolex camera which was mechanically operated by a spring; although its speed could not be validated by use of a stroboscope. Furthermore the slower film speed also increased the error in deciding when a tablet entered and left the spray zone, since one frame in error represented 0.0156 secs (17.1%) and 0.0025 secs (2.1%) at 64 and 400 fps respectively. Therefore the data from the Hycam camera was considered to be more accurate and was used in the design of the model system.

To ensure that tablets did not appear in the spray area intermittently, the black and white film was re-analysed after horizontally dividing the spray area marked on the screen into

Figure 4.10 Single frame from the black and white high speed cine film showing a blue compact in the spray area during a coating run in the Accela-Cota.

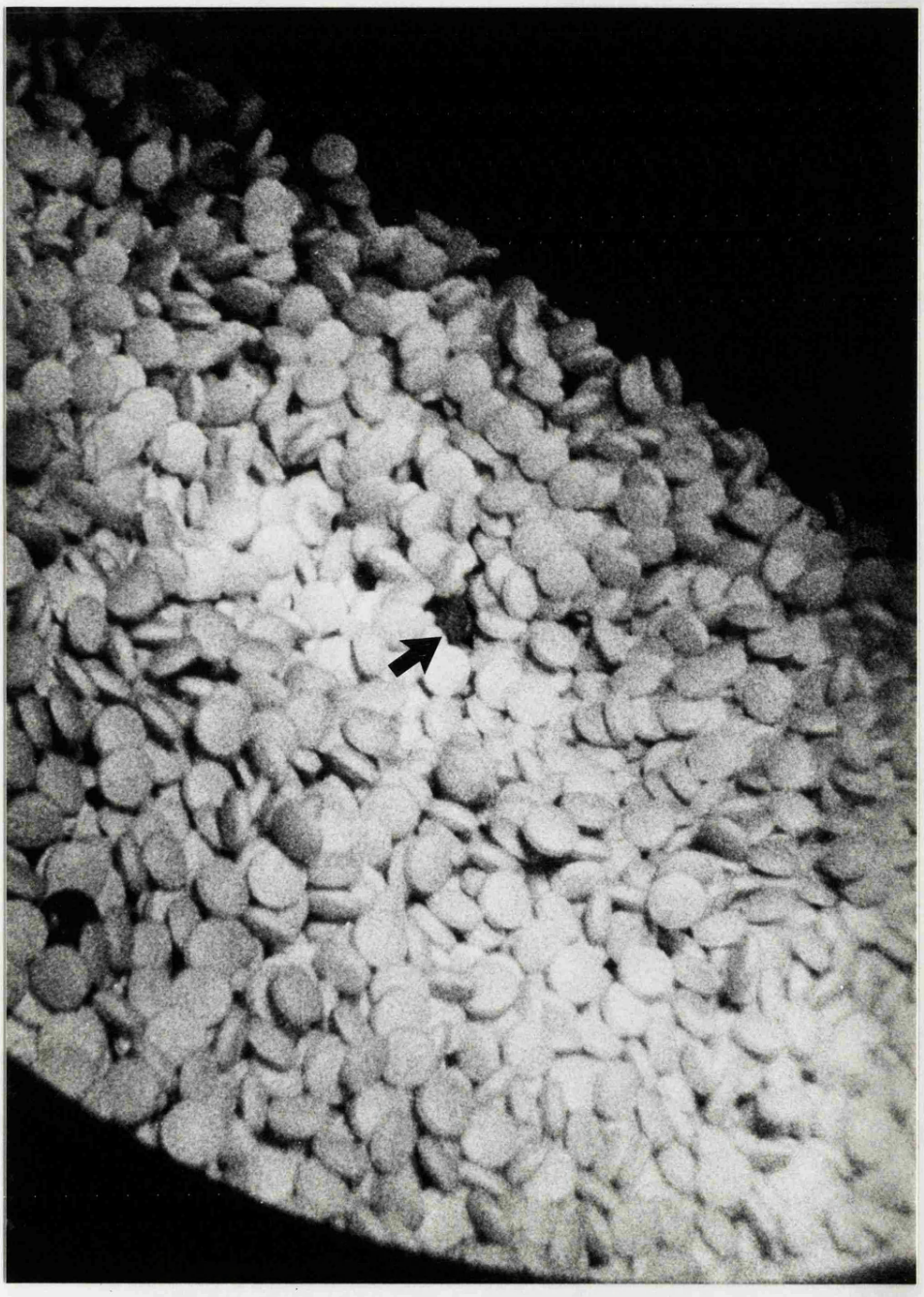

Table 4.8 The dwell time of single coloured compacts in the spray area of a 24" Accela-Cota, determined by high speed cine photography.

Camera	Film Speed (fps)	Number of frames in which compact appears in the spray zone during each passage		Mean dwell time in the spray zone		
		Mean	S.D.	(secs)	S.D.	C.V. (%)
Bolex	64	5.82	0.56	0.091	0.0088	9.67
Hycam	400	48.25	1.39	0.121	0.0035	2.90

S.D. = Standard Deviation

C.V. = Coefficient of variation $t_{calc} = 9.42$

$t_{tab}(P=0.05) = 2.02$

four equal parts. At no point could a coloured compact be positively identified as having appeared in less than all four regions, although fleeting shadows (< 0.005 sec) observed between white tablets may have been coloured compacts lower down in the bed. In addition, a few compacts were observed to encroach upon the outer margin of the spray area (< 0.0075 sec) before being forced outwards by the compressed air. Such appearances, being much shorter than a full passage through the spray were unlikely to contribute significantly to the build-up of the film coating.

Spray Interval

The interval between passes through the spray zone was recorded by observing the movement of one red and one blue compact added to 8 kg of white tablets. Since it was impracticable to record a coating run of twenty or thirty minutes on high speed cine, which uses 30 m of film in 5 to 10 seconds, the appearances of the coloured compacts in the spray area were recorded manually, with one person identifying the tablets and a second operating a digital lap timer (NTC Ltd.). This process was recorded onto cassette tape to allow retrospective checking of the data obtained.

The spray intervals recorded varied from 2 to 243 seconds, with no obvious pattern being discernible (Figures 4.11 to 4.13). The large variations observed in this interval indicated that mixing within the Accela-Cota was very poor. The mean time

Figure 4.11 .Plots of interval between appearance in the spray area against appearance number for single coloured compacts added to an 8 kg load of tablets in the Accela-Cota

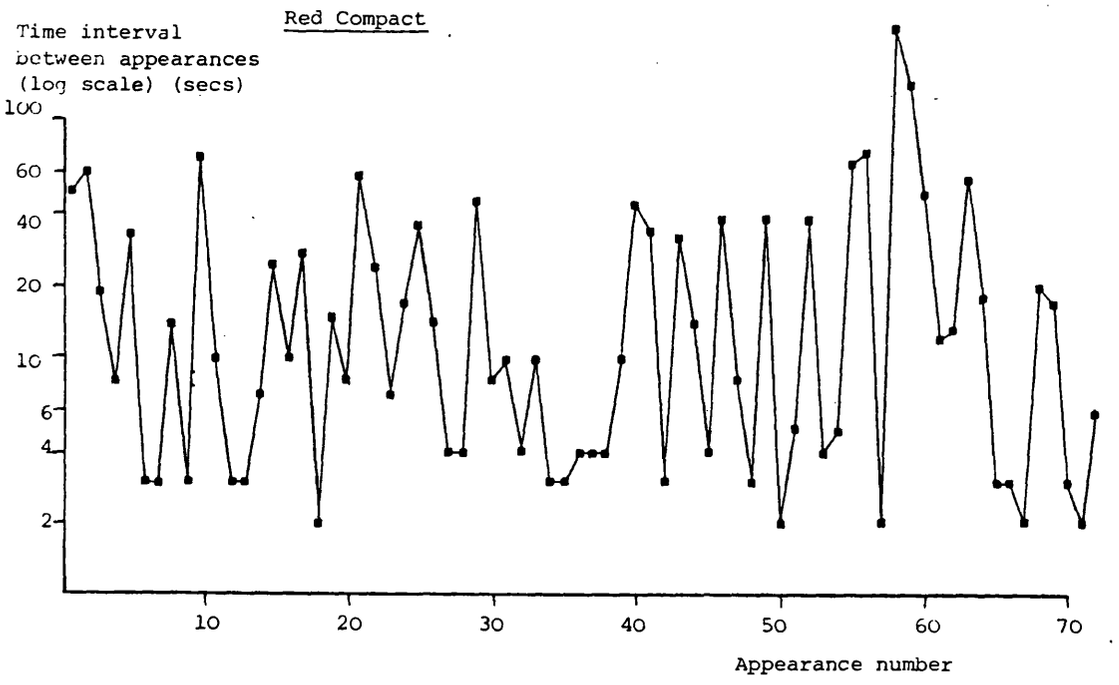

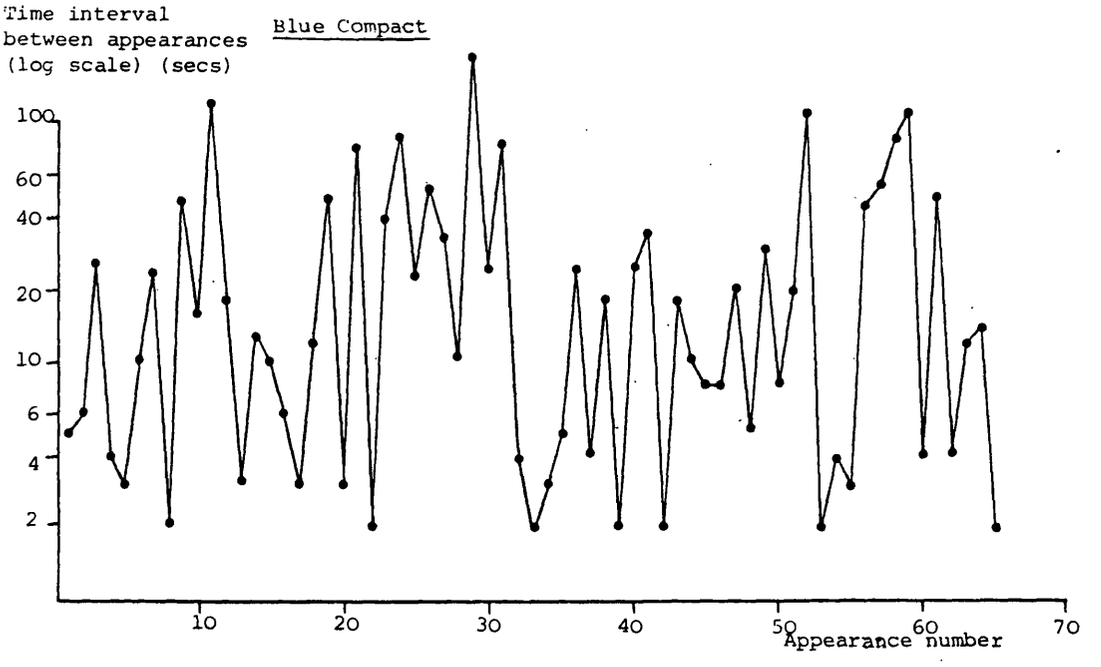

Figure 4.12 Plots of frequency versus interval between appearance in the spray area for single coloured compacts added to an 8 kg load of tablets in the Accela-Cota.

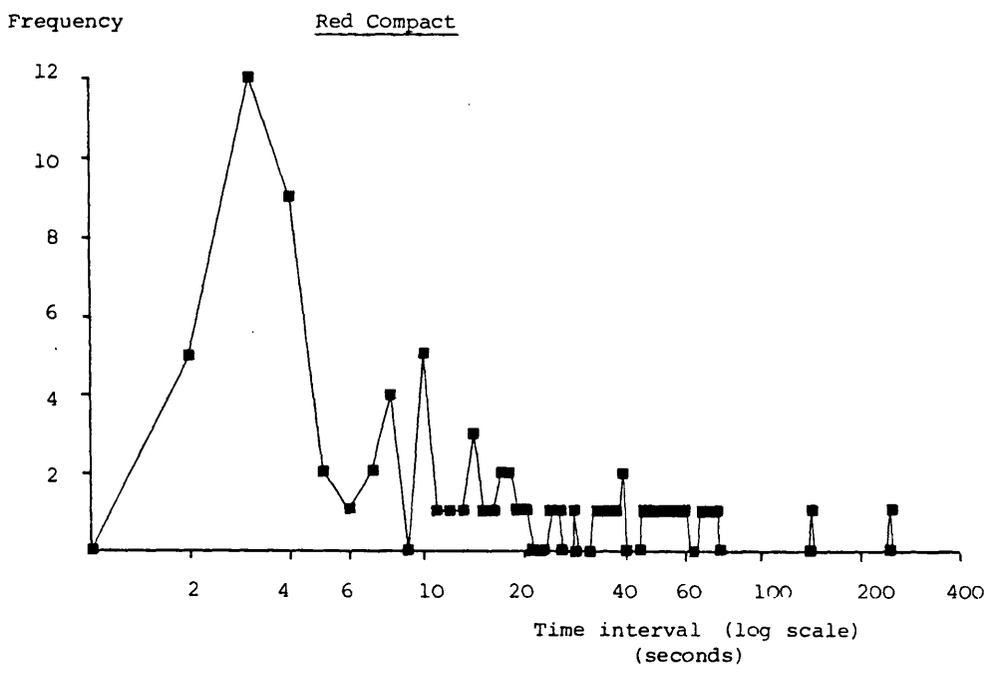

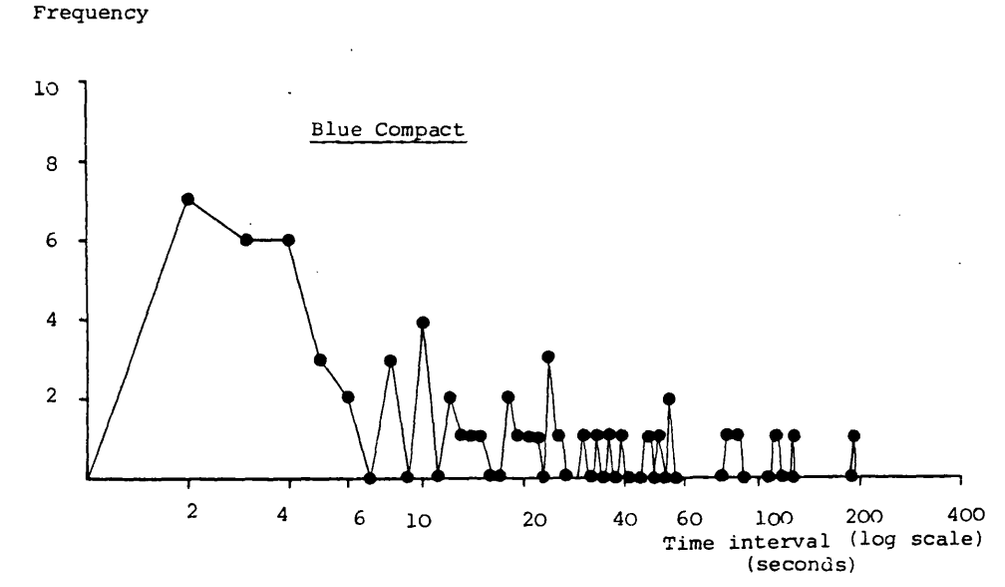

Figure 4.13 Plots of cumulative frequency against interval between appearances in the spray area for single coloured compacts added to an 8 kg load of tablets in the Accela-Cota

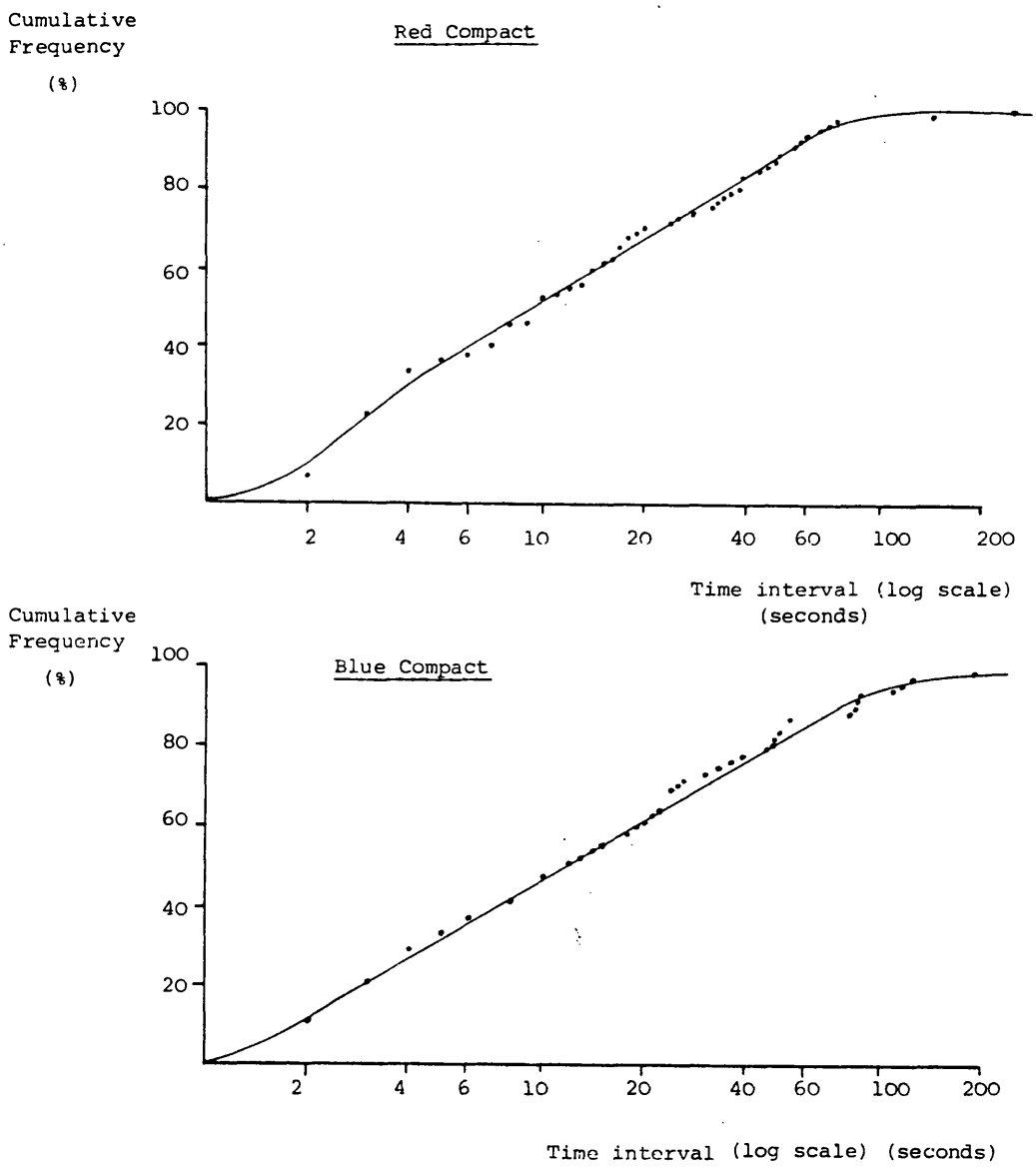

intervals for both red and blue compacts were similar (22.74 secs S.D. 34.71 and 26.86 secs S.D. 36.14 secs respectively) and their combined mean of 24.8 seconds (standard deviation 35.4 secs) was used in the design of the model system. The mean interval was chosen to equalize the number of passages through the spray area during a coating run.

4.3.1.3 The Imitation of Important Coating Parameters

A model coating system, designed to mimic the parameters measured in the previous section, was constructed around a modified fume cupboard, drying air being provided by an air conditioning fan and the exhaust removed by the fume cupboard extraction system.

a) Drying Air Volume and Temperature

An air conditioning fan (Imhofs Axial Fan, A. Imhof Ltd.), fitted with galvanised iron (Treman Ltd.) and articulated stainless steel (i.d. 101.6 mm) ducting, was used to provide inlet air for the model system (Figure 4.14). The baffle located at the end of the stainless steel ducting helped to deflect the air downwards on to the substrates being coated. The air was heated by a 3 kW electric element (Belling Lee Ltd.) installed in the galvanized iron ducting, the power to which was controlled by a variable transformer (Slideup, Yokoyama Electrical Works Ltd.). The equilibrium temperature of the inlet air , measured with a mercury in glass thermometer inserted through a grommet in the articulated ducting, could thus be varied from

Figure 4.14. Inlet air supply for the model system.

Key:

A Axial fan

B Galvanized Iron Ducting

C Articulated Stainless Steel Ducting

D Baffle

E 3 kw Heating Element

F Bimetal Thermal Sensor

G Thermometer

H Insulation

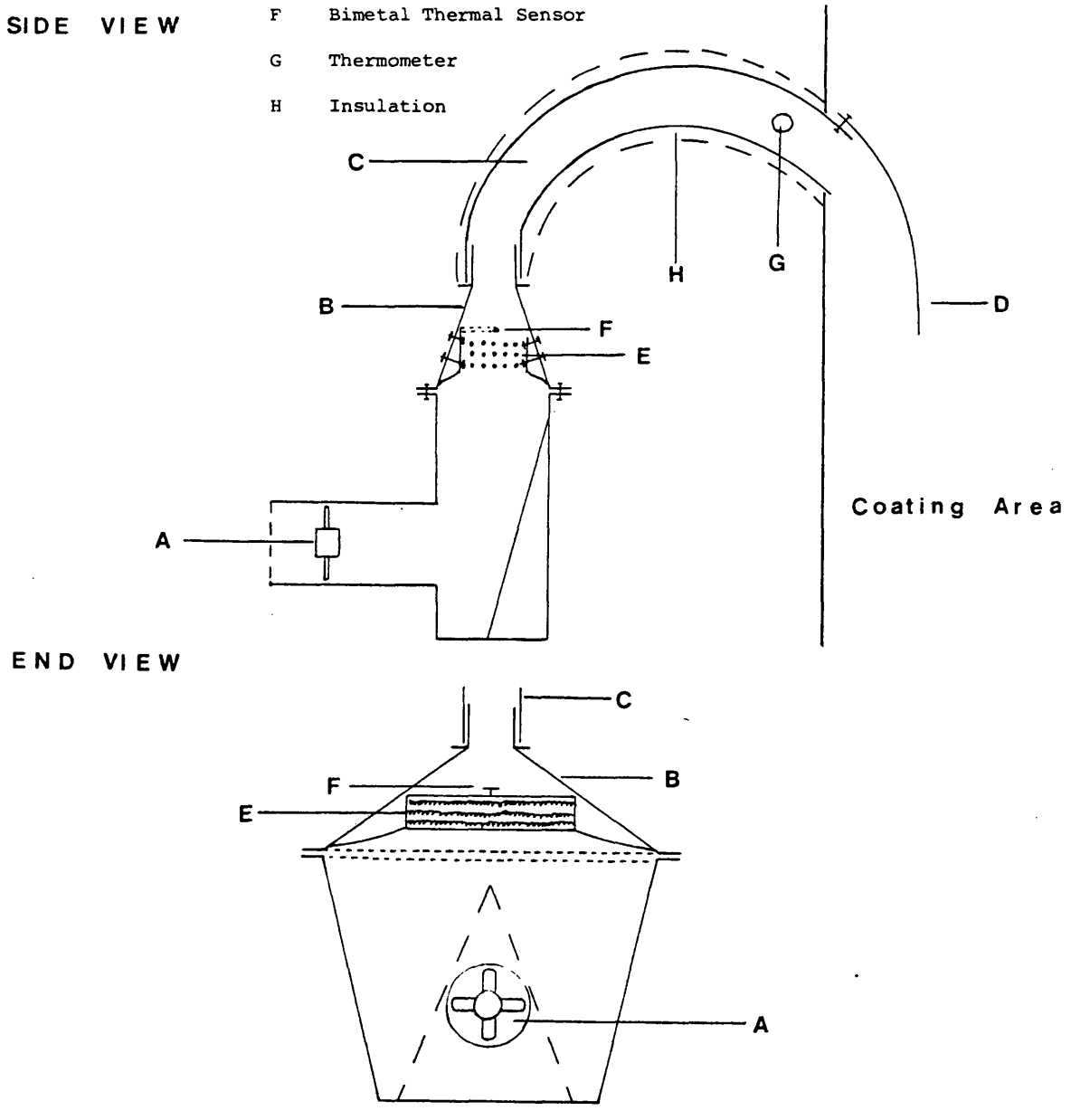

room temperature to 90°C (Figure 4.15). To minimize heat loss, the articulated ducting was lagged with a 25 mm thickness of cotton wool and covered with aluminium foil. Air temperatures above 90°C could not be obtained since the bimetal thermal sensor, located above the heating element, cut out, indicating that a further increase in the element temperature would cause permanent damage.

The air speed in the articulated ducting was measured with an anemometer (Minivane, E. Schictknecht Ing.) and converted to air volume by multiplication with the cross-sectional area of the ducting (8.107×10^{-3} m^2). Figure 4.16 shows that the volume of drying air produced at 90°C could not be adequately controlled by varying the voltage applied to the fan motor (Rotary Regavolt, British Electrical Resistance Co. Ltd.). The lack of control was attributed to the response of the fan motor being relatively unaffected by increases in voltage, once a threshold for rotation had been reached.

Consequently the fan was operated at 240 V, producing an inlet air volume of 4.13 m^3 min^{-1} at 90°C, which is within 5% of the value measured on the 24" Accela-Cota. For future studies a reduced inlet air volume could be obtained, if required, by installing a variable baffle before the fan, to reduce its air intake.

Figure 4.15 The variation of inlet air temperature with heater voltage, at constant fan speed, for the air supply to the model system.

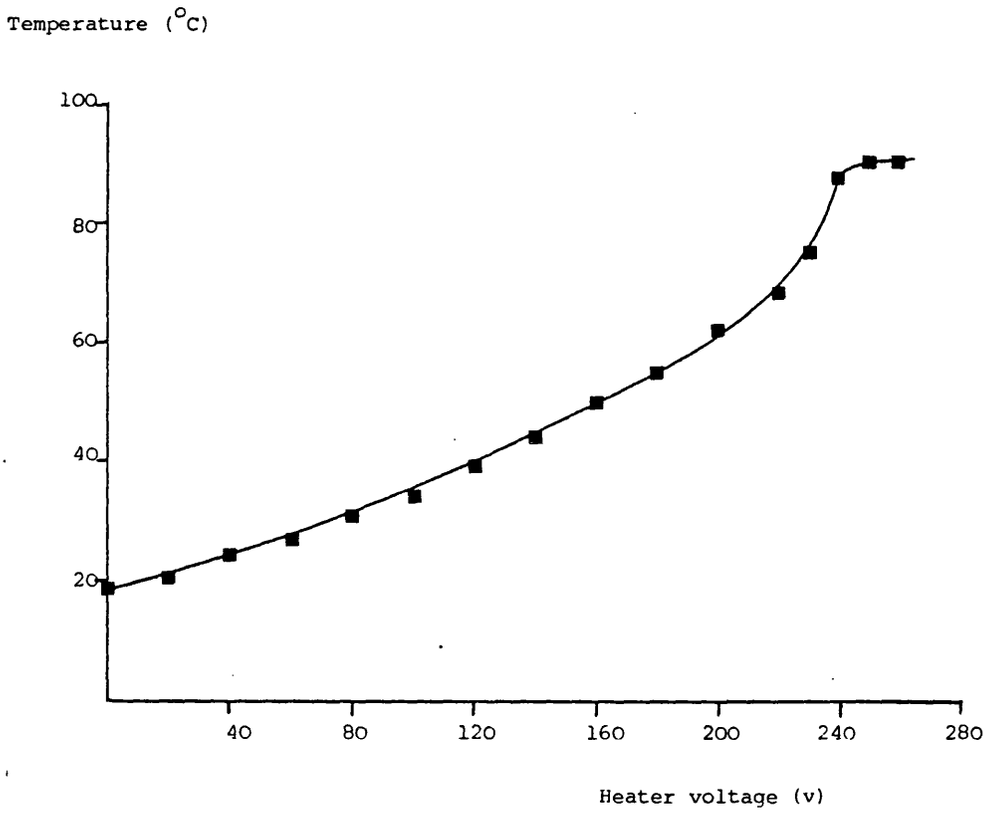

Figure 4.16 The effect of voltage applied to the fan motor on the drying air volume, at 90°C, supplied to the model system.

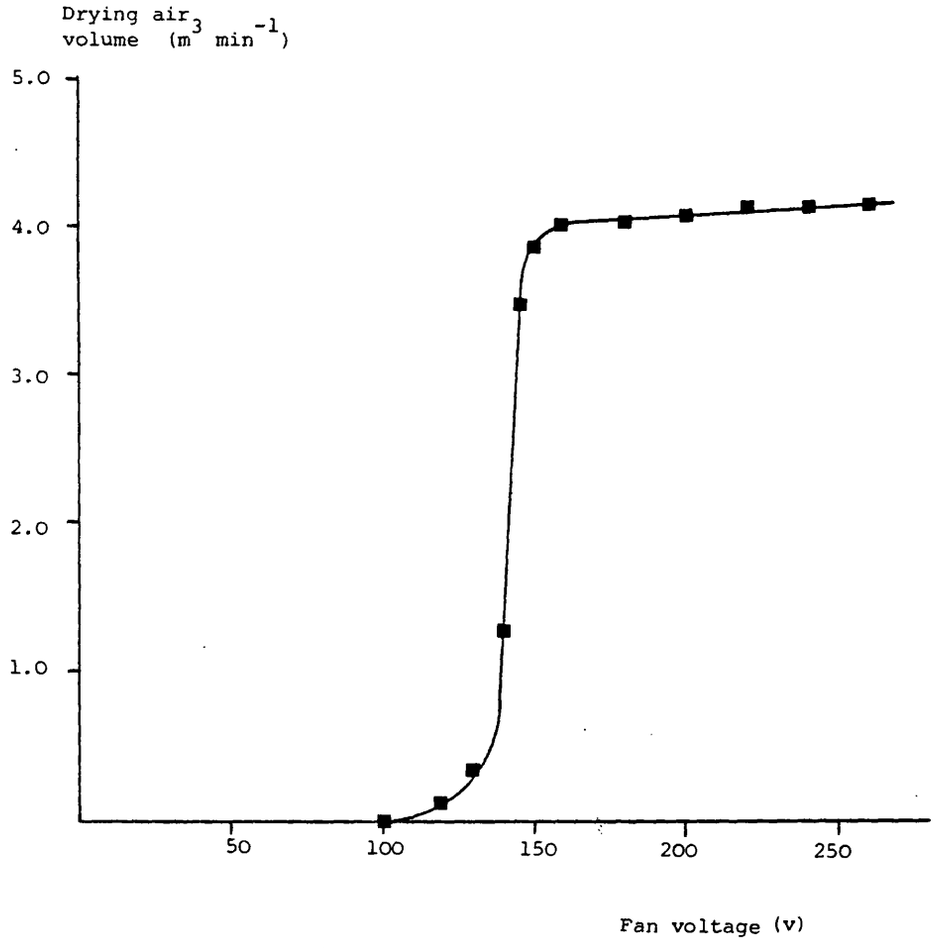

b) Exhaust Capacity and Temperature

For the model system, a fume cupboard was baffled such that air was extracted from a square opening (area 1.032 x 10^{-2} m^2) at the base of one wall (Figure 4.17). The sliding glass front was modified so it could be completely closed and a rubber seal installed to provide a leak-tight seal. The control flap located above the coating area enabled the exhaust capacity to be progressively reduced (Figure 4.18). The exhaust capacity of the model system, measured with an anemometer, could thus be varied from 7.63 m^3 min^{-1} to 10.20 m^3 min^{-1}.

The exhaust air temperature in the model system was measured with a mercury in glass thermometer, inserted in the ducting as shown in Figure 4.17.

c) Spraying System

The 2050/120 spray nozzle combination evaluated in Section 4.3.1.2.c was used for the model system. The quantity of material deposited across a 25 mm diameter substrate placed at the centre of the spray pattern was shown to vary by less than 7% and subsequent removal an area of coating, 21 mm in diameter, for testing further reduced this error.

Atomizing air at a pressure of 0.28 MPa (4" dial 407S/SM, British Steam Specialities) was provided from compressed air cylinders, after passing the gas through a heated water jacket to overcome the cooling effect caused by adiabatic expansion from the cylinder.

Figure 4.17 Exhaust facility for the model coating system

Key:

A	Baffle	D	Thermometer
B	Glass front	E	Air inlet
C	Control flap	F	Exhaust

SIDE VIEW

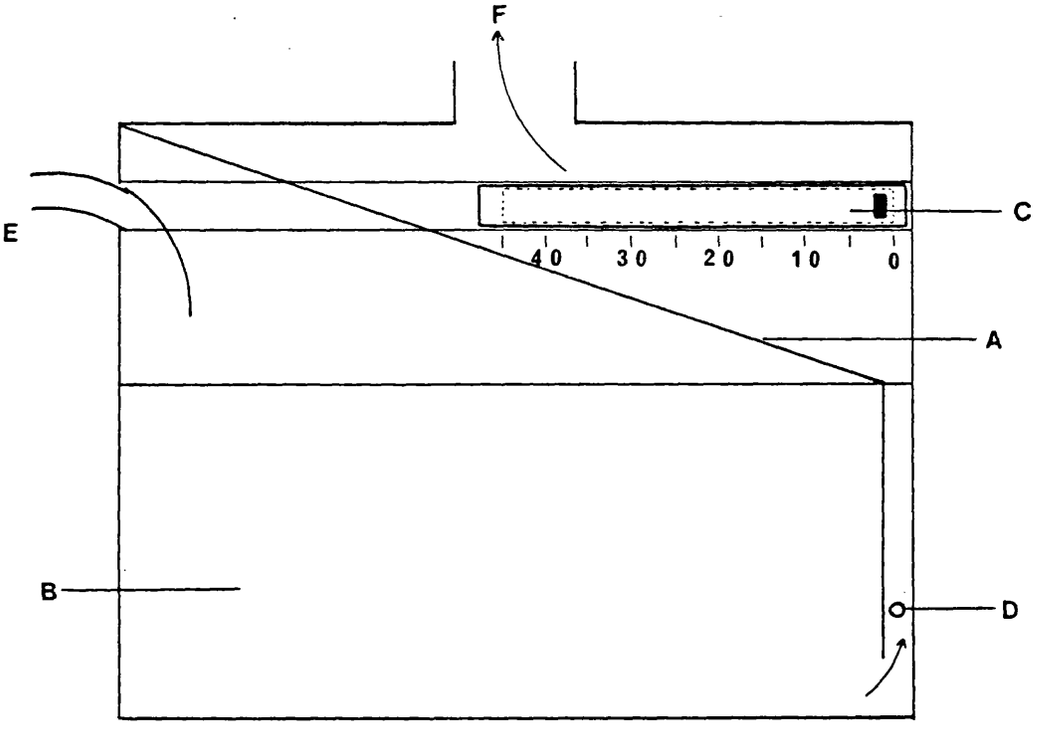

END VIEW

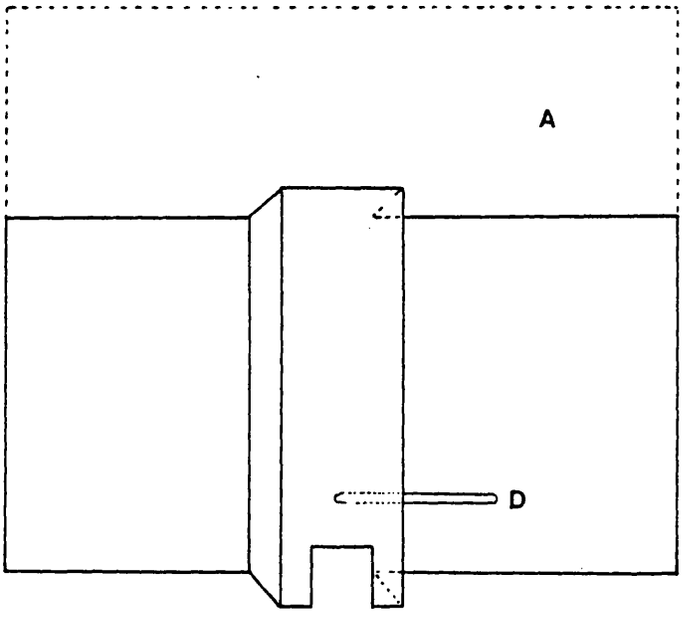

Figure 4.18 The variation in exhaust capacity with control flap setting for the model system.

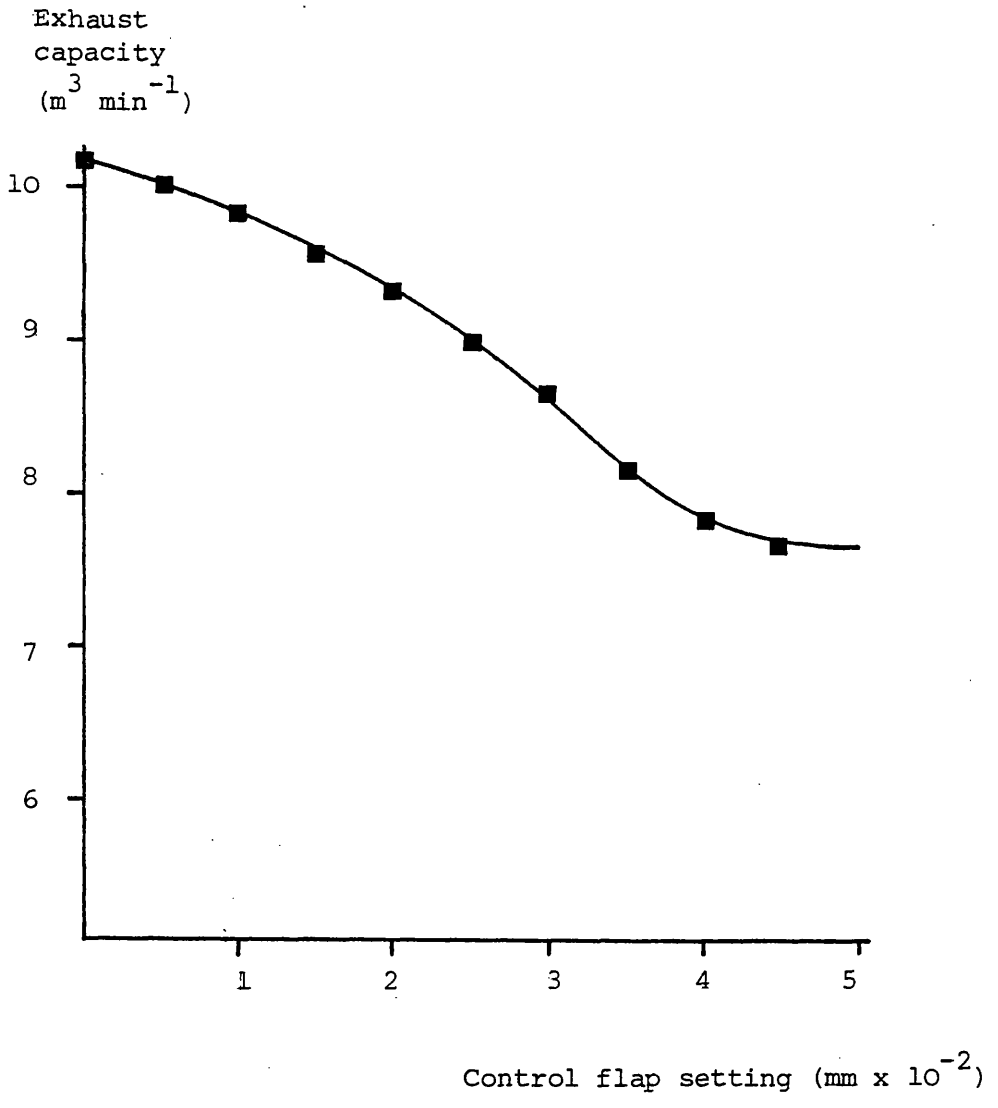

Liquid feed to the spray nozzle was provided by a peristaltic pump (MHR E100 Flow Inducer, Watson Marlow Ltd.) and regulated by the pump speed and use of a micro-metering valve (Whitey - B22RS4, Techmation Ltd.). Whilst spraying, the flow rate was adjusted, prior to each coating run, by measuring the volume of coating solution removed in 5 minutes from a 250 ml graduated measuring cylinder with an outlet fitted at the base. This technique of pre-calibration of the liquid flow rate was chosen in preference to use of a flow meter, since the calibration of the latter would be affected by changes in the viscosity and density of the coating solution or suspension used.

Throughout this study the gun to substrate distance was set at 200 mm (Accela-Cota gun to bed distance), although movement of the timing belt (Section 4.3.1.3e) could allow the distance to be varied between 30 and 900 mm.

d) Pan Speed and Tumbling Action

The pan speed of the Accela-Cota was of indirect importance in the design of the model system, since changes would to some extent alter the spray time parameters measured in Section 4.3.1.2e. Thus the effects of the pan speed can be accounted for by direct measurement of the spray time parameters.

The tumbling action of the tablets could not be mimiced since it was derived from the nature of the coating instrument. Furthermore, attempts to create such an action would cause

difficulties with large substrates as their high mass and hence inertia rapidly leads to damage such as chipping. Although this was recognised as a deficiency in the model, it was not thought to be of great importance since the coating solution was sprayed on to the tablets, giving little opportunity for tablet-tablet transfer of material. Indeed, contact of 'wet' tablets with subsequent drying and pulling apart is generally regarded as the cause of 'picking' of the coating. The rapid speed with which successive layers of coating dried also made it likely that any effects caused by the tumbling action, would be limited to mechanical stressing and damage of the dry film.

e) Spray Time Parameters

Due to the 200 to 1 ratio of interval to dwell time, a system was designed by which substrates could be attached to a rotating belt and moved through the spray in 0.12 secs, whilst an electronically controlled shutter, located next to the spray nozzle, allowed coating solution to reach the belt for only one revolution per 25 seconds.

The framework of the shutter system was constructed from 'Dexion' slotted angle with the fixed and moving shutters cut from 1.5 mm thick aluminium sheeting (Figure 4.19). A 27 mm diameter hole was cut in the fixed shutter, which was curved in an arc around the spray gun. The moving shutter was bent to fit the curvature of the fixed shutter and bolted to a carrying arm constructed from 3 x 12 mm mild steel. Activation of the

Figure 4.19 The shutter arrangement for control of the spray reaching the substrate on the model system

Key:

A Fixed shutter

B Moving shutter

C Shutter carrying arm

D Pivot

E Return stop

F Return spring

G 12 volt d.c. solenoid

H Waste suspension trough

I Cover

J Insulating bolt and washer

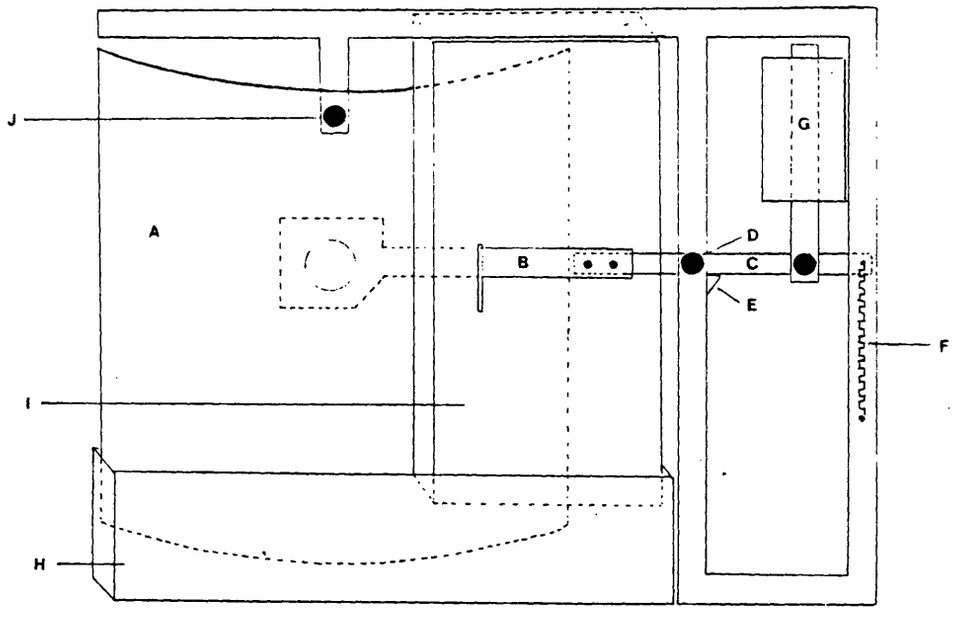

12 volt d.c. solenoid (Varley Type CMD3, Oliver Pell Control Ltd.) pulled the moving shutter away from the hole in the fixed shutter and allowed coating material to reach the substrate until deactivation enabled the return spring to close the shutter.

The solenoid was activated via the relay of an electronic timing circuit (Figure 4.20), all components of which were obtained from R.S. Components Ltd. and wired-up on stripboard. IC1 (555 integrated circuit timer) was connected for astable operation, such that the frequency with which it discharged was set by the values of resistors R_a (1 MΩ and 4.7 MΩ variable) and capacitor C_a (10 μF) according to the timing formula:

$$t = 0.7\ R_a\ C_a \qquad \text{... (equation 4.9)}$$

where t is in seconds, R_a in ohms and C_a in faradays.

The output from IC1 was fed to IC2 (555 integrated circuit timer), which was connected in the monostable mode and thus only fired when the output from IC1 began to rise. The duration of IC 2's output was controlled by resistors R_m (47 kΩ and 500 kΩ variable) and capacitor C_m (4.7 μF) according to equation 4.10:

$$t = 1.1\ R_m\ C_m \qquad \text{... (equation 4.10)}$$

The output from IC2 was amplified and used to activate a relay through which power was provided to the solenoid. To prevent arcing, a 47 μF solid tantalum capacitor was connected

Figure 4.20 Electronic timing circuit to control the shutter of the model system.

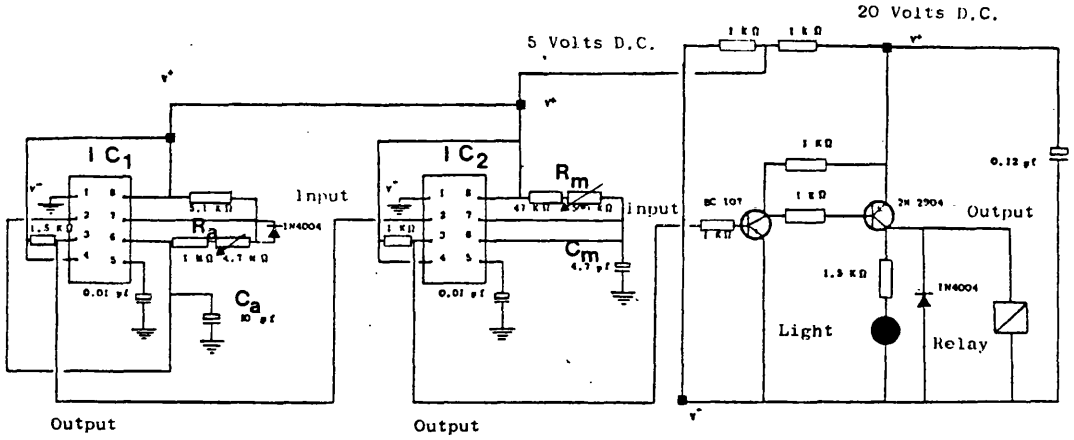

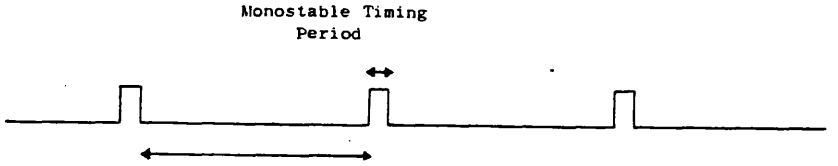

555 TIMER

V⁻	1	8	V⁺
Trigger	2	7	Discharge
Output	3	6	Threshold
Reset	4	5	Control Voltage

TIMING FORMULAE

ASTABLE

$T = 0{\cdot}7 R_a C_a$

MONOSTABLE

$T = 1{\cdot}1 R_m C_m$

UNITS

T - Seconds
R - Ohms
C - Faradays

across the 12 volt contacts of the relay.

The +20 volt power supply, required by the amplification circuit, was provided from a low voltage transformer. The transformer output (30 V a.c.) was fed to a silicone bridge rectifier, constructed from four 1N 4000 diodes, smoothed by a 2,200 μF electrolytic capacitor and dropped to 20 v. d.c. by a resistive network (17.1Ω and 78.0Ω). The +5v. rail for the timing circuits was derived from the smoothed 20 v. supply via a 1 kΩ resistor (Figure 4.20). The power supply for the solenoid was provided by a battery charging unit(Halfords Ltd.); the 20 v. a.c. transformer output was passed to a plate rectifier and dropped to 12 v. d.c. (3 amps) before being fed to the solenoid via the relay of the timing circuit.

To optimize and measure the speed of movement of the shutter, a millisecond stopclock (Type TSA 3314, Venner Electronics Ltd.) was connected between the moving and fixed shutters, which had been electrically insulated from each other by applying PVC tape (R.S. Components Ltd.) to the back of the moving shutter. An aluminium pointer was bolted to the carrying arm to remake electrical contact with the fixed shutter. By applying PVC tape selectively along the path of the pointer's movement, the timer circuit was closed during specific parts of the shutter movement, causing their time to be recorded. Thus the opening and closing times of the shutter were recorded and minimized by alterations of the return-spring tension and pivot

bearing (Table 4.9). The moving surfaces in the pivot were polished with a carborundum stone (Norton Ltd.) followed by Duraglit Metal Wadding (Reckitt Household Products Ltd.), or were separated by a layer of P.T.F.E. sheet.

The data in Table 4.9 demonstrated that the polished metal bearing allowed the quickest movement of the shutter and a reduced spring tension gave similar opening and closing times. Thus the minimum time to open and close the shutter was 33.36 milliseconds.

The rotating belt to which the substrates were attached (Figure 4.21) was constructed from a timing belt, circumference 1140 mm (Ford Motor Co. Ltd.), driven by a 125 mm diameter timing pulley (Fiat Motor Co. Ltd.) attached, via a bearing, to a high torque variable speed motor (Type KOJ11, Citenco Ltd.). The top idler pulley, diameter 125 mm, was constructed from bakelite and allowed to rotate freely about its bearing. Both pulley bearings were 127 mm long to enable the Dexion stand and motor to be clear of the spray area, thus preventing damage to the motor and minimizing interference with the spray pattern. To maintain the free-running nature of the bearings it was necessary to repack them with high temperature grease after 20 hours of use.

At a gun to substrate distance of 200 mm, the diameter of the spray area was 70.5 mm (Section 4.3.1.2c and Manufacturer's

Table 4.9. The effect of changes in the pivot bearing surfaces and return spring tension, on the opening and closing times of the moving shutter.

Bearing surfaces and return spring tension	Opening time			Closing time		
	Mean (msec)	S.D.	C.V. %	Mean (msec)	S.D.	C.V. %
PTFE Normal tension	28.38	(0.19)	0.67	23.90	(0.29)	1.21
PTFE Reduced tension	27.23	(0.65)	2.39	27.03	(0.25)	0.93
Polished metal Normal tension	21.02	(0.53)	2.52	15.47	(0.58)	3.75
Polished Metal Reduced tension	16.03	(0.78)	4.87	17.33	(0.91)	5.25

S.D. = Standard Deviation

C.V. = Coefficient of Variation.

Figure 4.21. The timing belt system for moving the substrates through the spray area on the model coating system.

Key: A, Timing Pulley; B, Idler Pully; C, Timing Belt; D, Polyurethane Foam; E, Substrate; F, Pulley Bearings; G, Stand; H, Variable Speed High Torque Motor; I, Cover; J, Spray Area.

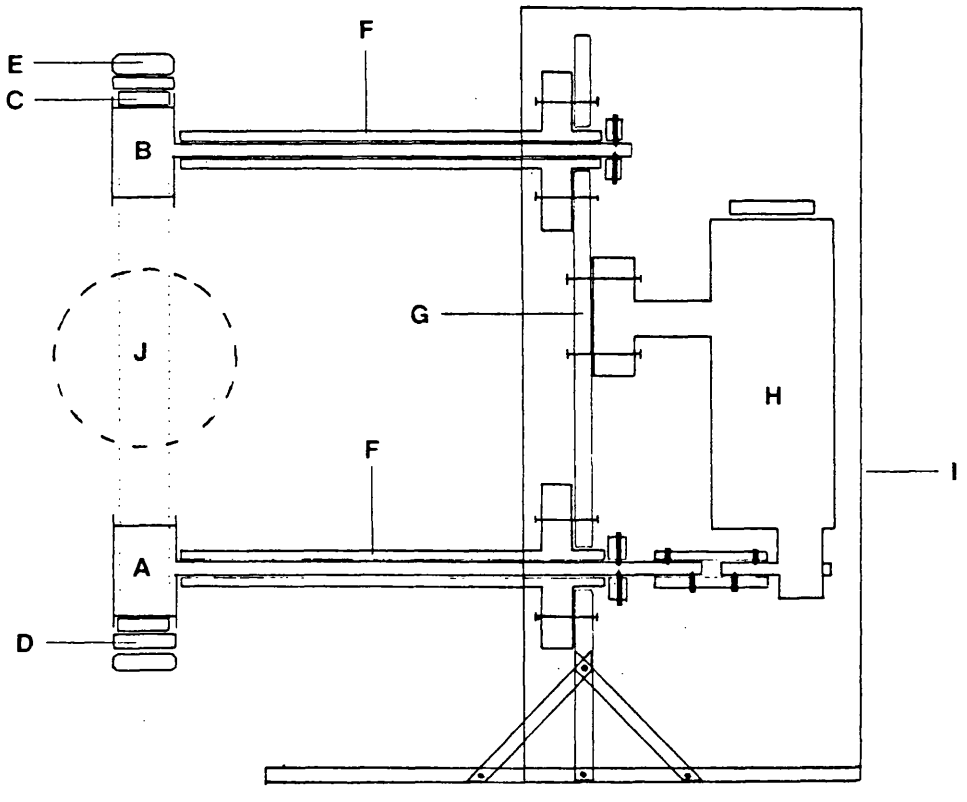

data). Thus for a substrate to spend 0.12 seconds in the spray area, the belt had to move at:-

$$\frac{70.5}{0.12} = 587.5 \text{ mm sec}^{-1}$$

Thus one complete revolution of the belt (circumference 1140 mm) took:-

$$\frac{1140}{587.5} = 1.94 \text{ seconds}$$

Since the driving pulley (diameter 125 mm) had a circumference of 392.699 mm, this belt speed represented

$$\frac{587.5}{392.699} \times 60 = 89.76$$

revolutions per minute of the pulley and driving shaft.

The timing pulley was marked with a white spot, its speed of rotation measured using a stroboscope (Griffin Xenon Stroboscope, Griffin and George Ltd.) and then set to 90 rpm by adjustment of the variable speed control on the motor. This procedure was repeated at regular intervals during use and after the pulley bearings had been repacked with grease. Figure 4.22 demonstrates that the pulley speed could be varied from 80 to 225 rpm, corresponding to belt speeds of 523.6 and 1,472.6 mm sec^{-1} and dwell times of 0.135 and 0.048 seconds respectively.

Using the electronic timer, the open time of the shutter was set to correspond to one revolution of the timing belt, by

Figure 4.22 The variation in timing pulley speed versus motor setting, for the belt drive of the model coating system.

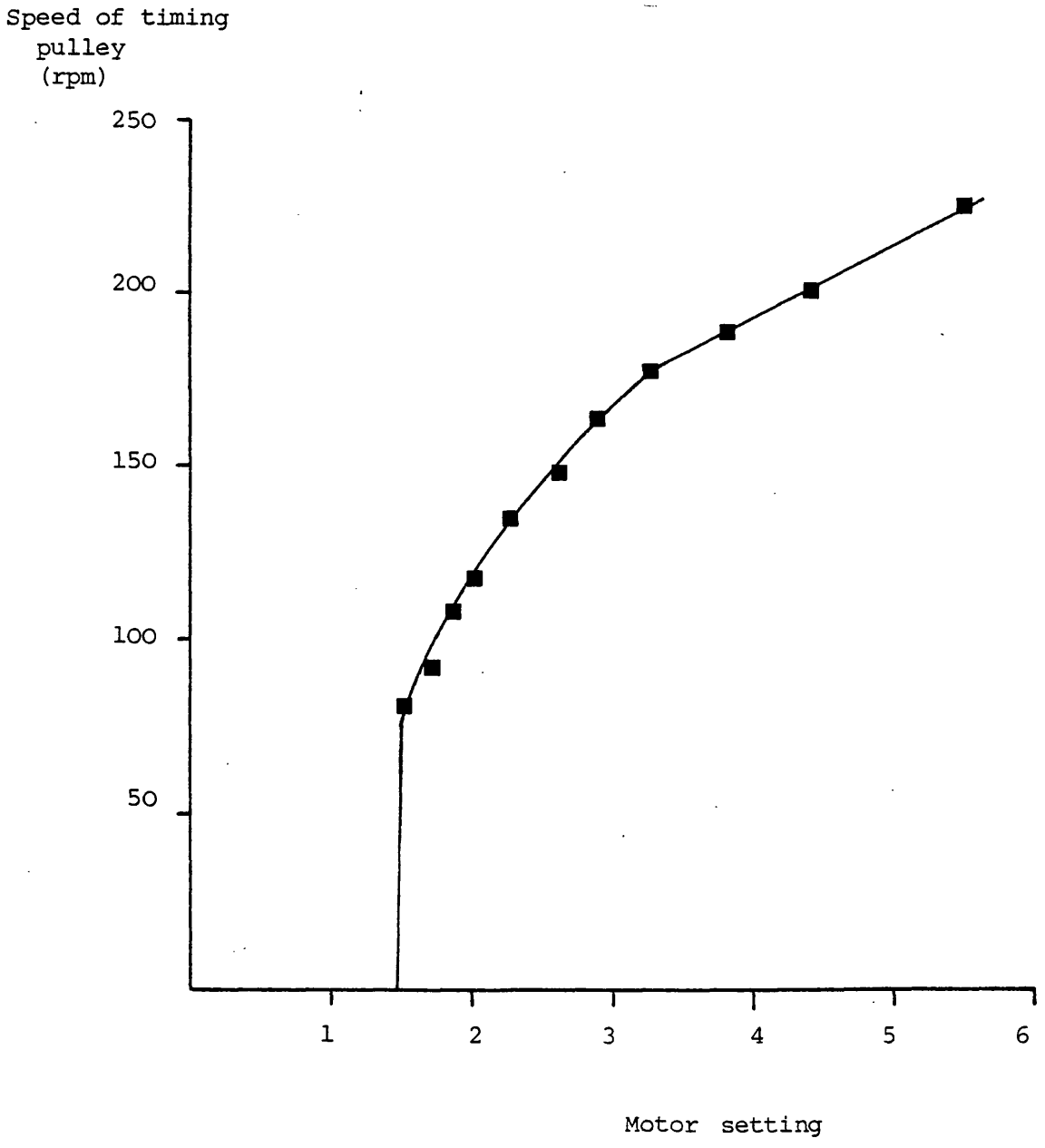

adjustment of variable resistor R_m in the timing circuit (Figure 4.20). During this adjustment, a 5% w/v solution of Pharmacoat 606 was sprayed to allow for any changes in the shutter movement resulting from the force of polymer solution and compressed air on the moving shutter. The closest to 1.94 seconds that the open time could be set was 1.925 secs (standard deviation 0.0127 secs). Open times ranging from 0.24 to 2.83 secs were available by variation of R_m, but an even greater range could be produced by substitution of components C_m and R_m, subject to a minimum of 33 msec. due to friction in the shutter bearing.

The interval between openings of the shutter was measured with a digital lap timer and adjusted, using variable resistance R_a of the timing circuit, to 25.02 secs (standard deviation 0.14), whilst spraying a 5% w/v solution of Pharmacoat 606 . Spray intervals from 7 to 40 seconds were available by variation of R_a and substitution of components R_a and C_a would allow an even greater range.

The spray time parameters were thus set to within one percent of the values derived from a 24" Accela-Cota (Table 4.10).

To prevent stressing and occasional detachment of the substrates on passage over the pulleys, a 5 mm thick layer of polyurethane foam was attached to the timing belt and the substrates stuck to this using contact adhesive (Thixofix,

Table 4.10 Comparison of the spray time parameters determined in the Accela-Cota and achieved on the model.

	Spray Interval	Spray Dwell Time	
Accela-Cota Measurement	24.8 secs S.D. 35.4 secs C.V. 142.7%	0.12 secs S.D. 0.0035 C.V. 2.92%	
Model requirements	24.8 secs	Pulley Speed 89.76 rpm	Shutter Open Time 1.94 secs
Model settings (10 replicates)	25.02 secs S.D. 0.14 C.V. 0.56%	90 rpm S.D. 0 C.V. 0%	1.925 secs S.D. 0.0127 C.V. 0.66%
Percentage error	0.89	0.27	0.77

Dunlop Ltd.). Forty 25.4 mm diameter substrates could thus be accommodated on the belt and coated under identical conditions.

Figures 4.23 and 4.24 show the complete model coating system. The timing pulley, revolving at 90 rpm, moves substrates through the spray region in 0.12 seconds and the electronically controlled shutter allows coating solution to pass for one revolution of the belt every 25 seconds (Figure 4.25). 4.13 $m^3 min^{-1}$ air at 90°C was provided by the axial fan and heating element, whilst the baffled fume cupboard had an exhaust capacity of 10.20 $m^3 min^{-1}$. The air flow pattern indicated by the arrows in Figure 4.23 was observed by placing a smoke canister (P.H. Smoke Products Ltd.) at the air intake of the axial fan. The optimized spray set up of a 2050 liquid nozzle and 120 air cap, was located 200 mm from the substrates attached to the timing belt. Compressed air, from cylinders was passed through a heat exchanger, shut-off valve and pressure gauge, to provide atomizing air at 0.28 MPa. The flow of liquid to the spray head was induced by a peristaltic pump and controlled via the pump speed and a metering valve.

This system therefore closely mimiced the conditions which had been successfully used for aqueous film coating in a 24" Accela-Cota.

4.3.2 Evaluation of The System

To evaluate the model, the rate at which film coatings

Figure 4.23. Diagrammatic representation of the model coating system

Key

A Compressed air cylinder

B Cylinder regulator

C Water jacket

D Shut off valve

E Pressure gauge

F 2050/120 spray nozzle

G Metering valve

H Peristaltic pump

I Shut off valve

J Coating suspension reservoir

K Axial fan

L Galvanized ducting with heating element

M Articulated ducting

N Variable transformer

O Moving shutter

P Fixed shutter

Q Waste suspension trough

R Timing belt

S Substrates to be coated

T Idler pulley

U Timing pulley

V Baffle

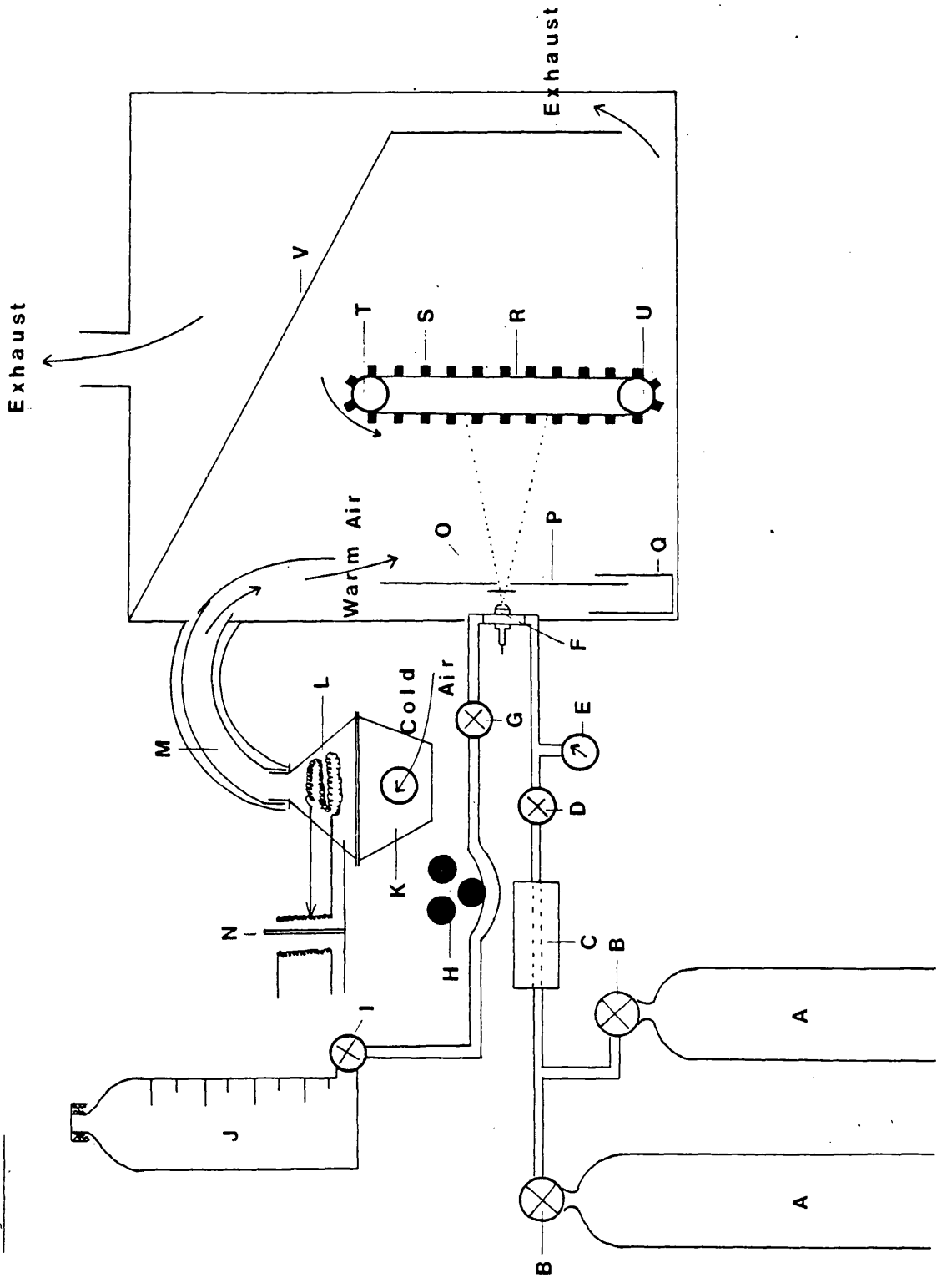
Exhaust
Exhaust
V
T
S
R
U
Warm Air
O
P
Q
F
L
Cold Air
G
E
M
D
K
N
H
C
B
I
A
J
A
B

Figure 4.23

Figure 4.24 Photograph of the model coating system.

Figure 4.25 Photograph of the coating area of the model system, showing the timing belt, shutter system and air inlet.

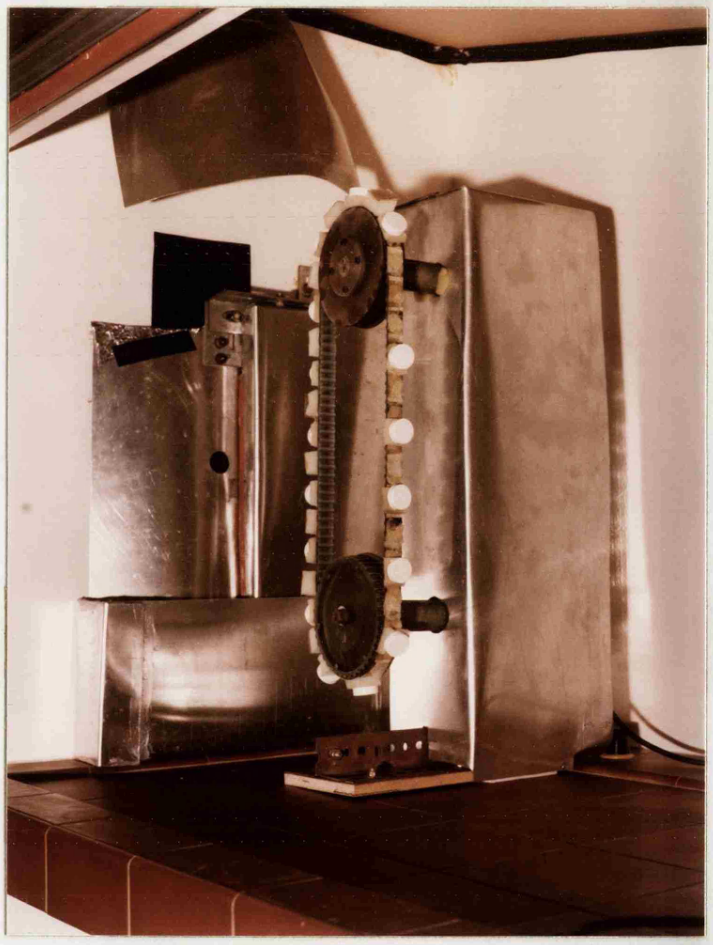

were built up and the water vapour permeabilities of films prepared in the Accela-Cota and on the model were compared.

4.3.2.1 Rate of Coating Deposition

a) Weight Increase: 10.32 mm diameter normal convex tablets were compressed from the lactose/Avicel formulation described in Section 4.3.1.2e. Five samples of ten tablets were removed at random, individually weighed to 0.01 mg (Unimatic CL4D, Stanton Instruments Ltd.) and the intra- and inter-sample variation calculated. Table 4.11 shows that both the intra- and inter-sample variations were under 1%. Analysis of variance showed that the within group variance (4.73) was greater than that between groups (3.80). An F test confirmed that the samples were not significantly different at the 5% level.

8 kg of these tablets were placed in the 24" Accela-Cota, pre-warmed for 10 minutes and coated with the following formulation:-

	% w/w
Pharmacoat 606	3.00
Klucel L.F.	3.00
Talc U.S.P.	0.91
Titanium Dioxide	3.01
F.D. and C. yellow No 6 aluminium lake (26% dye)	0.07
Purified water	90.01

Table 4.11 Intra- and Inter-sample weight variation for a batch of Lactose/Avicel tablets, showing analysis of variance data.

Sample number (K)	1	2	3	4	5
Mean tablet weight ($\bar{x}$ mg)	360.97	361.57	360.20	360.57	360.75
Standard deviation	1.76	1.70	3.45	1.38	1.97
C of V (%)	0.49	0.47	0.96	0.38	0.58
Sum of weights ($\sum_{1}^{10} x$)	3609.7	3615.7	3602.0	3605.7	3607.5
Sum of squares of weights ($\sum_{1}^{10} x^2$)	1303021.4	1307354.5	1297547.3	1300124.4	1301440.4
Number in sample (n)	10	10	10	10	10
A $\sum_{1}^{5}\sum_{1}^{10} x^2$		6,509,488.0			
B $\sum_{1}^{5} \frac{\left[\sum_{1}^{10} x\right]^2}{10}$		6,509,275.2			
C $\frac{\left[\sum_{1}^{5}\sum_{1}^{10} x\right]^2}{10 \times 5}$		6,509,260.0			
Between groups sum of squares		B - C = 15.2	Degrees of freedom 5 - 1	Variance $s_2^2 = \frac{15.2}{4} = 3.80$	
Within groups sum of squares		A - B = 212.8	10x5-5	$s_1^2 = \frac{212.8}{45} = 4.73$	
Total sum of squares		A - C = 228.0	10x5-1	$s_T^2 = \frac{228}{49} = 4.65$	

$$F = \frac{s_2^2}{s_1^2} = \frac{3.80}{4.73} = 0.80$$

$$F = 0.80 < F_{4,45}\ (0.05) = 2.61$$

This plasticizer-free formulation was chosen to avoid any error resulting from the loss of plasticizer during coating[106].

The following coating conditions were used:-

Liquid nozzle	2050
Air cap	120
Atomizing air pressure	0.28 MPa
Liquid pressure	69 KPa
Liquid feed rate	32 g min^{-1}
Inlet air temperature	89°C
Exhaust air temperature	42°C

The weight of coating deposited per tablet, assuming 100% efficiency was calculated as follows:-

Liquid spray rate	=	32 g min^{-1}
Solids content	=	9.99% w/w
Solid sprayed per minute	=	3.197 g min^{-1}
Number of tablets	=	$\frac{8000}{0.3608}$ = 22,172.95
Weight solids deposited per minute per tablet	=	1.442 x 10^{-4} g min^{-1} $tablet^{-1}$

Thus after 60 minutes 8.65 mg of coating would be deposited on each tablet.

At five minute intervals during the coating run, samples of ten tablets were withdrawn from the Accela-Cota, placed in a vacuum desiccator over magnesium perchlorate for two hours, to

remove any residual water and individually weighed to 0.01 mg. The data presented in Table 4.12 clearly demonstrates that the mean tablet weight only increased by 3.01 mg after 60 minutes coating, giving an indicated coating efficiency of 34.8%. This could be attributed to a very low coating efficiency, but a more probable explanation was that as the tablets were tumbled and heated in the coating pan, weight was lost due to abrasion and water loss from the cores. These explanations were corroborated by the large standard deviations observed, relative to those before coating (Table 4.11) and the mean weight decreasing 2.4 mg after the tablet bed had been heated for 10 minutes in the Accela-Cota prior to coating. Observations made by other workers[254] also supported this interpretation of the data.

Consequently the weight change of individual tablets could not be regarded as an accurate indication of the rate of film coating deposition.

b) Ingredient Assay

An alternative method of measuring the rate of coating build-up was to assay coated tablets for an ingredient of the film, such as the pigment. Initially the following formulation was prepared as being typical of coating suspensions:-

Table 4.12 The weight change of individual tablets (10 replicates) removed from the Accela-Cota at five minute intervals during aqueous film coating

Time (minutes)	Mean weight increase (mg)	Standard deviation	Coefficient of variation (%)
0	0.00	4.37	-
Pre-heated for 10 minutes	-2.42	6.84	283
5	0.00	2.48	-
10	-0.95	6.59	694
15	-0.87	3.79	436
20	3.68	1.98	54
25	-0.37	6.52	1762
30	1.44	6.22	432
35	2.69	4.96	184
40	4.29	4.42	103
45	4.91	3.09	63
50	1.53	4.91	321
55	3.54	3.62	102
60	3.01	5.39	179

	% w/w
Pharmacoat 606	4.81
Titanium dioxide	0.84
Propylene glycol	0.80
F.D. and C.Yellow No. 5 aluminium lake (25% dye)	0.08
Purified water	93.47
Percentage solids	6.53%

Aliquots of this suspension ranging from 30 to 250 mg were weighed (Model R20, Oertling Ltd.) into glass centrifuge tubes and dried in a vacuum desiccator. To displace the dye (tartrazine) from the aluminium lake,5 ml of 5 M hydrochloric acidwere added and the tubes shaken for 30 minutes. After centrifugation at 6,000 rpm (Bench Centrifuge, M.S.E. Ltd.) for 20 minutes, the supernatent was withdrawn and assayed spectrophotometrically (SP 500, Pye Unicam) using 4 cm path length microcells, at 434 nm, the wavelength of maximum absorbance.

A plot of weight of coating solids taken against absorbance at 434 nm clearly demonstrated that the Beer Lambert relationship was not obeyed by this system (Figure 4.26). Two possible explanations for the decrease in absorbance at higher solid contents were that the efficiency of dye extraction from the aluminium lake was limited, or that the dye was adsorbed by the titanium dioxide present in the coating suspension.

Further experiments, using alkaline extraction of the dye

Figure 4.26 Plot of weight of coating solids taken versus absorbance due to tartrazine at 434 nm after extraction from the aluminium lake with 5 M hydrochloric acid.

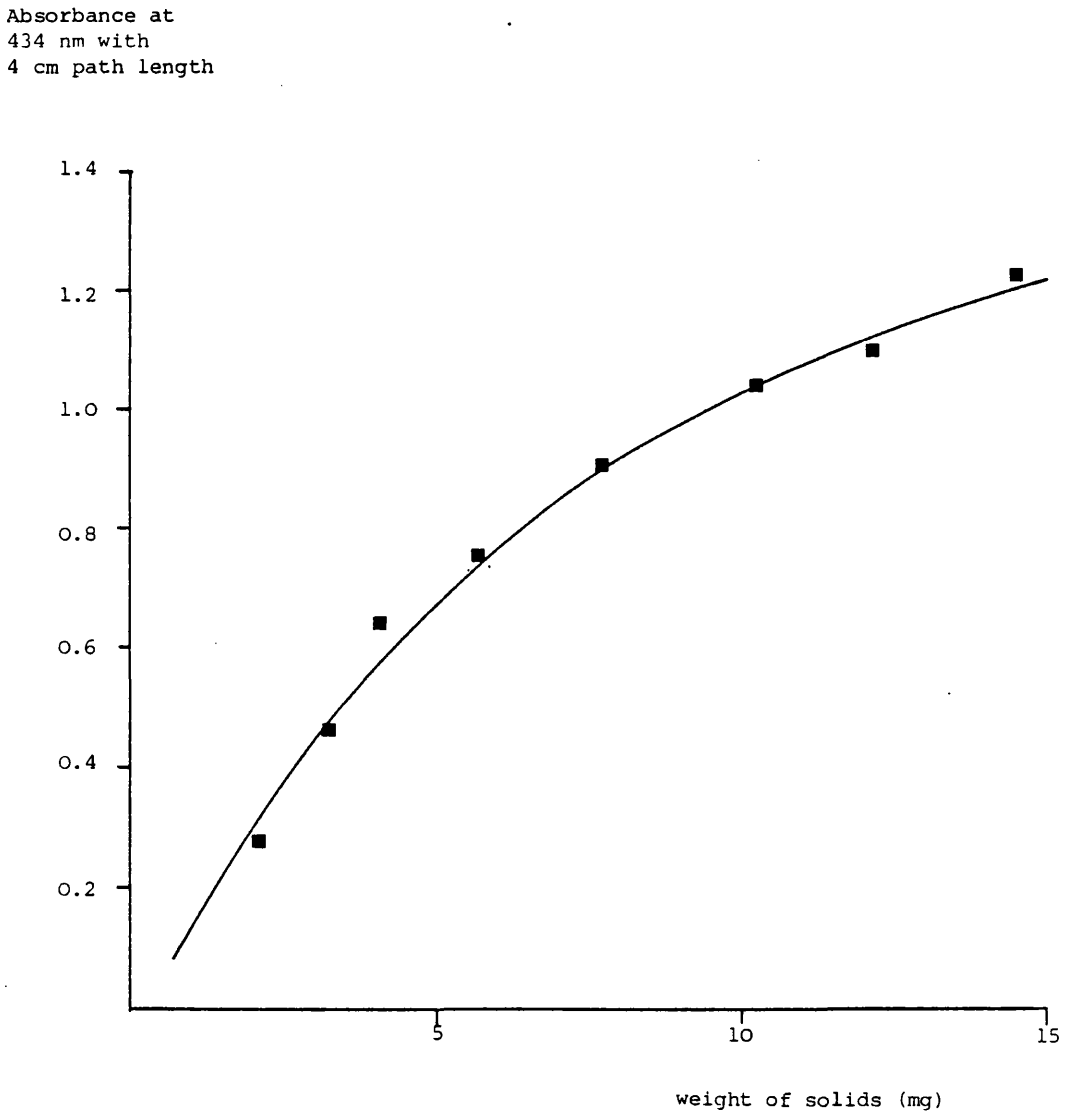

could not overcome this problem and in addition allowed an unidentified compound to be extracted from the tablet formulations, which would have interfered with the tartrazine peak.

c) Addition of a Marker Compound

As a result of the problems described above, evaluation of the rate of coating deposition was therefore carried out with the simple tartrazine-Pharmacoat solution described previously (section 4.3.1.2c). The tartrazine concentration in the stock coating solution used for this experiment, determined as before, was 0.281 % w/v.

To test the ability to recover the tartrazine after drying, a 1 in 10 dilution of the stock coating solution was prepared, aliquots weighed into 15 ml centrifuge tubes and evaporated to dryness under a stream of nitrogen, in a water bath at 90°C. The dried solids were redissolved by shaking with 10 ml of distilled water for 30 minutes and the absorbance at 425 nm measured after dilution where necessary. The thermal stability of tartrazine was demonstrated by the absorbance of a solution containing 0.0012 % w/v tartrazine and 0.02 % w/v Pharmacoat 606 being unchanged after 2 hours at 90°C.

From the weight of dilution taken (W_{soln}) and its solids content (0.528% w/v), the weight of solids (W_{solid}) added to each tube could be calculated:

$$W_{solid} = W_{soln} \cdot \frac{0.528}{100}$$

$$W_{solid}(mg) = W_{soln}(g) \cdot 5.28$$

Similarly the theoretical tartrazine concentration in the reconstituting fluid (C_c) can be calculated from its concentration in the dilution (0.281% w/v) and W_{soln}:-

$$C_c = W_{soln} \cdot \frac{0.0281}{100} \cdot \frac{100}{10}$$

$$C_c \text{ (\% w/v)} = W_{soln}(g) \cdot 0.00281$$

The detected tartrazine concentration (C_D) after drying and redissolving was calculated from the absorbance:-

$$C_D(\text{\% w/v}) = \frac{A_{425}}{338.70} \cdot DF$$

where DF is the dilution factor. Since tartrazine comprised 5.325% w/w of the solids, the detected weight of solids (W_D) can be calculated:-

$$W_D \text{ (mg)} = \frac{A_{425}}{338.70} \cdot DF \cdot \frac{10}{100} \cdot \frac{100}{5.321} \cdot 1000$$

$$W_D \text{ (mg)} = A_{425} \cdot DF \cdot 5.549$$

Table 4.13 compares the linear regression data obtained for the plots of theoretical tartrazine concentration (C_c), calculated from the weight of dilution, versus absorbance of the reconstituting fluid, with that of the Beer-Lambert plot determined earlier (Table 4.5). The 't' test showed that neither slope nor intercept were altered significantly by drying and subsequent reconstitution in 10 ml of water.

Table 4.13 Linear regression data for absorbances at 425 nm versus concentration for tartrazine in the presence of HPMC and after drying and reconstituting with distilled water.

	Slope ($\%^{-1}cm^{-1}$)	Standard Deviation of slope	Relative Standard Deviation of slope	Intercept	Standard Deviation of Intercept	Correlation Coefficient
Beer-Lambert Data from Table 4.5	338.70	4.97	1.47	-0.0102	0.0074	0.9997
Dried and Reconstituted	342.71	5.05	1.48	0.0036	0.0062	0.9991
$t_{slope} = 0.57$				$t_{intercept} = 1.43$		
t_{tab} (P=0.05) = 2.20						

Figure 4.27 shows the weight of solids detected (W_D) plotted against the weight of solids added (W_{solid}) and the regression analysis data given in Table 4.14 demonstrates that the assay technique could accurately detect the amount of coating added; the intercept and slope values lying within two standard deviations of zero and one respectively.

The effect of the presence of tablets on the recovery of tartrazine was investigated by adding one Lactose/Avicel tablet (Section 4.3.1.2e) to each centrifuge tube prior to the addition of the diluted coating suspension. After reconstitution in 10 ml of distilled water, it was necessary to centrifuge the suspension for 30 minutes at 6,000 rpm to sediment particles, since experiments using millipore filters or glass sinters had indicated that between 10 and 20% of the tartrazine could be removed during filtration. The absorbance of the resulting supernatent was read against a pooled blank derived from the supernatent above a tablet core to which coating solution had not been added. The mean absorbance of 10 individual blank assays was 0.150 (SD 0.008, CV 5.3%) indicating that although significant extraction and carry-over of particles from the core were occurring, they were fairly reproducible. Consequently the individual blank supernatents were pooled and the absorbance of the test supernatent read against this. If dilution was necessary prior to measurement, both the sample and pooled blank were diluted equally.

Figure 4.27 Weight of coating solids detected versus weight of solids taken, by analysis of the tartrazine added as a marker compound.

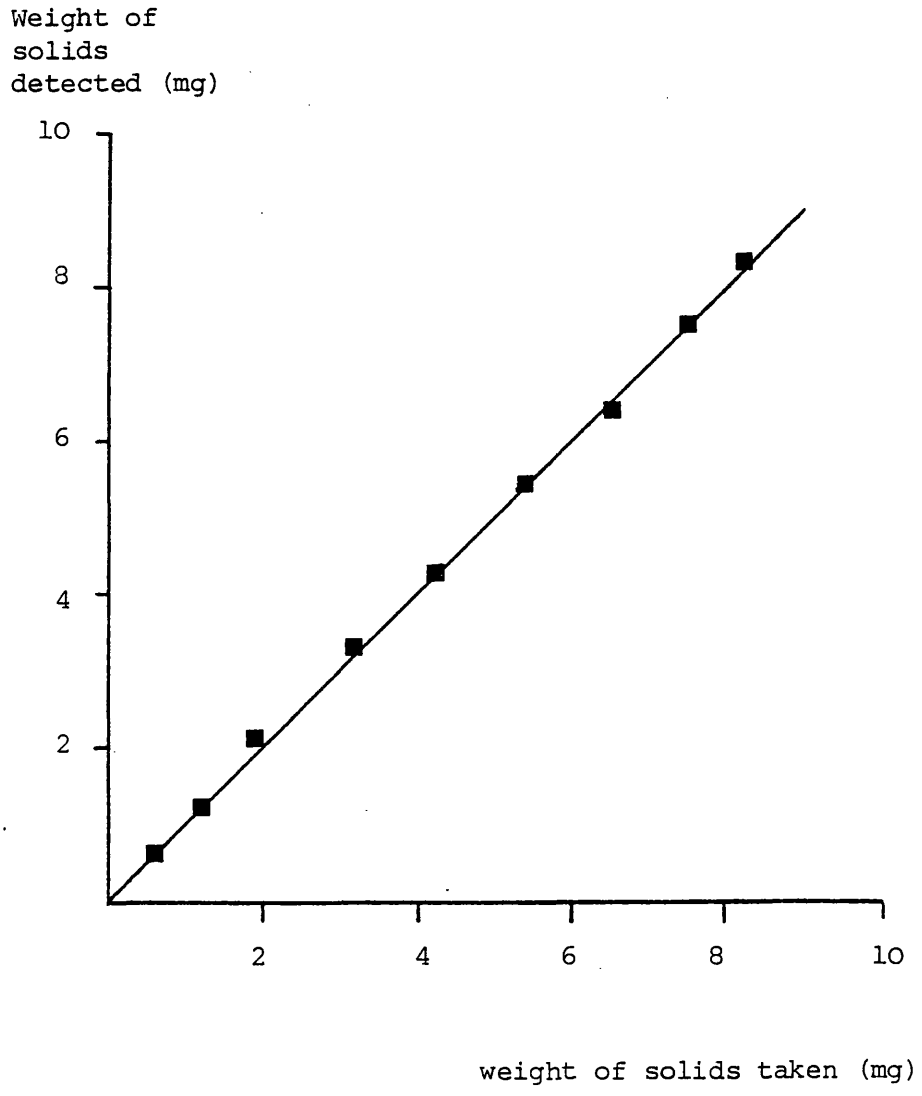

Table 4.14 Least squares regression data for the weight of solids detected versus weight of solids added, detected by an assay for tartrazine.

Slope	0.9966
S.D. slope	0.0116
Rel. S.D. Slope (%)	1.16
Intercept (mg)	0.0783
S.D. Intercept	0.0574
Correlation Coefficient	0.9995

S.D. = Standard Deviation

Rel. S.D. = Relative Standard Deviation

To enable the accuracy and reproducibility of recovery to be established, a second coating solution was prepared, the tartrazine concentration determined as 0.279% w/v and the experiment repeated.

The absorbance was plotted against the theoretical concentration of tartrazine, calculated from the weight of diluted coating solution taken (Figure 4.28). Least squares regression analysis gave the data in Table 4.15. Both plots were linear and appeared coincident, although they did not pass through the origin; the relative standard deviation of the intercepts being 23.7 and 18.4%. The 't' test confirmed that neither slope nor intercept were significantly different from each other, indicating that the assay technique was reproducible. The combined data gave a mean slope and intercept, in the presence of tablet cores, of $314.47\%^{-1}cm^{-1}$

Figure 4.28 Graph of absorbance at 425 nm against tartrazine concentration calculated from the volume of coating solution taken, in the presence of Lactose/Avicel tablets

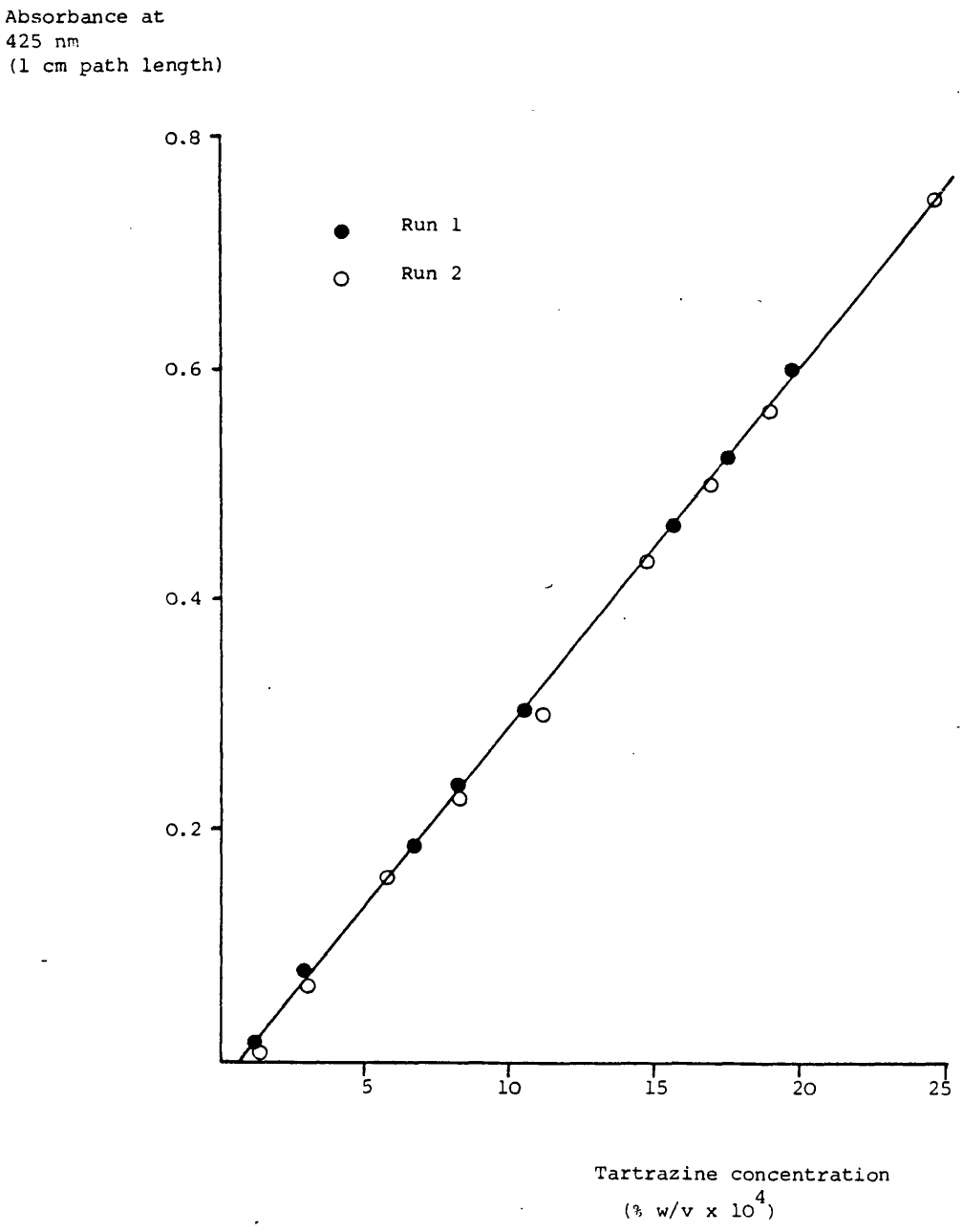

Table 4.15. Least squares regression data of the absorbance at 425 nm versus concentration for tartrazine in the presence of HPMC, after drying with a tablet core and reconstituting with distilled water

Experiment	Slope ($\%^{-1}cm^{-1}$)	Standard Deviation of slope	Relative Standard Deviation of slope	Intercept	Standard Deviation of Intercept	Correlation Coefficient
1	311.95	3.37	1.08	-0.0173	0.0041	0.9997
2	316.98	4.29	1.35	-0.0320	0.0059	0.9994
t_{slope} = 0.92				$t_{intercept}$ = 2.04	$t_{tab}(P=0.05)$ = 2.16	

(S.D. 3.56) and -0.0247 (S.D. 0.0104) respectively. Thus the slope, but not intercept, was significantly different from the extinction coefficient obtained in the absence of tablets (Table 4.5). (t_{slope} = 3.97, $t_{intercept}$ = 1.13, t_{tab} (P=0.05) = 2.26). The observed decrease in the percentage extinction coefficient from 338.70 to 314.47$\%^{-1}cm^{-1}$ can be explained by adsorption of tartrazine by the solids present in the tablet core. However, since these changes were reproducible, (Figure 4.28 and Table 4.15), the tartrazine content in the presence of tablets was calculated using the latter values of slope and intercept (314.47 and -0.0247 respectively). In addition, it should be noted that extent of adsorption of the tartrazine by the cores was dependent upon the nature and batch of raw materials used in the tablet manufacture. Preliminary experiments using tablets containing 88% w/w calcium phosphate demonstrated that approximately 27% of the tartrazine was lost on contact with the cores, whilst Lactose/Avicel tablets prepared from a different batch of ingredients did not significantly alter the slope and intercept values from those recorded in Table 4.5 ($E^{1\%}_{1cm}$ = 347.11, S.D. 9.86, Intercept -0.038, S.D. 0.028; $t_{calc\ slope}$ = 0.76, $t_{calc\ intercept}$ = 0.95, t_{tab} (P=0.05) = 2.08).

A coating solution containing 0.279% w/v tartrazine and 5% w/v Pharmacoat 606 was applied to 8 kg of 10.32 mm diameter normal convex tablets in the Accela-Cota, under the following conditions:

Liquid nozzle	2050
Air cap	120
Air pressure	0.28 MPa
Liquid pressure	69 KPa
Liquid feed rate	28.2 g min^{-1}
Inlet air temperature	90°C
Exhaust air temperature	41°C
Time	60 minutes
Total weight sprayed	1690 grams
Mean tablet weight	385 mg
Theoretical weight deposited per tablet after 60 minutes	4.29 mg

At 10 minute intervals, 10 tablets were removed and the weight of coating deposited on each tablet determined by the technique described above.

The data presented in Figure 4.29 and Table 4.16 indicate that the rate of coating deposition in the Accela-Cota was linear, but did not pass through the origin. The coating efficiency was 87.7%. From the large standard deviation bars, it was clear that mixing within the Accela-Cota was very poor, leading to an uneven distribution of coating between the tablets. This added further weight to the data obtained in Section 4.3.1.2e, which showed large variations in the time interval between passages through the spray. Such mixing problems had been identified in the past, especially with the larger diameter Accela-Cota, by the presence of relatively uncoated tablets

Figure 4.29 The weight of film coating deposited on each tablet versus time for a coating run in the 24" Accela-Cota (showing the Standard Deviation bars)

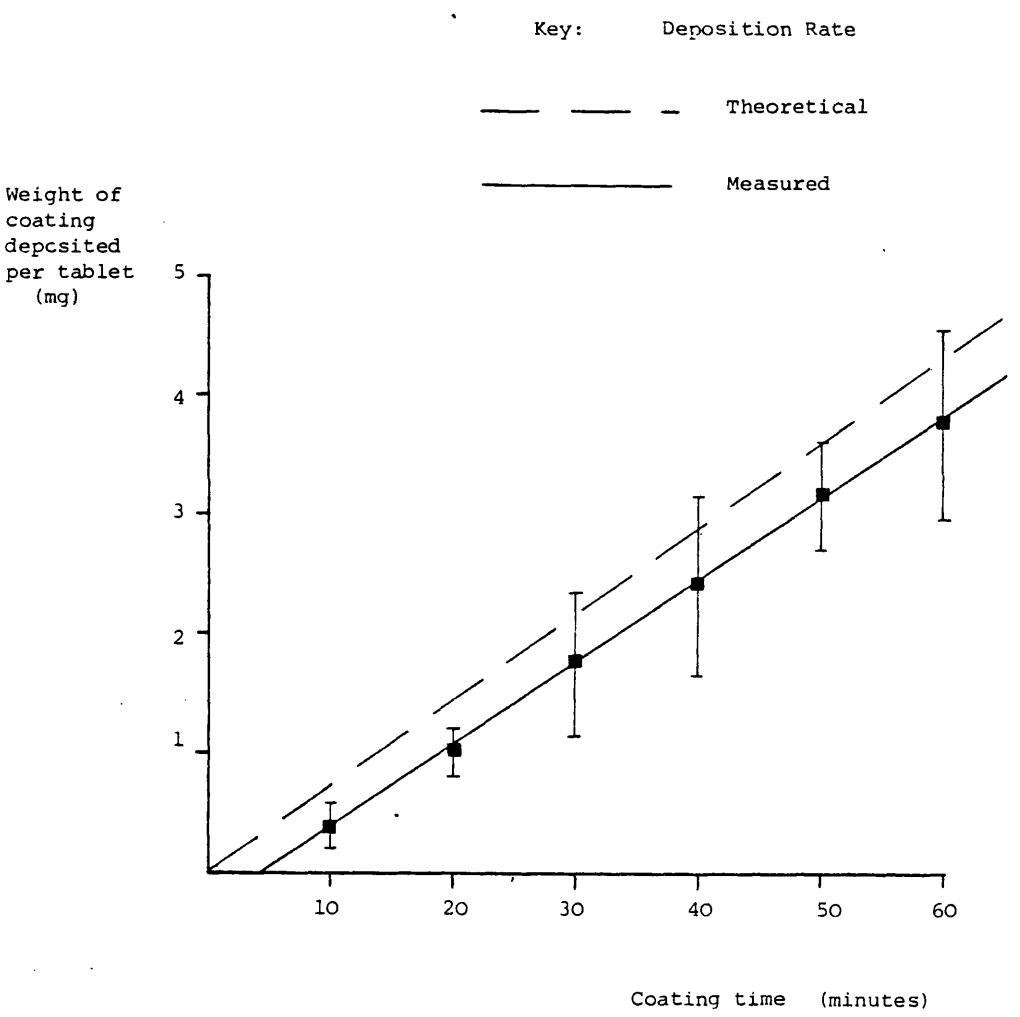

Table 4.16 The deposition of film coating solids on individual tablets, during aqueous film coating in a 24" Accela-Cota.

Time (minutes)	Mean weight of solids deposited (mg tablet^{-1})	Standard Deviation	Coefficient of Variation (%)
10	0.39	0.21	54.01
20	1.02	0.22	21.57
30	1.75	0.61	34.96
40	2.40	0.75	31.06
50	3.16	0.45	14.37
60	3.76	0.82	21.83

Least squares regression data

Slope = 6.8232×10^{-2} mg min^{-1} tablet^{-1}

Standard Deviation = 0.0902×10^{-2}

Relative S.D. = 1.32%

Intercept = -0.3069 mg tablet^{-1}

Standard Deviation = 0.0351

Correlation coefficient = 0.9997

after quite long process times[254].

The negative intercept may have arisen as a consequence of the poor mixing, since a time interval may have been required before the compacts were presented to the spray. The possibility that adsorption of the dye by the pipework of the spray gun created the negative intercept was eliminated, since the absorbance of a 1 in 250 dilution of the coating solution was unchanged by prolonged contact with the tubing.

To allow the comparison of deposition rates on different substrates, the same surface area must be considered. Thus the surface area of a 10.32 mm diameter normal convex tablet was calculated using equation 4.11:-

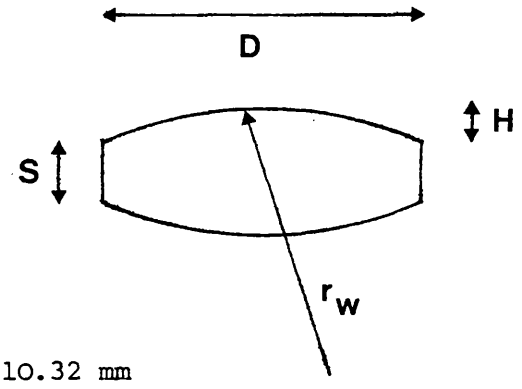

D = 10.32 mm

H = 1.09 mm

——— From tooling manufacturer's drawings

r_w = 12.70 mm

S = Thickness - 2H = 4.8 - 2 x 1.09 mm = 2.62 mm

$$S_A = \Pi DS + 2(2r_w \Pi H) \quad \text{...(equation 4.11)}$$

$$= (\Pi \times 10.32 \times 2.62) + 2(2 \times 12.70 \times \Pi \times 1.09)$$

$$= 258.90 \text{ mm}^2$$

The rate of deposition per unit area, in the Accela-Cota, was thus calculated as 2.6354×10^{-4} mg min^{-1} mm^{-2} (S.D. 0.0348×10^{-4}) with an intercept of -1.1854×10^{-3} mg mm^{-2} (S.D. 0.1356×10^{-3}).

To evaluate the rate of coating deposition with the model system, a solution containing 0.288 % w/v tartrazine and 5% Pharmacoat 606 was applied to 25.4 mm squares of glass, attached to the timing belt, using the following conditions:-

Liquid nozzle	2050
Air cap	120
Air pressure	0.28 MPa
Liquid feed rate	28 ml min^{-1}
Inlet air temperature	88^{o} C
Exhaust air temperature	43^{o} C
Time	60 mins
Total volume sprayed	1680 ml

At 10 minute intervals 5 glass plates were removed, each placed in 10 ml of distilled water, shaken for 30 minutes and the absorbance at 425 nm measured against a distilled water blank. The weight of coating deposited was calculated as described previously. To overcome slight variations in the area of the glass plates, these were measured (Model 1140 Vernier Callipers, Moore and Wright Ltd.) and the weight of coating deposited per unit area calculated.

The data obtained with the model system is presented in Figure 4.30 and Table 4.17 and demonstrates that the coating deposition on the model was also linear. The reason for the positive intercept was unclear, but may have been associated with a slight decrease in the spray rate during the first 5 minutes. This phenomenon was observed in some later experiments and has been attributed to either a slight deformation in the tubing used with the peristaltic pump, or a settling of the metering valve stem after the initial adjustment.

The coating was built up much more evenly on the model system, with coefficients of variation in the range 2 - 7% rather than the 15 to 55% observed for the Accela-Cota. This was expected since the model did not create random variations in the time interval between passages through the spray area for individual substrates.

Comparison of regression data for coating deposition in the Accela-Cota and model system, under identical process conditions, demonstrated that the model system built up the film coating almost four times faster than the Accela-Cota (Table 4.18). There were two main reasons for this discrepancy, neither of which could be overcome easily. Firstly, on the model system the substrates always passed through the centre region of the spray area, where the liquid density was greatest. Even using the 2050/120 nozzle combination, a tablet passing around the

Figure 4.30 The weight of film coating deposited per unit area versus time for a coating run in the model system (showing the standard deviation bars)

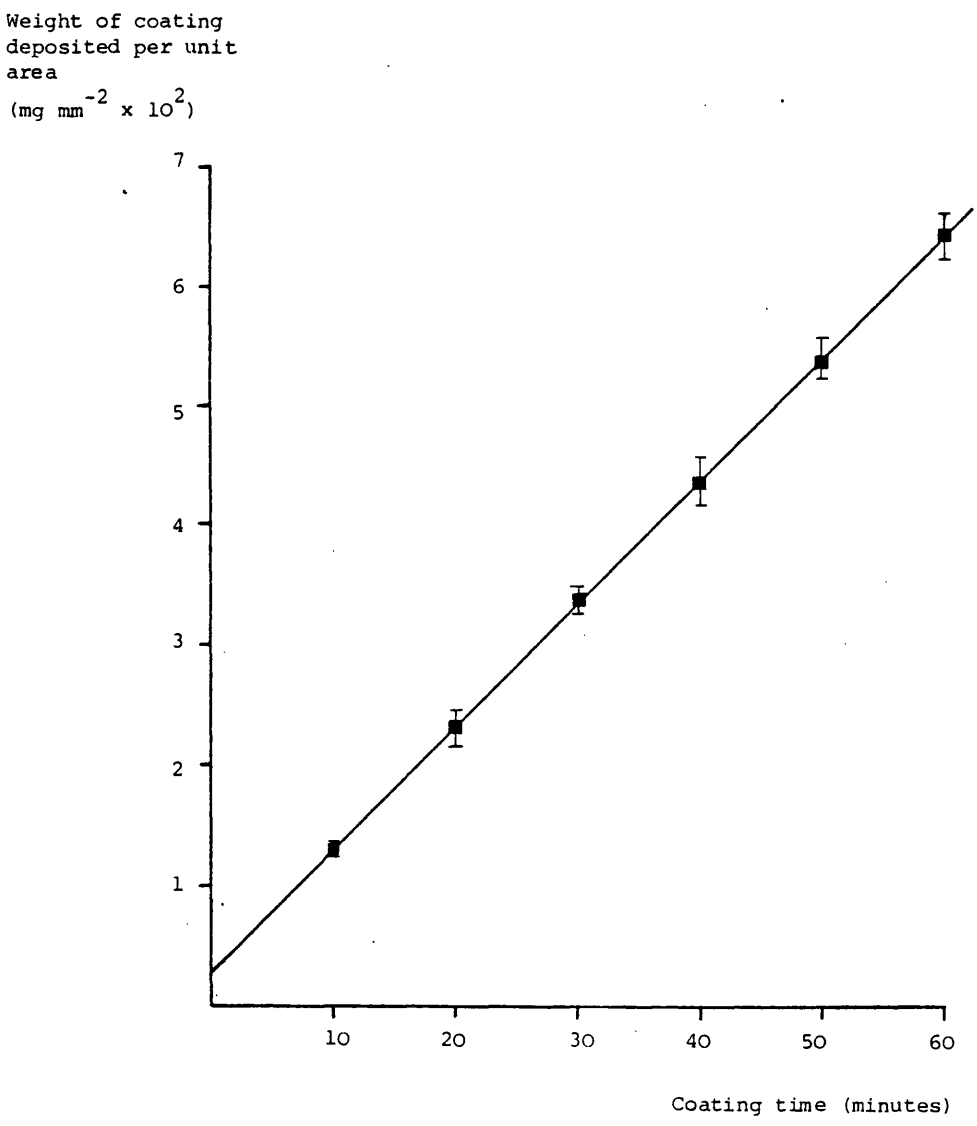

Table 4.17 The deposition of film coating solids on glass plates during coating on the model system

Time (mins)	Mean weight of solids deposited per unit area ($mg\ mm^{-2} \times 10^{2}$)	Standard Deviation ($\times 10^{3}$)	Coefficient of variation (%)
10	1.31	0.58	4.43
20	2.30	1.66	7.22
30	3.37	0.75	2.23
40	4.35	2.54	5.84
50	5.38	1.73	3.22
60	6.40	1.93	3.02

Least squares regression data

Slope = 10.191×10^{-4} mg mm^{-2} min^{-1}

Standard Deviation = 0.0459×10^{-4}

Relative S.D. = 0.45%

Intercept = 2.8467×10^{-3} mg mm^{-2}

Standard Deviation = 0.1785×10^{-3}

Correlation coefficient = 0.9999

Table 4.18 Least squares regression data for the deposition of coating solids per unit area in the Accela-Cota and model system

	Slope ($mg\ min^{-1}\ mm^{-2} \times 10^{4}$)	S.D. Slope ($\times 10^{4}$)	Rel. S.D. Slope (%)	Intercept ($mg\ mm^{-2} \times 10^{3}$)	S.D. Intercept ($\times 10^{3}$)
Accela-Cota	2.6354	0.0348	1.32	-1.1854	0.1356
Model system	10.191	0.0459	0.45	2.8467	0.1785

t_{slope} = 131.17

t_{int} = 17.99

t_{calc} = 2.31 (P=0.05)

edge of the spray area would receive less than half of the quantity of material deposited on one passing through its centre (Section 4.3.1.2c, Figure 4.6). Re-analysis of the black and white high speed cine film indicated that tablets were often forced around the edges of the spray area and thus picked up less coating than would otherwise be expected. Such an action was impossible to mimic and its effects could not be reduced any further since all the spraying systems evaluated showed a dense centre region.

A further inaccuracy was that the model system produced a dwell time within the spray of 0.12 seconds for the whole surface of the substrate, whilst a tablet passing through the spray area in the Accela-Cota possessed a tumbling action, such that each surface only faced the spray directly for some

fraction of 0.12 seconds. Since this tumbling action was non-uniform it was impossible to calculate a reliable factor by which the dwell time on the model system could be reduced.

4.3.2.2 Water Vapour Permeability

The properties of film coatings derived from tablets coated in the 24" Accela-Cota and on the model were very difficult to compare since most tests required an area of film greater than that obtainable from conventionally sized tablets. However, a miniature water vapour permeability cell was developed to accept films approximately 8 mm in diameter (Figure 4.31).

An autosampler vial (ASA 100, 0.8 ml, Perkin Elmer Ltd.) was filled with approximately 0.6 g of magnesium perchlorate and a thin film of Apiezon M grease (Edwards High Vacuum Ltd.) applied to the top edge. The test film was cut using a number 4 cork borer (i.d. approximately 8 mm) and placed across the neck of the vial. A hole was cut in the cap and silicone rubber septa of the sample vial using a number 1 cork borer, producing a hole of mean diameter 4.047 mm (S.D. 0.003, Model 1140 Vernier Callipers, Moore and Wright Ltd.). The cap was crimped onto the vial, sealing the film over the desiccant with an exposed area of 1.2863×10^{-5} m^2. The complete vial was then placed in a desiccator containing a saturated sodium chloride slush at $30^{\circ}C$ (vapour pressure 23.8 mm Hg) and the weight increase, due to the passage of water vapour across the film, recorded to 0.01 mg (Unimatic, Stanton Instruments Ltd.) at 12 hourly intervals.

Figure 4.31 Diagrammatic representation of the miniature cell used in the determination of the water vapour permeability of small areas of film coatings.

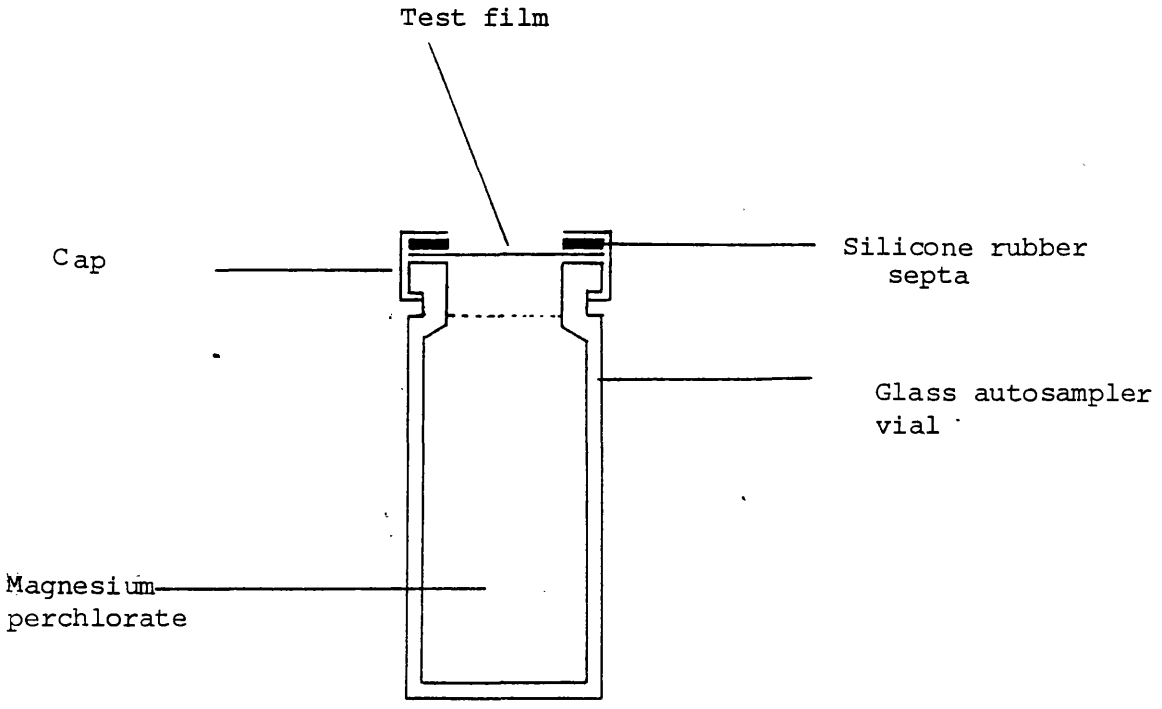

The water vapour permeability, P, was thus calculated from equation 4.12:-

$$P = \frac{R_{WT}\, L}{A\, C_D} \qquad \ldots \text{(equation 4.12)}$$

R_{WT} = rate of water vapour transmission ($g\ sec^{-1}$) (from regression analysis slope of weight increase versus time)

L = Film thickness (m)

A = Film area ($1.2863 \times 10^{-5}\ m^2$)

C_D = Concentration gradient across film ($22.687\ g\ m^{-3}$)

The concentration gradient across the film was calculated from the vapour pressure at 30°C (23.8 mm Hg)[244] using the Ideal Gas Law. Two 8 kg batches of 10.32 mm diameter normal convex tablets (lactose/Avicel formulation, section 4.3.1.2e) were coated with a 5% w/v solution of Pharmacoat 606 in the Accela-Cota under the following conditions:-

	Accela-Cota	Model
Liquid nozzle	2050	2050
Air cap	120	120
Air pressure	0.28 MPa	0.28 MPa
Liquid pressure	69 KPa	-
Liquid feed rate	30 g min^{-1}	30 ml min^{-1}
Inlet air temperature	90°C	88°C
Exhaust air temperature	43°C	44°C

Twenty tablets were removed at 30 minute intervals for 150 minutes and the films carefully detached using the technique described in Section 5.2 . 150 10.32 mm diameter tablets, from the same manufacturing lot, were stuck to the belt of the model coating system and coated with the same 5% w/v solution of Pharmacoat 606 under the conditions shown above. 15 tablets were removed at 10 minute intervals for 60 minutes and the films carefully detached.

The thickness of the detached films, produced in the Accela-Cota and the model system, were measured using a high precision micrometer (L.S. Starrett and Co. Ltd.) and films of similar thickness (87 - 106 μm) selected for use in the miniature permeability cell. The rate of water vapour transmission was thus measured for each of four films from the replicate coating runs in the Accela-Cota and the model system. In addition, the rate of water uptake in the absence of a film and across an aluminium foil sheet (Bacofoil, 19 μm thick) were recorded.

Table 4.19 clearly demonstrates that the water uptake across an aluminium film was negligible; both slope and intercept values lay within $\pm$ two standard deviations of zero. Thus a good seal was obtained between the neck of the vial and the film. The rate of water uptake in the absence of the film was approximately ten times that with films present, indicating that the uptake was limited by permeation through the film and not reaction with the desiccant.

Table 4.19 Least squares regression data for the uptake of water vapour across films in a miniature permeability cell. *S.D. = Standard Deviation; Rel. S.D. = Relative Standard Deviation

Film Origin	Film Thickness (μm)	Rate of water vapour transmission: Mean ($g sec^{-1} \times 10^{7}$)	* S.D. ($\times 10^{7}$)	* Rel. S.D. (%)	Intercept: Mean ($g \times 10^{3}$)	S.D. ($\times 10^{3}$)	Correlation Coefficient
Absent	-	3.7349	0.1228	3.29	5.1049	2.8599	0.9978
Foil	19	0.0024	0.0018	73.77	-0.0373	0.0415	0.5611
		0.0001	0.0001	86.00	-0.0235	0.0171	0.5026
Run 1	96	0.4332	0.0178	4.11	-0.2476	0.2623	0.9958
	95	0.4460	0.0095	2.13	0.1292	0.1395	0.9989
Accela-Cota	92	0.3749	0.0089	2.34	0.2872	0.1311	0.9986
	87	0.4999	0.0112	2.24	0.2161	0.1646	0.9988
Run 2	93	0.3295	0.0119	3.61	0.3065	0.1747	0.9968
Accela-Cota	87	0.3228	0.0092	2.83	0.2836	0.1347	0.9980
	99	0.3870	0.0131	3.39	0.3265	0.1929	0.9972
	90	0.6309	0.0133	2.11	0.3883	0.1954	0.9989
Run 1	95	0.2643	0.0173	6.55	0.5120	0.2539	0.9895
Model System	105	0.5668	0.0067	1.18	0.0295	0.0982	0.9997
	109	0.2924	0.0099	3.41	0.3167	0.1460	0.9971
	106	0.3680	0.0101	2.70	0.3377	0.1484	0.9981
Run 2	88	0.5121	0.0104	2.04	0.2925	0.1530	0.9990
Model System	94	0.2660	0.0107	3.99	0.5010	0.2359	0.9973
	99	0.3867	0.0111	2.87	0.3256	0.1991	0.9979
	90	0.6300	0.0139	2.21	0.3782	0.1594	0.9989

In the presence of film coatings, the intercept values were effectively within $\pm$ two standard deviations of zero, as expected for a technique which measured the total weight of permeant within and crossing the film. The water vapour permeability coefficients were calculated from the transmission rates and are listed in Table 4.20. Analysis of variance (Table 4.21) indicated that the within group variance (0.1707) was larger than the between group variance (0.0083) and an 'F' test confirmed that the water vapour permeability of films produced on the model system and in the Accela-Cota were not significantly different ($F = 0.05$, $F_{3,12}(P=0.05) = 3.49$).

The large variations observed within the groups can, in part, be attributed to errors inherent in the experimental method. The film thickness, measured with a micrometer, contained an error due to the presence of tablet particles adhering to the lower surface. Despite choosing films of similar measured thickness removed from identical tablets, considerable variation in the size and quantity of adhering particles was possible, leading to differences in the error associated with the film thickness. In addition, the area of film exposed to the permeant was subject to considerable variation, since during crimping of the cap a slight deformation of the silicone rubber seal could produce a relatively large change in this small area.

Thus using this technique, the water vapour permeabilities of films produced in the 24" Accela-Cota and on the model system, were not significantly different.

Table 4.20 The water vapour permeability coefficients for HPMC films prepared under similar conditions in the Accela-Cota and the model system

Film Origin	Film Thickness (μm)	Water vapour permeability coefficient ($m^2 s^{-1} \times 10^8$)	S.D. ($\times 10^8$)	Mean water vapour permeability coefficient ($m^2 s^{-1} \times 10^8$)	S.D. ($\times 10^8$)	C.V. (%)
Run 1 Accela-Cota	96	1.4251	0.0586	1.3873	0.1395	10.06
	95	1.4519	0.0393			
	92	1.1819	0.0281			
	87	1.4903	0.0334			
Run 2 Accela-Cota	93	1.0501	0.0379	1.3178	0.4443	33.72
	87	0.9623	0.0274			
	99	1.3129	0.0444			
	90	1.9457	0.0410			
Run 1 Model system	95	0.8604	0.0563	1.3322	0.5100	38.29
	105	2.0394	0.0241			
	109	1.0921	0.0370			
	106	1.3367	0.0367			
Run 2 Model System	88	1.5442	0.0312	1.4140	0.4537	32.09
	94	0.8568	0.0345			
	99	1.3119	0.0377			
	90	1.9429	0.0429			

S.D. = Standard Deviation

C.V. = Coefficient of Variation

Mean Coefficient = 1.3628×10^{-8} $m^2 s^{-1}$

S.D. = 0.0454×10^{-8}; C.V. = 3.33

Table 4.21 Analysis of variance data for the water vapour permeability of HPMC films prepared under similar coating conditions in the Accela-Cota and the Model System.

Film Origin	Accela-Cota Run 1	Accela-Cota Run 2	Model System Run 1	Model System Run 2
Mean permeability ($m^2\ s^{-1}$) (transformed by 10^8)	1.3873	1.3178	1.3322	1.4140
Standard deviation	0.1395	0.4443	0.5100	0.4537
C of V (%)	10.06	33.72	38.29	32.09
Sum of weights ($\sum_1^4 x$)	5.5492	5.2710	5.3286	5.6558
Sum of squares of weights ($\sum_1^4 x^2$)	7.7568	7.5382	7.8789	8.6146
Number in sample (n)	4	4	4	4
A $\sum_1^4 \sum_1^4 x^2$	31.7885			
B $\sum_1^4 \frac{(\sum_1^4 x)^2}{4}$	29.7398			
C $\frac{(\sum_1^4 \sum_1^4 x)^2}{4 \times 4}$	29.7150			
Between groups sum of squares	B - C = 0.0248		Degrees of freedom 4-1	Variance S_2^2=0.0083
Within groups sum of squares	A - B = 2.0487		4x4-4	S_1^2=0.1707
Total sum of squares	A - C = 2.0735		4x4-1	S_T^2=0.1382

$$F = \frac{S_2^2}{S_1^2} = \frac{0.0083}{0.1707} = 0.05$$

$$F = 0.05 < F_{3,12}(0.05) = 3.49$$

5. EVALUATION OF THE APPEARANCE, ELEMENTAL DISTRIBUTION AND THICKNESS OF FILM COATINGS

5.1 Electron Microscopy

a) Scanning Electron Microscopy (S.E.M.)

Three instruments were used during this work, a 100 CX combined transmission and S.E.M. (Joel Instruments Ltd.), a 35C S.E.M. (Joel Instruments Ltd.) and an S4 Steroscan S.E.M. (Cambridge Instruments Ltd.). In all cases the samples were sputter coated (Polaron Ltd.) with gold to enhance their ability to dissipate surplus electrons, thus preventing a negative charge developing which would repel the incoming electron beam . The layer of gold (10 - 20 nm) did not affect detail visible under the S.E.M. .

Depending on their nature, samples were stuck to the carrier stubs using either double-sided tape (3 M Ltd.) or silver high conductivity paste (Electrodag 915, Acheson Colloids Co.). Coated tablets were examined after fracture had exposed the coating/core boundary. Fracture at room temperature often caused the film coating to become detached from the substrate and tear rather than break cleanly. Therefore to prevent fracture stresses disturbing the coating/core boundary, tablets were embedded in Spurr's Resin and cut with a microtome or fractured. No detail could be seen in the cut surfaces since they completely lacked relief and the fractured surfaces indicated that part of the coating formulation had dissolved in the resin, making this preparation technique unsatisfactory (Figure 5.1).

Figure 5.1 Scanning Electron Micrographs of film coated tablets embedded in Spurr's Resin

20 µm

To prevent plastic deformation and tearing of the coating, a freeze fracture technique was then developed and used for all subsequent S.E.M. of coated tablets. The tablets were dropped into liquid nitrogen, left to cool for 3 minutes and fractured by applying force to a pointed metal seeker. Thus the fracture was tensile and apart from the area under the seeker the film was undamaged. To prevent atmospheric moisture condensing and freezing on the fragments, they were transferred to a desiccator over phosphorus pentoxide until the remaining liquid nitrogen had evaporated and the sample regained room temperature.

b) Energy Dispersive Analysis of X-Rays (EDAX)

The 100 CX instrument was equipped with an EDAX facility enabling the distribution of certain elements within the coating and core to be identified and analysed semi-quantitatively.

When incoming electrons of several KeV energy collide with the surface of the specimen, an electron can be ejected from its orbit in an atom, leaving the atom in an excited state. When an electron fills this vacant site in the orbital and the atom returns to its stable state, the energy difference can be emitted as an X-ray of appropriate wavelength. Since the energy and hence wavelength of the emitted X-ray is specific to the atom and electron orbitals involved in the transition, the elements present in the surface can be identified.

For quantitative analysis of these X-rays a wavelength dispersive

spectrometer(WDS) is used, in which the intensity of particular X-ray lines is measured after separation by diffraction.

For qualitative and semi-quantitative analysis an energy-dispersive detection system is employed (EDAX), in which an emitted X-ray strikes a semiconductor detector, producing an electrical current of under 1 μs duration, which is proportional to the energy of the incident X-ray. These current pulses are amplified and passed to a multichannel analyser which classifies them into different energy levels, allowing the intensity of X-rays at each level to be recorded. X-rays of energy less than 1 KeV cannot be detected using this system, effectively preventing the analysis of all elements lighter than sodium. Thus to prevent background interference from the specimen holder, samples for EDAX are usually fixed to the stub with graphite paste (E. Mscope Laboratories Ltd.) and coated with carbon instead of gold. The latter was unnecessary in this work since the X-ray lines for gold are well separated from those due to the components of the tablet core and coating.

To enable the positive identification of the coating-core boundary, which was often unclear on a S.E.M. (Figure 5.2a), tablet cores composed of 87% w/w calcium phosphate were coated with a suspension containing 5% w/v Pharmacoat 606 and 1% w/v titanium dioxide. Samples were freeze-fractured and examined by S.E.M. and EDAX. Figure 5.2a demonstrates that the film was approximately 20 μm thick but the coating-core boundary was

Figure 5.2 SEM and EDAX of calcium phosphate tablets coated with 80% w/pw HPMC and 20% w/pw titanium dioxide

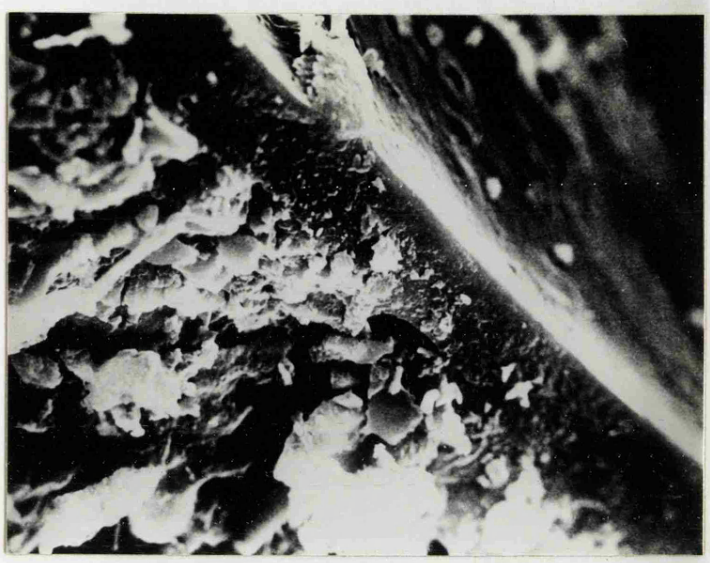

a. S.E.M.

40 µm

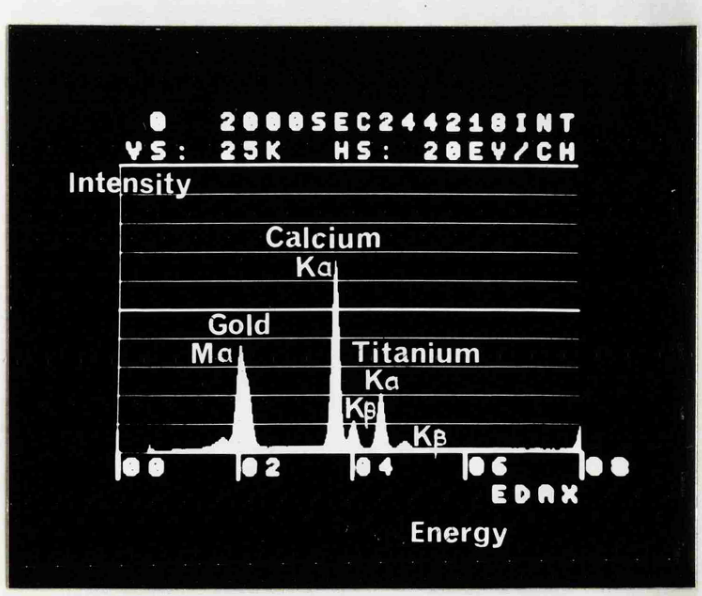

b. EDAX spectrum

Figure 5.2 SEM and EDAX of calcium phosphate tablets coated with 80% w/pw HPMC and 20 w/pw titanium dioxide

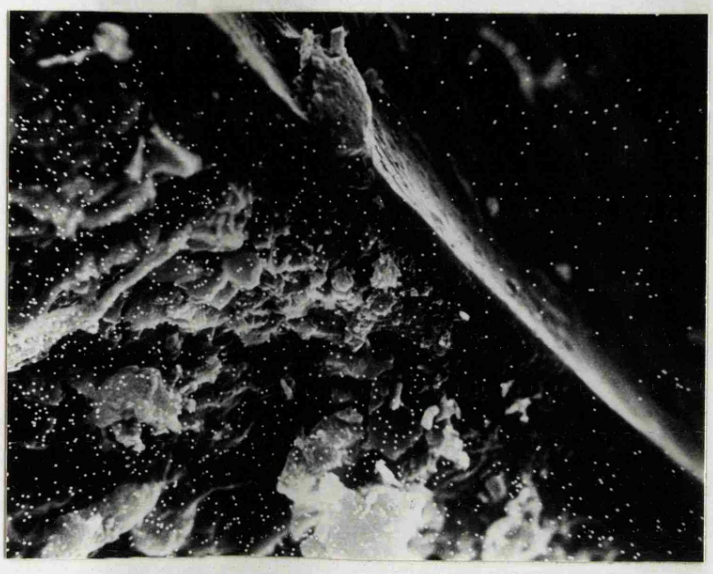

c. X-ray map for calcium

40 µm

d. X-ray map for titanium

indistinct in places. Figure 5.2b shows the X-rays given off by the sample were those of titanium and calcium (Table 5.1). X-ray maps for calcium (Figure 5.2c) and titanium (Figure 5.2d) clearly demonstrated the areas of core and coating, although by moving the sample out of the electron beam background radiation was shown to be responsible for approximately 15% of the counts.The variation in background count both within and between energy levels was such as to prevent the application of a reliable correction factor to the data.

The electron beam was focussed to a point 1 μm in diameter and the X-rays produced by this area of coating analysed. Table 5.2 shows the X-ray counts per minute (cpm) for calcium and titanium obtained from point analyses of tablet cores and the upper and lower surfaces of film coatings stripped from similar cores. The tablet clearly produced X-rays characteristic of calcium and the coating those of titanium, but the latter also exhibited a count due to calcium, which was greater for the lower surface. The difference was highlighted by calculation of the ratio titanium to calcium cpm. This could not be attributed solely to adhering tablet particles since none could be seen on the upper surface and a more probable explanation was that dust from the cores became trapped in the film during the coating process.

Point analyses were therefore carried out at intervals through the cross-section of the coating to establish the variation in calcium content across the film. Figure 5.3 clearly demonstrates the

Table 5.1 The energy and origin of X-rays given off by calcium phosphate tablets, coated with 80% w/ pw HPMC 20% w/pw titanium dioxide, when subjected to EDAX

X-Ray Energy KeV	Identification and electron shell involved in transition	Probable Origin
1.72	Silicon kα	Escape peak from detector
2.03	Gold Mα	Gold coating
3.70	Calcium Kα	Tablet core
4.02	Calcium Kβ	Tablet core
4.52	Titanium Kα	Tablet coating
4.96	Titanium Kβ	Tablet coating

Table 5.2 Point analyses of the X-rays given off by calcium phosphate cores and HPMC film coatings containing 20% w/pw titanium dioxide stripped from these cores.

Sample	X-ray counts per minute		
	Titanium Kα (4.52 KeV)	Calcium Kα (3.70 KeV)	Ratio Ti:Ca
Core	0	1,579	0
Lower surface of film	268	136	1.97
Upper surface of film	370	109	3.40

Figure 5.3 Point analyses (at the centre of the white squares) of a cross-section of coating (20% w/v titanium dioxide) and calcium phosphate core.

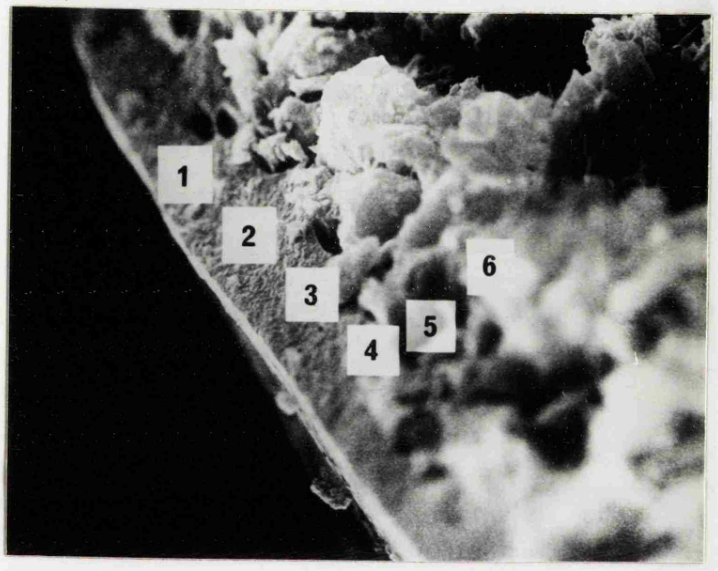

Point Number	Counts per Minute		Ratio Ti:Ca
	Titanium Kα (4.52 KeV)	Calcium Kα (3.7 KeV)	
1	432	145	2.98
2	382	182	2.10
3	340	223	1.53
4	390	304	1.28
5	202	923	0.22
6	52	1,111	0.05

change from coating to core and the increase in calcium present in the coating nearer the core. There was good agreement between the ratios of titanium to calcium cpm observed in Figure 5.3 and Table 5.2 further indicating the presence of calcium in the coating. Since the volume of the X-ray envelope in the film was only 1 μm^3, interference from the core was unlikely to be significant except at the core-coating boundary. Thus the theory that dust from the tablet cores became trapped in the coating was supported since the amount of dust present would decrease as the coating thickness increased.

5.2 Removal of Film Coatings From Substrates

Film coatings cast or sprayed onto glass which had been cleaned with chromic acid exhibited little adhesion and could be lifted off the substrate.

Films applied to compacts were removed by cutting around the edges of the compact with a scalpel, until the film could be lifted off and any adhering particles gently removed by scraping. Care was taken to avoid peeling the film from the substrate, as such a procedure could easily distort the coating. The adherence of particles to the underside of such coatings could have been minimised or eliminated by producing compacts of very low porosity with a dense surface[280]. However, such compacts would be atypical and contrary to the aim of studying films applied to tablets rather than non-porous substrates such as glass and teflon.

The removal of films by a pull-off technique similar to that used for adhesion testing[175] was discounted due to the possibility of damage to the film by the adhesive or applied stress and problems in the subsequent separation of the film and adhesive.

The possibility of selectively dissolving the compact without affecting the coating was investigated, but discounted for routine use since HPMC was only insoluble or did not swell in solvents such as benzene and cyclohexane, which would not dissolve all the exipients required for regular tablet manufacture. The preparation of compacts from materials such as waxes, whilst overcoming this problem, would produce atypical surface characteristics which could affect the properties of applied films.

5.3 Measurement of Film Thickness

The thickness of films cast or sprayed onto glass was routinely measured using a high precision micrometer (L.S. Starrett and Co. Ltd.). The instrument could be read to ±0.5 μm, creating a possible error of 3.3% for very thin films (15 μm). However, since the majority of films tested were considerably thicker (25 - 50 μm), errors in the measurement of film thickness were negligible compared to those involved in the evaluation of film properties. Both upper and lower surfaces of the film coatings sprayed onto glass were smooth (Figure 5.4), although droplet marks could be seen on the former, probably due to partial drying of the coating liquid upon atomization. Such irregularities were unlikely to significantly affect the film thickness measured by a micrometer.

Figure 5.4 S.E.M. of a sprayed HPMC film removed from a glass substrate

Top surface

10 µm

Lower surface

100µm

The measurement of thickness for films applied to compacts was complicated by particles adhering to the lower surface. The data in Table 5.3 demonstrates that for films sprayed simultaneously onto tablets and glass, the measured thickness of the former was almost twice that of the latter. The use of a point micrometer (Moore and Wright Ltd.) reduced this discrepancy slightly by allowing the micrometer tip to penetrate between some of the adhering particles, although the risk of film damage during measurement was increased due to the small contact area. The reason for the consistently higher thickness recorded by the point micrometer for films sprayed on to glass was unclear, since the calibrations of both instruments, as checked with a 25 μm feeler gauge (Moore and Wright Ltd.), were almost identical. However, the larger graduation intervals of the point micrometer may have resulted in an increased error of measurement.

To evaluate the effects of particles adhering to the film, 10.32 mm diameter normal convex tablets were compressed (Hand Machine, Manesty Machines Ltd.) from pure phenothiazine,

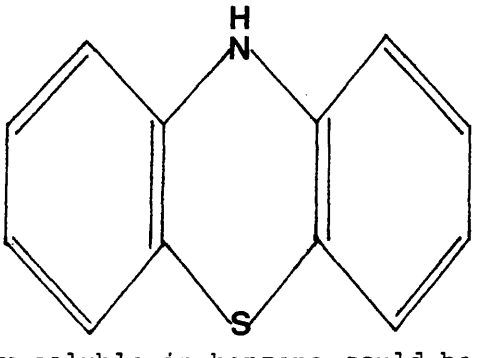

which being freely soluble in benzene could be selectively dissolved without affecting the HPMC film coating. To prevent lamination of the tablets, a slug of magnesium stearate was compressed in between each phenothiazine tablet, thus enabling good compacts

Table 5.3 The measured thickness (10 replicates) of HPMC films containing 20% w/pw titanium dioxide, cast on to glass or sprayed on to glass and tablet substrates under identical conditions.

Micrometer used		Starrett High Precision Micrometer			Moore and Wright Point Micrometer		
Graduations		1 μm			0.0001" = 2.54 μm		
Contact area		28 mm^2			0.80 mm^2		
Preparation Technique	Substrate	Mean Thickness (μm)	S.D.	C.V. (%)	Mean Thickness (μm)	S.D.	C.V. (%)
Cast	Glass	64.1	0.5	0.78	67.0	2.5	3.73
		31.5	0.9	2.86	34.0	3.0	8.82
Sprayed	Glass	16.8	0.4	2.38	19.5	1.3	6.67
	Tablet	32.2	2.5	7.76	27.1	1.5	5.54
	Glass	36.3	0.6	1.65	39.8	1.3	3.27
	Tablet	86.9	5.7	6.56	68.6	4.0	5.83
	Glass	25.2	1.1	4.37	29.9	1.1	3.68
	Tablet	48.0	11.3	23.54	46.7	4.3	9.21

Tablet= Lactose/Avicel compact

S.D. = Standard Deviation

C.V. = Coefficient of Variation

to be obtained without the use of adjuvants. 30 tablets and 10 glass plates were attached to the belt of the model coating system (Section 4.3.1.3) and coated under the following conditions:

Liquid nozzle	2050
Air cap	120
Atomizing air pressure	0.28 MPa
Coating liquid	5% w/v Pharmacoat 606
Liquid feed rate	30 ml min^{-1}
Inlet air temperature	89° C
Exhaust temperature	45° C

4 glass plates and 10 phenothiazine tablets were removed after 25 and 50 minutes, the films carefully detached and the thickness measured with both high precision and point micrometers. Each film was placed in repeated changes of benzene for 40 hours, agitating at regular intervals in an ultra-sonic bath to aid dissolution of the adhering phenothiazine particles. The films were dried for 24 hours at 40°C in a vacuum oven and the thickness re-measured with both micrometers.

Table 5.4 further demonstrates the effects of tablet particles adhering to the film prior to washing in benzene and the reduction of this error by use of a point micrometer. Treatment with benzene did not alter the thickness of films sprayed on to glass, indicating that HPMC was not grossly affected by the solvent. Although the measured thickness of films sprayed on to phenothiazine

Table 5.4 The measured thickness (10 replicates) of HPMC films sprayed on to glass and phenothiazine substrates under identical conditions, before and after treatment with benzene to dissolve adhering particles of phenothiazine.

Micrometer used		Starrett High Precision Micrometer			Moore and Wright Point Micrometer		
Graduations		1 μm			0.0001"= 2.54 μm		
Contact Area		28 mm^2			0.80 mm^2		
Substrate and treatment after removal		Mean Thickness (μm)	S.D.	C.V. (%)	Mean Thickness (μm)	S.D.	C.V. (%)
Glass	A_1	19.9	0.4	2.01	21.6	1.4	6.48
	B_1	40.2	1.4	3.48	40.6	3.1	7.64
Glass treated with benzene	A_2	20.4	0.8	3.92	21.3	1.4	6.57
	B_2	40.1	0.8	2.00	40.2	1.9	4.73
Phenothiazine	A_3	35.7	7.3	20.45	24.4	1.4	5.74
	B_3	81.9	15.7	19.17	61.4	13.8	22.48
Phenothiazine treated with benzene	A_4	27.4	3.1	11.31	23.9	1.4	5.86
	B_4	53.7	5.4	10.06	48.3	4.3	8.90

S.D. = Standard Deviation
C.V. = Coefficient of Variation
t_{tab} (P=0.05) = 2.10

't' test	Precision Micrometer	Point Micrometer	't' test	Precision Micrometer	Point Micrometer
t_{calc} A_1/A_2	1.77	0.48	t_{calc} B_1/B_2	0.20	0.35
t_{calc} A_1/A_3	6.83	4.47	t_{calc} B_1/B_3	8.37	4.65
t_{calc} A_1/A_4	7.59	3.67	t_{calc} B_1/B_4	7.91	4.59

tablets decreased on treatment with benzene, it was still significantly greater than that for films stripped from glass substrates. The reason for the greater quantity of phenothiazine particles adhering to thick films, as indicated by the decrease in measured thickness on washing, was unclear, but may have been associated with the thinner films flexing during removal and adversely affecting particle adhesion. S.E.M. of the films indicated that the upper surfaces of these coatings were fairly smooth, although droplet marks could be seen clearly before and after benzene treatment, indicating partial spray drying of the coating solution (Figure 5.5). The underside of these films were rough with many adhering particles of phenothiazine (Figure 5.6), which were not completely removed by treatment with benzene (Figure 5.7). The most probable explanation for this phenomenon was that during coating, polymer solution penetrated the porous surface of the tablet, surrounding or impregnating particles of phenothiazine which were then removed with the film coating. Subsequent treatment with benzene would have little effect on these particles since the HPMC associated with them acts as an insoluble barrier to the solvent.

An additional error in the measured thickness of films removed from tablets may arise from the surface roughness of the substrate producing an uneven film (Figure 5.8), since the wavelength of such asperities was much shorter than the contact area of either micrometer (Section 7.3). However, the magnitude of such errors will probably be less than those due to the presence of adhering particles.

Figure 5.5 Upper surface of HPMC films sprayed on to phenothiazine tablets before and after treatment with benzene to remove adhering phenothiazine particles.

Before treatment

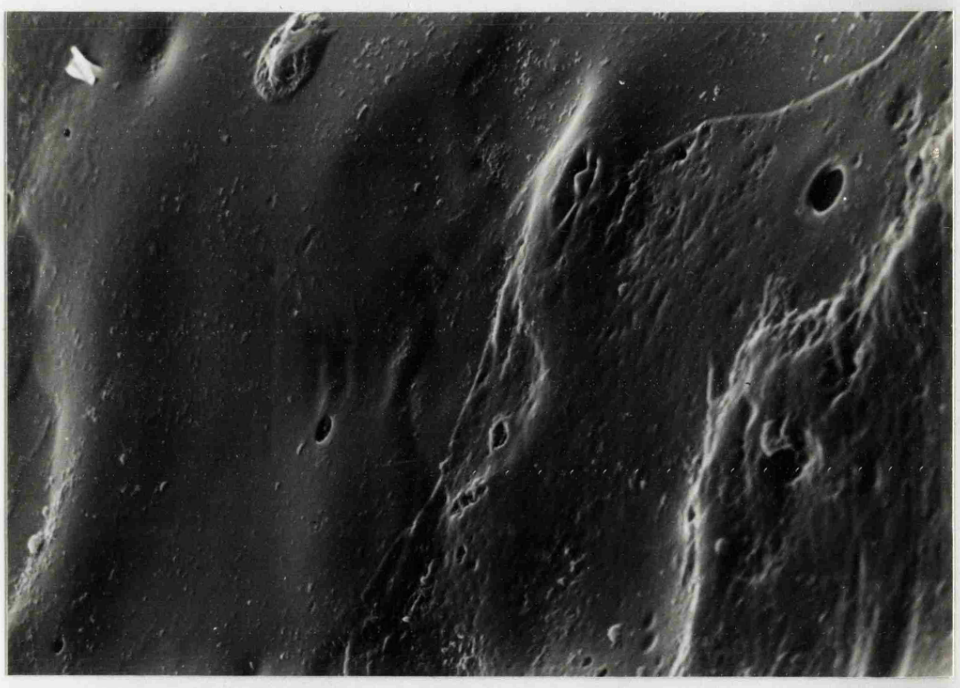

After treatment

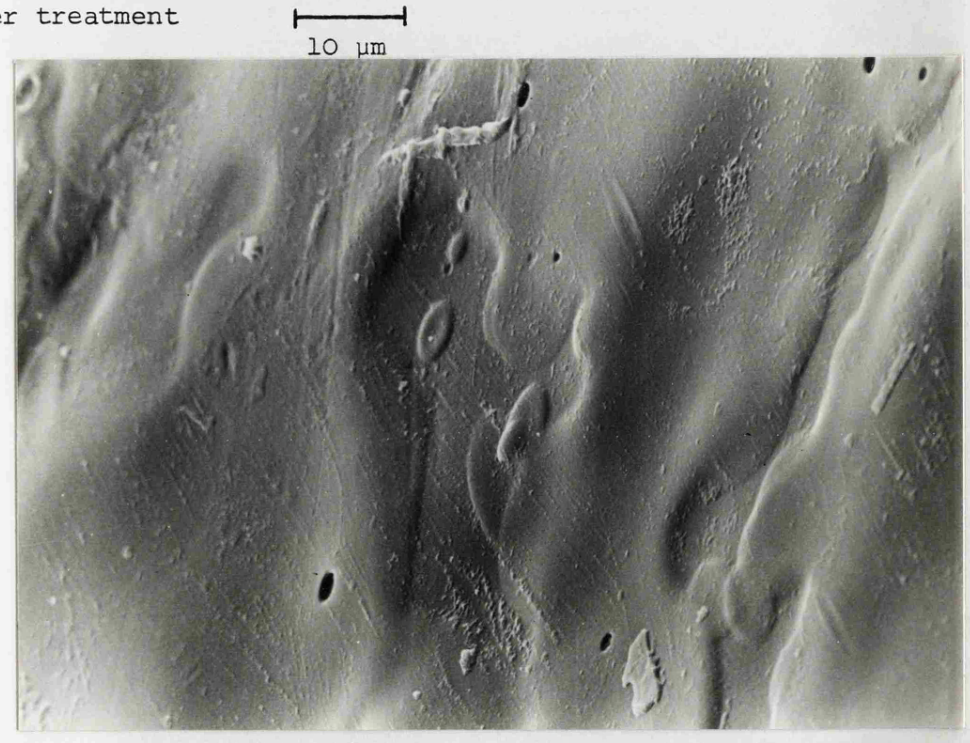

Figure 5.6 Lower surface of HPMC films sprayed on to phenothiazine tablets before treatment with benzene to remove adhering particles

10 μm

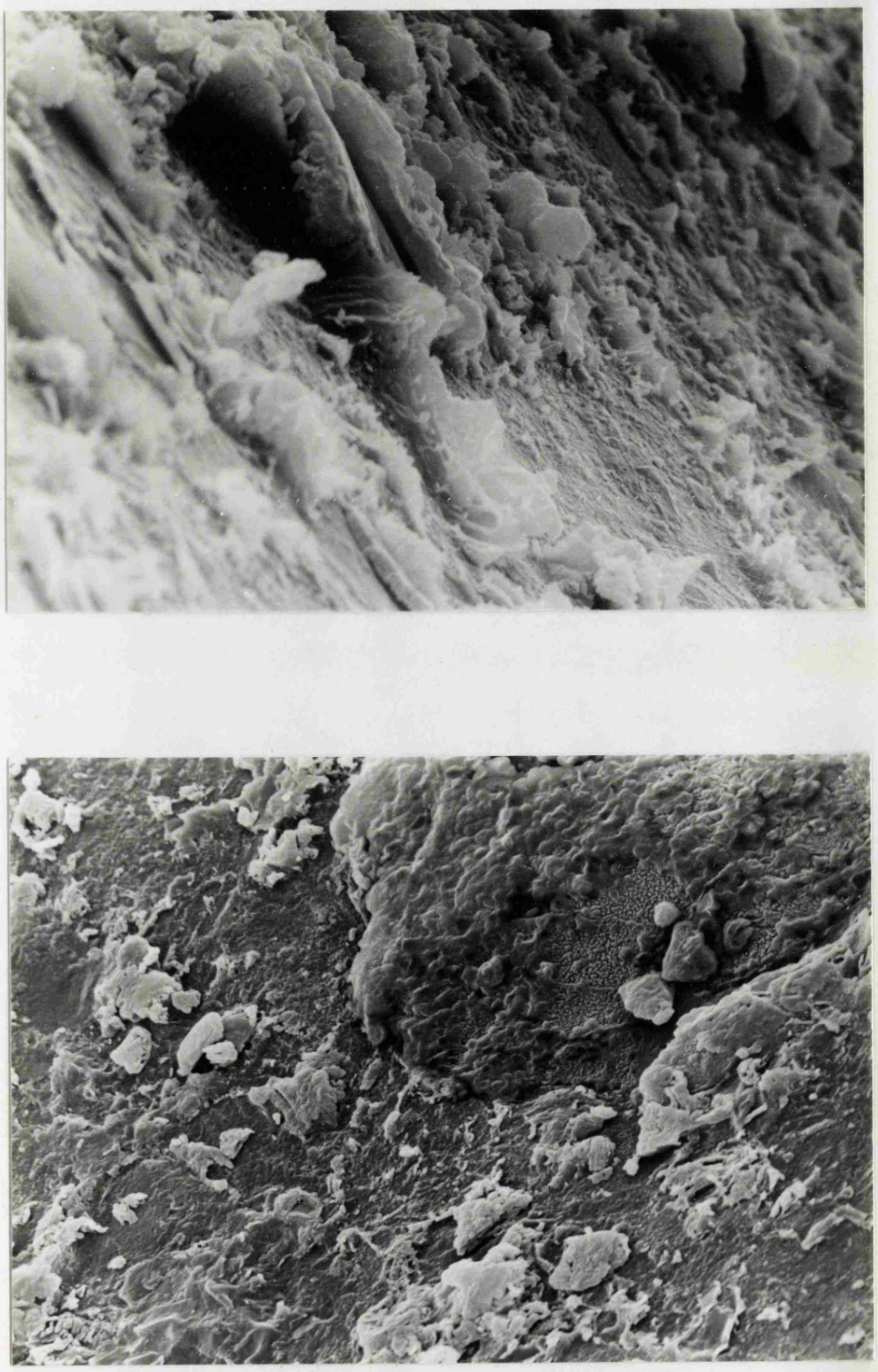

Figure 5.7 Lower surface of HPMC films sprayed on to phenothiazine tablets after treatment with benzene to remove adhering particles.

10 μm

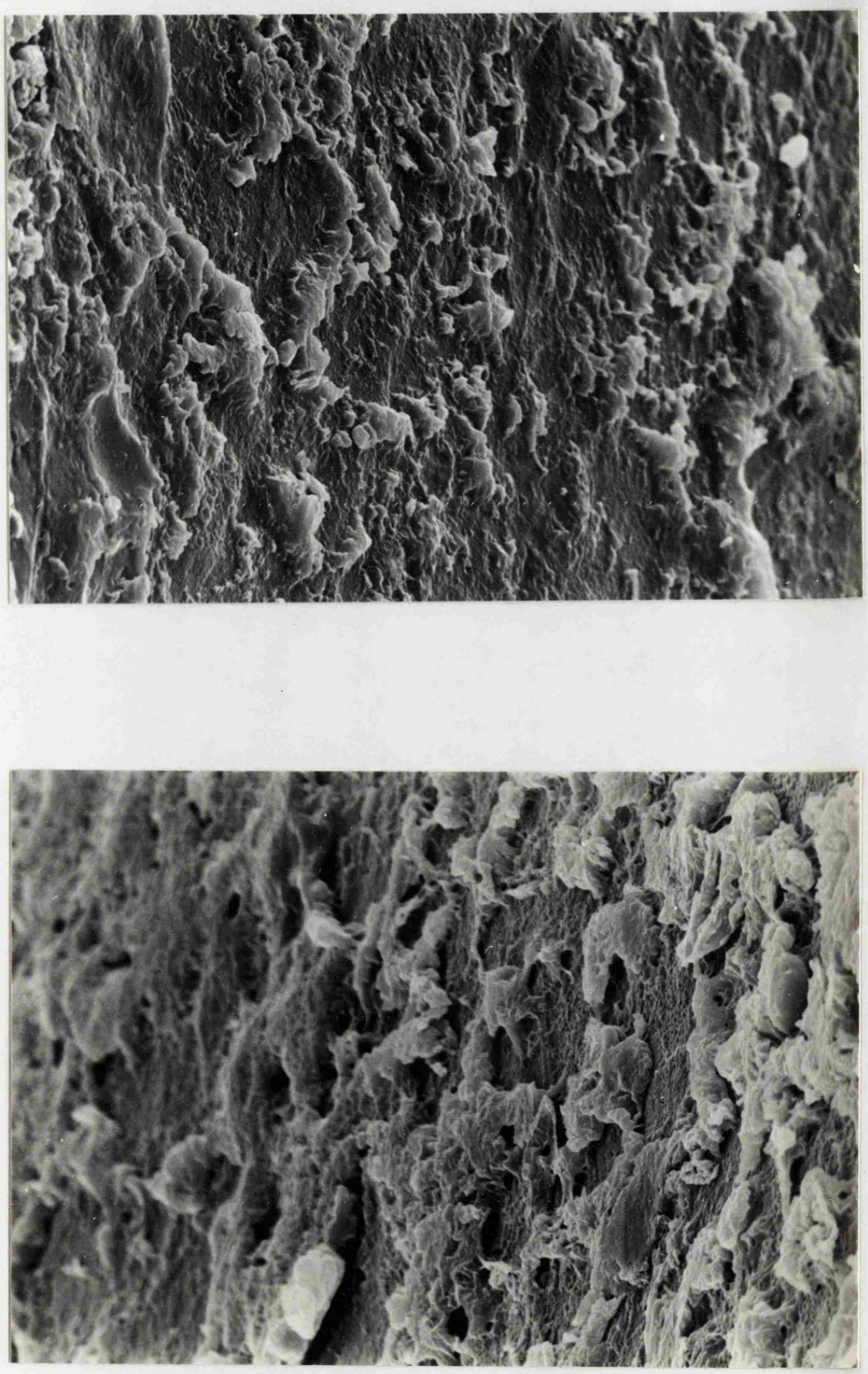

Figure 5.8. The effect of surface roughness on the thickness of film coatings as measured by a micrometer.

Smooth Film

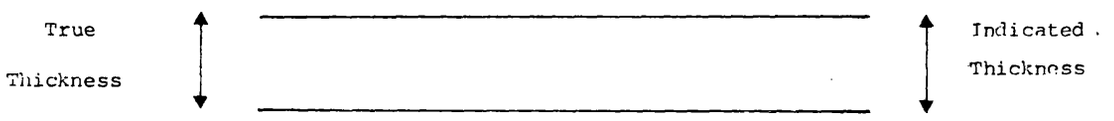

Rough film

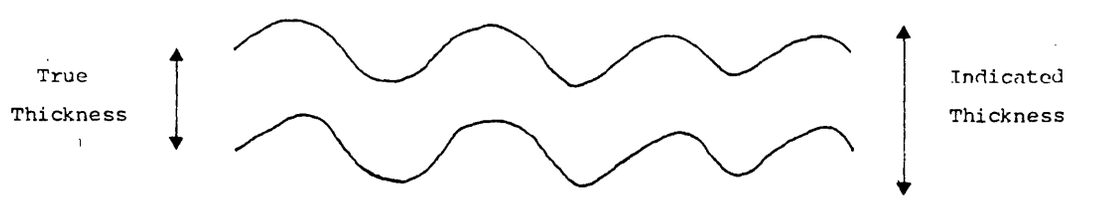

Consequently it was impossible to accurately measure the thickness of films applied to tablet substrates although a close approximation could be obtained by the use of the mean measured thickness of films sprayed on to glass substrates placed in between the tablets on the belt of the model coating system (Section 4.3.1.3). Hence this approach was used throughout this study to determine the effective film thickness.

6. EVALUATION OF FILM PROPERTIES

6.1 The Development of a Mass Spectrometric Technique for the Determination of the Gas and Vapour Permeability of Thin Films

6.1.1 Introduction

The use of film coatings to provide tablets which are resistant to abrasion and taste-masked is well established. That such coatings might also provide protection for the active ingredients against the potential degradative effects of atmospheric oxygen, carbon dioxide and water vapour has led to considerable interest in the barrier properties of film coating materials. However, the techniques used for evaluating such properties, described in Section 1, suffer several disadvantages. Those based on applying an absolute pressure difference across a film create problems with relatively weak or highly plastic films, which may bulge, distort or rupture, even when supported by some kind of grid which, in turn, will interfere with the area of film exposed to the permeant gas. Furthermore with the exception of gas chromatographic and mass spectroscopic detection systems, these techniques will only follow the transfer of a single component, unless elaborate systems for selectively trapping gases and vapours, or a combination of several specific detectors are employed. This lack of selectivity prevents any study of the interaction of two or more permeants, for example hydrophilic films may be plasticized by water vapour, so affecting the oxygen permeability.

It was therefore decided to develop a mass spectrometry technique which had the potential to detect the low level transfer

of an individual species from a multicomponent gaseous mixture.

6.1.2 Development of the Experimental Technique

A detection system based on the Micromass 2 mass spectrometer was selected. This instrument gives a 10% valley resolution at mass 44, but quantitative estimation of any component below mass 60 is possible provided that the partial pressure of components at adjacent mass numbers is low. The gaseous sample is admitted to the analyser head of the mass spectrometer through a molecular leak, enabling a pressure differential to be established between the high vacuum mass spectrometer system and the sample inlet. To maintain the versatility of the mass spectrometer for uses other than permeability measurement, an inlet system was adopted in which gas samples could be removed from a permeability cell remote from the instrument, using a gas-tight syringe and injected in to a sample chamber connected to the analyser head by the molecular leak.

6.1.2.1 The Permeability Cell Design and Construction

It was proposed to study films prepared by spraying aqueous film coating solution on to 25.4 mm diameter tablet cores using the laboratory model of the 24" Accela-Cota described in Section 4.3.1.3. Consequently the permeability cell design of Ashworth[256] was extensively modified to accept films 21 mm in diameter and allow intermittent sampling from a receptor chamber approximately 50 ml in volume. Thus up to ten 0.25 ml samples of gas could be withdrawn for analysis without greatly

affecting the pressure within the receptor chamber. A trial cell was manufactured from 76.2 mm diameter perspex rod (F.R. Warren and Co. Ltd.), to evaluate and optimize the design prior to construction of the test cell from stainless steel (Figures 6.1 and 6.2).

The main body of the cell (A) was machined from a single piece of stainless steel rod (EN58 AN grade, Righton Henry and Co.Ltd.) and the bottom (B) then arc-welded on. C and D are two-way Whitey ball valves (B - 4254, Techmation Ltd.), screwed directly in to the main body of the cell (thread 7/16x20 t.p.i. UNF); the valve extension arms (E) allow their operation from outside the temperature controlled cabinet which housed the cell. The septum holder (G), the stainless steel sealing washer (H) and ledge (I) were hand ground with successively finer carborundum then diamond discs (Knuth Rotor, Struers Ltd. and Griffin and George Ltd.) and finally finished with Duraglit metal wadding (Reckitt Household Products Ltd.) to ensure a scratch-free, highly polished surface on which the silicone rubber septum (J) (Jones Chromatography) and film (K) can seal. For use, the stainless steel top of the cell (L) was bolted down, applying even pressure to the sealing washer (H) via a viton 'O' ring (M) (Edwards High Vacuum Ltd.). To ensure a reliable seal, a thin film of Apiezon M grease (Edwards High Vacuum Ltd.) was applied to the ledge (I) and film facing surface of the sealing washer (H), thus eliminating the need for a mercury seal which had been incorporated in Ashworth's original design. The cell was tested for leaks by linking the

Figure 6.1 DIAGRAMMATIC REPRESENTATION OF THE PERMEABILITY CELL

KEY

A. Body of cell (EN58 AN Grade Stainless Steel, Righton Henry & Co. Ltd.)

B. Base of cell (EN58 AN Grade Stainless Steel, Righton Henry & Co. Ltd.)

C. Receptor Isolation Valve (Whitey ball-valve B-4254, Techmation Ltd.)

D. Receptor Isolation Valve (Whitey ball-valve B-4254, Techmation Ltd.)

E. Valve Extension Arm

F1. Donor Gas Inlet

F2. Donor Gas Outlet

F3. Receptor Gas Inlet

F4. Receptor Gas Outlet

G. Septum Holder (EN58 AN Grade Stainless Steel, Righton Henry & Co. Ltd.)

H. Sealing Washer (EN58 AN Grade Stainless Steel, Righton Henry & Co. Ltd.)

I. Film Sealing Ledge

J. Silicone Rubber Septum (3mm x 10mm, Jones Chromatography Ltd.)

K. Test Film

L. Top of Cell (EN58 AN Grade Stainless Steel, Righton Henry & Co. Ltd.)

M. Viton 'O' Ring (1119 VIT, Edwards High Vacuum Ltd.)

N. Bolt (6 recessed Head)

P. Donor Compartment

R. Receptor Compartment

S. Access For Mercury Seal.

Figure 6.1

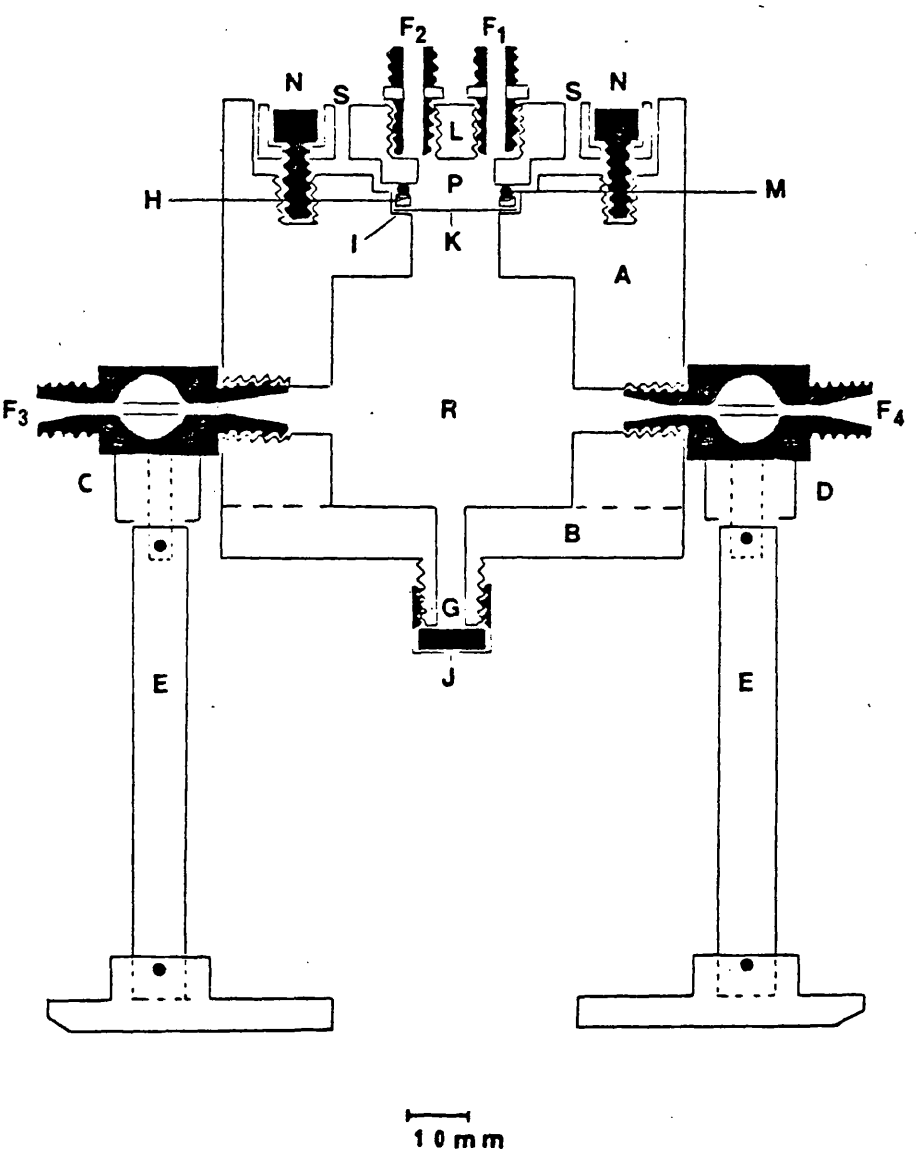

Figure 6.2 Photograph of permeability cell.

donor and receptor compartments and pressurising both to 0.69 MPa with nitrogen from a gas cylinder. No gas bubbles were visible when the pressurised cell was totally immersed in water. Furthermore, no drop in pressure was observed when the cell was isolated for 8 hours by closing the gas cylinder valve.

The films for use in the permeability cell, were cut using a specially designed stainless steel punch (Figure 6.3) of internal diameter 21 mm. The screws (A) allowed the centre section to be removed, placed in a lathe and the cutting edge re-sharpened.

Operation

The donor (P) and receptor (R) compartments were both flushed with the same carrier gas (usually high purity nitrogen) at a rate of 25 and 500 ml min^{-1} respectively, these rates being measured by flow meters located in the outlet gas streams of the donor (manometer) and receptor (Rotameter) compartments. The receptor compartment (R) was then isolated by first closing the receiver gas inlet valve (C) followed immediately by closure of the receiver gas outlet valve (D); this sequence prevented pressure build-up within the receptor compartment. The donor gas was then switched from the carrier gas to the test gas mixture through a 3-way Whitey ball valve (BL2x5A, Techmation Ltd.) and the increase in concentration of permeant in the receptor followed by withdrawing 0.25 ml samples of gas via the septum (J) at appropriate time intervals using a gas tight syringe.

Figure 6.3 Punch for cutting 21 mm diameter films to fit the permeability cell.

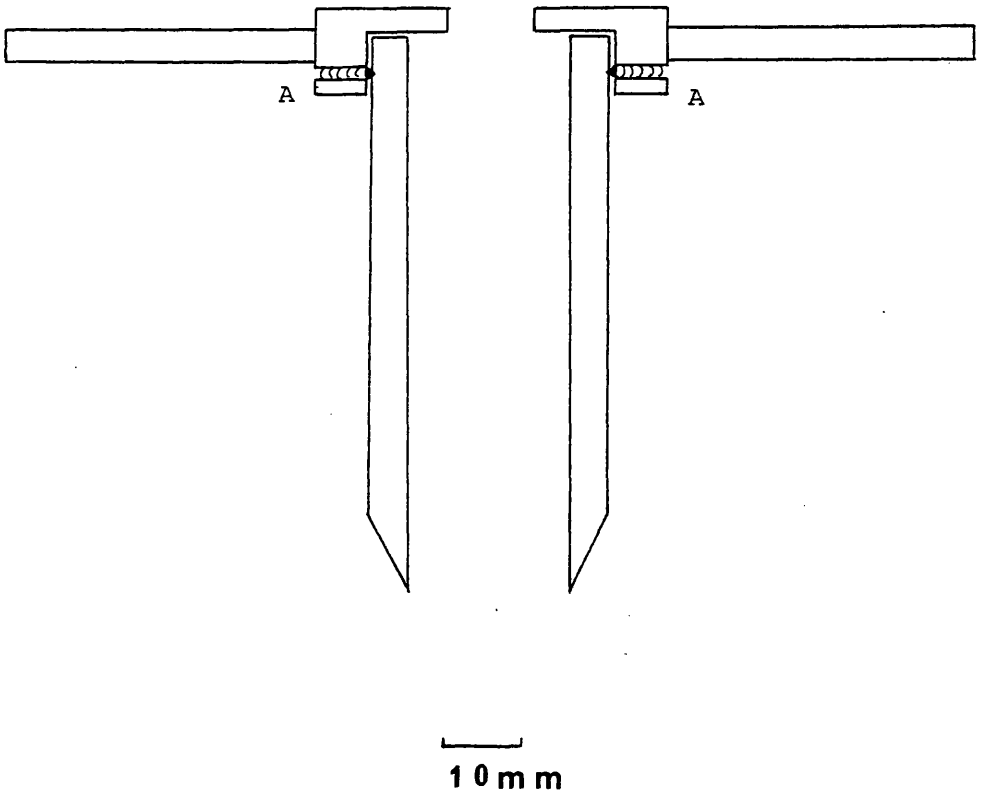

6.1.2.2 Evaluation of 'Gas Tight' Syringes

Syringes from a number of manufacturers (Table 6.1) were evaluated but found to leak when used in conjunction with the mass spectrometer system.This was demonstrated by monitoring the oxygen mass 32 peak, as a function of time, after isolating the sample chamber with the syringe 'in situ'. The most satisfactory syringes were found to be the 'Pressure-Lok' A2 range (Pierce and Warriner (U.K.) Ltd.), which had the additional advantage of a 'built-in' sealing valve rather than the 'add-on' valves fitted to other manufacturers' syringes. The importance of using a syringe valve was demonstrated with the 'Pressure-Lok' A2 0.25 ml syringe; the partial pressure of oxygen in high purity nitrogen indicated by the mass spectrometer, being greater due to the ingress of atmospheric gases into the sample when the valve was left open (Table 6.2). The 0.25 ml 'Pressure-Lok' A2 syringes presented problems due to the rapid break-up of the PTFE plunger tips, with subsequent leakage after minimal use, often after only one or two injections (Figure 6.4). Consequently 1 ml 'Pressure-Lok' A2 syringes (050033, Pierce and Warriner (U.K.) Ltd.) were used in all subsequent experiments since these represented the best compromise between a syringe which remained gas-tight and one with which a 0.25 ml sample could be accurately taken.

The use of side port rather than conventional needles (Figure 6.5) was found to improve the reliability of injection and increase septum life, since the latter tended to tear the

Table 6.1 'Gas-Tight' syringes evaluated for use with the mass spectrometer gas detection system.

Manufacturer	Model	Capacity (ml)	Result of leak test
Hamilton	1000 series	0.25	Fail
		0.5	Fail
		1.0	Fail
		2.5	Fail
	1800 series	0.25	Fail
Scientific Glass Engineering	GSGA	0.25	Fail
		0.50	Fail
Pierce and Warriner	Pressure-Lok A2	0.25	Pass/Fail
		1.00	Pass

Table 6.2 The effect of the use of the syringe valve, fitted to a 0.25 ml 'Pressure-Lok' A2 gas syringe, on the partial pressure of oxygen detected in a 0.25 ml sample of high purity nitrogen

Time interval between filling syringe and injecting into mass spectrometer (secs)	State of Syringe Valve	Partial pressure of oxygen detected in sample ($Pa \times 10^7$)
10	Closed	1.40
	Open	1.60
30	Closed	1.40
	Open	2.30

Figure 6.4 Mass 32 peak versus time during injection of a sample of high purity nitrogen

a 'Gas Tight' syringe

Key:

A Syringe through septum and chamber isolated

B Syringe valve opened, plunger pushed to 0 ml

C Syringe valve left open

D Syringe valve closed

E Syringe removed

b Syringe leaking past plunger tip.

Key:

As Fig. 6.4a

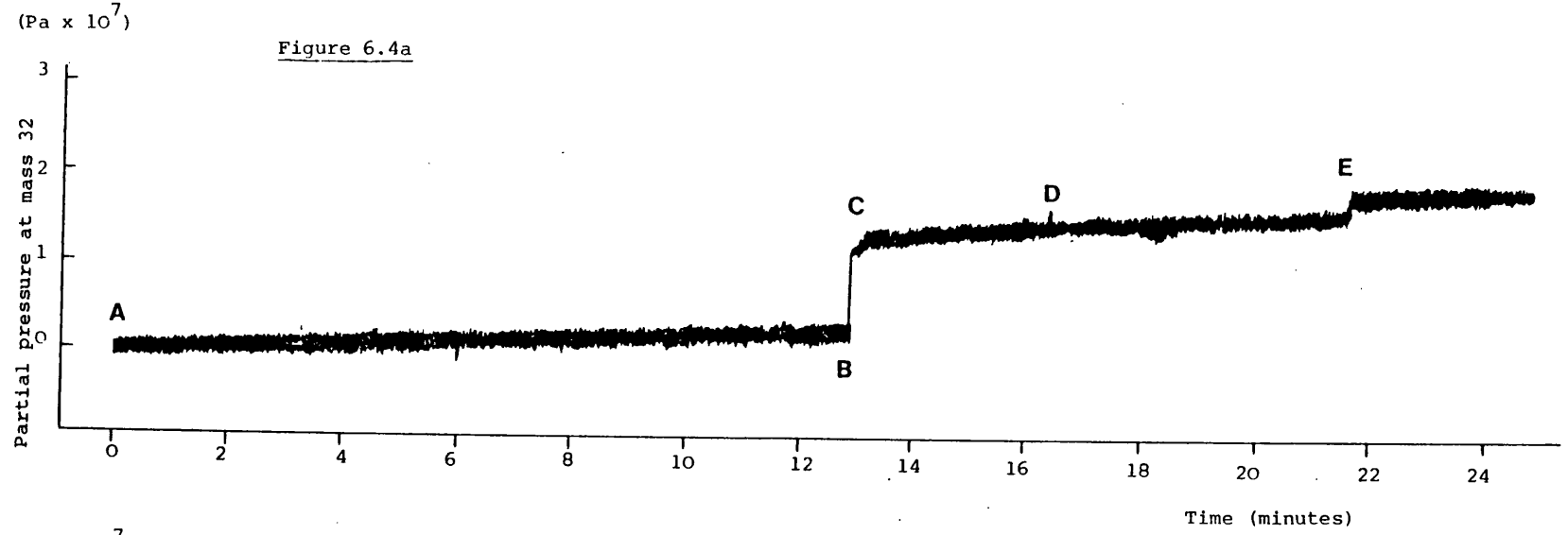

Figure 6.4a

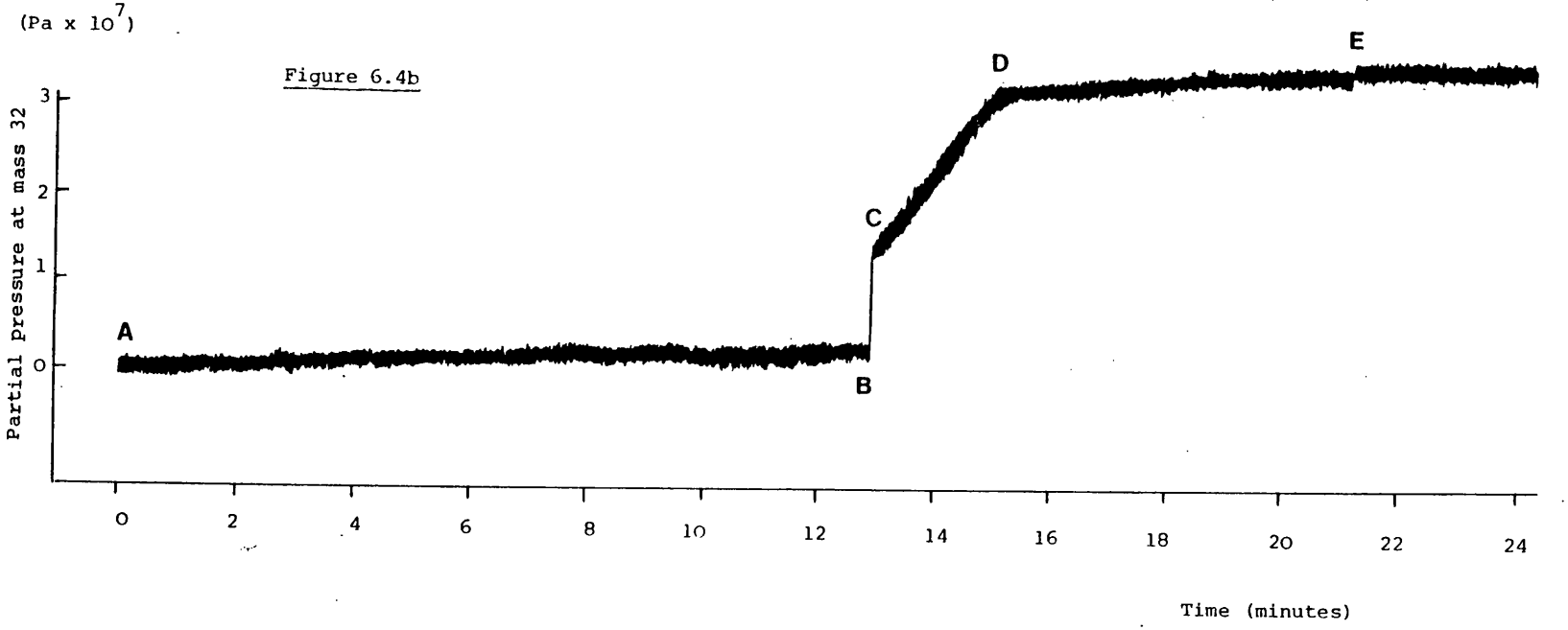

Figure 6.4b

Figure 6.5 Diagrammatic representation of the syringe needles used with the 'Pressure-Lok' A2 gas syringe.

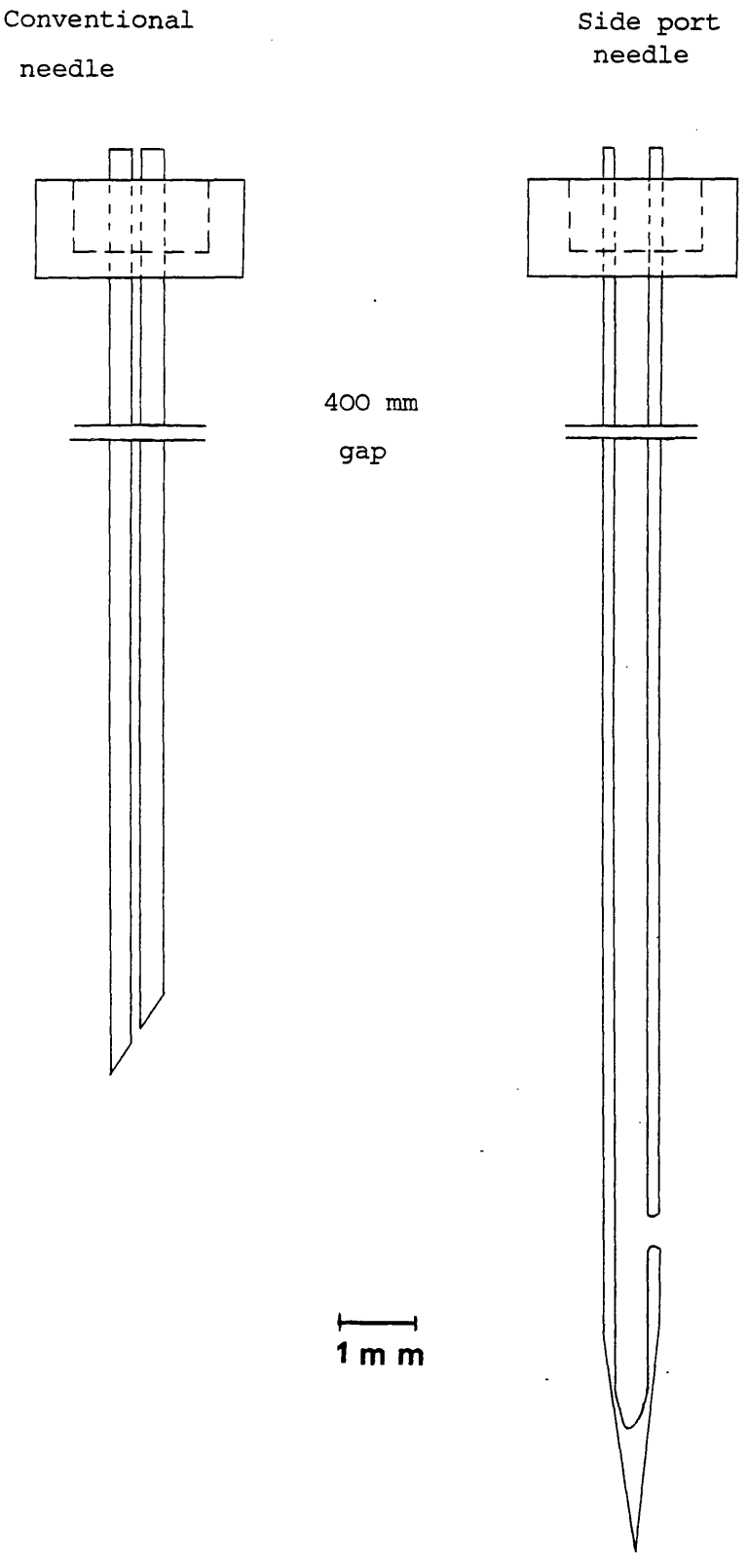

septa and block easily. Thus injections were lost due to leakage around the septum or an inability to deliver the whole sample volume. Blockages could be minimized by removing the needle and cleaning it with fine wire prior to each injection, but the wear so created at the needle/syringe junction rapidly led to leakage.

6.1.2.3 Temperature Control

As film permeabilities are temperature dependent, it was important to ensure that the cell and all gases entering it were at constant temperature.

A copper water jacket was constructed to fit around the outside of the permeability cell, allowing water at constant temperature to be circulated. All gas entering the cell passed through temperature equilibration coils (6.35 mm o.d. copper tube) submerged in a water bath. The temperature within the permeability cell was monitored with a thermocouple unit (Light Laboratories Ltd.), which demonstrated that the cell could be maintained at $30^{o}C \pm 0.1^{o}$ without gas entering it, but at flow rates of between 25 and 500 ml min^{-1} the gas was found to be at room temperature. Repeated lagging of the temperature equilibration coils between the water bath and cell did not improve the situation, although the temperature drop could be reduced by increasing the gas flow rate above 1 l min^{-1}.

To overcome this problem a temperature controlled cabinet was constructed from 10 mm plywood to accommodate the permeability

cell, gas mixers, vapour saturators and temperature equilibration coils (Figure 6.6). Air circulation and heating within the cabinet were effected by a radial fan (Belling-Lee), air capacity 2.1 m^3 min^{-1}, to which a 1 kW heating element was fitted. The power to the heating element was supplied via the relay of a thermistor control circuit (Figure 6.7). As the temperature within the cabinet fell, the resistance of the thermistor probe increased, reducing the input to IC1 (741 operational amplifier). The resistive network R2 and R3 was adjusted such that the resistance equalled that of the thermistor probe at the required temperature. Consequently, the input currents to each arm of IC2 (741 operational amplifier) were matched, producing zero output to IC3 (2N3053 transistor) and preventing operation of the relay. When the temperature fell, the increasing resistance of the thermistor probe caused an imbalance between the 2 inputs to IC2. The output so produced activated IC3, allowing the relay to close and current to pass through the heating element.

All components for the temperature control circuit were obtained from R.S. Components Ltd. and wired up on a stripboard, To prevent arcing on activation of the relay, a 1 µF 600 V electrolytic capacitor was attached in parallel across the contacts. To minimize temperature fluctuations, the heater voltage was reduced to 80 V allowing the air within the cabinet to be gently warmed by the heating element which now consumed only 110 watts of power. By adjustment of R3 (coarse control) and R2 (fine control) the air temperature within the cabinet was set at 30°C.

Figure 6.6 Photograph of the temperature controlled cabinet.

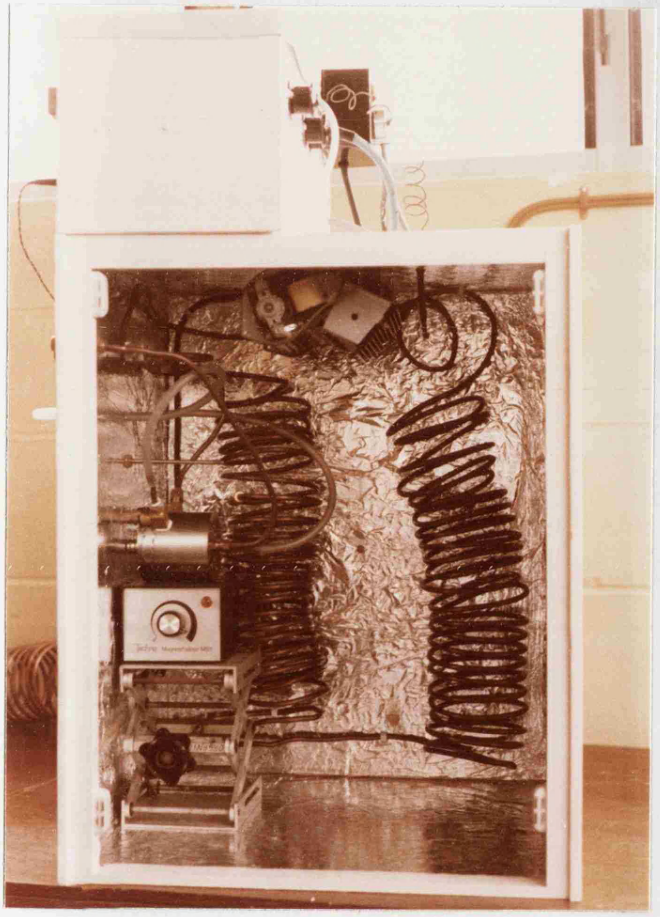

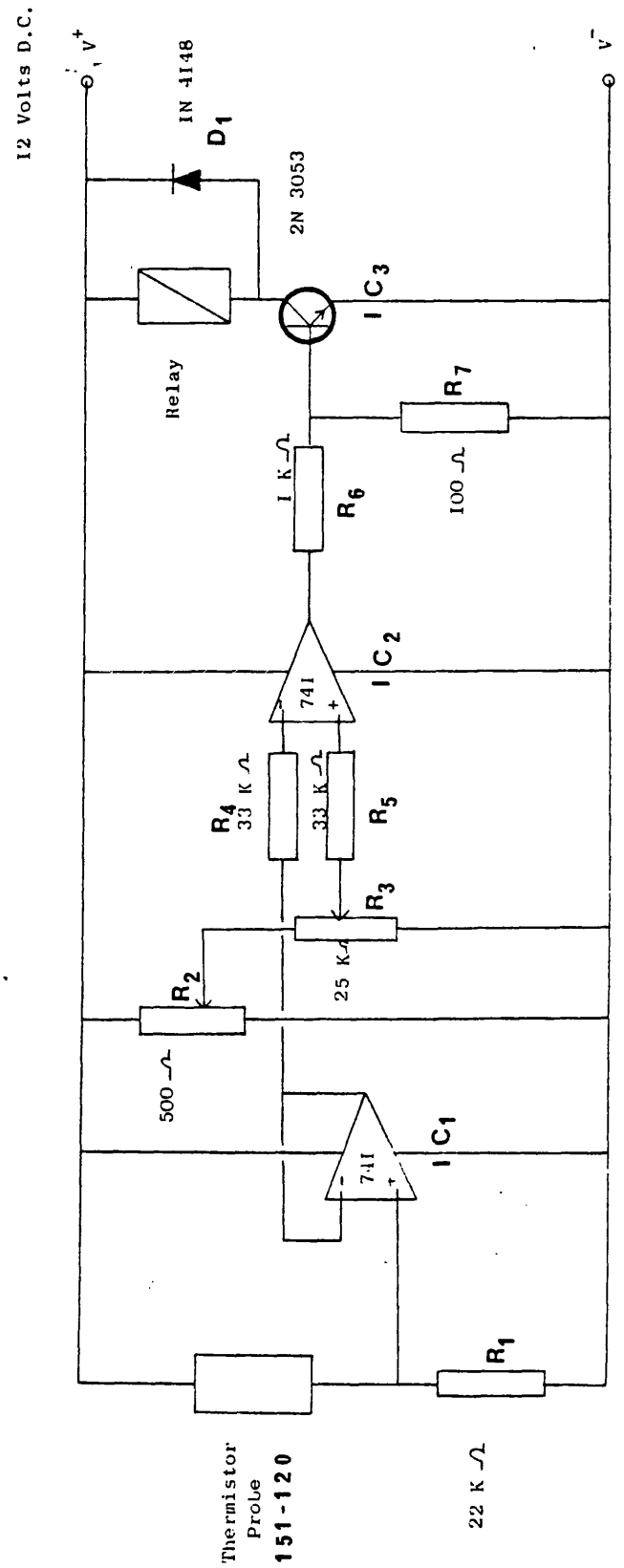

Figure 6.7 Thermistor temperature control circuit.

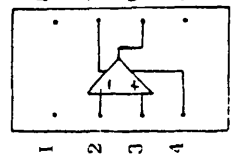

741
Operational Amplifier

Using this system, temperature control within $\pm$ 0.1° at 30°C was achieved, as demonstrated with the thermocouple unit. No variation in temperature was detectable when the thermocouple probe was located within the permeability cell itself, nor when gases from the temperature equilibration coils were passed through the cell.

6.1.2.4 Gas Mixing and Vapour Saturation

To enable the investigation of the permeation of films by mixtures of gases and vapours, a system was employed by which gases could be accurately mixed in known ratios. The flow rate of each gas entering a 'T' piece was monitored with a Porter Flow Meter (Model F150A 0-36 ml min^{-1}, Jones Chromatography Ltd.) and controlled by a precision control valve (Series 60PV 1000, Supelco Inc.). Further calibration of the flow meters was unnecessary since each was supplied with the manufacturer's calibration curve. The accuracy with which such mixing could be performed was demonstrated by the preparation of gas mixtures for the calibration of the mass spectrometer using a similar technique (see Section 6.1.2.5e).

A glass saturator was designed to saturate the test gas with water vapour (Figure 6.8). The sinters (A and B) broke up the gas flow into a stream of fine bubbles, maximizing the area of contact between the gas and the distilled water and promoting rapid saturation of the gas. The sinter on the outlet (C) helped to prevent water droplets entrapped in the air stream

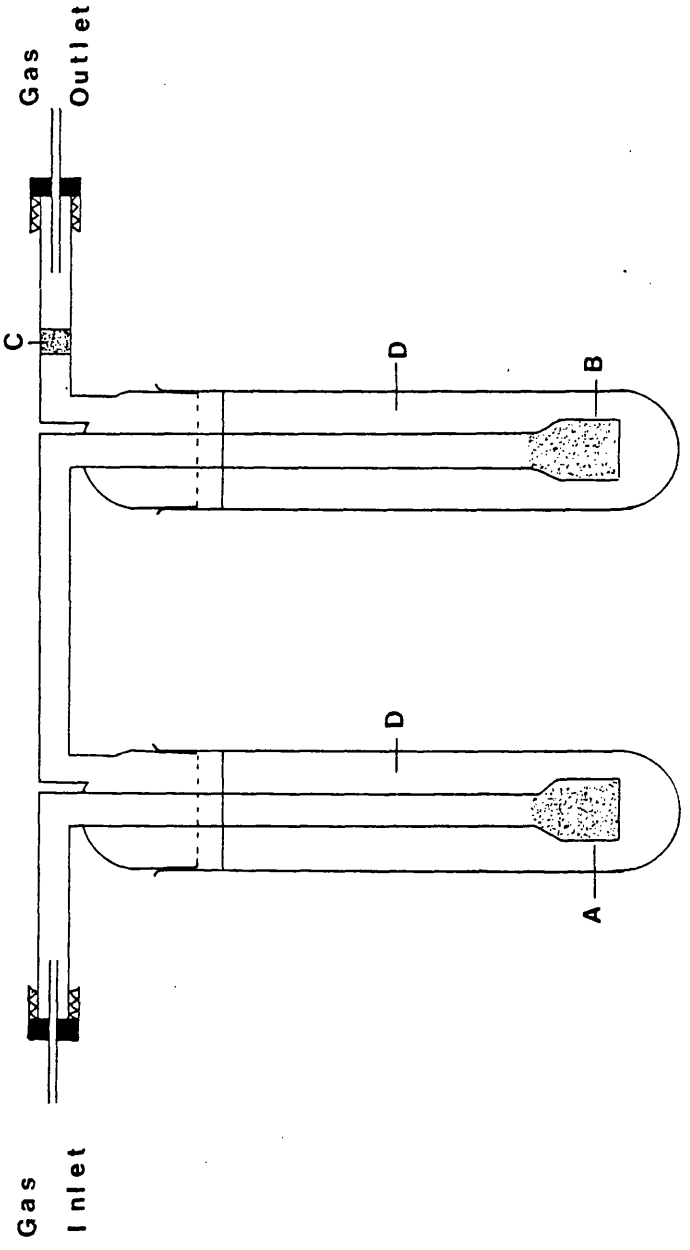

Figure 6.8 Gas Saturator

from leaving the saturator, although the low flow rates (25 ml min^{-1}) used did not produce the turbulence and gas velocity necessary for significant droplet carry-over.

To ensure that complete saturation had occurred, high purity nitrogen was passed through the saturator and then a liquid nitrogen trap, at a rate of 25 ml min^{-1}, for 60 minutes (Figure 6.9). Thus the weight increase of the trap, measured to 0.01mg (Unimatic, Stanton Instruments Ltd.) was due to water vapour condensed from 1.5 litres of gas. During these weighings, it was necessary to handle and wipe the glass trap with a chamois leather to prevent finger grease and condensation on the outer surface interfering with the results. Experiments with unsaturated high purity nitrogen indicated that a weight increase of 0.2 mg (standard deviation 1.291×10^{-2} mg) occurred when 1.5 litres of dry gas (dew point - $75^{o}C$, < 1 ppm by volume water vapour) was passed through the trap. This was due to the very small amount of water vapour contained in the nitrogen and/or moist air from the room being drawn in to the U-tube by the rapid contraction in volume of gas within the cold trap when initially immersed in liquid nitrogen after weighing.

The theoretical weight of water present in 1 litre of saturated gas was calculated, using the Ideal Gas Law and a knowledge of the vapour pressure and temperature, as 17.29 mg l^{-1} at $20^{o}C$.

Figure 6.9. Gas saturator and liquid nitrogen trap.

Key:

A, B, C	No.1 sinters
D	Distilled water
E	Glass U-tube
F	Liquid nitrogen
G	Dewar flask
H	Insulation
I	Glass wool

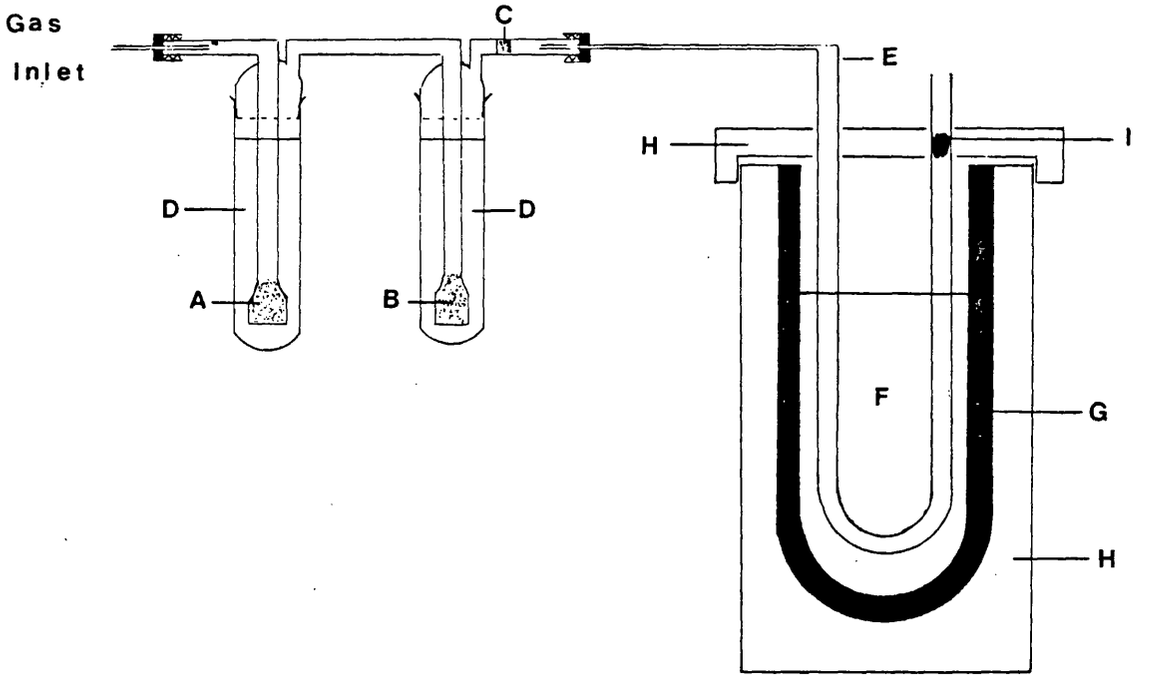

Triplicate determination of the water held in saturated high purity nitrogen at 20°C yielded a mean of 17.56 mg l^{-1} (standard deviation 0.15 mg l^{-1}, C.V. 0.84%), thus agreeing with the predicted water vapour content to within 1.6%. Such agreement was considered satisfactory allowing for the errors possible in the measurement of gas flow rates, weighings and the effect of the blank value (0.2 mg) discussed above.

An alternative saturation system was evaluated whereby water from a syringe (500 µl series 700, Hamilton Ltd.) and syringe pump (Model 341A, Sage Instruments Ltd.) was dropped on to a 'hot finger' placed in the gas stream. (Figure 6.10). Although this system was found to work satisfactorily, it did not represent any advantage over the more conventional technique described earlier and was practically more difficult to use at low gas flow rates.

The use of saturated salt solutions to provide atmospheres of limited water vapour pressure is well documented in the literature[244,257-260]. It was therefore thought that test gas mixtures of intermediate vapour pressure could be produced by replacing the distilled water, present in the saturator, with saturated salt solutions. Initially saturated solutions of sodium chloride and sodium bromide were evaluated for the production of vapour pressures of 23.87 and 18.07 mm Hg respectively at 30°C [244, 257-260]. As previously, the quantity of water contained in 1 litre of gas was calculated and compared

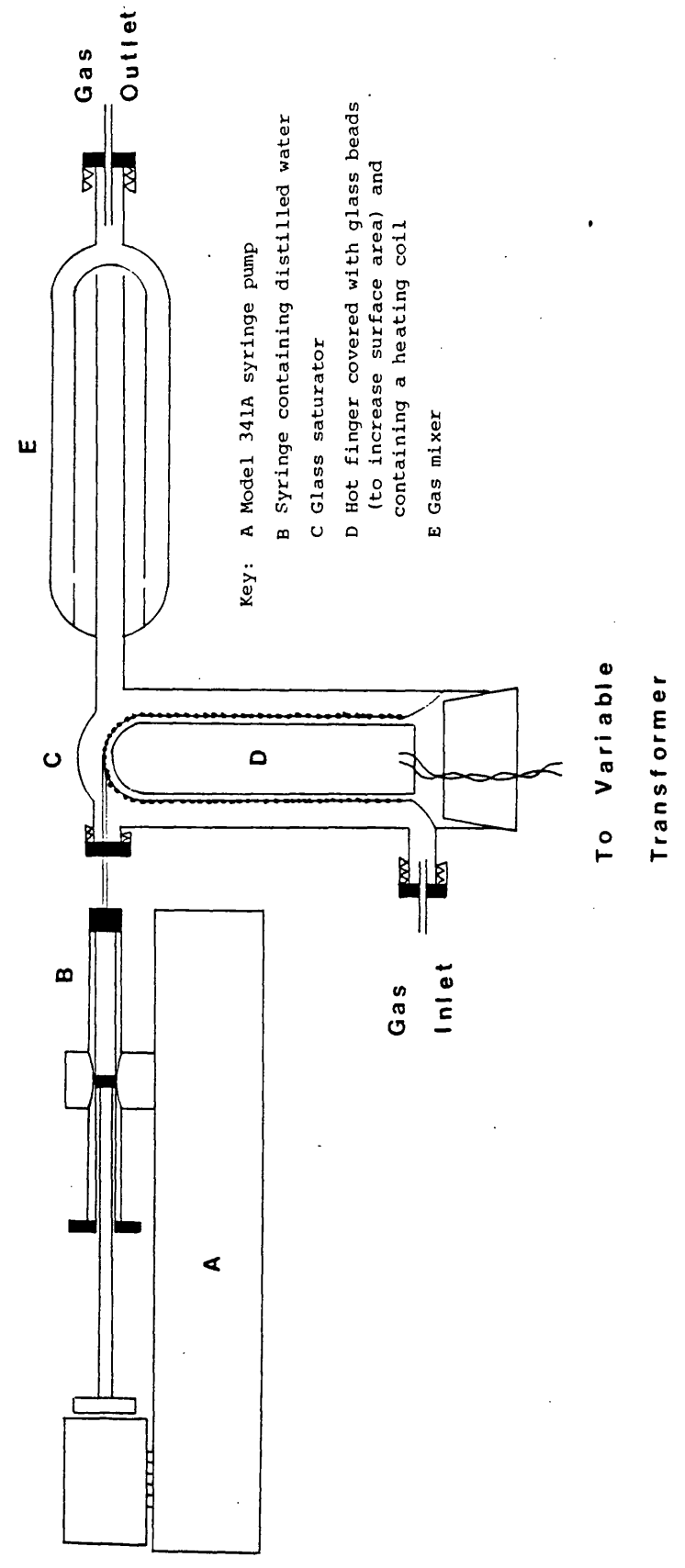

Figure 6.10 Hot Finger Gas Saturator

with that measured by use of a liquid nitrogen trap. Table 6.3 clearly demonstrates that the evaporation of water was not being adequately limited by the saturated salt solutions. A satisfactory explanation for this phenomenon has not been obtained; one explanation considered was that it may be associated with the formation of concentration gradients within the solutions[261]. However, this could not be substantiated when samples of the salt solutions, taken from at and below the surface, were evaporated and the salt content determined by weight.

To overcome this problem an alternative system was therefore adopted in which saturated and dry gas streams were mixed, using the flow meters and controllers described earlier, to produce the desired vapour pressure.

6.1.2.5 Mass Spectrometer Gas Detection System

a. Theory

(i) Mass Spectrometer

If a charged particle is injected into a magnetic field at constant velocity, it will move in a circular path of constant radius.The radius of this orbit (r) is dependent upon the velocity (V), mass (M) and charge (e) of the particle and the strength of the magnetic field (H) as shown by equation 6.1; the particle charge is equivalent to the number of electrons lost.

$$r^2 = \frac{MV}{H^2 e} \times \text{constant} \qquad \text{...(equation 6.1)}$$

Table 6.3 The water vapour content of high purity nitrogen obtained by passage through a saturator, at 30°C, containing sodium chloride or sodium bromide saturated solutions

	Saturated salt solution	
	Sodium chloride	Sodium bromide
Vapour pressure at 30°C (mm Hg)	23.87	18.07
Predicted water content (mg l^{-1})	22.75	17.23
Mean detected water content (mg l^{-1})	29.11	25.33
Standard Deviation	1.06	3.10
Coefficient of Variation (%)	3.64	12.24
Percentage Error	+28.0	+47.0

If the radius is fixed, equation 6.1 reduces to:-

$$\frac{M\ V}{e\ H^2} = \text{constant} \qquad \ldots\text{(equation 6.2)}$$

The charged particles can now be focussed according to the ratio of $\frac{M}{e}$, on a predetermined radius, by variation of either the accelerating voltage or the magnetic field strength. The latter being used in electromagnetic focussing instruments and the former in permanent magnet instruments such as the Micromass 1/2.

Atoms or molecules to be analysed pass into the ion source (Figure 6.11), where they collide with or pass close to an electron beam, causing electrons to become detached from the molecule, forming a charged ion. The electron beam is derived from a hot wire filament and is focussed magnetically through the ion source. The electrons are drawn towards the ion source by a positive potential, pass through it and are collected on the electron trap. The exit slit is positioned close to the electron beam and, by applying a negative potential (relative to the source) to the source slit, positioned close to the exit slit, ions are drawn out of the ion source. The potential applied to the source slit is known as the acceleration potential and in addition to extracting ions, acts as an electrostatic lens focussing the ion beam.

The ion repeller was originally operated at a positive potential relative to the source to increase the ion extraction efficiency by repelling positive ions. However, in the Micromass it is used at a negative potential to improve the electrostatic focussing of the ion beam. Furthermore, by making its potential proportional to the acceleration voltage, any effects on the electron beam will be counteracted. The number of ions formed is dependent on the number of molecules in the ion source, which in turn is dependent upon the system pressure and the electron current. Thus, a feedback circuit controls the filament emission so as to maintain the electron current at pre-set levels.

Figure 6.11 Ion source of a mass spectrometer.

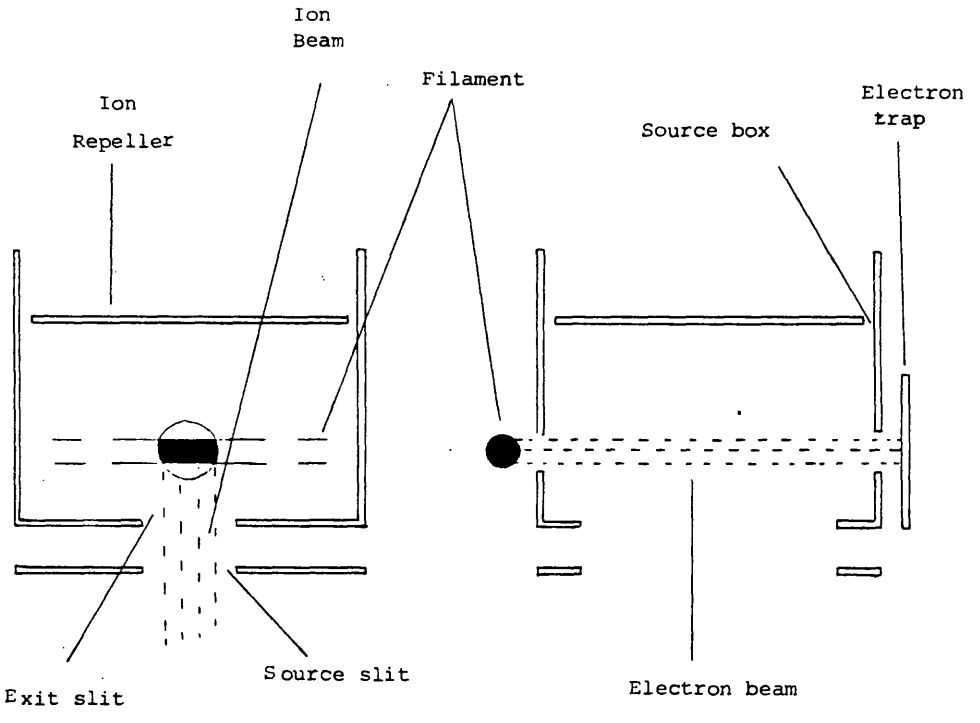

The region of magnetic field in which the ions orbit is termed the analyser (Figure 6.12). The ions leaving the source slit pass through the analyser slit and orbit under the influence of the magnetic field. Those ion species with an orbit radius of 1 cm arrive at the collector slit and can be detected. To reduce peak broadening and thus improve resolution, the alpha slit helps remove ions on 'wrong' trajectories and the collector slit is kept as small as possible. However, the reduction in slit size will reduce the number of ions accepted by the collector, so decreasing the sensitivity.

Ions passing through the collector slit are detected by either an electron multiplier or a plate collector. Since an electron multiplier necessitates a maximum operating pressure of 1.33×10^{-3} Pa, the Micromass 1/2, which is required to operate at pressures up to 1.33 Pa, utilizes a plate collector for ion detection.

Thus as the acceleration voltage is scanned, ions of particular $\frac{M}{e}$ ratio are sequentially brought to a focus at the collector slit, where they are detected by a plate collector.

(ii) Vacuum System

In order for the mass spectrometer to function properly, the probability of collisions between ions and molecules in the analyser must be low. This requirement, together with the need to reduce electrode contamination and filament deterioration

Figure 6.12 Micromass 1/2 analyser

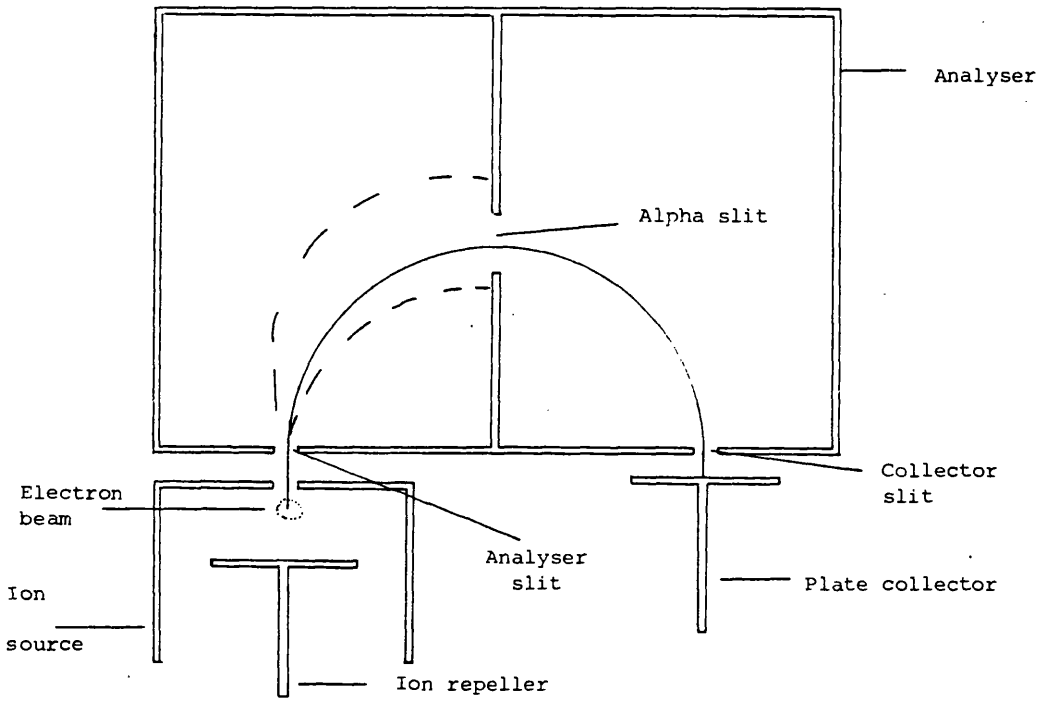

Magnetic field perpendicular to plane of paper -

necessitates operation at low pressures. At 1.33×10^{-2} Pa and room temperature, the mean distance travelled between collisions is approximately 50 cm, falling to 5 cm at 0.133 Pa. Thus even in a 1 cm path length 180^{o} mass spectrometer, good quantitative results can only be obtained at pressures below 1.33×10^{-2} Pa.

The necessary high vacuum can be obtained by use of either an ion pump or a diffusion pump. The former is not generally recommended for analytical work, despite the 'clean' vacuum obtained, since the pumping speed is dependent upon the chemical properties of the vapour; oxygen is readily adsorbed whilst inert gases are pumped more slowly and may be regurgitated at higher operating pressures, giving memory effects. In contrast, the pumping speed of oil diffusion pumps is approximately related to the molecular weight of the vapour. The general design of an oil diffusion pump is shown in Figure 6.13. The pump fluid in the boiler (A) is heated to produce a pressure within the jet system (B,C and D). The resultant vapour travels upwards through the jet stages and emerges from the jet nozzles as high velocity vapour streams which impinge and condense on the cooled pump-body wall (G) and subsequently drain to the boiler. A portion of any gas arriving at the pump inlet (E) is trapped, compressed and transferred to the next stage, where the process is repeated until the gas is removed by a rotary pump via the cooled backing connection (F).

Figure 6.13 Diagrammatic representation of an oil diffusion pump

Key:
- A Boiler
- B Top jet nozzle
- C Middle jet nozzle
- D Bottom jet nozzle
- E Pump inlet
- F Backing connection
- G Water cooled pump body

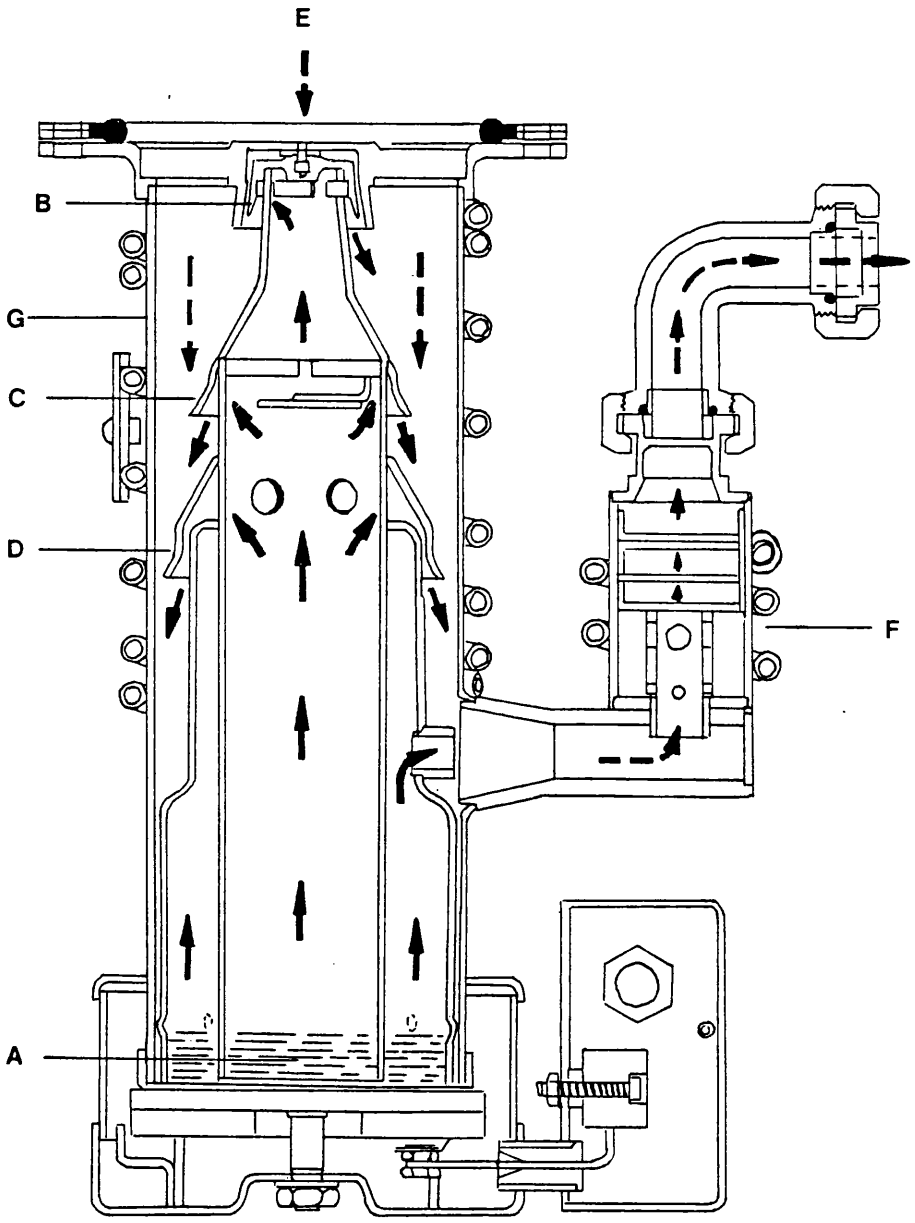

The choice of pump fluid can be critical in mass spectrometry applications since siliconeoils can be deposited on the electrodes, forming a tenacious insulating film which decreases the instrument's performance. In contrast, polyphenyl ether oils produce conducting films which can be easily removed by baking at 250^{o}C, although their chemical and thermal stability is not as good as the best silicone oils[262,263].

Pressure measurement in the high vacuum region is carried out using an ionization gauge. Cold cathode instruments work in the range 10 to 10^{-5} Pa and utilize a magnetic field to increase the ionization of the gas and hence sensitivity. Hot cathode ionization gauges, such as the Ion 7 (Edwards High Vacuum), are used in the range 10^{-1} to 10^{-8} Pa; the increased sensitivity being obtained by use of a heated filament to produce ionizing electrons and a fine wire ion collector. It should be noted that the sensitivity of both ionization gauges and mass spectrometers is dependent upon the degree of ionization of the gas concerned and that correction factors, specific for each instrument, have to be applied to obtain the true pressure of gases other than nitrogen.

Low vacuum measurement is best carried out by thermal conductivity gauges. Thermocouple gauges utilize a thermocouple attached to a heated filament to directly measure its increase in temperature as the pressure of gas decreases. Pirani gauges use a Wheatstone Bridge to measure the changing resistance of a

heated filament as the temperature changes due to cooling by the surrounding gas. Since the thermal conductivity depends upon the nature of the gas, correction factors have to be applied to obtain the true pressure of gases other than nitrogen.

b) Design and Construction of the System

The mass spectrometer gas detection system is shown diagrammatically in Figure 6.14. The analyser head (A) and cross-piece(D) (V.G. Micromass Ltd.) could be evacuated to 2.67×10^{-6} Pa by an EO_2 oil diffusion pump (J) (Edwards High Vacuum Ltd.), baffled to reduce the pumping speed from 150 to 2 $lsec^{-1}$ in order to produce a stable base pressure. The baffle consisted of a stainless steel plate,with six 2 mm diameter holes, which was bolted to the base of the cross-piece. The sample chamber (G) (V.G. Micromass Ltd.) could be evacuated to about 1.33×10^{-3} Pa by an EO_1 oil diffusion pump (K) (Edwards High Vacuum Ltd.). The separate parts of the high vacuum system were linked by FC 38 knife-edged flanges (o.d. 70 mm) sealed with copper gaskets; the fixing bolts being tightened in diagonally opposite pairs to ensure even compression of the gasket between the opposing knife edges. A new copper gasket was used each time a joint was reassembled,to ensure a reliable seal. The EO_2 and EO_1 diffusion pumps were linked to the high vacuum system by a Viton Co-Seal and 'O' ring respectively. The septum isolation valve (V3) (Hoke International Ltd.) allowed the septum (H) (Jones Chromatography Ltd.) to be changed without switching off the vacuum system. To prevent leakage under

Figure 6.14 Diagrammatic representation of mass spectrometer gas detection system

Key

A. Micromass 2 Analyser Head (V.G. Micromass Ltd.)

B. Magnet (V.G. Micromass Ltd.)

C. Ion Collector (V.G. Micromass Ltd.)

D. Cross-Piece (V.G. Micromass Ltd.)

E. IG5G Ionization Gauge Head (Edwards High Vacuum Ltd.)

F. Molecular Leak (V.G. Micromass Ltd.)

G. Sample Chamber (V.G. Micromass Ltd.)

H. Silicone Rubber Septum (3mm x 10mm Jones Chromatography Ltd.)

I. Baffle Plate (V.G. Micromass Ltd.)

J. EO_2 Water Cooled Oil Diffusion Pump (Edwards High Vacuum Ltd.)

K. EO_1 Water Cooled Oil Diffusion Pump (Edwards High Vacuum Ltd.)

L. SC10 Flexible Bellows (Edwards High Vacuum Ltd.)

M. FL20 Foreline Trap (Edwards High Vacuum Ltd.)

N. GDR1 Rotary Vacuum Pump (Kratos Ltd.)

P1 PR10 Pirani Gauge Head (Edwards High Vacuum Ltd.)

P2. PR10 Pirani Gauge Head (Edwards High Vacuum Ltd.)

R1. Micromass 1/2 Control Lead (V.G. Micromass Ltd.)

R2. Micromass 1/2 Control Lead (V.G. Micromass Ltd.)

R3. Ion 7 Ionization Gauge Control Lead (Edwards High Vacuum Ltd.)

R4. Pirani 11 Control Lead (Edwards High Vacuum Ltd.)

R5. Pirani 11 Control Lead (Edwards High Vacuum Ltd.)

V1. VRD 38R Viton Sealed Valve (V.G. Micromass Ltd.)

V2. VRD 38R Viton Sealed Valve (V.G. Micromass Ltd.)

V3. 4100 Series 316SS Bellows Sealed Valve (Hoke International Ltd.)

V4. SC10 Speedivalve (Edwards High Vacuum Ltd.)

V5. AV10 Air Admittance Valve (Edwards High Vacuum Ltd.)

Figure 6.14

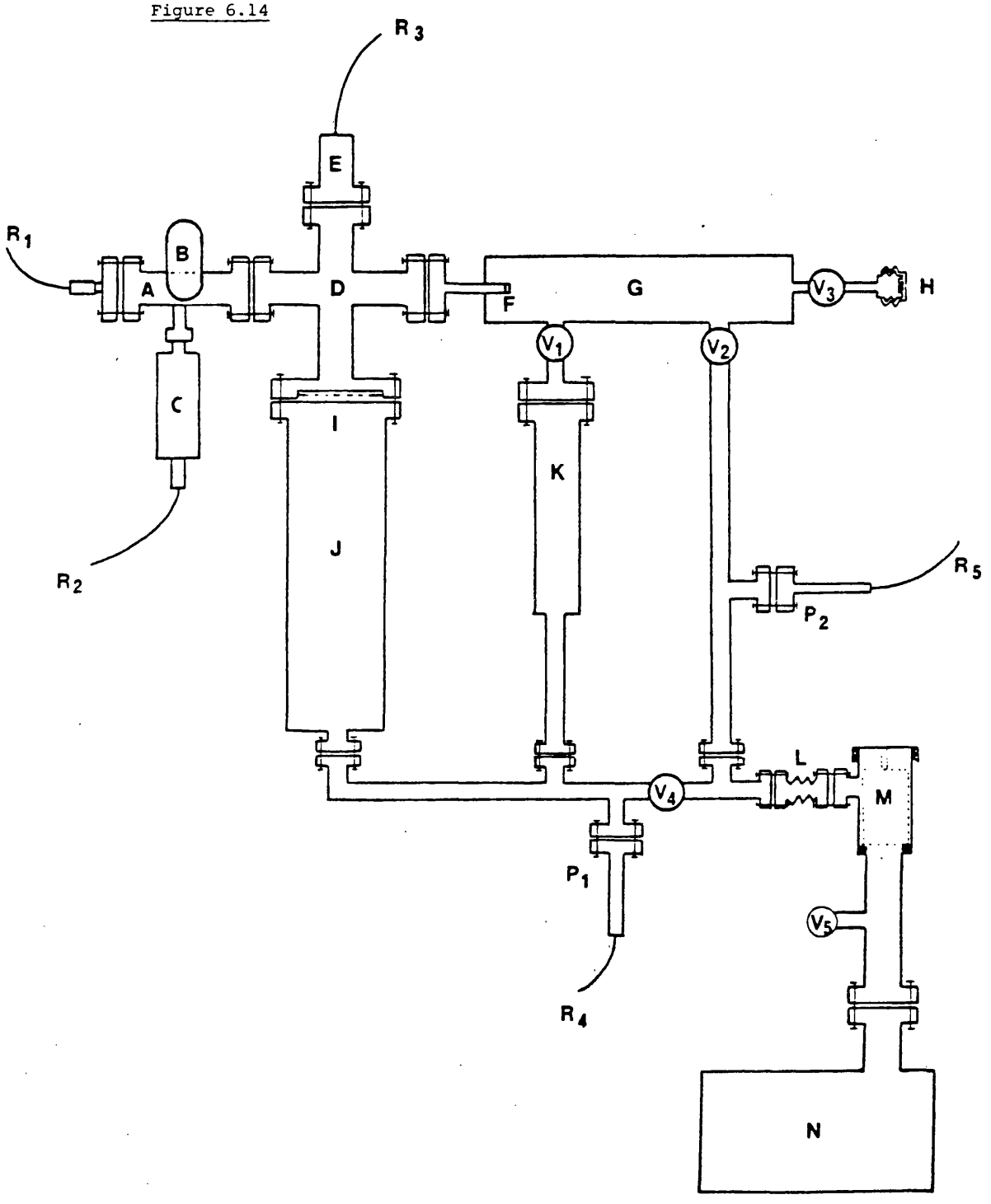

vacuum, the nut and ferrule seal of the valve were supplemented with 6.35 mm diameter gold wire seals placed at the front of the ferrules.

The backing line for the oil diffusion pumps and roughing line for the sample chamber were constructed from 15 mm o.d. copper pipe, using 'yorkshire' fittings for bends and 'T' junctions. The tubing ends were cleaned with OO grade steel wool and flux (Fluxite, Fry Ltd.) prior to assembly and soldering. To aid the attainment of a vacuum tight joint, an additional fillet of solder was run around the outside edge of each joint and 'wiped' with a chamois leather to give a smooth surface. The connections to the diffusion pumps, Pirani gauge heads (P1 and P2), backing line isolation valve (V_4), flexible bellows (L), foreline trap (M) and air admittance valve (V5)were made by'muff coupling' the tube and fittings (Figure 6.15). To ensure that a good seal was produced by the 'O' ring and muff it was necessary to slightly swage the ends of the copper tubing prior to cleaning with OO grade steel wool and Duraglit metal wadding. To minimise contamination of the vacuum system, the roughing and backing lines were thoroughly cleaned with trichloroethane ('Genklene', ICI Ltd.), RBS 25 (Chemical Concentrates (R.B.S.) Ltd.) and distilled water, before drying at 100^{o}C for 24 hours prior to the final assembly of the muff coupled joints. The connection to the GDR1 rotary vacuum pump was made via a flexible bellows (L) and foreline trap, charged with an activated alumina sorbent (M) (Edwards High Vacuum Ltd.) to isolate the high vacuum system from

Figure 6.15 'Muff coupling' of backing and roughing lines

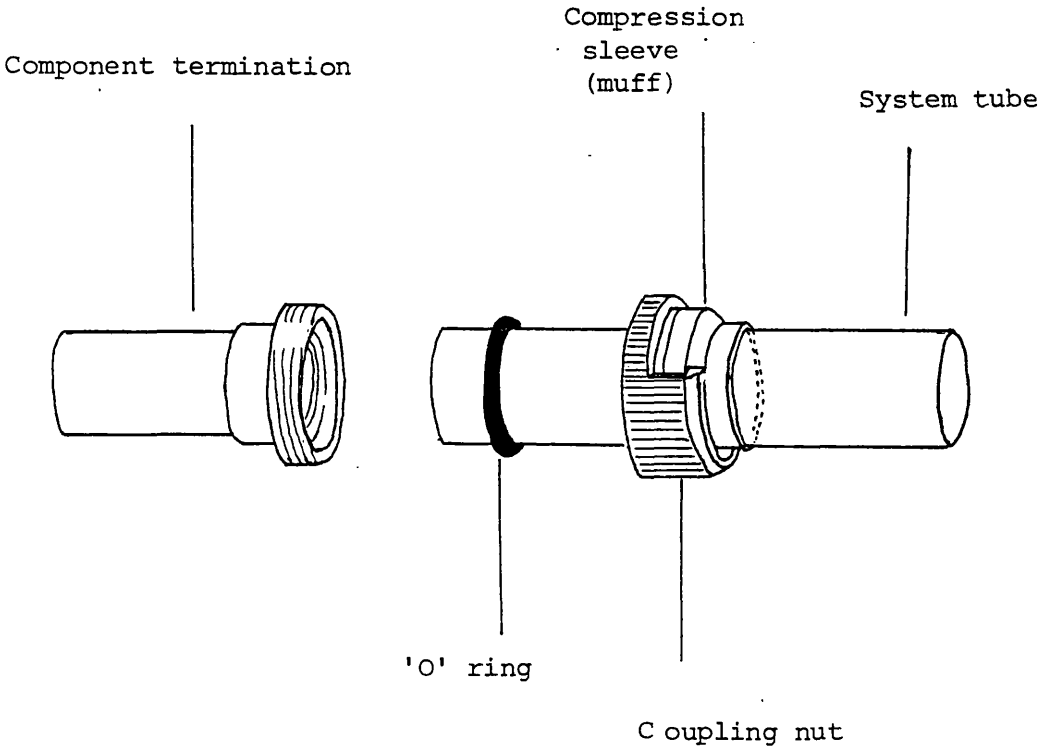

vibration and 'backstreaming' of oil vapour respectively.

The cooling water to the diffusion pumps (minimum flow rate 1 l min^{-1} at 20°C) was supplied through 6.35 mm o.d. annealed copper tubing; the two pumps being plumbed in series to minimize water wastage. To prevent the pumps from overheating in the event of cooling water failure, a thermal snap switch (Edwards High Vacuum Ltd.) was bolted to the side of the EO_2 pump. The power to both diffusion pumps was wired via this device which consisted of a bimetallic strip designed to break the circuit if the temperature exceeded 46°C and automatically reset at 35°C.

To protect the system from failure of the backing line, a control unit was built to switch off the diffusion pumps if the backing line pressure, sensed by Pirani gauge head P1 (Edwards High Vacuum Ltd.), rose above 8 Pa (Figure 6.16). The control circuit required feeds of +12 V, -12 V and a regulated + 5 V. 240 volts was applied to the 12-0-12 transformer (TR1), the 24 V output rectified by diodes D1-4 and then smoothed by C1 and C2, using the centre tap of the transformer, to provide a +12 V and -12 V supply. The regulated +5V rail was then derived from the +12V rail via the regulator IC1, with C3 and C4 providing additional smoothing. The Pirani gauge output, applied to socket A of the control circuit, was amplified by the operational amplifier IC2, with negative feedback via the resistive network R2 and RV1. The input was thus amplified from 0-10 mV to 0-5 V to be compatible with the following logic system. IC3d was a two input NOR gate, used as inverting Schmidtt Trigger, the state of whose output was controlled by the output of the operational amplifier (IC2). The switching point, or point at

Figure 6.16 Vacuum Pump Control unit

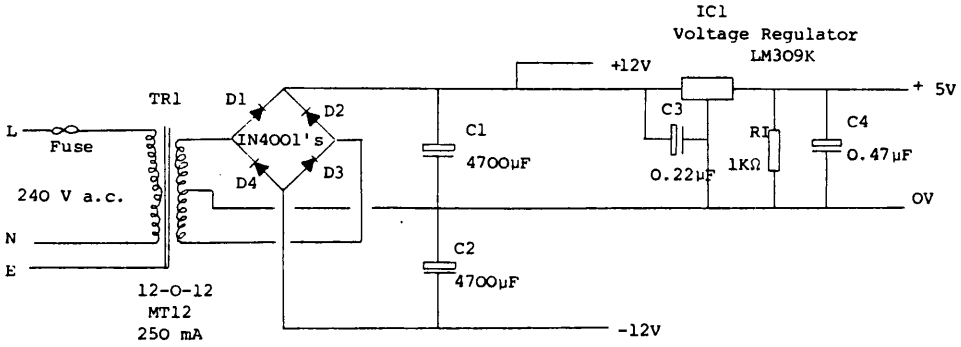

Power supply

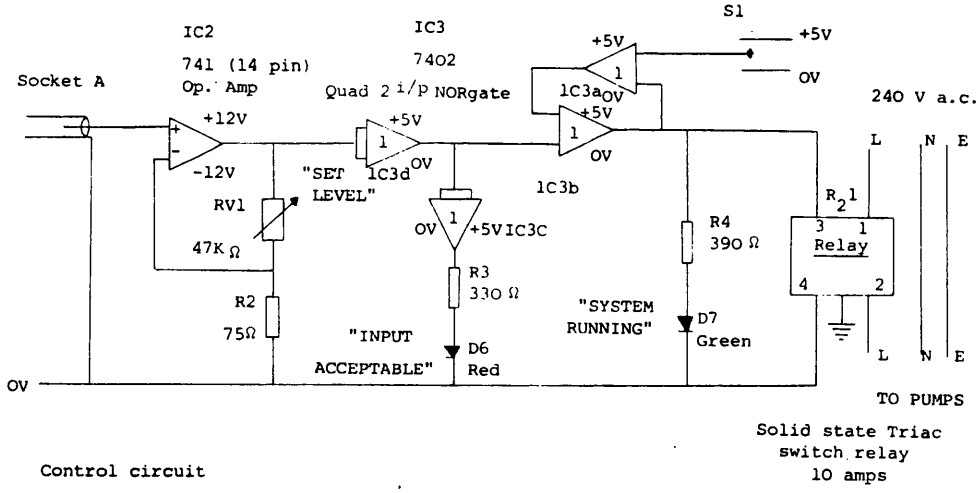

Control circuit

which the output of IC3d changed from a 0 to a 1 was set by the 'set level' potentiometer RV1, which controlled the amplification of IC2. This was adjusted to correspond to an input of approximately 6 mV, representing a backing line pressure of 8 Pa. IC3c , R3 and D6 gave an indication of an acceptable input for the diffusion pumps to run by a red light emitting diode (L.E.D.). The logic IC3a and IC3b required an additional pulse from switch S1 to provide an output to the relay (assuming a satisfactory input). Once S1 had been operated with a satisfactory input, the system ran by the feedback output of IC3a until either the input fell below the set level or the power supply failed. The system then remained inoperative until S1 was again operated. The green L.E.D.,D7, buffered by R4, provided an indication that the system was running. The output from IC3b was fed to a solid state relay, which utilized a 400 V 10 amp Triac to switch the power to the oil diffusion pumps. A 4 μF electrolytic capacitor had to be connected between the output of IC3b and the zero volt rail (across 3 and 4 of the relay) to prevent momentary 'dips' in voltage, due to mains switching and interference, interrupting the feedback to IC3a and switching the pumps off.

The sample chamber volume and leak rate of the sintered molecular leak (F) (V.G. Micromass Ltd.) were tailored around a gas sample volume of 0.25 ml, the pumping speed of the baffled EO_2 oil diffusion pump and the maximum pressure at which the analyser head can be operated on full emission without a drastic reduction in filament life ($3.33 - 6.67 \times 10^{-3}$ Pa).

The sample chamber (volume 1 litre) and molecular leak initially supplied had to be modified, as the pressure in the analyser head only rose to 8×10^{-5} Pa on injection of a 0.25 ml gas sample. Since the minimum detection limit of the mass spectrometer was directly related to the total pressure in the analyser head, this resulted in a system incapable of detecting less than 1345 ppm oxygen. The minimum detection limit was calculated as follows:-

$$\frac{P_m}{S \; P_T} = \frac{C_m}{C_T} \qquad \text{...(equation 6.3)}$$

where P_m = minimum detectable partial pressure

S = sensitivity factor of mass spectrometer for oxygen

C_m = minimum detectable concentration

C_T = total gas content

Although partial pressures are directly related to the concentration expressed in mole fraction rather than parts per million, the error in using the latter was insignificant for these approximations.

$$\frac{6.67 \times 10^{-8}}{0.62 \quad 8 \times 10\text{-}5} = \frac{C_m}{10^6}$$

$$C_m = 1345 \text{ ppm}$$

A larger molecular leak was installed in the sample chamber, increasing the total pressure in the analyser head to 2.4×10^{-4} Pa

and the minimum detection limit for oxygen to 448 ppm. To further increase the leak rate of the gas, the sample chamber was remade to reduce the internal volume from approximately 1 litre to 300 ml. The combination of the larger molecular leak and the higher sample pressure (resulting from the reduced chamber volume) produced a leak rate such that at a pressure of 3.33×10^{-3} Pa it was balanced by the pumping speed of the EO_2 oil diffusion pump. This produced a minimum detection limit of 32 ppm.

To minimize contamination of the vacuum system by oil vapour, a polyphenylether oil (Santovac 5, Edwards High Vacuum Ltd.) was used in the diffusion pumps and an uninhibited mineral oil (No. 16 grade, Edwards High Vacuum Ltd.) in the rotary vacuum pump[262].

c) Operation of the System

For analysis, the sample chamber was evacuated to approximately 1.33×10^{-3} Pa and isolated by closing valve V1. The gas sample was introduced via the septum, causing the sample chamber pressure to rise to about 80 Pa. Gas diffused through the molecular leak causing the pressure in the analyser head and cross-piece to rise from 2.67×10^{-6} Pa to 3.33×10^{-3} Pa, at which point the leak rate was balanced by the pumping speed of the EO_2 oil diffusion pump. The mass spectrometer was then tuned to each gas species of interest and the partial pressure recorded from the gauge on the Micromass 1/2 control unit or a potentiometric recorder. When the analysis was complete, valve

V_4 was shut, valve V_2 opened and the sample chamber evacuated to 4 Pa, indicated by Pirani gauge head P2. Valve V_2 was shut and valves V_4 and V_1 opened, allowing the EO_1 oil diffusion pump to evacuate the sample chamber to approximately 1.33×10^{-3} Pa. The total analysis time was about 2 minutes, although a further 10 minutes was required to ensure complete evacuation of the sample chamber prior to the next injection.

d) Evaluation of the System

Initially, the detection limit of the apparatus for oxygen in the samples was found to be some five times greater than the 32 ppm envisaged in the design. This was eventually traced to a gettering (reactive oxidation) action of the tungsten filament of the ionization gauge head which was effectively consuming oxygen, so lowering the partial pressure in the detection system. Table 6.4 clearly demonstrates that the response of the mass spectrometer to oxygen increased as the ionization gauge head was switched off and then completely removed. Comparison of the mass 32 and 28 peaks when a sample of high purity oxygen was injected indicated that as the peak due to oxygen increased, the mass 28 peak decreased. This phenomenon can be attributed to the reaction of oxygen at the surface of the tungsten filament, leading to the production of carbon monoxide. Such a comparison could not be made for the sample containing 540 ppm oxygen in nitrogen since the high partial pressure of nitrogen at mass 28 effectively masked any small changes due to the conversion of some of the oxygen to carbon monoxide.

Table 6.4 The effect of the ionization gauge head on the detected partial pressure at mass 32 (oxygen) and mass 28 (nitrogen and carbon monoxide) from 0.25 ml samples of high purity oxygen and 540 ppm oxygen in nitrogen

Ionization gauge head operating condition	High Purity Oxygen		540 ppm oxygen in nitrogen
	Partial pressure mass 32 - oxygen ($Pa \times 10^4$)	Partial pressure mass 28 - carbon monoxide ($Pa \times 10^4$)	Partial pressure mass 32 - oxygen ($Pa \times 10^7$)
on	4.665	9.666	3.607
off	9.000	2.000	6.667
removed	17.999	0.667	8.133

This problem, which has also been observed in relation to mass spectrometer filaments by other workers[264-267], can be minimized by use of low work function filaments such as rhenium, lanthanum hexaboride coated rhenium and thoria coated iridium[266,268]. Since ionization gauge heads containing such filaments were not compatible with the Ion 7 gauge control unit, the situation was resolved by removing the gauge head for oxygen analysis. The ionization gauge was not essential to operation once the system had been thoroughly checked out to ensure that the pressures in the analyser head before and after injection of a sample were correct. However, since the total pressure was not monitored, it was possible to overlook an error in the sample volume injected (e.g. a blocked needle could prevent complete evacuation of the syringe). Such errors were minimized by checking that the pressure indicated by the Pirani gauge head P2 rose to 15 Pa on evacuation of the sample chamber after each analysis, although it must be recognised that the reproducibility of such a value was dependent upon the pumping speed of the rotary vacuum pump and the time taken for analysis, since the sample was continuously removed by the EO_2 pump.

To remove adsorbed gases and vapour, chiefly water and hydrocarbons, from the vacuum system it was necessary to bake the system at 250^{o}C under vacuum, over a period of four weeks (Table 6.5). This was achieved by wrapping heating tapes (Electrothermal tape, A. Gallenkamp and Co. Ltd.) around the

analyser head, cross-piece and sample chamber after removal of the magnet, ion collector and control cables. The power to the heating tapes was regulated by a variable transformer (Rotary Regavolt, The British Electrical Resistance Co. Ltd.) to achieve the required temperature, which was measured using a digital thermometer (model 3001, Comark Electronics Ltd.). Although the majority of the system could be baked up to 400°C, the Viton sealed valves could not exceed 140°C to prevent damage to the seals. After baking for 28 days it was necessary to repeatedly inject samples containing oxygen until a stable response was obtained at mass 32, which did not fall with time. This was attributed to the 'clean' stainless steel surfaces adsorbing and reacting with oxygen, thus reducing the partial pressure detected until the binding sites had been saturated with oxygen.

Table 6.5 The effect of baking the vacuum system at 250°C on the residual water vapour peak (mass 18)

Time at 250°C (days)	Residual water vapour peak (mass 18) ($Pa \times 10^{6}$)
Nil	13.333
7	5.333
14	2.667
28	1.867

Considerable background noise was present on the more sensitive amplification ranges, such that measurements on the $0 - 3 \times 10^{-9}$ range would be inaccurate unless the response time of the instrument was increased to approximately 5 seconds by switching from the "fast" to the "normal" operating mode. In this mode, automatic mass scanning would require a new scan motor to reduce the scan speed from 1 AMU sec^{-1} to 0.1 AMU sec^{-1} and manual tuning to each peak was very tedious since the response took about 10 seconds to stabilise after each movement of the fine tune control. Furthermore, at higher partial pressures a voltage can develop on the ion collector, due to the ion charge, which causes ion suppression and amplifier non-linearity.

As an alternative to using the highest amplification range, the filament emission could be increased, so producing more ions which could be collected. However, this introduced other problems by reducing the filament life and increasing the background peaks due to the higher emission electron beam promoting reactions such as:- (Table 6.6)

$$CH_4 + O_2 \rightarrow CO + H_2O + H_2$$

$$2H_2 + O_2 \rightarrow 2H_2O$$

$$2CO + O_2 \rightarrow 2CO_2$$

Although such peaks could be resolved from that due to oxygen (mass 32), the concentration of oxygen available within the system for detection was reduced by these reactions. Measurements at different filament emissions were also a problem since they were not strictly comparable, as the cracking pattern of the spectra and hence the relative sensitivity for each gas was

Table 6.6 The effect of increased filament emission on the residual spectrum recorded by the mass spectrometer

Filament Emission	Partial pressure in residual spectrum			
	Mass 17 HO^+ ($Pax10^{-6}$)	Mass 18 H_2O^+ ($Pax10^{-5}$)	Mass 28 CO^+ N_2^+ ($Pax10^{-5}$)	Mass 44 CO_2^+ ($Pax10^{-6}$)
High (Torr Multiplier x 1)	16.000	5.973	6.453	31.465
Low (Torr Multiplier x 10)	4.160	1.707	1.867	4.320

affected[153]. Of these problems the use of the highest amplification range was considered to be the greatest. Consequently all measurements were routinely made at the higher filament emission, the fast response speed and the most sensitive amplification range avoided.

Figures 6.17, 6.18 and 6.19, show typical mass spectra obtained from the residual vacuum, high purity nitrogen and air respectively. The major peaks have been identified and listed in Table 6.7.

The mass 32 peak detected for high purity nitrogen (< 5 ppm oxygen) was unexpected since the minimum detection limit for oxygen was 30 ppm. The influence of the sample injection technique on this peak is examined later in this section and the reason

Figure 6.17 Typical residual mass spectrum

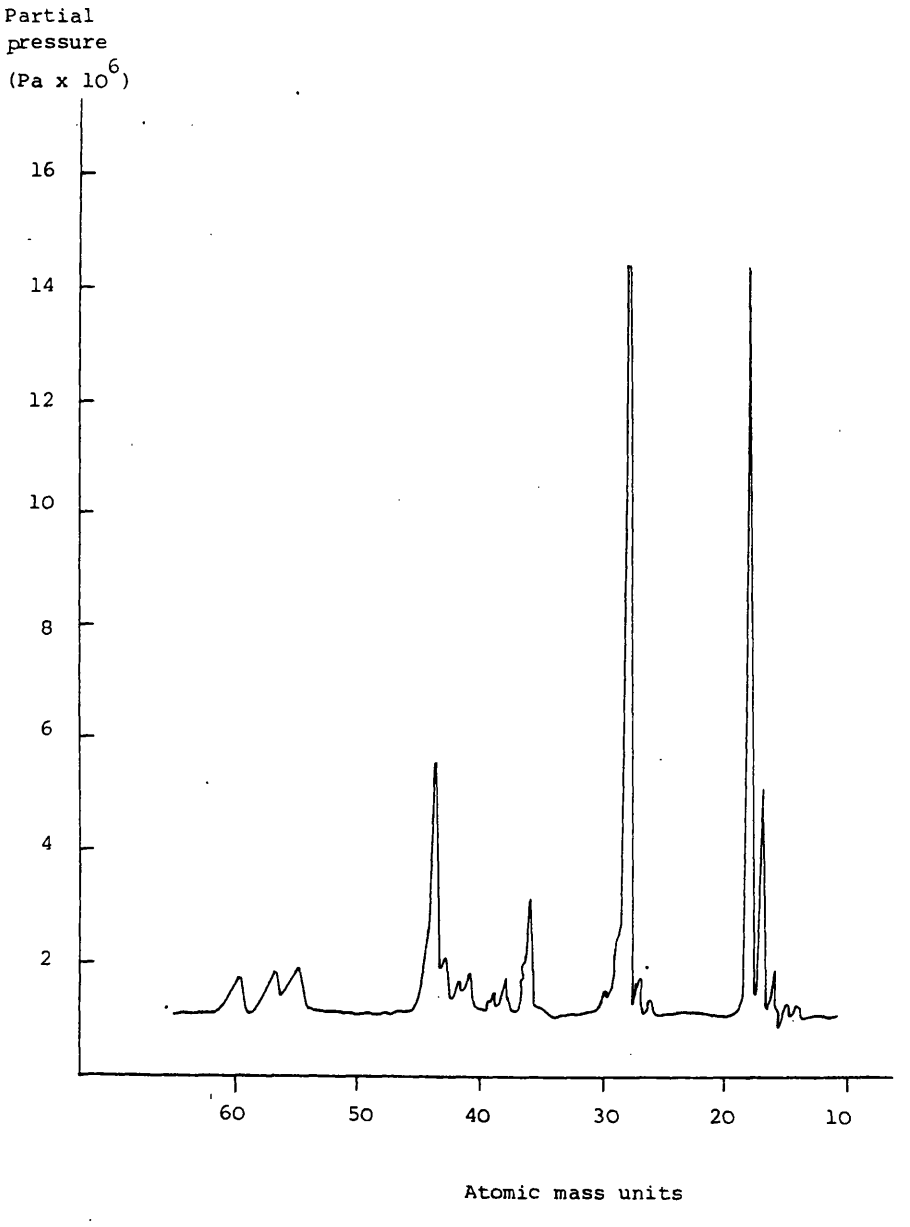

Figure 6.18 Typical mass spectrum of high purity nitrogen

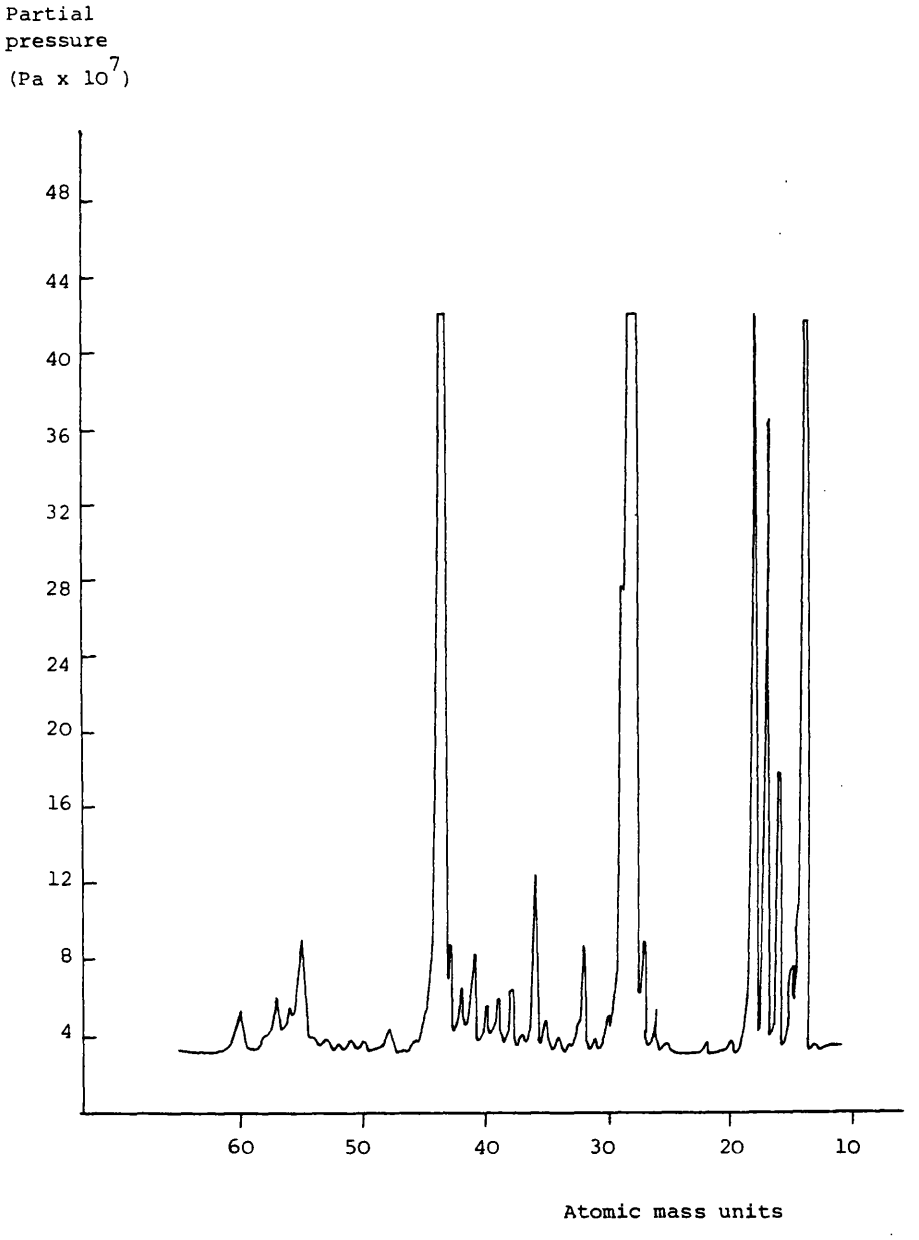

Figure 6.19 Typical mass spectrum for air.

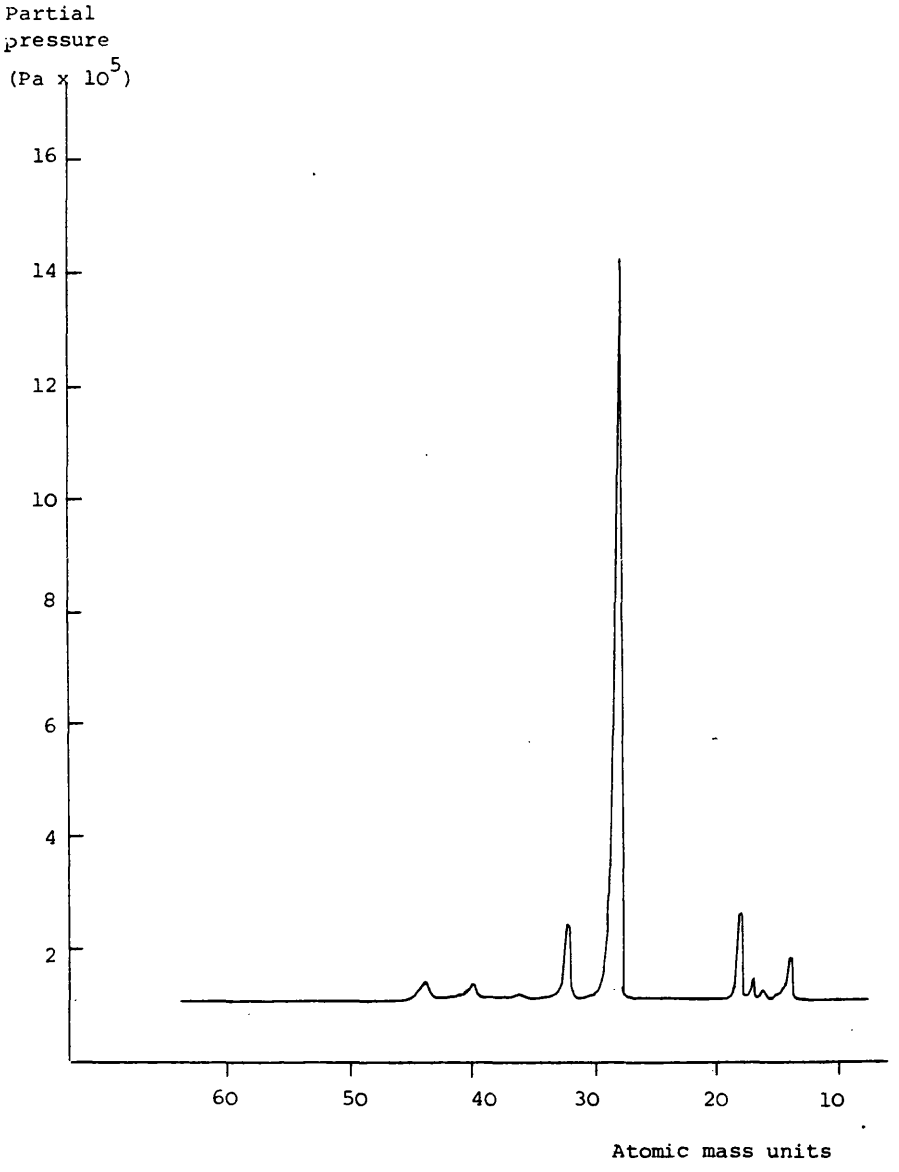

Table 6.7 Mass numbers, partial pressures and identification of the major peaks in the spectra of the residual vacuum and 0.25 ml samples of high purity nitrogen and air.

Mass Number	Residual vacuum		High purity nitrogen		Air	
	Partial Pressure ($Pa \times 10^6$)	Identification	Partial Pressure ($Pa \times 10^6$)	Identification	Partial Pressure ($Pa \times 10^6$)	Identification
14	0.27	CO^{++} (N_2^{++})	3.94	N_2^{++} (CO^{++})	7.47	N_2^{++} (CO^{++})
16	0.91	CH_4^+ (O_2^{++})	1.50	O_2^{++} CH_4^+	1.07	O_2^{++} (CH_4^+)
17	4.11	HO^+	3.41	HO^+	3.47	HO^+
18	13.40	H_2O^+	> 4.00	H_2O^+	15.47	H_2O^+
26			0.24	Hydrocarbon		
27	0.69	Hydrocarbon	0.61	Hydrocarbon		
28	13.40	CO^+ (N_2^+)	> 4.00	N_2^+ (CO^+)	>132	N_2^+ (CO^+)
29			2.50	Hydrocarbon		
30			0.21	Hydrocarbon		
32			0.56	O_2^+	13.33	O_2^+
36	2.13	HCl^+ Ratio 3:1 from Cl isotopes	0.94	HCl^+ from traces of cleaning fluid trichloroethane	1.07	HCl^+
38	0.64	at mass 36 and 38	0.37			
39			0.29			
40			0.26	A^+	3.20	A^+
41	0.75	Hydrocarbon	0.56	Hydrocarbon		
42			0.34	Hydrocarbon		
43	1.07		0.59	Hydrocarbon		
44	5.53	CO_2^+	>4.00	CO_2^+	3.20	CO_2^+
48			0.14	Hydrocarbon		
55	0.85	Hydrocarbon	0.62	Hydrocarbon		
57	0.80	Hydrocarbon	0.30	Hydrocarbon		
60	0.69	Hydrocarbon	0.26	Hydrocarbon		

Notes: 1. Ions in brackets e.g. (N_2^{++}) are least preferred

2. Hydrocarbon - from the cracking pattern the most likely source is the stainless steel and rotary vacuum pump oil, rather than the polyphenylether oil.

for the phenomenon discussed in section 6.1.2.5e, with reference to the calibration of the mass spectrometer for oxygen.

When the system was used in conjunction with a potentiometric recorder (TE 200, Tekman Ltd. or CR 6505, J.J. Instruments Ltd.) it became apparent that the peak height recorded was significantly lower than that indicated by the meter on the Micromass 1/2 control unit, demonstrating that the response speed of the recorder was too slow for the scan rate being used (1 AMU sec^{-1}). Comparison of the gauge deflection during automatic mass scanning and manual tuning indicated that even this was unable to respond fast enough. Five replicate determinations of the partial pressure of oxygen indicated for a single 0.25 ml sample of both air and high purity nitrogen, showed that use of the automatic scan unit gave a lower result and that the reproducibility of such values was poor (Table 6.8). The 't' test showed that the differences in partial pressure detected by the two methods were significant for both gas samples.

Consequently the mass spectrometer was manually tuned to each mass number of interest and the partial pressure read from the gauge on the control unit. By reading the partial pressure from the gauge rather than using a potentiometric recorder, occasional large peaks of background noise could be accounted for rather than appearing as a falsely high reading.

It was thought that the mass 32 peaks produced by samples of high purity nitrogen could be due to leakage around the septum/

Table 6.8 The effect of tuning method on the partial pressure of oxygen detected in single 0.25 ml samples of high purity nitrogen and air.

Tuning Method	High Purity Nitrogen			Air		
	Partial pressure at mass 32 (oxygen) ($Pa \times 10^{7}$)	S.D.	C.V. (%)	Partial pressure at mass 32 (oxygen) ($Pa \times 10^{5}$)	S.D.	C.V. (%)
Automatic	2.656	0.136	5.13	1.413	0.119	8.42
Manual	4.193	0.027	0.64	1.626	0.023	1.42
	$t_{calc} = 22.17$			$t_{calc} = 3.52$		
	S.D. = Standard Deviation					
	C.V. = Coefficient of Variation			t_{tab} (P=0.05) = 2.31		

needle junction during injection. However, the data in Figure 6.4a demonstrated that the mass spectrometer response remained practically constant even when the syringe was left 'in situ' for a period of 15 minutes.

The diffusion of air into the open end of the syringe needle was demonstrated by injecting five replicate samples of high purity nitrogen by two different techniques. Firstly, when the sample chamber was isolated prior to injection, the peak at mass 32 could have arisen from the nitrogen held in the body and needle of the syringe and any air which had diffused into the needle or leaked past the septum as it was punctured. Secondly, by continuously pumping the sample chamber during insertion of the needle through the septum, all gas held in the needle and leaking past the septum was removed prior to isolation of the chamber and admittance of the sample from the body of the syringe by opening the syringe valve.

Table 6.9 demonstrates that a significant proportion of the oxygen indicated for a 0.25 ml sample of high purity nitrogen was due to gas in the needle and leakage past the septum on penetration. The approximate volume of gas held in the needle, calculated from its internal dimensions, was 1.647×10^{-3} ml or 0.66% of the total sample volume, whilst the difference in partial pressure of oxygen detected by the two injection techniques was over 200%. Figure 6.4a showed that leakage past the septum with the syringe 'in situ' was

Table 6.9 The effect of injection technique on the partial pressure of oxygen detected in five replicate 0.25 ml samples of high purity nitrogen

Injection Technique	Partial pressure of oxygen detected in 5 replicate 0.25 ml samples of high purity nitrogen		
	Mean ($Pa \times 10^7$)	Standard Deviation ($Pa \times 10^7$)	C.V. (%)
Sample chamber isolated prior to injection and opening of syringe valve	2.473	0.146	5.90
Sample chamber pumped during injection and isolated prior to opening of syringe valve	0.803	0.014	1.74
$t_{calc} = 22.77$		$t_{tab}(P=0.05) = 2.31$	

minimal indicating that the discrepancy between the two injection techniques was due to air diffusion into the needle and/or leakage on penetration of the septum. Table 6.9 also demonstrates that the reproducibility was increased by use of the second injection technique. Consequently during all subsequent injections the sample chamber was only isolated prior to opening the syringe valve.

e. Calibration of the System

The mass spectrometer was initially calibrated using 0.25 ml samples of certified oxygen-nitrogen mixtures (55, 540

5100 and 50,000 ppm oxygen in nitrogen, Air Products Ltd.). These exhibited a thousand fold variation in concentration which was too great for accurate generation of permeability data. Day to day calibrations, over the desired working range, were therefore obtained by mixing the certified gases with high purity nitrogen (Air Products Ltd.). The maximum possible error in assuming that the latter contained no oxygen (maximum 5 ppm) was 4.6% at the lower end (108 ppm) and 0.013% at the upper end (40,000 ppm) Two Porter Flow Controllers (VCD 1000/A60, Jones Chromatography Ltd.) were used to control the flow rate (0 - 50 ml min^{-1}) of each gas entering a 'T' piece before a 0 - 150 ml min^{-1} Rotameter (Rotameter Manufacturing Co. Ltd.); gas ratios varying from 4:1 to 1:4 oxygen in nitrogen: nitrogen being used.

The calibration of the rotameter was checked using a dry gas meter (Gelsenkirchen Lange). High purity nitrogen was passed through the rotameter, at indicated flow rates varying from 10 to 100 ml min^{-1} and then through the dry gas meter. The true flow rate was calculated from the volume of gas which passed through the dry gas meter in 10 minutes. The calibration plots produced (Figure 6.20) were linear and least squares regression analysis gave the data shown in Table 6.10. Neither slope nor intercept were significantly different and regression of the combined data gave the values listed in Table 6.10. Although the intercept passed through the origin within $\pm$ two standard deviations, the slope was significantly greater than one (1.034 ± 0.010). However, this error in the manufacturer's

Figure 6.20 Calibration plot for the flow rate of high purity nitrogen indicated by a 0 - 150 ml min^{-1} Rotameter

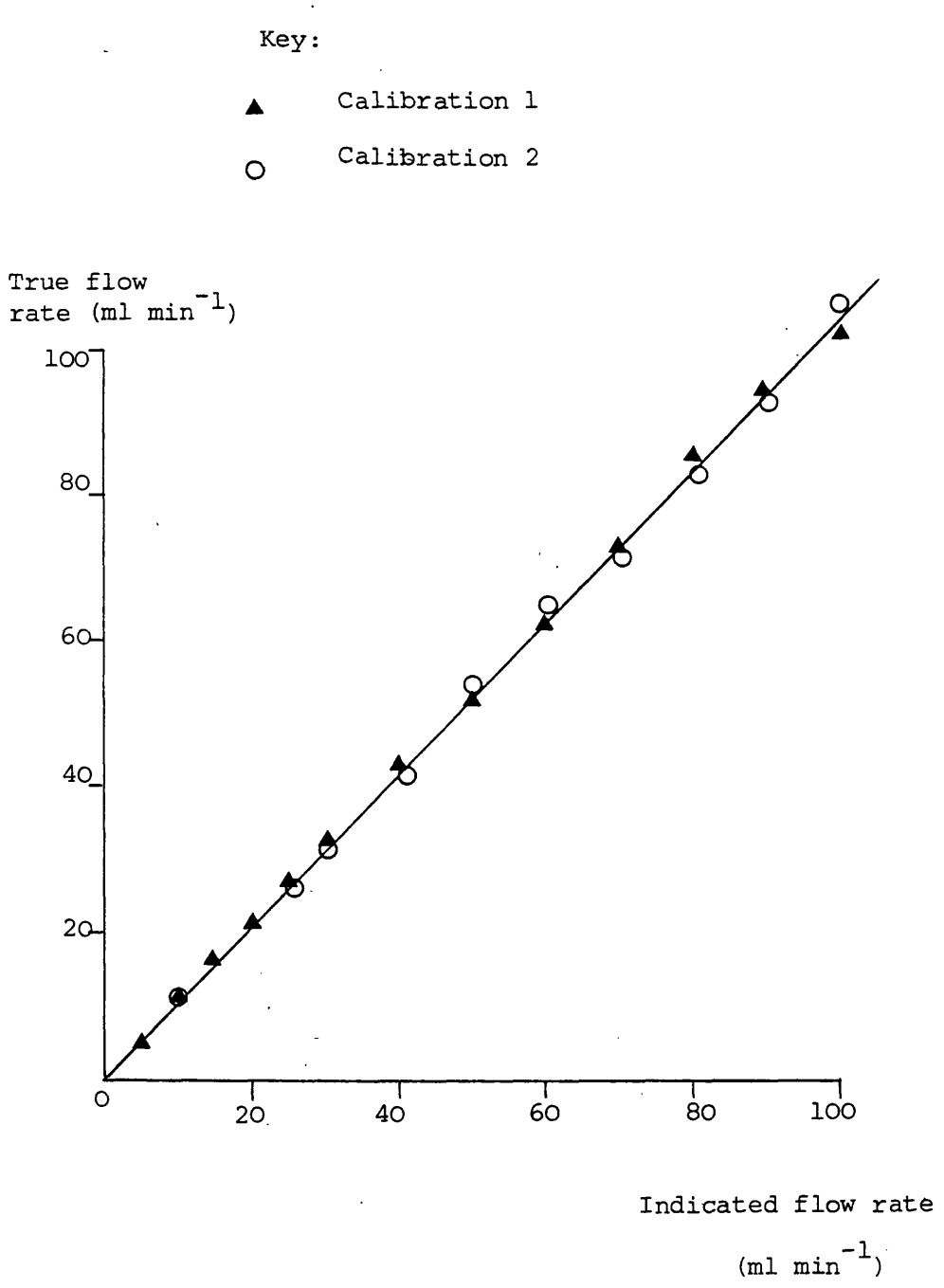

Table 6.10 Calibration data obtained for a 0 - 150 ml min^{-1} Rotameter, using a dry gas meter to record flow rates in the region 10 - 100 ml min^{-1}

Calibration	Slope ($\frac{\text{True Flow Rate}}{\text{Indicated flow rate}}$)	S.D. Slope	Rel. S.D. Slope (%)	Intercept (ml min^{-1})	S.D. Intercept	Correlation Coefficient
1	1.027	0.012	1.18	0.780	0.641	0.9992
2	1.045	0.015	1.46	0.176	0.899	0.9991
Combined	1.034	0.010	0.96	0.602	0.561	0.9990

$t_{slope\ 1,2} = 0.94$ $t_{int\ 1,2} = 0.55$

$t_{tab}\ (P=0.05) = 2.06$

calibration (3.4%) was too small to enable a correction to be applied to the flow settings used with the rotameter, due to the instrument's logarithmic scale.

The reproducibility of detection was determined by five replicate analyses at each concentration level using the certified gases (Table 6.11). This demonstrated that coefficients of variation were less than 1.1% at all concentrations studied. Therefore, subsequent data points were obtained from duplicate or triplicate determinations.

The mass spectrometer detects partial pressure which is directly proportional to the mole fraction of gas species under consideration in the gas mixture. Consequently calibration curves of oxygen partial pressure against oxygen concentration, expressed as ppm cannot, theoretically be linear. However, the error in assuming that the partial pressure was proportional to ppm oxygen in the sample was less than 0.7% over the concentration range 50 to 50,000 ppm oxygen in nitrogen:-

Oxygen concentration ppm	Ratio of the concentrations	Oxygen concentration mole fraction	Ratio of the concentrations	Percentage Difference between ratios
50 50,000	1×10^{-3}	4.375×10^{-5} 4.403×10^{-2}	9.936×10^{-4}	0.64

Table 6.11 The reproducibility of the partial pressure of oxygen detected in five replicate samples of certified oxygen:nitrogen mixtures

Oxygen Concentration (ppm)	Partial pressure of oxygen detected		
	Mean (Pa)	Standard Deviation (Pa)	Coefficient of Variation (%)
55	3.293×10^{-7}	3.600×10^{-9}	1.09
540	8.333×10^{-7}	4.667×10^{-9}	0.56
5100	6.253×10^{-6}	5.600×10^{-8}	0.90
50,000	5.205×10^{-5}	4.372×10^{-7}	0.84

Consequently a linear mass spectrometry calibration plot was obtained over this three decade concentration range, when the log of partial pressure less the injection constant (see below) was plotted against the log of the oxygen concentration in the sample (Figure 6.21). The log-log plot allowed better presentation of the three decade concentration range, but necessitated the subtraction of an injection constant equal to the response of the system when high purity nitrogen (< 5 ppm oxygen) was injected.

Figure 6.22 confirmed that the certified gas mixtures could be accurately mixed with high purity nitrogen, to produce samples of intermediate oxygen concentration. The calibration plot produced by mixing the certified gases was linear over the concentration range 216 to 50,000 ppm, with a relative standard

Figure 6.21 CALIBRATION PLOT FOR THE DETERMINATION OF OXYGEN IN NITROGEN OVER THE CONCENTRATION RANGE 50 - 50,000 ppm, USING 0.25ml GAS SAMPLES.

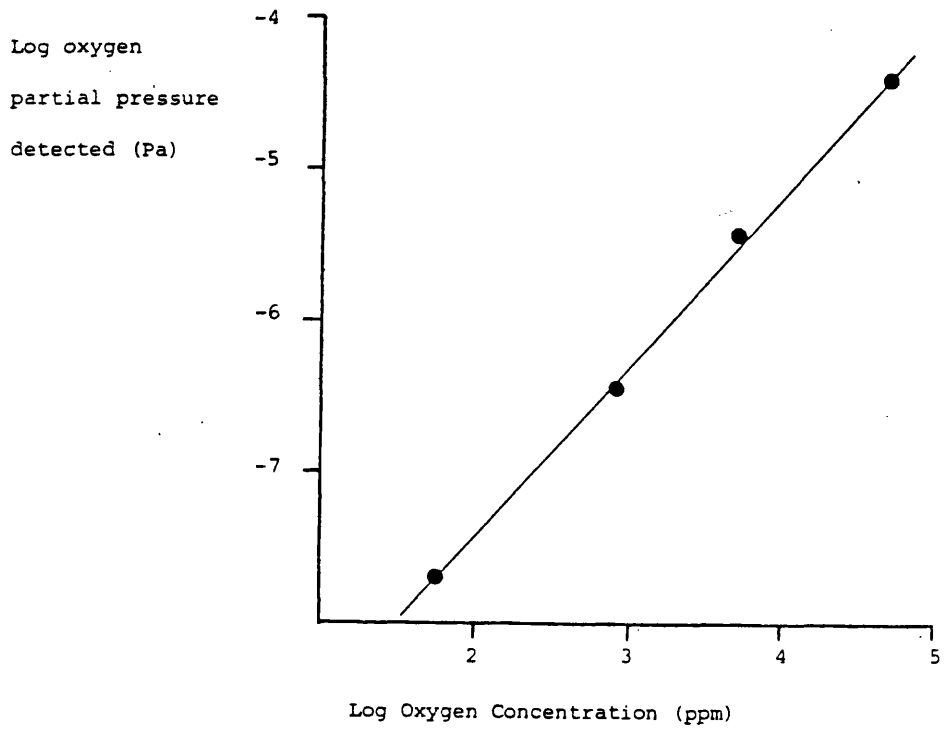

Figure 6.22 Calibration plot for the determination of oxygen in nitrogen over the concentration range 216 - 50,000 ppm using 0.25 ml gas samples produced by mixing certified gases with high purity nitrogen.

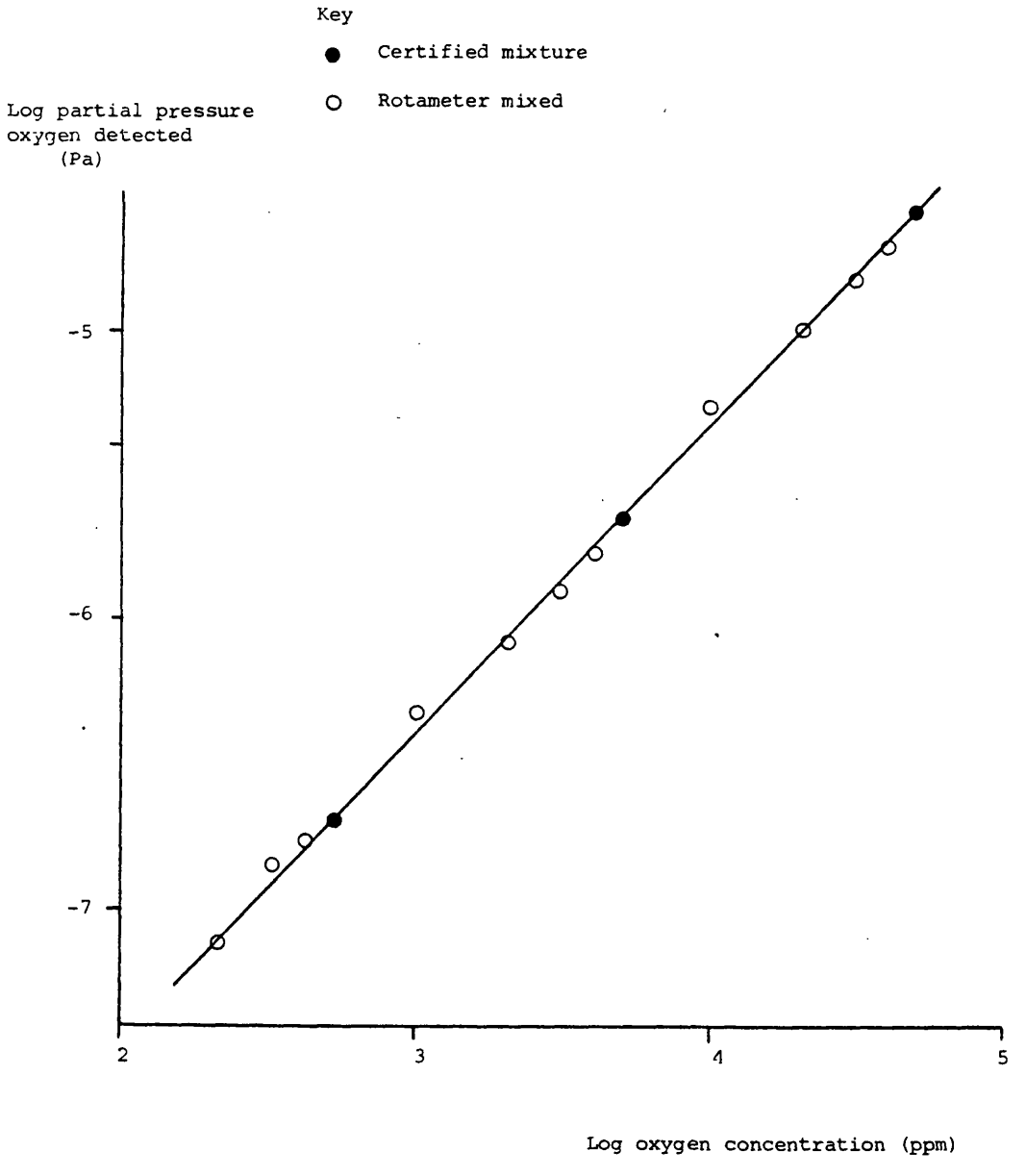

deviation of the slope of 1.19% and correlation coefficient of 0.9992.

Figure 6.23 shows a typical working range calibration plot, each point being the mean of at least two determinations. Replicate calibration plots determined on successive days were subjected to linear least squares regression analysis and the results shown in Table 6.12. Figure 6.23 and Table 6.12 both show that whilst the daily calibration curves were linear, they did not pass through the origin. The intercept values of about 2.67×10^{-7} Pa were not simply a measure of the residual oxygen in the system; base-line response at mass 32 was some twenty fold less at about 1.33×10^{-8} Pa. Values equivalent to the intercepts were also obtained when high purity nitrogen (< 5 ppm oxygen) samples were injected. Control experiments, described earlier in Sections 6.1.2.2 and 6.1.2.5d, eliminated the possibility of this being due to air leaking past the septum during injection. By continuously pumping the sample chamber whilst inserting the syringe needle through the septum, any air diffusing into the open end of the needle, or ingressing on puncturing the septum was removed prior to admission of the gas sample by opening the syringe valve. The most probable explanation for this phenomenon was, that on injection of the sample, the pressure in the sample chamber rose abruptly from 1.33×10^{-3} Pa to 80 Pa and that in the mass spectrometer from 2.67×10^{-6} Pa to 3.33×10^{-3} Pa. This was largely the consequence of the nitrogen component of the sample and may have resulted in the displacement of oxygen bound to the

Figure 6.23 CALIBRATION PLOT FOR THE DETERMINATION OF OXYGEN IN NITROGEN OVER THE CONCENTRATION RANGE 50 - 1100 ppm, USING 0.25ml GAS SAMPLES

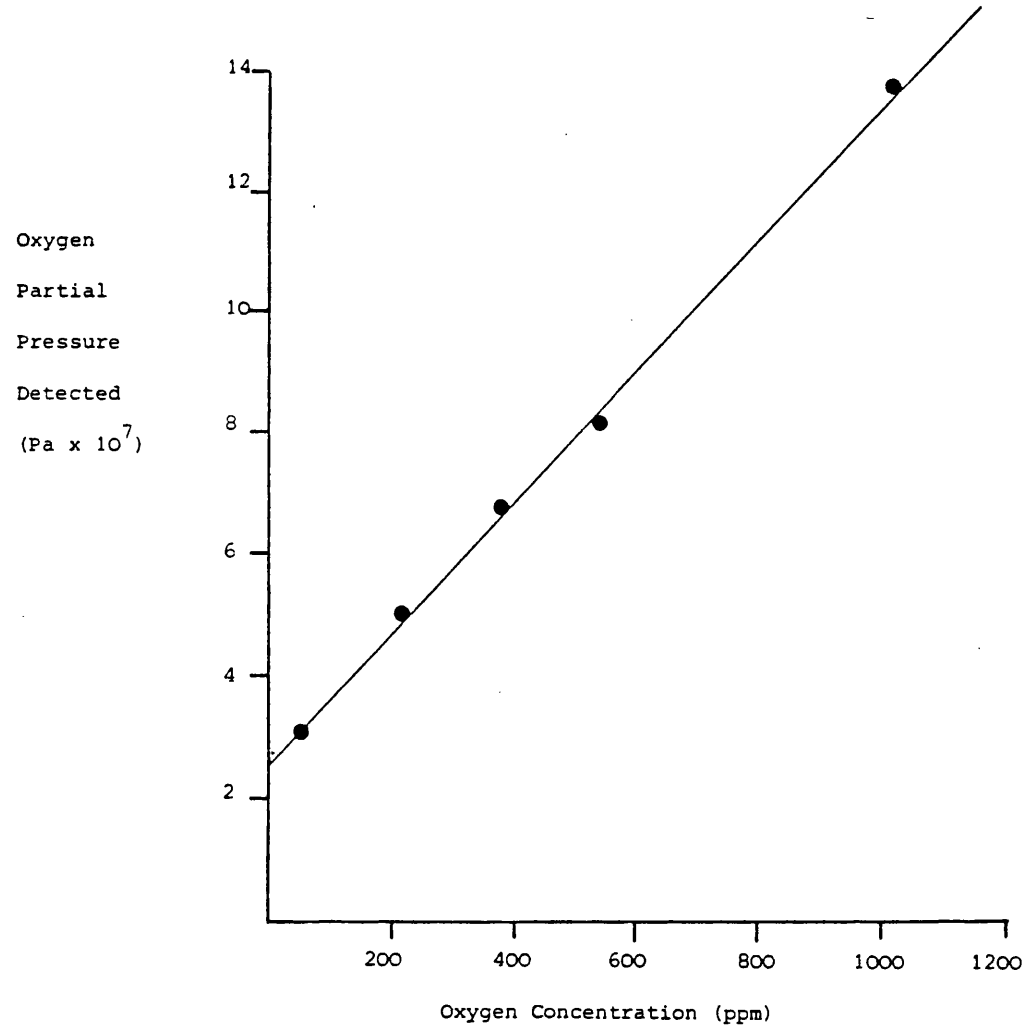

Table 6.12 Calibration Data obtained on Successive Days for the Determination of Oxygen in Nitrogen over the Concentration Range 50 - 1100 ppm using a 0.25ml Sample

Slope ($Pa\ ppm^{-1} \times 10^{9}$)	Stand. Dev. Slope ($\times 10^{9}$)	Rel. Stand. Dev. Slope (%)	Intercept ($Pa \times 10^{7}$)	Stand. Dev. ($\times 10^{7}$)	Correlation Coefficient
1.042	0.0155	1.5	2.453	0.080	0.9996
1.086	0.0227	2.1	2.595	0.125	0.9994
1.035	0.0144	1.4	2.819	0.079	0.9997
1.178	0.0172	1.5	2.843	0.095	0.9997
1.048	0.0164	1.6	2.688	0.091	0.9996
1.050	0.0129	1.2	2.745	0.101	0.9997
Mean Slope 1.073×10^{-9}			Mean Intercept = 2.691×10^{-7}		
Coeff. Variation = 5.1%			Coeff. Variation = 5.5%		$X^2_{tab} = 11.07$ ($p = 0.05$)
X^2 Slope 52.25			X^2 Intercept = 11.65		

stainless steel surfaces of the high vacuum system. The effect however, was fairly reproducible (Table 6.12) and does not therefore invalidate the method.

Table 6.12 shows that all the calibration plots were linear with correlation coefficients better than 0.999 and relative standard deviations for the slopes of under 2.1%. However, there was a slight day to day variation in the regression equations, the mean slopes and intercepts both having a coefficient of variation of about 5%. Slope and intercept values were therefore subjected to a Bartlett test, giving χ^2 values of 52.3 and 11.7 respectively, compared to the tabulated value of 11.1 (P=0.05), thus indicating that the differences, although fairly small, were significant. This day to day variation was possibly associated with the mass spectrometer side of the system being switched off overnight. After discarding the first four injections of the day, which allowed the oxygen displaced by injection of a sample to reach an equilibrium, calibration data carried out at any point within a normal day's working were always reproducible. Consequently a calibration plot was determined each day, injecting standard gas samples at intervals between samples for analysis. The regression equations for these calibrations are tabulated in Appendix I.

After replacement of the mass spectrometer filament, the slope of the calibration plots increased steadily due to

incomplete baking of the system allowing contaminants, introduced when the vacuum was broken, to be slowly removed during use. Complete baking of the system for four weeks was not carried out since the mass spectrometer could be used reproducibly for oxygen analysis after 7 to 10 days, thus reducing 'down time'. The fall in the calibration slope prior to failure of the filament resulted from thinning of the filament causing a reduction in its emission and hence ionization of the gas sample (Appendix I).

For experiments involving the use of gas and vapour mixtures, it was important that the presence of water vapour did not affect the mass spectrometer's response to oxygen. Such an effect could arise from competitive effects at adsorptive and reactive sites within the high vacuum system and electron beam. The detected partial pressure of oxygen in four replicate samples containing 5,100 ppm oxygen in nitrogen was measured before and after the gas was passed through the saturator at a rate of 25 ml min^{-1} (Table 6.13). The 't' test demonstrates that the partial pressure of oxygen detected was not significantly affected by the presence of water vapour.

6.1.3 Evaluation of Oxygen Permeability Measurement Using The System

By use of the techniques, optimized in section 6.1.2, oxygen permeability measurements were evaluated.

Table 6.13 The effect of water vapour on the partial pressure of oxygen detected in four replicate samples of gas containing 5100 ppm oxygen in nitrogen

Water Content	Partial pressure of oxygen detected in 0.25 ml samples of gas containg 5100 ppm oxygen in nitrogen		
	Mean ($Pa \times 10^{-6}$)	Stand. Dev. ($\times 10^{-6}$)	Coeff. Var. (%)
Nil	7.075	0.064	0.91
Saturated at 30°C	7.093	0.077	1.09
$t_{calc} = 0.36$	t_{tab} (P=0.05) = 2.45		

6.1.3.1 Film Seal Integrity

Although the cell had been leak tested at 0.69 MPa, this test did not establish that gas leakage from the donor to receptor compartment could not occur around the film seating. The cell was fitted with an aluminium film (19 μm thick domestic grade, Bacofoil), flushed with high purity nitrogen and the receptor compartment isolated. Pure oxygen was passed through the donor compartment and the oxygen level in the receptor compartment monitored as a function of time at various intervals ranging from every 15 minutes to a single sample ,withdrawn after 3 hours. The results are shown in Tables 6.14 and 6.15 and Figures 6.24 and 6.25.

With an aluminium foil film in the cell, no increase in the partial pressure of oxygen in the receptor was observed when a

single sample was withdrawn after intervals up to 3 hours (Table 6.14). This indicated that neither the receptor compartment nor film seal were leaking. However, if several samples were taken for analysis at intervals during the three hour period, a rise in oxygen concentration was observed which could be minimized but not eliminated by repeatedly flushing the syringe and needle with high purity nitrogen prior to sampling (Figure 6.24). The negative points at time zero arose due to the standard deviation of the intercept of the calibration plot (see Table 6.12) causing a 5 to 10 ppm error in the indicated oxygen concentration. Figure 6.24 also demonstrates that the greater the number of samples taken over the three hour period, the greater the rise in oxygen content in the receptor compartment of the cell. The slope of the line for all samples taken at 30 minutes intervals, other than the first 15 minutes sample, was about half that when samples were taken every 15 minutes (Table 6.15) and the first sample at 15 minutes did not fit on the 30 minute line very well. Figure 6.25 shows the data replotted as receptor oxygen concentration against the number of samples taken, when the lines based on the standard sampling technique became coincident. Least squares regression of this data gave the results shown in Table 6.15, which confirmed that the increase in oxygen content of the receptor compartment, with an aluminium film in place, was associated with sampling and not leakage past the membrane. The relative standard deviation of the slope became smaller for the 30 minute sample plot when time was translated to sample number (Table 6.15) and the 't' test showed that both slopes and intercepts for this plot were not significantly

Table 6.14 The partial pressure of oxygen detected in a single sample of gas withdrawn, at intervals up to 3 hours, from the receptor compartment of a permeability cell fitted with an aluminium foil film .

Time before withdrawing a single 0.25 ml sample (Hours)	Partial pressure of oxygen detected ($Pa \times 10^{7}$)
Nil	1.73
0.5	1.80
1.0	1.81
1.5	1.73
2.0	1.76
2.5	1.79
3.0	1.73
Mean detected partial pressure	$= 1.764 \times 10^{-7}$ Pa
Standard deviation	$= 3.289 \times 10^{-9}$
Coefficient of variation	= 1.87%

different from those obtained with the 15 minute sampling data. The explanation for this phenomenon was associated with the needle of the syringe being evacuated as the sample was introduced into the mass spectrometer and consequently filled with air on withdrawal.This volume of air was then injected into the receptor compartment when the next sample was taken. Since this effect could not be eliminated by flushing the syringe and needle with nitrogen prior to sampling it was probable that either oxygen diffused into the needle very rapidly, or that some air leaked into the cell as the septum was punctured.

Figure 6.24 The effect of sampling time on the concentration of oxygen found in the receptor compartment of the permeability cell fitted with an aluminium film.

KEY

○ Samples withdrawn at 30 minute intervals

▲ Samples withdrawn at 15 minute intervals

● Syringe flushed with nitrogen prior to sampling at 30 minute intervals

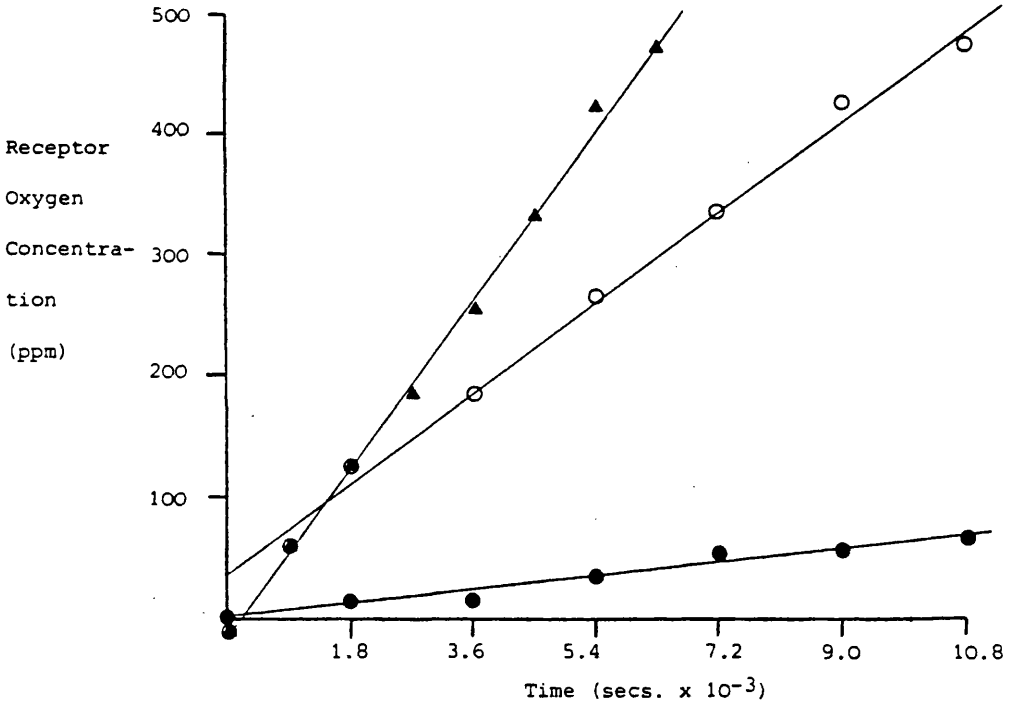

Table 6.15 Least Squares Regression Analysis Data for the Build-up of Oxygen in the Receptor Compartment of the Permeability Cell fitted with an Aluminium Film

Time Intervals	Data Plotted on Time Basis				Data Plotted on Sample Number Basis			
	Slope (SD) (ppm sec^{-1} x 10^2)	Rel SD (%)	Intercept (SD) (ppm)	r	Slope (SD) (ppm $injection^{-1}$)	Rel SD (%)	Intercept (SD) (ppm)	r
15 mins.	7.778 (0.187)	2.4	-14.96(7.03)	0.9983	70.00 (1.68)	2.4	-14.96(7.03)	0.9983
30 mins.	4.346 (0.178)	4.09	23.14(10.81)	0.9950	70.09 (1.45)	2.06	-11.95(6.04)	0.9987

(SD) = Standard deviation

r = correlation coefficient

t Slope 0.04

t Intercept 0.29

t tab 2.18 (p = 0.05)

Figure 6.25 THE EFFECT OF SAMPLING NUMBER ON THE CONCENTRATION OF OXYGEN FOUND IN THE RECEPTOR COMPARTMENT OF THE PERMEABILITY CELL FITTED WITH AN ALUMINIUM FILM

KEY

○ Samples withdrawn at 30 minute intervals

▲ Samples withdrawn at 15 minute intervals

● Syringe flushed with nitrogen prior to sampling at 30 minute intervals

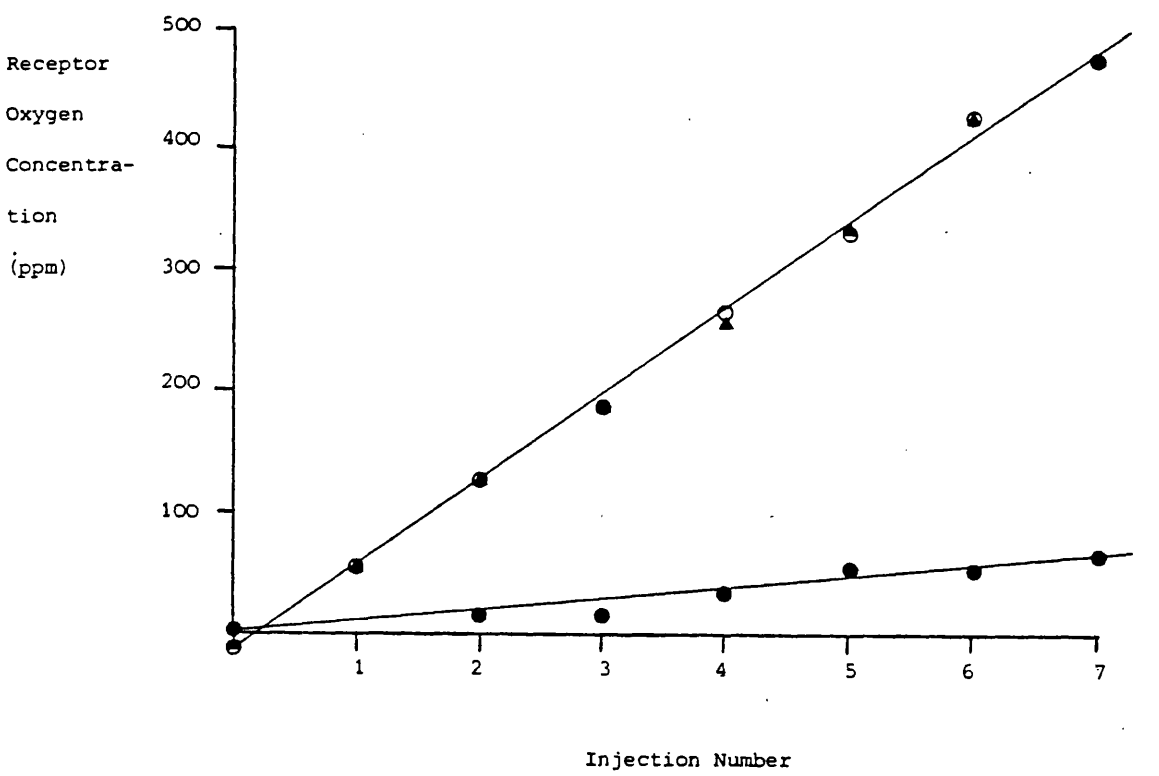

As Table 6.15 showed the sampling error to be consistent, since the plots were linear and passed through the origin effectively within $\pm$ two standard deviations, a correction factor equal to the slope multiplied by the sample number could be subtracted from the sample oxygen content, to give the correct concentration in ppm. Five replicate determinations of this slope were carried out using a side port needle and three with the conventional needle, the results being shown in Tables 6.16 and 6.17 respectively. The correction factor for the conventional needle, which was smaller due to its lower volume, was required as some initial work had been carried out prior to the change to side port needles (Section 6.1.2.2).

The mean results of 30.35 and 71.57 ppm injection^{-1} for the conventional and side port needles respectively, were subtracted from all subsequent determinations of the oxygen concentration in the receptor compartment.

6.1.3.2 Receptor Compartment Volume

The receptor compartment was designed to have an internal volume of 50 ml, but addition of the isolation valves and engineering inaccuracies necessitated the precise determination of this figure. The cell was fitted with an aluminium foil film, flushed with high purity nitrogen and the receptor compartment isolated. 1 ml of high purity oxygen was injected into the receptor compartment and after two minutes a 0.25 ml sample withdrawn for analysis; the time interval being to ensure

Table 6.16 Least squares regression analysis data for replicate determinations of the correction factor to be applied for side port needles.

Slope (ppm injection^{-1})	Stand. Dev. Slope (ppm injection^{-1})	Rel. Stand. Dev. slope (%)	Intercept (ppm)	Stand. Dev. Intercept (ppm)	Correlation Coefficient
73.53	1.89	2.57	-14.86	7.90	0.9980
71.09	1.45	2.04	-11.95	6.04	0.9987
73.06	1.00	1.37	-14.07	4.16	0.9949
70.61	1.48	2.10	-14.01	6.18	0.9987
69.58	1.68	2.42	-14.96	7.03	0.9983

Mean slope = 71.57 ppm injection^{-1}

S.D. = 1.67

C.V. = 2.34%

χ^2 Slope = 4.78

χ^2_{tab} (P=0.05) = 9.49

Mean intercept = -13.97 ppm

S.D. = 1.21

C.V. = 8.67%

χ^2 Intercept = 0.14

Table 6.17 Least squares regression analysis data for replicate determinations of the correction factor to be applied for conventional needles

Slope (ppm injection^{-1})	Stand. Dev. Slope (ppm injection^{-1})	Rel. Stand. Dev. slope (%)	Intercept (ppm)	Stand. Dev. Intercept (ppm)	Correlation Coefficient
30.27	0.87	2.86	10.18	3.62	0.9976
31.71	1.66	5.23	5.16	6.94	0.9919
29.07	0.98	3.37	-28.35	4.10	0.9966

Mean slope = 30.35 ppm injection^{-1}

S.D. = 1.32

C.V. = 4.36

χ^2 Slope = 2.34

Mean intercept = -4.34 ppm

S.D. = 20.95

C.V. = 482.65%

χ^2 Intercept = 33.72

$\chi^2_{tab}(P=0.05) = 5.99$

complete diffusional mixing, although no evidence of incomplete mixing was observed if samples were withdrawn earlier. To prevent errors due to leakage of air into the cell during penetration of the septum, the syringe was not withdrawn between injecting 1 ml of high purity oxygen and taking a 0.25 ml gas sample for analysis. This also avoids using the correction factor determined in Section 6.1.3.1.

The procedure was repeated six times and the volume of the receptor compartment (V_R) calculated from the mean oxygen concentration (C_R) using equation 6.4

$$C_o V_I = C_R(V_R + V_I)$$

$$V_R = \frac{1.10^6}{C_R} - 1 \qquad \text{...(equation 6.4)}$$

C_o = concentration of oxygen in high purity oxygen (10^6 ppm)

V_I = volume of oxygen injected (1 ml)

V_R = volume of receptor compartment

C_R = concentration of oxygen detected in the receptor compartment.

The mean oxygen concentration was determined as 19379 ppm (standard deviation 79, C.V. 0.41%) and the volume of the receptor compartment calculated as 50.61 ml (5.061×10^{-5} m^3)

The area of the film exposed to the permeant was defined by the inside diameter of the sealing ring and ledge. This was measured as 15.00 mm with vernier callipers (model 1140, Moore and Wright Ltd.), giving an exposed film area of 176.72 mm^2 (1.7672×10^{-4} m^2).

6.1.3.3 Effect of donor gas flow rate and stirring of the receptor compartment on film permeability

A 40 μm thick HPMC film was prepared by spraying a 5% w/v aqueous solution of Pharmacoat 606 on to a glass plate, at a rate of 32 ml min^{-1}, under the conditions described in Section 4.3.1.3. This film was fitted into the cell and the effect of increasing the donor gas flow rate from 25 to 50 ml min^{-1} evaluated (Table 6.18 and Figure 6.26).

If good mixing was not rapidly achieved in the receptor compartment then a concentration gradient could be established leading to incorrect assessment of permeability coefficients. The effect of stirring the receptor compartment, by mounting the cell on a magnetic stirrer (model MS1, Techne Ltd.) with the stirrer bar inside, was therefore determined using a 40 μm thick sprayed HPMC film (Table 6.18 and Figure 6.26). Visual inspection with the cell top removed ensured stirring did, in fact, take place and significant turbulence was demonstrated by injecting smoke (Smoke Canister, P.H. Smoke Products Ltd.) into the receptor compartment, via the septum, whilst stirring.

Figure 6.26 shows the Barrer plot for oxygen permeation through a 40 μm thick HPMC film under donor gas flow rates of 25 ml min^{-1}, with and without stirring and at 50 ml min^{-1}. The negative intercepts were consistent with permeability theory which predicts lag times before steady state transport is achieved. Least squares regression analysis of the data showed that neither stirring nor donor gas flow rate affected the transport rate of oxygen across the film (Table 6.18). This confirmed that a flow rate representing approximately ten changes of donor gas per minute (donor volume approximately 2.5 ml) was sufficient to prevent the depletion of oxygen, or the formation of stagnant layers within the donor compartment.

Consequently 25 ml min^{-1} was adopted as the standard flow rate of donor gas in subsequent work and the system was not stirred.

6.1.3.4 Oxygen permeability coefficient for polyethylene film at 30°C.

Oxygen transport rates were determined for 38 μm thick non-orientated polyethylene sheeting (Trans-Atlantic Plastics Ltd.). As the oxygen concentration in the receptor compartment was always well under 1% of that in the donor compartment, sink conditions were assumed to be operating and the Barrer equation[243,269] (equation 1.5) was applicable. A plot of receptor compartment concentration (C_R) against time (t) should therefore exhibit a steady state slope ($\frac{dC_R}{dt}$) from which

Figure 6.26 THE EFFECTS OF DONOR GAS FLOW RATE AND STIRRING IN THE RECEPTOR COMPARTMENT, ON THE RATE OF OXYGEN TRANSFER ACROSS A 40μm THICK HPMC FILM

KEY

■ 50ml $min.^{-1}$ donor gas flow rate

▲ 25ml $min.^{-1}$ donor gas flow rate

○ 25ml $min.^{-1}$ donor gas flow rate with stirring of the receptor compartment.

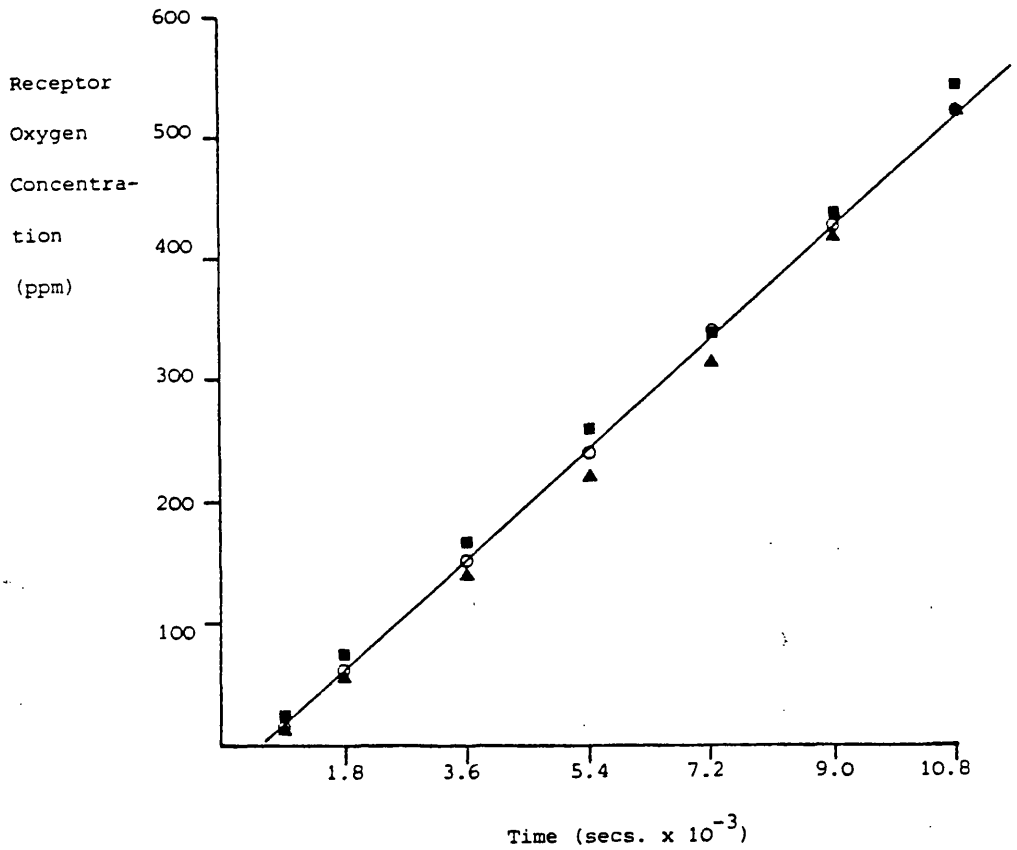

Table 6.18 Data derived from Barrer Plots for Oxygen Transport through a 40μm HPMC Film at 30°C

Experimental Conditions	Slope (SD) (ppm s^{-1} x 10^2)	Rel. SD (%)	Intercept (SD) (ppm)	r
1. 25ml min^{-1} (unstirred)	5.081 (0.122)	2.40	- 42.3 (7.9)	0.9986
2. 25ml min^{-1} (stirred)	5.092 (0.036)	0.71	- 32.9 (2.4)	0.9999
3. 50ml min^{-1} (unstirred)	5.097 (0.090)	1.76	- 19.9 (5.9)	0.9992
$t^{1:2}_{slope}$ = 0.09		$t^{1:2}_{intercept}$ = 1.14		
$t^{1:3}_{slope}$ = 0.11		$t^{1:3}_{intercept}$ = 2.17	t_{tab} = 2.23 (p=0.05)	

the permeability constant (P) can be calculated (equation 6.5)

$$C_R = \frac{P_A C_D}{L V_R} \cdot \left[t - \frac{L^2}{6D} \right] \qquad \text{...(equation 1.5)}$$

$$P = \frac{L V_R}{A C_D} \frac{dC_R}{dt} \qquad \text{...(equation 6.5)}$$

A and L are the area (1.7672×10^{-4} m^2) and thickness (3.8×10^{-5} m) of the film respectively, V_R is the volume of the receptor compartment (5.061×10^{-5} m^3), C_D is the concentration of the species of interest in the donor compartment (10^6 ppm) and D is the diffusion coefficient within the film matrix.

Using this standard method the oxygen transfer rate for the sample of polyethylene film was determined as 0.2866 ppm sec^{-1} (standard deviation 5.256×10^{-3} - 3 replicates).

Equation 6.5 was used to calculate the oxygen permeability coefficient. This gave a value of $3.12 \times 10^{-12} m^2 s^{-1}$ (C.V. 1.8%), as compared with figures of $3.32 \times 10^{-12} m^2 s^{-1}$ derived from data supplied by the manufacturer and values calculated from the literature[270] of 2.79 and 2.91×10^{-12} $m^2 s^{-1}$ which can be considered to validate the method. The methods by which the literature and manufacturer's data were converted to S.I. units and $30^{o}C$ are described in Appendix II.

6.2 The Measurement of the Water Vapour Permeability of Free Films by a Gravimetric Technique

Whilst developing the mass spectrometric permeability technique, the water vapour permeability of films was measured using a conventional gravimetric technique. A multidose injection vial ('clinbritic') was developed into a permeability cell for the measurement of the rate of water vapour transmission across free films (Figure 6.27). Desiccant was used inside the cell, rather than a saturated salt solution, to avoid errors due to accidental wetting of the film, as the solution would have to come within 5 mm of the film to minimize the development of a vapour pressure gradient within the cell[131,139]. To obtain a good film seal, it was necessary to lightly grease (Silicone Stopcock Grease, Dow Corning Ltd.) the silicone rubber washer and glass neck of the bottle prior to crimping the cap on. Once assembled, the cells were weighed (Model R20, Oertling Ltd.) and placed in a desiccator containing 200 ml of saturated sodium chloride solution, which had been equilibrated to 30°C in an oven (Townson and Mercer Ltd.). The saturated salt solution was vigorously stirred to reduce the formation of concentration gradients within the solution and vapour pressure gradients within the air. The cells were removed and weighed at 12 hourly intervals, the weight increase recorded and the rate of water vapour transmission obtained by least squares regression analysis of a plot of weight increase versus time.

Anhydrous magnesium perchlorate, calcium chloride and silica gel were evaluated as desiccants by measuring their

Figure 6.27 Diagrammatic representation of the permeability cell used for determining the water vapour permeability of film coatings.

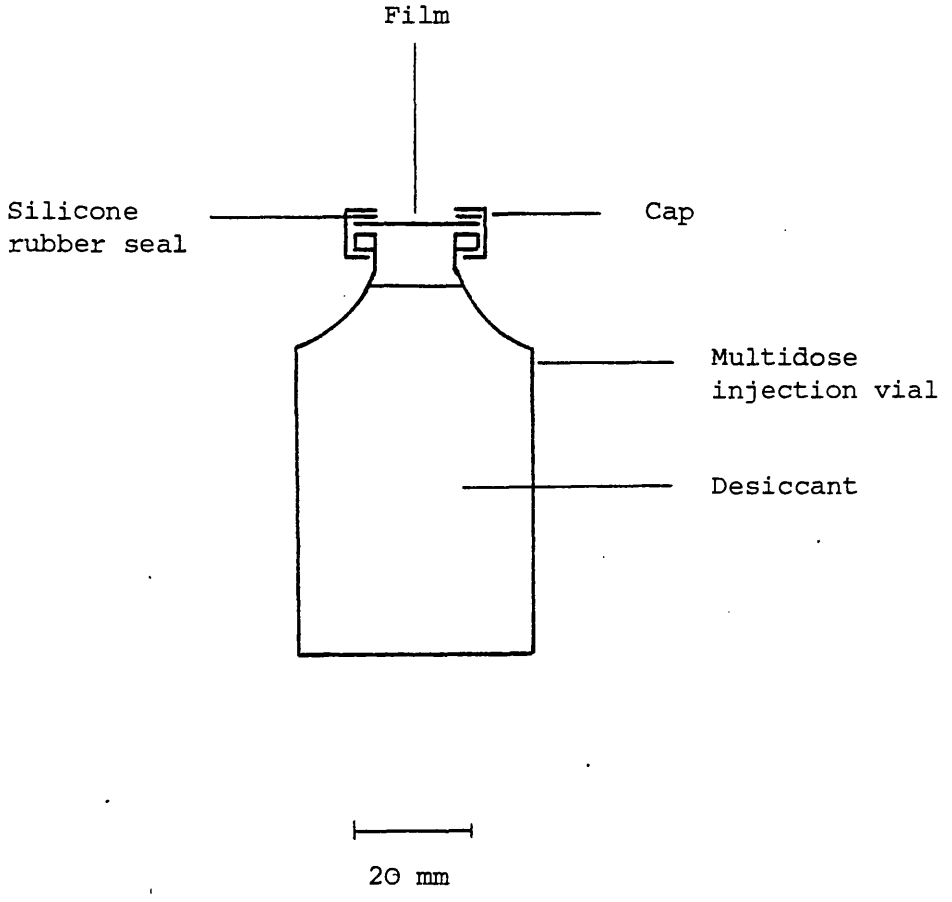

weight increase, due to absorption of water, when 10 g of material were placed in a cell without a film present. The former desiccant was shown to be most suitable (Figure 6.28), since its rate of water uptake was higher and remained linear for a longer period. No weight increase was detectable when an aluminium foil film was installed in the cell, indicating that film sealing was adequate.

The permeability coefficient for water vapour was calculated as described in Section 4.3.2.2.

6.3 The Mechanical Properties of Free Films

The mechanical properties of the films were evaluated using an Instron Table Model Tensile Tester (Type 1026, Instron Ltd.) equipped with pneumatic action specimen grips and tension load cell B (Figure 6.29). All measurements were carried out at ambient temperature and humidity (18^{o}C, 70% RH), although the films were stored in a desiccator until testing. Thus the effects of humidity on the mechanical properties of the films were constant, but as the films could not be equilibrated to different relative humidity levels on the tester, the mechanical properties at different moisture levels were not evaluated. To enable small areas of coating to be evaluated, strips of film 5 mm wide and 20 mm long were cut using a sharp scalpel and metal template and the distance between the grips (gauge length) set to 5 mm by adjustment of the crosshead motion limit switches. The strips of film were fixed between the jaws of

Figure 6.28. Weight increase versus time for the absorbtion of water vapour by approximately 10 g of desiccant placed in the permeability cell, at 30°C and 23.8 mm Hg vapour pressure

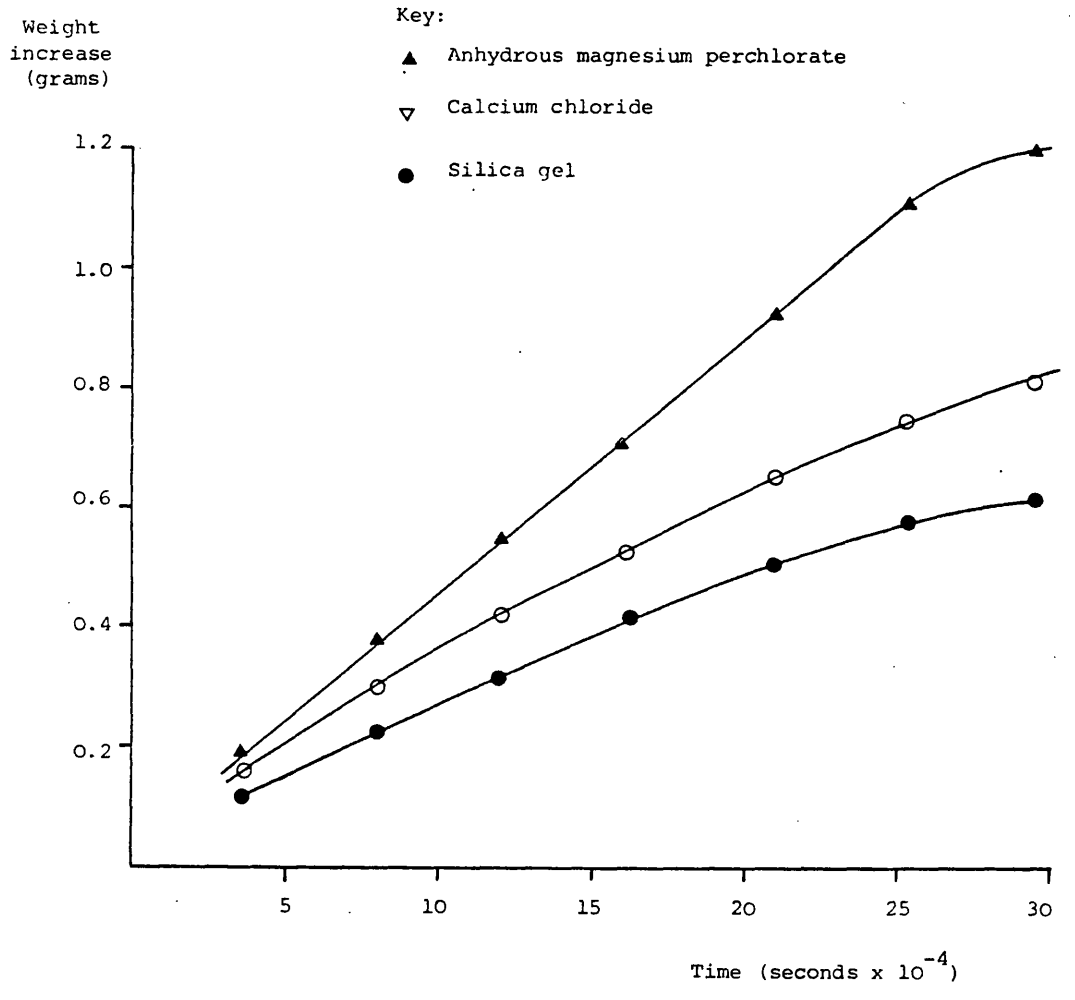

Figure 6.29 Diagrammatic representation of Instron Tensile Tester

Key A = Drive screws

B = Load cell

C = Moving crosshead

D = Specimen grips

E = Chart

F = Load cell amplifier controls

G = Recorder controls

H = Crosshead controls

I = Change gear unit (for control of crosshead and chart speed)

J = Crosshead motion limit switches.

Figure 6.29 Diagrammatic representation of Instron Tensile Tester.

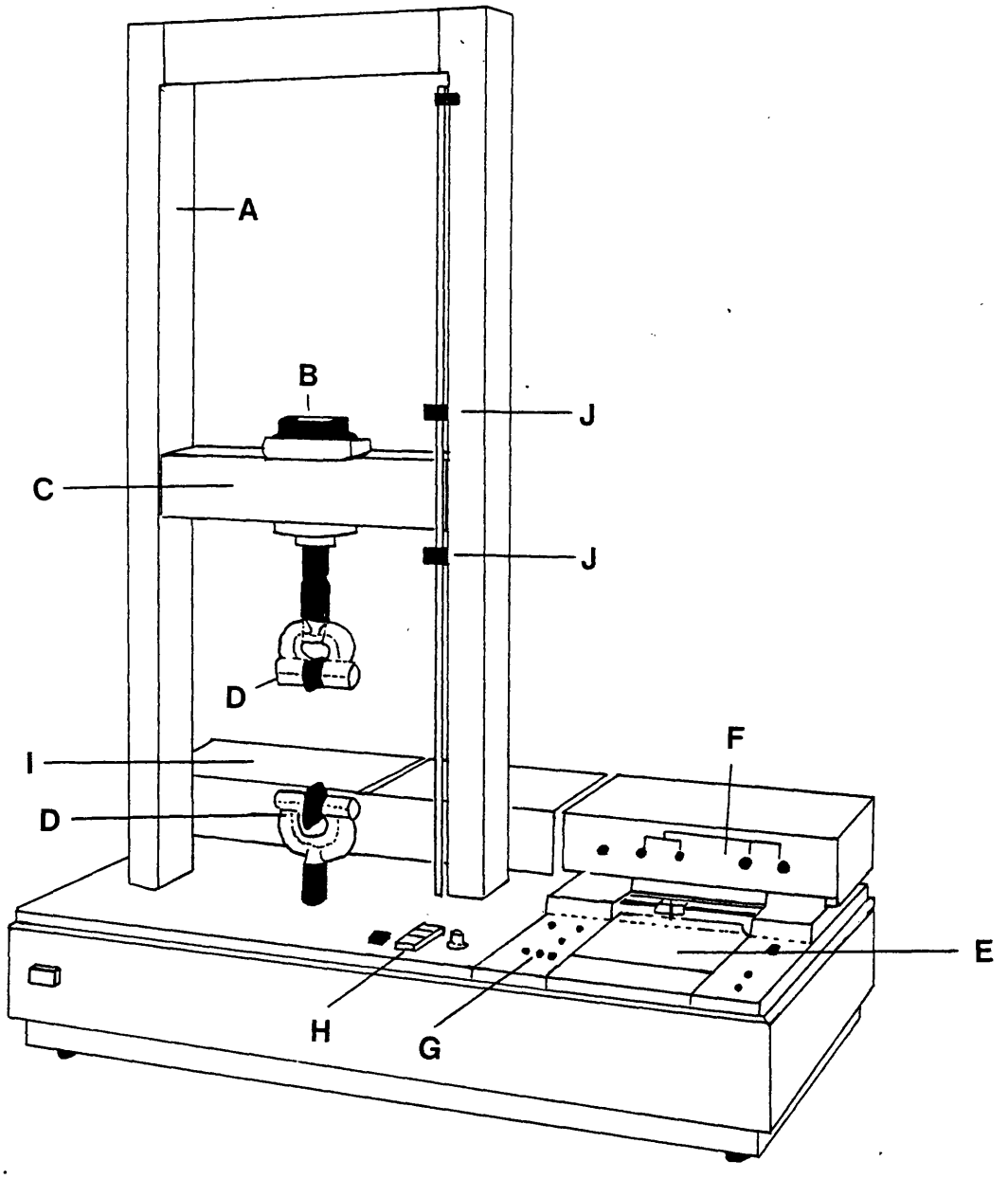

the grips and elongated at a constant rate of 1 mm min^{-1} until rupture took place. The applied load was recorded on a strip chart moving at 500 mm min^{-1} (500 mm of chart representing 1 mm of crosshead movement) and the trace (Figure 6.30) characterized as follows:-

$$\text{Stress} \doteq \text{Force per unit area} = \frac{\text{Load x Acceleration due to gravity}}{\text{Original cross-sectional area}}$$

$$\text{Strain} = \frac{\text{Film extension}}{\text{Original length}}$$

a) Ultimate Tensile Strength

The maximum stress at rupture was calculated from the load per unit cross sectional area of the original specimen.

b) Elastic Modulus

The modulus of elasticity (E) for a material, within its elastic limit, was defined as:-

$$E = \frac{\text{Stress}}{\text{Strain}} = \frac{\text{Force}}{\text{Area}} \times \frac{\text{Original length}}{\text{Elongation}}$$

The elastic modulus was obtained from the slope of a tangent to the elastic region of the curve, since for the films tested this was very short in comparson with the prolonged plastic region. Repeated application of stress, within the elastic limit, to a film cast from 5% w/v Pharmacoat 606 indicated no trend in the variation in elastic modulus (3.59×10^9 Pa, C.V. 3.94% - 10 replicates), but up to 20% stress relaxation occurred in 20 seconds when a constant stress, within the apparent elastic limit, was applied.

Figure 6.30 Typical stress-strain curve for HPMC films

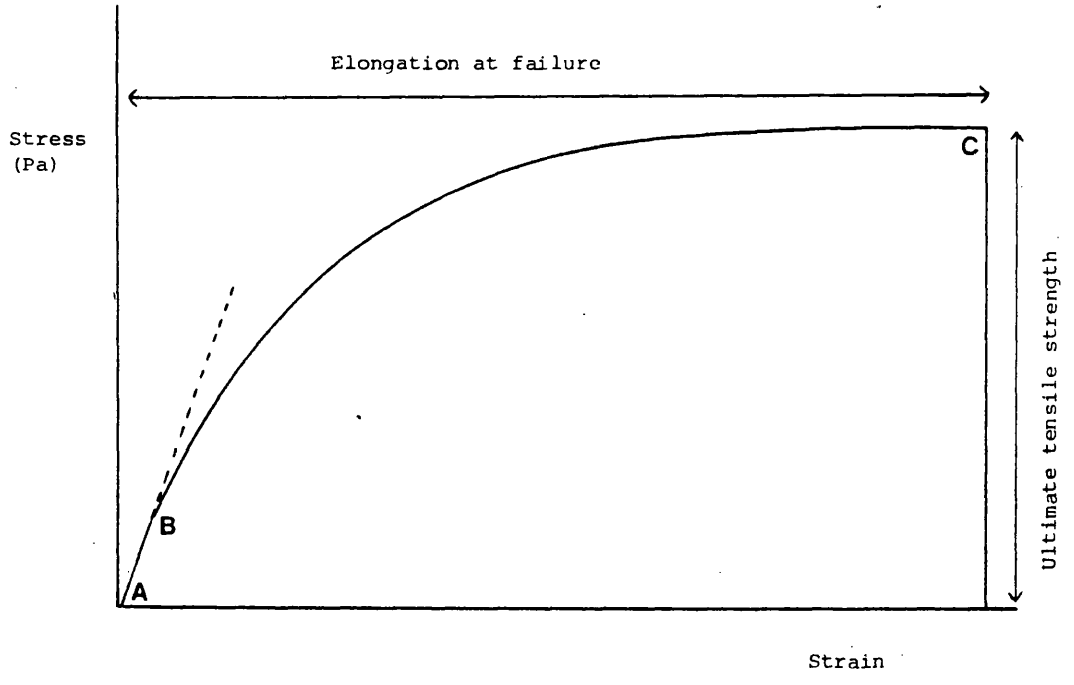

A - B = Elastic region

B - C = Plastic region

Despite this the values obtained for the elastic modulus were recorded, whilst recognizing that they will only be comparable with measurements performed under identical conditions.

c) Elongation at Failure

The strain at failure was calculated and expressed as a percentage of the gauge length.

d) Elongation and Stress at Yield

The values of strain and stress at the yield point could not be defined for this system due to the absence of a sharp transition from elastic to plastic behaviour.

e) Work of Failure

The work of failure is defined as the area under the force-displacement curve. The area under the load-displacement curve was measured using a planimeter (compensating polar planimeter, W.F. Stanley and Co. Ltd.) and the work of failure, work per unit cross-sectional area and work per unit volume calculated.

6.3.1 Reproducibility of Measurements

Films were prepared by casting a 5% w/v solution of Pharmacoat 606 onto glass, or spraying on to glass, calcium phosphate/lactose or lactose/Avicel compacts, at a rate of 32 ml min^{-1}. The mean mechanical properties were evaluated for 10 samples of each type of film (Table 6.19), although the thickness variation between films available from each preparation technique prevented their comparison. Subsequent work, at constant film thickness, presented in Section 9 did however, allow such comparisons.

Table 6.19 The mean mechanical properties (10 replicates)of films prepared from a 5% w/v solution of Pharmacoat 606, by casting or spraying on the model system

S.D. = Standard Deviation, C.V. = Coefficient of Variation

Preparation method	SPRAYED						CAST	
Substrate	Glass		Calcium phosphate/ Lactose placebo		Lactose/Avicel Placebo		Glass	
Film thickness (μm)	20		20		52.33		40	
	Mean (S.D.)	C.V. %	Mean (S.D.)	C.V. %	Mean (S.D.)	C.V. %	Mean (S.D.)	C.V. %
Ultimate tensile strength ($Pa \times 10^{-7}$)	5.84 (0.51)	8.73	5.63 (0.73)	12.97	6.43 (0.37)	5.75	6.98 (1.01)	14.47
Elongation at failure (%)	3.80 (0.92)	24.21	4.44 (1.28)	28.82	3.52 (0.57)	16.19	6.73 (2.2)	32.69
Elastic modulus ($Pa \times 10^{-9}$)	4.34 (0.41)	9.45	4.52 (0.34)	7.52	4.71 (0.30)	6.37	4.21 (0.45)	10.69
Work done in failure ($Jx10^{3}$)	0.82 (0.22)	26.83	1.00 (0.43)	43	2.19 (0.52)	23.74	4.09 (1.90	46.46
Work done per unit cross section ($Jm^{-2}x10^{-3}$)	8.19 (2.16)	26.37	9.99 (4.27)	42.74	8.38 (1.98)	23.63	20.46 (9.50)	46.43
Work done per unit volume ($Jm^{-3} \times 10^{-6}$)	1.64 (0.43)	26.22	2.00 (0.86)	43	1.68 (0.4)	23.81	4.09 (1.90)	46.46

The data demonstrated that the technique, when applied to small areas of film, was not very reproducible, with coefficients of variation between 5 and 15% for the ultimate tensile strength, 6 and 10% for the elastic modulus, 16 and 32% for the elongation at failure and 24 to 46% for the work done in failure. The very large variations in the work of failure (force x displacement) were largely due to the variability of the elongation at break (displacement), since the shape of the stress-strain curve (Figure 6.30) was such that premature failure of the film, due to the presence of flaws, had a greater effect on the elongation at break than on the ultimate tensile strength. The magnitude of the variations in mechanical properties could, in part, be attributed to the small area of film tested (5 mm x 5 mm), increasing the importance of errors in film thickness, width and length. For example, a 0.5 mm error in the gauge length could alter the calculated elongation at break by 20%.

6.4 Variables Investigated

6.4.1 Reproducibility of Films Prepared by the Model Coating System

Glass substrates were attached to the belt of the model coating system (Section 4.3) and coated under the following conditions:-

Solution	5% w/v Pharmacoat 606
Liquid feed rate	25 ml min^{-1}
Inlet air temperature	90°C
Exhaust temperature	48°C

8 substrates were removed at 25 minute intervals up to 100 minutes, the films carefully detached and stored between cartridge paper in a desiccator until required for testing. This procedure was repeated twice more using fresh batches of coating solution.

The oxygen permeabilities of these films were determined by the methods described in Section 6.1. The reproducibility of the measured permeability coefficient was evaluated for a single film reseated in the cell on four successive days (Table 9.1), several films of similar thickness and all the films tested from one coating run (Table 9.2). The permeability coefficient of six films from each coating run, thickness 25 to 30 μm and 45 to 55 μm, were also compared (Table 9.5) (duplicate determinations for three films at each thickness).

The mechanical properties of the films were measured using the techniques described in Section 6.3. The reproducibility of measurement was established for four films of each thickness and the effect of thickness variations evaluated (Table 9.4). The mechanical properties of five films, thickness 39 to 40 μm, from each coating run were compared (Table 9.7).

6.4.2 The Effects of Film Preparation Technique, Substrate and Titanium Dioxide Content

Film coatings were prepared from solutions containing 5% Pharmacoat 606 and 0, 0.5, 1.0, 2.0 or 3.0 % w/v titanium dioxide. The solutions and suspensions were cast on to glass

plates and sprayed on to glass, lactose/Avicel and calcium phosphate/lactose substrates attached to the model coating system using the following coating conditions:-

Liquid feed rate	31.5 - 32.5 ml min^{-1}
Inlet air temperature	83 - 87°C
Exhaust temperature	42 - 45°C

The films were detached from the substrates and stored between cartridge paper in a desiccator prior to testing.

The oxygen permeabilities at each concentration of titanium dioxide were determined in duplicate for three films prepared by casting on to glass, spraying on to glass and calcium phosphate/lactose substrates and two films prepared by spraying on to a lactose/Avicel substrate. The results are shown in Table 9.8 and Figure 9.5.

The water vapour permeabilities were determined, using the gravimetric technique described in Section 6.2, for two films from each preparation technique, at the 20% w/p w level of titanium dioxide. The results are shown in Figure 9.13 and Tables 9.10 and 9.11.

The mechanical properties at every titanium dioxide concentration, were determined for four films from each preparation

technique and substrate. The results are shown in Figures 9.14 to 9.19.

6.4.3 The Effect of Water Vapour on the Oxygen Permeability of HPMC films

A solution containing 5% w/v Pharmacoat 606 was sprayed on to glass plates , attached to the belt of the model coating system, under the following conditions:-

Liquid feed rate	25 ml min^{-1}
Inlet air temperature	90°C
Exhaust temperature	48° C

The oxygen permeabilities of two films, 18 and 68 µm thick were determined in duplicate at donor oxygen relative humidities of 0, 30, 60 and 100%. The results are shown in Figure 9.20 and Table 9.12.

7. THE DEVELOPMENT OF A RELOCATION TECHNIQUE FOR THE STUDY OF THE EFFECTS OF FILM COATING ON TABLET SURFACE ROUGHNESS

7.1 Introduction

Surface roughness parameters determined by stylus instruments are important in the interpretation of tablet film coating adhesion data[172,174,192] and in quantifying the physical appearance of the coat during formulation and process optimization[213,234]. This approach however is severely limited due to the large variations inherent in the surface topography of tablets which tend to mask any changes resulting from the application of a film coating. Thus values reported in the literature for roughness parameters are averages of a large number of different profiles and will only indicate gross trends during coating.

Relocation profilometry[271-273], when combined with the model coating system described earlier (Section 4.3), can overcome this disadvantage by allowing a specimen to be precisely remounted on the stylus instrument, enabling the identical area of surface to be recorded during film coating. Consequently the precise effect of coatings on the surface roughness can be readily assessed by eliminating variations due to an inability to monitor the identical section of surface (2.5 μm stylus width and 3.8 mm travel) before and after coating.

The most reliable relocation systems are based on the passive interaction of three or four points of contact between a relocation table bolted to the stylus instrument and a removable

relocation stage. Therefore, to investigate the feasibility of using such a technique in the future, a system was developed to allow a tablet, attached to a relocation stage, to be precisely remounted on the stylus instrument at intervals during the application of a film coating by the model system described in Section 4.3.

7.2 Development of the Experimental Technique

All surface roughness measurements were made using a Talysurf 3 surface measuring instrument (Rank Taylor Hobson) (Figure 7.1). A four-sided 90° diamond pyramid stylus, with a slightly rounded tip 2.5 μm wide, was attached to a stylus arm located within a pickup (A) fixed to the gearbox (B). Vertical movements of the stylus were converted to an electrical signal by a variable inductance located at the rear end of the stylus arm. A skid nosepiece served to protect the fragile stylus and act as a datum against which movements of the stylus were recorded. For surfaces with crests greater than 750 μm apart an external datum was required. The stylus and pick-up were moved across the surface under test by a motor driving through the gearbox. The speed control knob (C) allowed a choice of three motor speeds which, with a constant recording speed, allowed the surface profile to be magnified horizontally by x100, x20 and x5; the latter being used for computation of the arithmetical mean deviation (R_a). The length of surface examined was controlled by the stroke knob (D) and the setting lever (E) returned the pick-up to the start of its movement

Figure 7.1 Talysurf 3 surface measuring instrument

Key
- A Pickup
- B Gearbox
- C Speed knob
- D Stroke knob
- E Setting lever
- F Base table
- G Lead screw hand wheel
- H Carriage clamp knob
- I Amplifier
- J Rectilinear recorder
- K Triple cut-off average meter
- L Magnification switch
- M Cut-off control

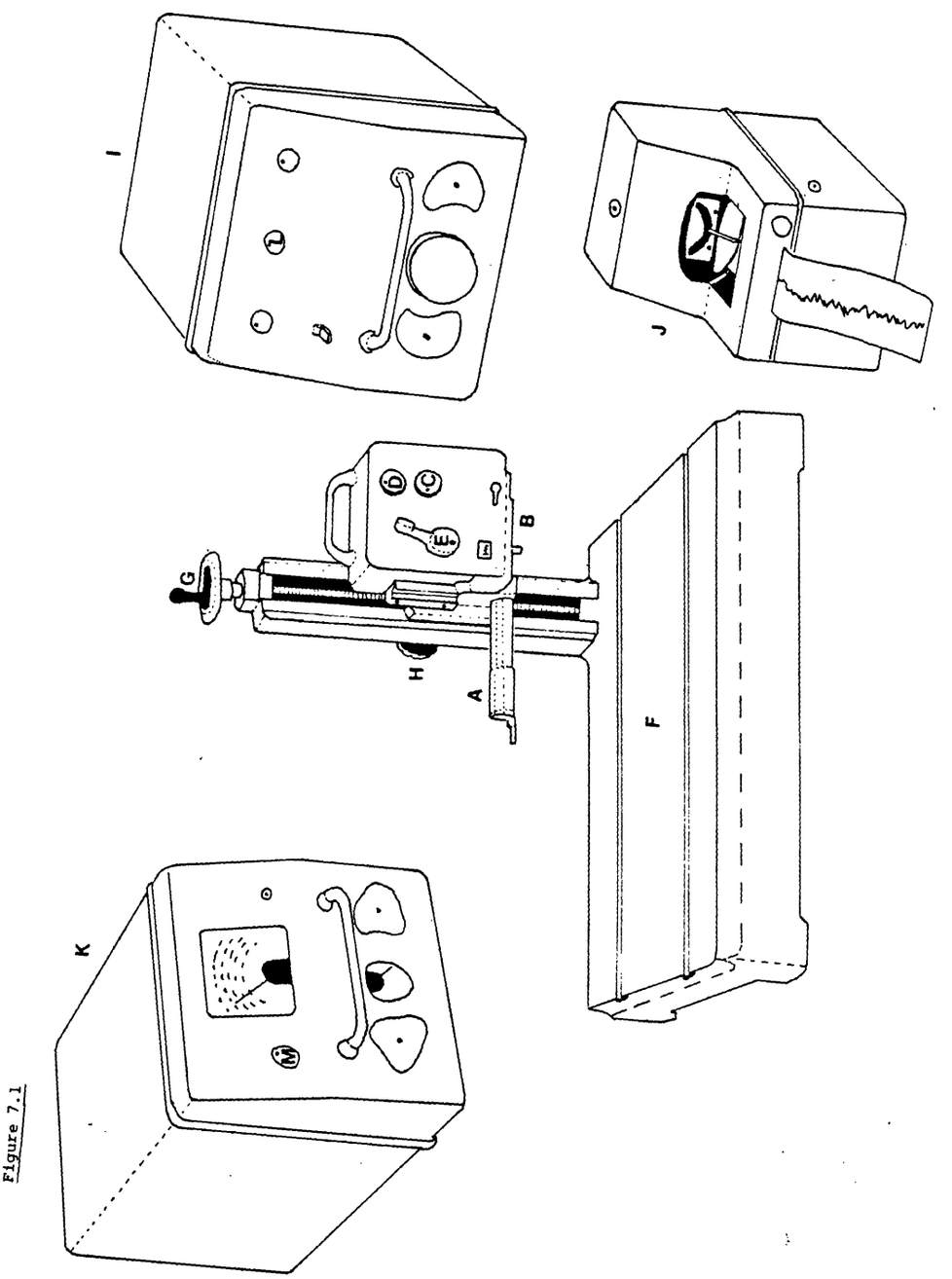

Figure 7.1

after each profile had been recorded. The gearbox and motor unit were fixed to the vertical carriage at one corner of the base table (F). The carriage was raised and lowered by means of a Lead Screw Handwheel (G) at the top of the column and clamped by the carriage clamp knob (H).

The signal from the pick-up was amplified (I) and fed to a rectilinear recorder (J), to give a permanent representation of the surface profile and to a triple cut-off Average Meter (K), for computation of R_a; a process represented diagrammatically in Figure 7.2. The 6 position magnification switch (L) of the amplifier allowed vertical magnifications of 1, 2, 5, 10, 20 and 50 thousand. The average meter cut-off control (M) enabled surface waviness of long wavelengths to be electrically filtered from the roughness signal prior to the computation of R_a (Figure 7.3).

A cut-off of 0.8 mm was selected since the crests were fairly closely spaced and this value can be regarded as the most suitable for a variety of surfaces[274]. The stroke knob was set to 11.7 mm (k position) as the traverse length must relate to the chosen cut-off. The magnification and speed controls were selected to give the best representation of the surface under study.

The instrument was calibrated using the glass Roughness Standard supplied with the Talysurf (Figure 7.4). The left hand

Figure 7.2 Calculation of arithmetic mean deviation (B.S. 1134 definition)

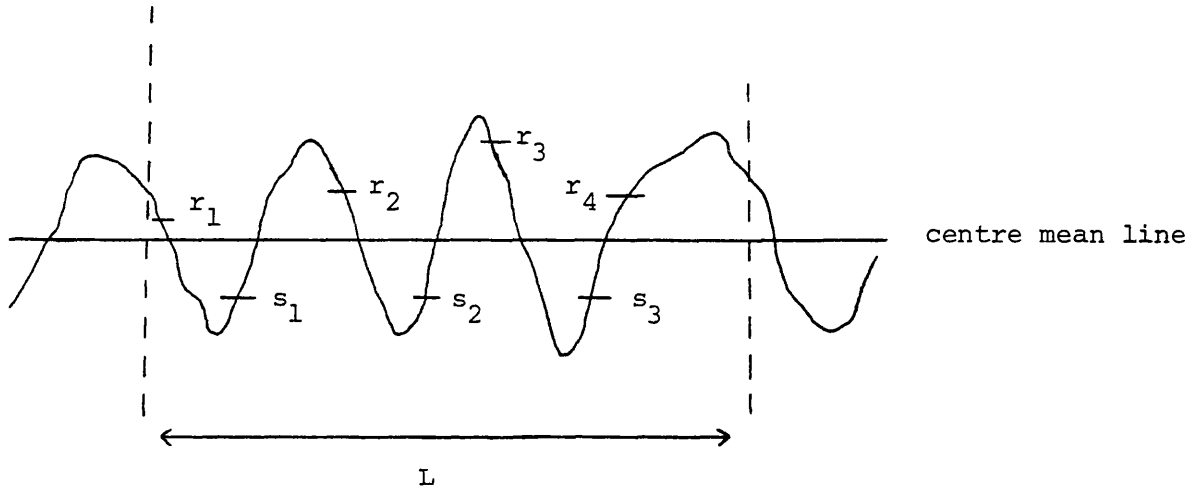

$$R_a = \frac{\text{sum of areas (r) + sum of areas (s)}}{L} \times \frac{1000}{V_v}$$

R_a = Arithmetical mean deviation (μm)

V_v = Vertical magnification

L = Sampling length (mm)

r and s = Areas on trace (mm^2)

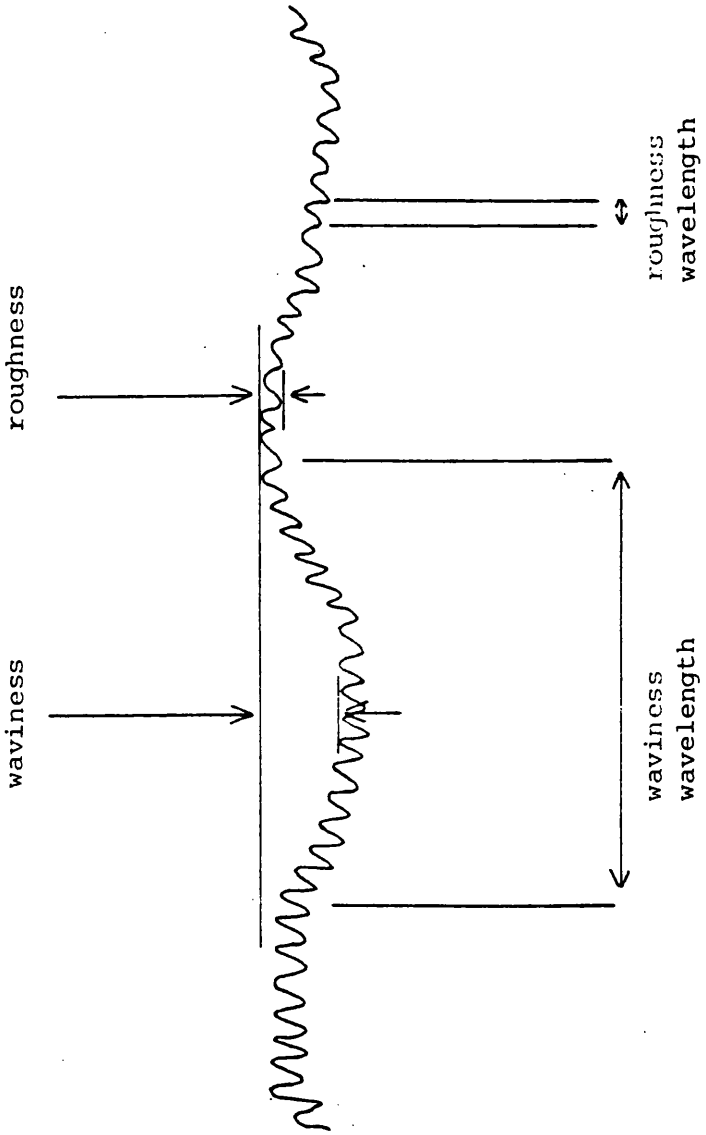

Figure 7.3 Waviness and roughness of a surface profile

Figure 7.4 Talysurf Glass Roughness Standard

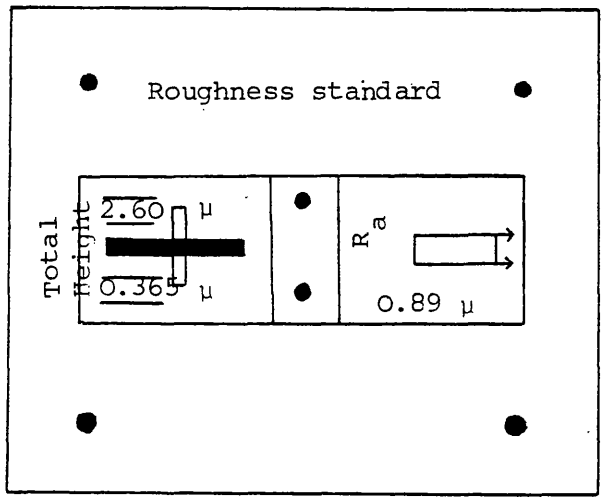

plate carried three coarse and three fine lines, spaced at 254 μm, of height 2.60 μm and 0.365 μm respectively, enabling the recorder pen/stylus magnification to be set by use of a potentiometer in the amplifier. The right hand plate contains a grid of 76 μm spacing, R_a 0.89 μm, to allow calibration of the average meter once the pen/stylus magnification had been set.

The relocation system developed was based around the contact between three ball bearings attached to a relocation table and three holes drilled in a relocation stage. A three point contact system was chosen in preference to a four point contact system since the latter required a higher degree of precision in the construction of the relocation system. Furthermore, in contrast to many engineering applications, the relocation stage and attached tablet were very light making it unnecessary to spread the load between four contact points.

A relocation table was constructed from mild steel (Righton Henry and Co. Ltd.) (Figure 7.5) and bolted firmly to the Talysurf 3 using T-slot nuts, thus providing an immobile platform on which relocation could take place. The top and bottom of the relocation table were surface ground to ensure they were parallel to the base table and movement of the pick-up. The relocation stage was constructed from surface ground 5/16" (7.94 mm) gauge plate (Righton Henry and Co. Ltd.) and three 4 mm diameter holes accurately drilled and reamed out (Figure 7.6a). The holes were equally spaced from the centre of the stage, as far apart as was

Figure 7.5 Side view of relocation table

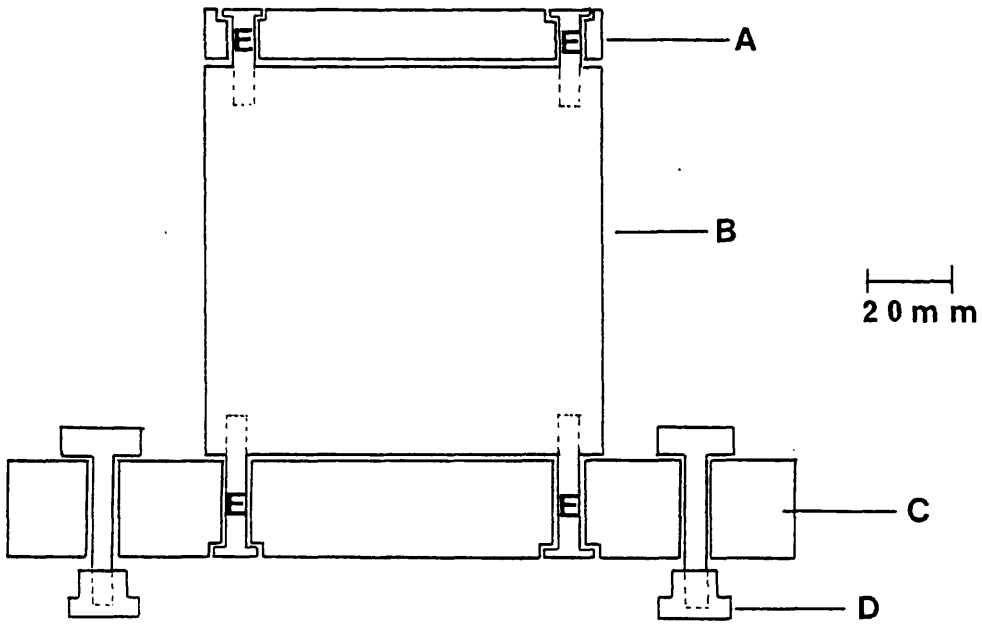

Key:
- A Removable top (½" x 4" x 4" mild steel)
- B Relocation table (4" x 4" x 4" mild steel)
- C Base of table (4" x 8" x 2" mild steel)
- D T-slot nuts (mild steel)
- E Recessed bolts

Figure 7.6a Relocation Stage

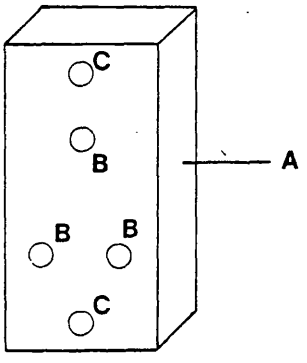

Key

A Relocation stage (5/16" gauge plate)

B 4 mm diameter drilled and reamed holes for relocation

C 4 mm diameter drilled holes for fixation to backing plate

Figure 7.6b Relocation stage attached to coating system

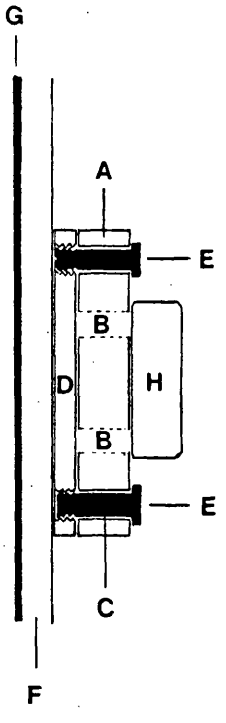

Key

A Relocation stage

B 4 mm holes for relocation

C 4 mm holes for fixation to backing plate

D Aluminium backing plate

E Fixing bolts

F Polyurethane foam

G Timing belt

H 25.4 mm diameter flat-bevelled edge compact

consistent with their upper surfaces being covered by a 25.4 mm diameter flat bevelled edge compact, so preventing coating suspension from reaching the relocating surfaces during coating. The 4 mm diameter holes at either end of the stage allowed it to be bolted to an aluminium backing plate which was fixed to the belt of the model coating system using cyanoacrylate adhesive (Radio Spares Ltd.) (Figure 7.6b). The relocation stage was inverted on a flat surface and three 5 mm diameter hardened steel ball bearings placed in the reamed holes. A spot of epoxy adhesive (Araldite, Ciba-Geigy Plastics Division) was applied to the free surface of each ball bearing and the removable top of the relocation table placed on top until the adhesive had set.

The table top and attached balls were reassembled with the relocation table and the surface profile of the stage recorded after successive relocations. The recording of the surface profile was a critical test for the accuracy of location since identical traces could only occur if relocation was to within the width of the stylus track (2.5 μm). Figure 7.7 shows that repeatedly raising and lowering the gearbox, with the carriage clamp lightly tightened, did not affect the trace and therefore any changes in the profile after removal and replacement of the relocation table must show inefficient relocation. Figure 7.8 clearly demonstrates that satisfactory relocation was not obtained with this system; the major changes in the profile being indicated by the arrows. Examination of the relocation system with a

Figure 7.7 Surface roughness traces of the first relocation stage, showing the effect of raising and lowering the gearbox between the recording of each profile

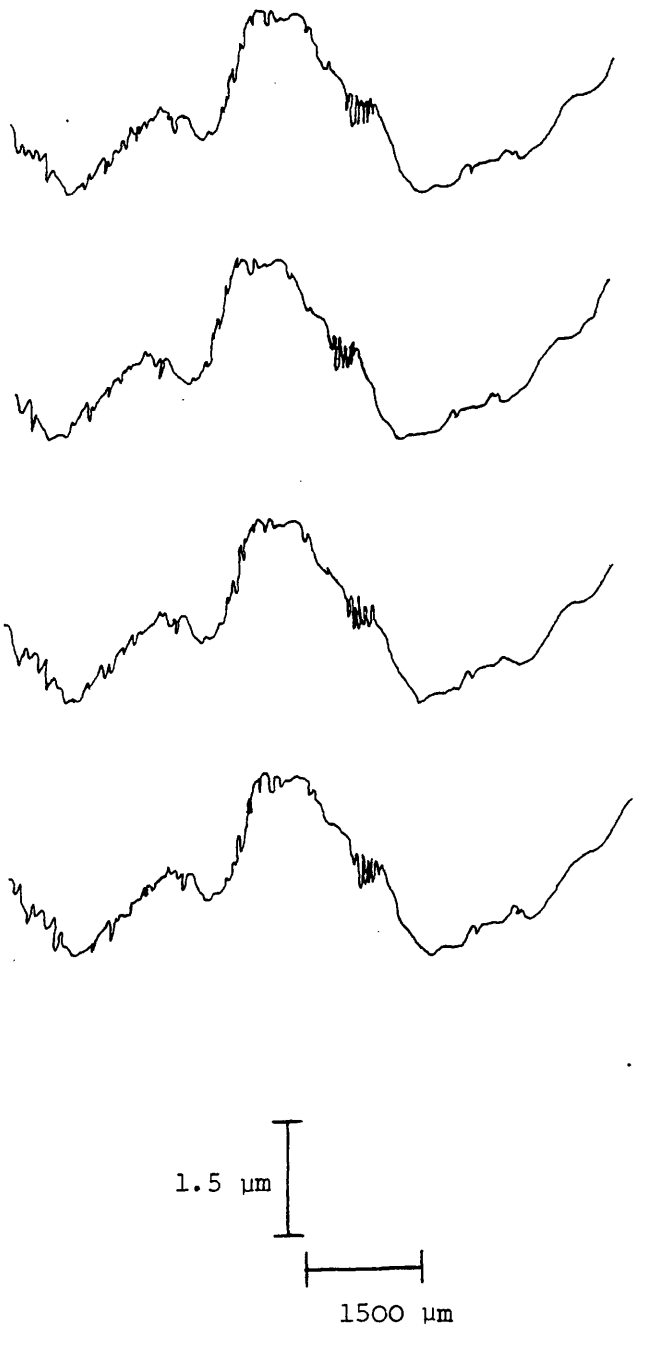

Figure 7.8 Surface roughness traces of the first relocation stage, showing six consecutive relocations.

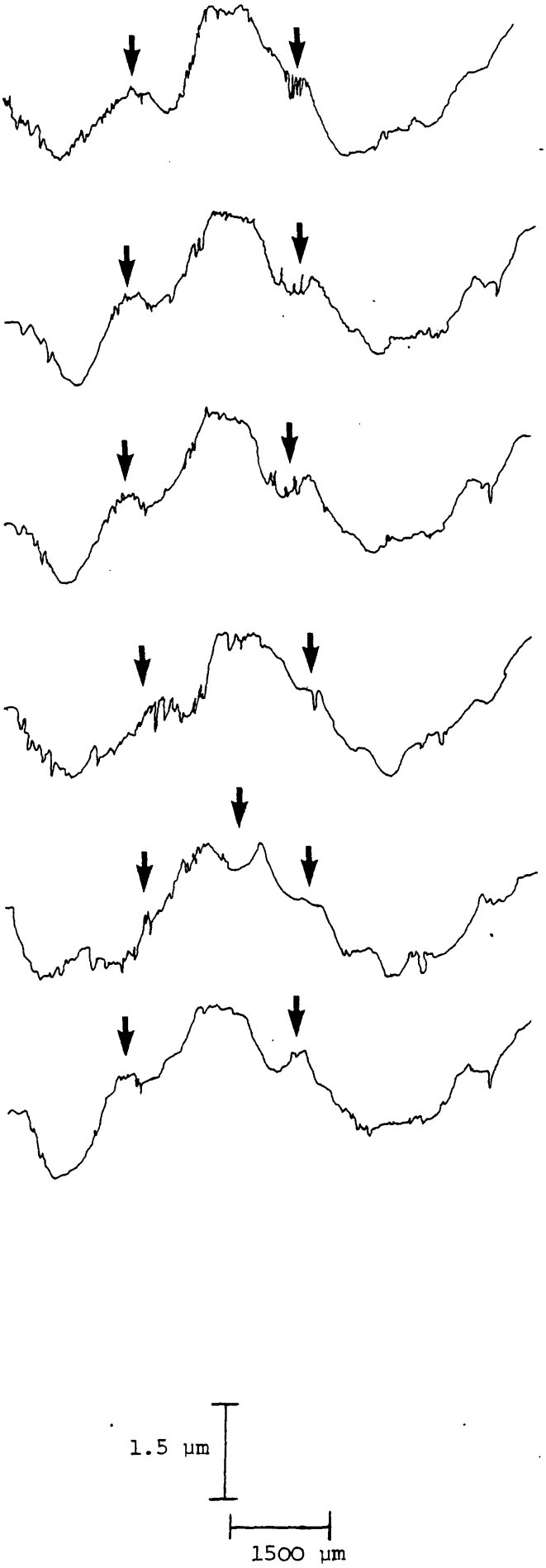

travelling microscope revealed that whilst setting the viscous adhesive had allowed the balls to be displaced slightly from their seat in the holes of the relocation stage. Furthermore, the position of the balls on the relocation table was only fixed by the adhesive and the point contact of a sphere with a flat surface.

To overcome these problems, a new relocation stage was made, clamped to the removable top of the relocation table and three 4 mm diameter holes accurately drilled and reamed out. The relocation table and its top were reassembled on the Talysurf base. Cyanoacrylate adhesive was applied to the edges of the holes in the table top, in which 5 mm diameter hardened steel ball bearings were placed and the relocation stage placed on top until the adhesive had set. Thus the balls were firmly located in holes on the relocation table and held in place by a very thin layer of low viscosity adhesive (Figures 7.9 and 7.10). Replicate surface roughness traces of the stage (Figure 7.11) demonstrated that relocation to better than 2.5 μm (the stylus width) was obtained by this three point contact of the balls and holes in the stage. It should be noted that the traces had to be manually aligned by their predominant surface features since the axial positioning of the stylus could vary due to mechanical backlash in the resetting mechanism.

When tablets consisting of lactose and microcrystalline cellulose (Section 4.3.1.2) were attached to the relocation stage with cyanoacrylate adhesive, significant changes could be seen in

FIGURE 7.9

SIDE VIEW OF RELOCATION TABLE AND STAGE.

KEY

A. 25.4mm Flat Bevelled edge compact.

B. Relocation Stage - ($^5/_{16}$" Mild Steel Gauge Plate)

C. 5mm Diameter Hardened Steel Balls.

D. Removable Top of Relocation Table. ($\frac{1}{2}$" x 4" x 4" Mild Steel)

E. Relocation Table (4" x 4" x 4" + 4" x 8" x 2" Mild Steel)

F. T - Slot Nuts (Mild Steel)

G
H 4mm Diameter drilled and reamed holes

I. 4mm Diameter drilled holes for fixing relocation stage to belt of Model Coating System.

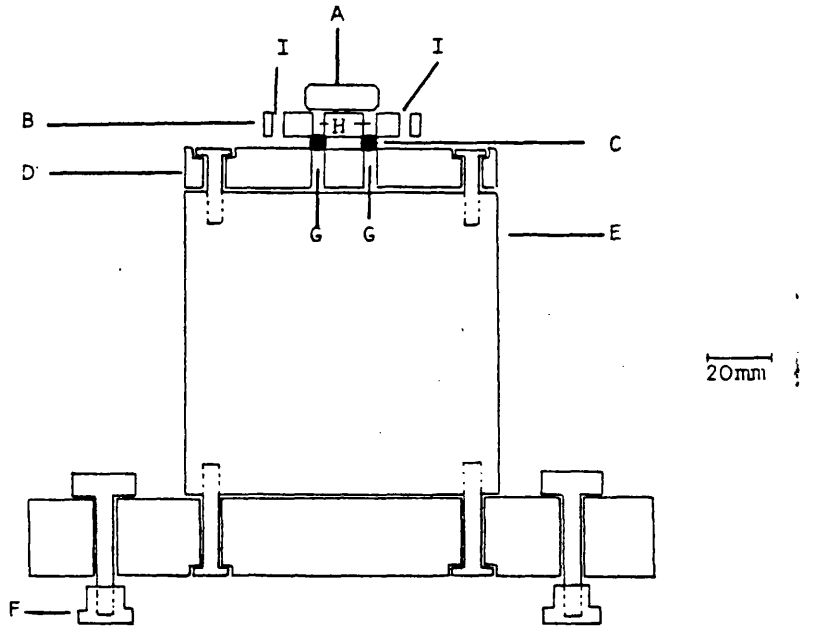

PLAN VIEW OF RELOCATION TABLE AND STAGE.

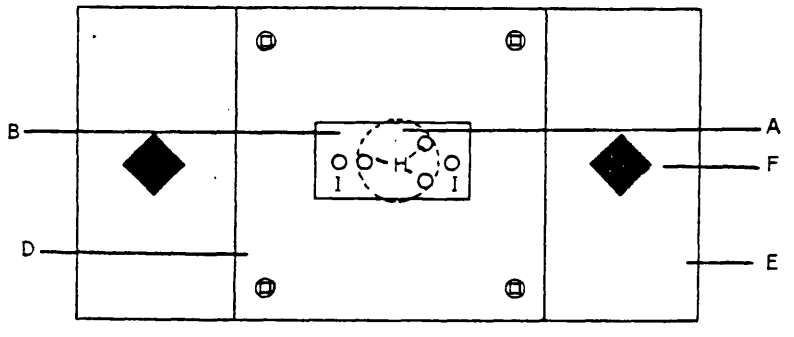

Figure 7.10 Photograph of Talysurf 3 surface measuring instrument fitted with the nylon skid and relocation rig.

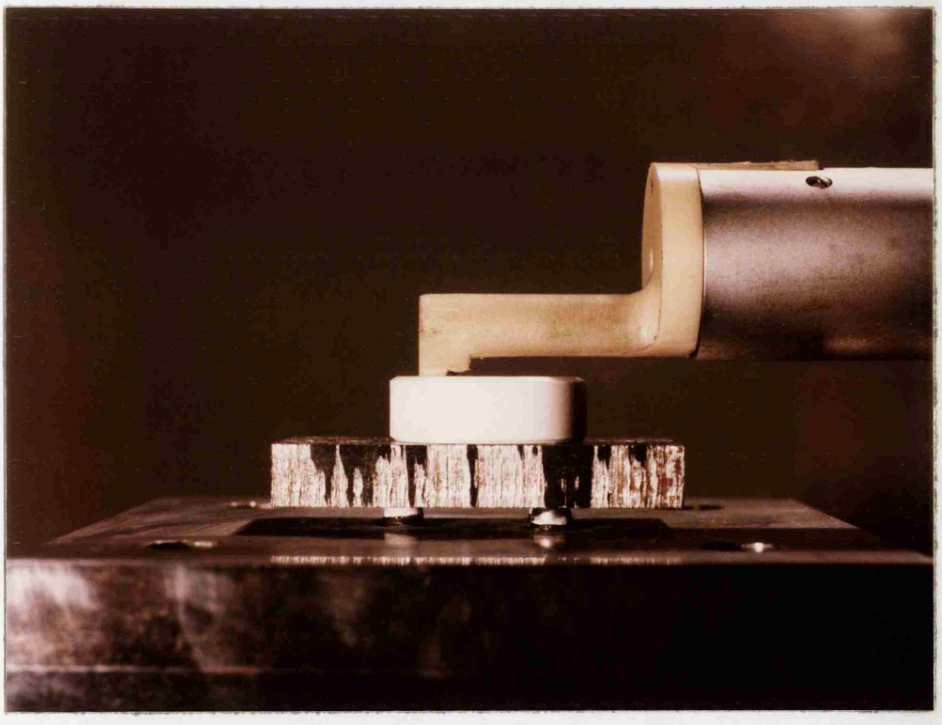

Figure 7.11 Surface roughness traces of the second relocation stage, showing the effect of seven successive relocations.

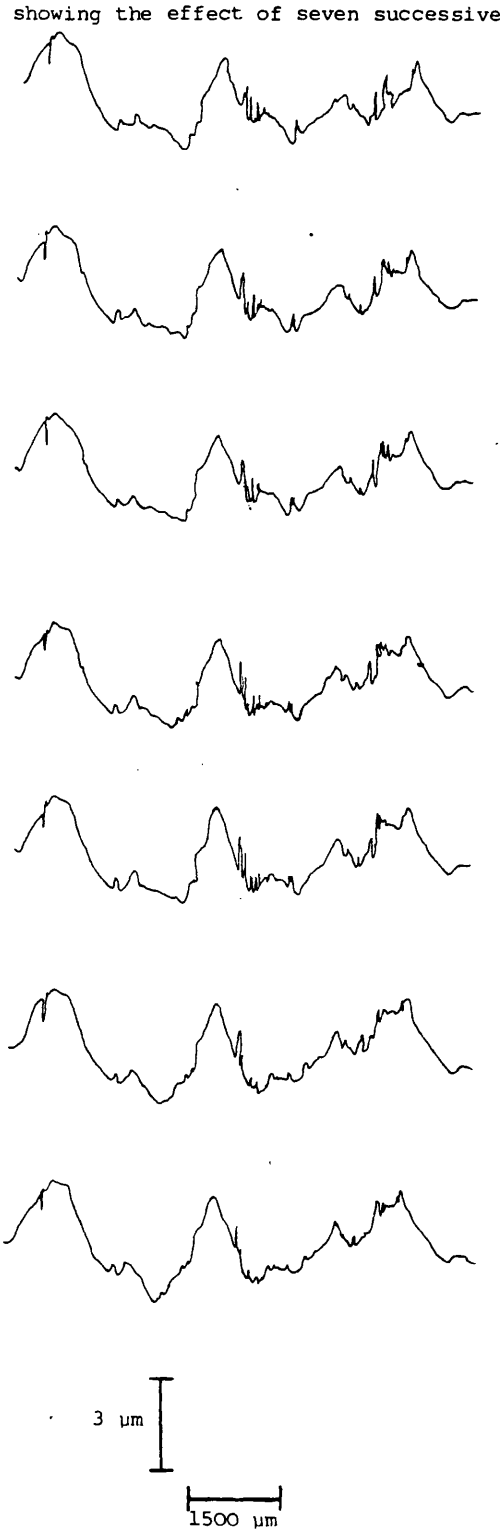

both replicate and relocated surface profiles (Figure 7.12). Examination of the tablets indicated that the surface was being damaged by the tungsten carbide skid fitted to the pick-up. Removal of the skid nosepiece prevented the damage from occurring, but the unrestrained movement of the stylus produced a complex trace, much of which could be attributed to vibrational movements (Figure 7.13). To alleviate the damage, a skid nosepiece was machined from cast Nylon 12 block (F.R. Warren and Co. Ltd.) and fitted to the pick-up such that the loading of the surface under study was reduced.

Figures 7.14 and 7.15 demonstrate that only minimal changes occurred in replicate and relocated surface profiles respectively. The minor changes which did occur in certain regions of the traces could be attributed to damage by the repeated passage of the nylon skid and diamond stylus under a load of 100 mg, since these did not occur on relocation of a roughened metal surface (Figure 7.16). Not withstanding these changes, the value of R_a recorded by the average meter was a constant 2.85 μm (standard deviation zero) during successive relocations. For similar surfaces on lactose-starch tablets Rowe[174], who did not use relocation, found coefficients of variation ranging from 14 to 30%.

To follow the changes in surface topography during film coating, the relocation stage and tablet were bolted to the backing plate attached to the belt of the model coating system. A 5% w/v aqueous solution of Pharmacoat 606 was applied at a rate of

Figure 7.12 Surface roughness traces of a 25.4 mm diameter lactose-microcrystalline cellulose tablet showing three replicate and two relocated profiles

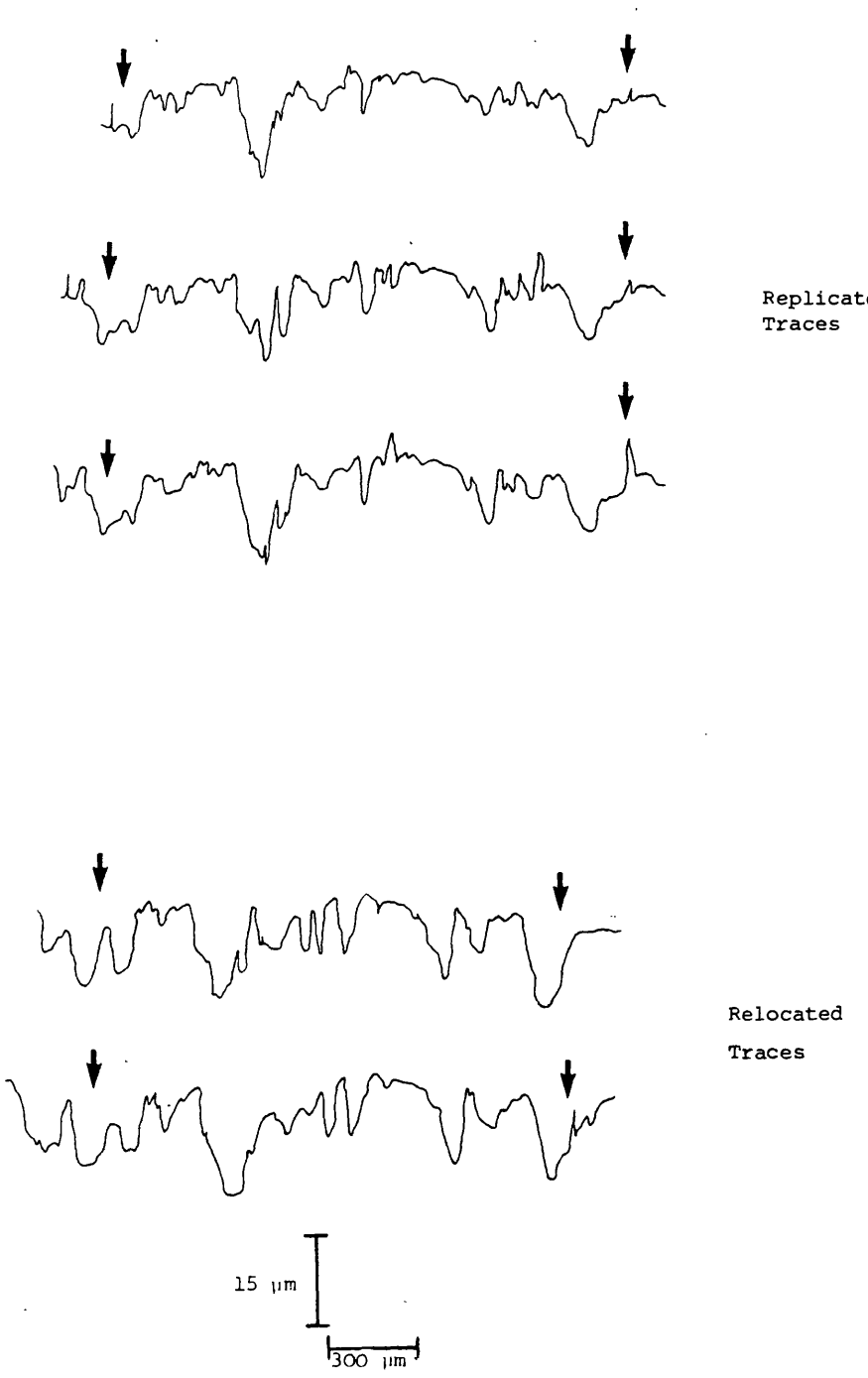

Figure 7.13 Surface roughness traces of a 25.4 mm diameter lactose-microcrystalline tablet, with skid removed, showing six consecutive relocations.

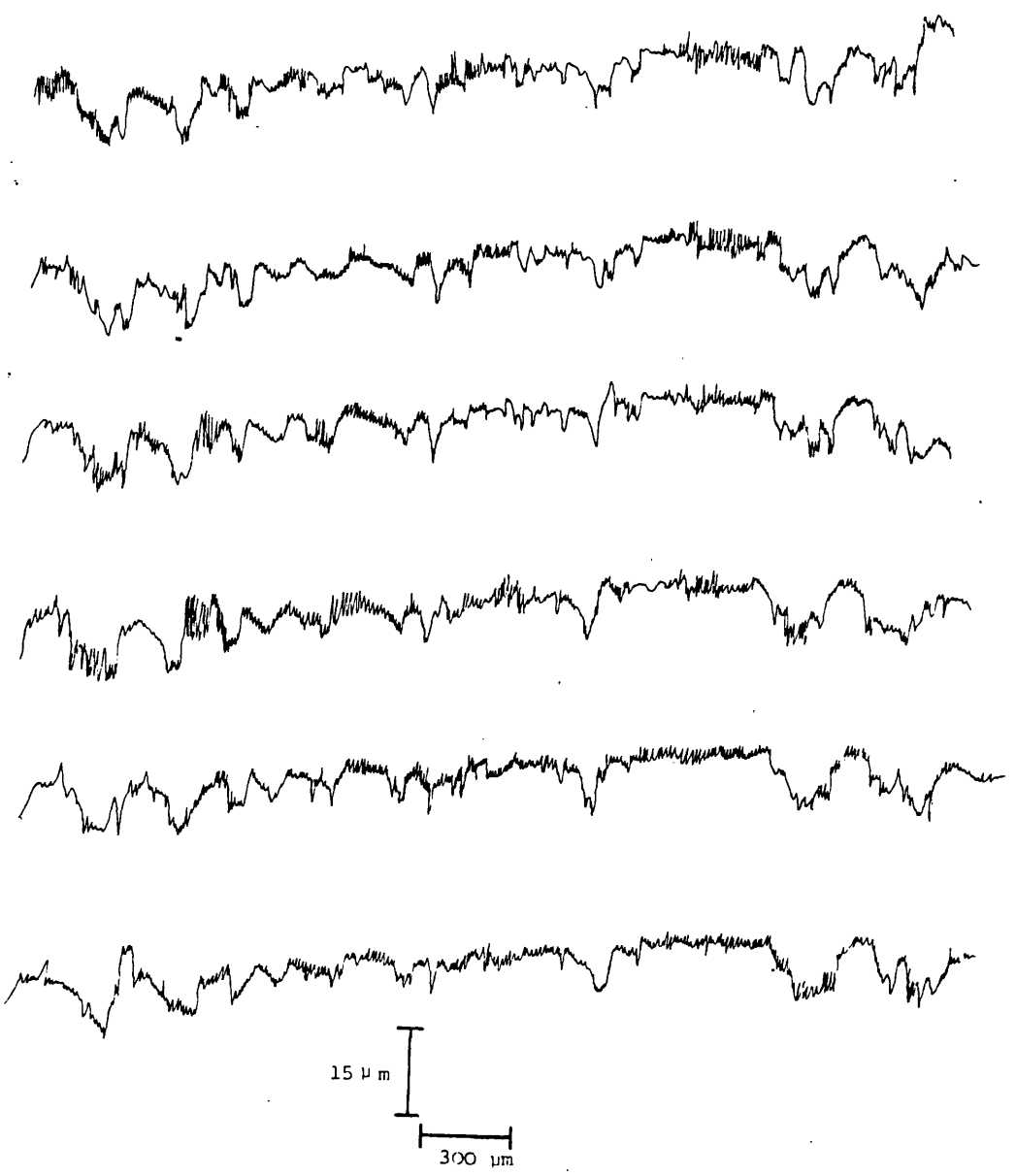

Figure 7.14 Surface roughness traces of a 25.4 mm diameter lactose-microcrystalline cellulose tablet, using a nylon skid, showing four replicate profiles.

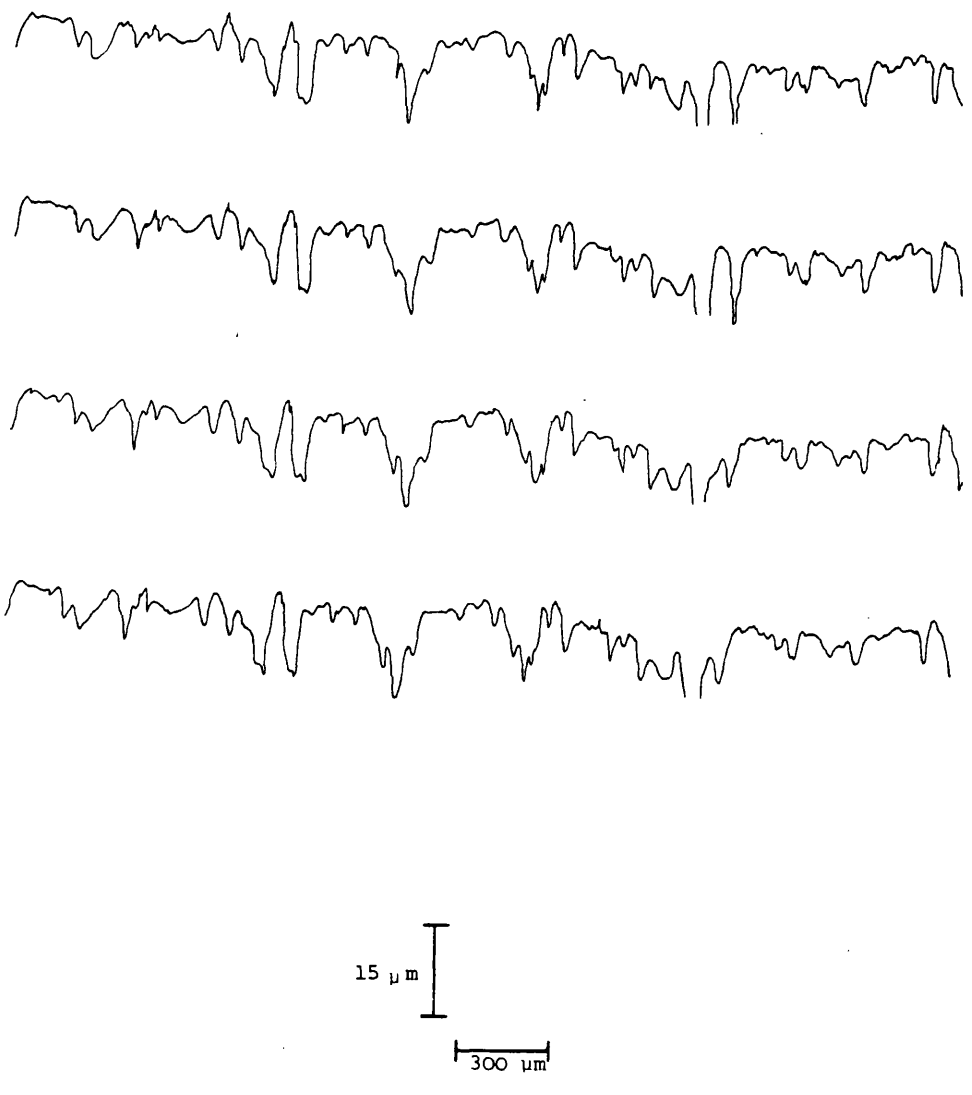

Figure 7.15 Surface roughness traces of a 25.4 mm diameter lactose - microcrystalline cellulose tablet, using a nylon skid, showing seven consecutive relocations.

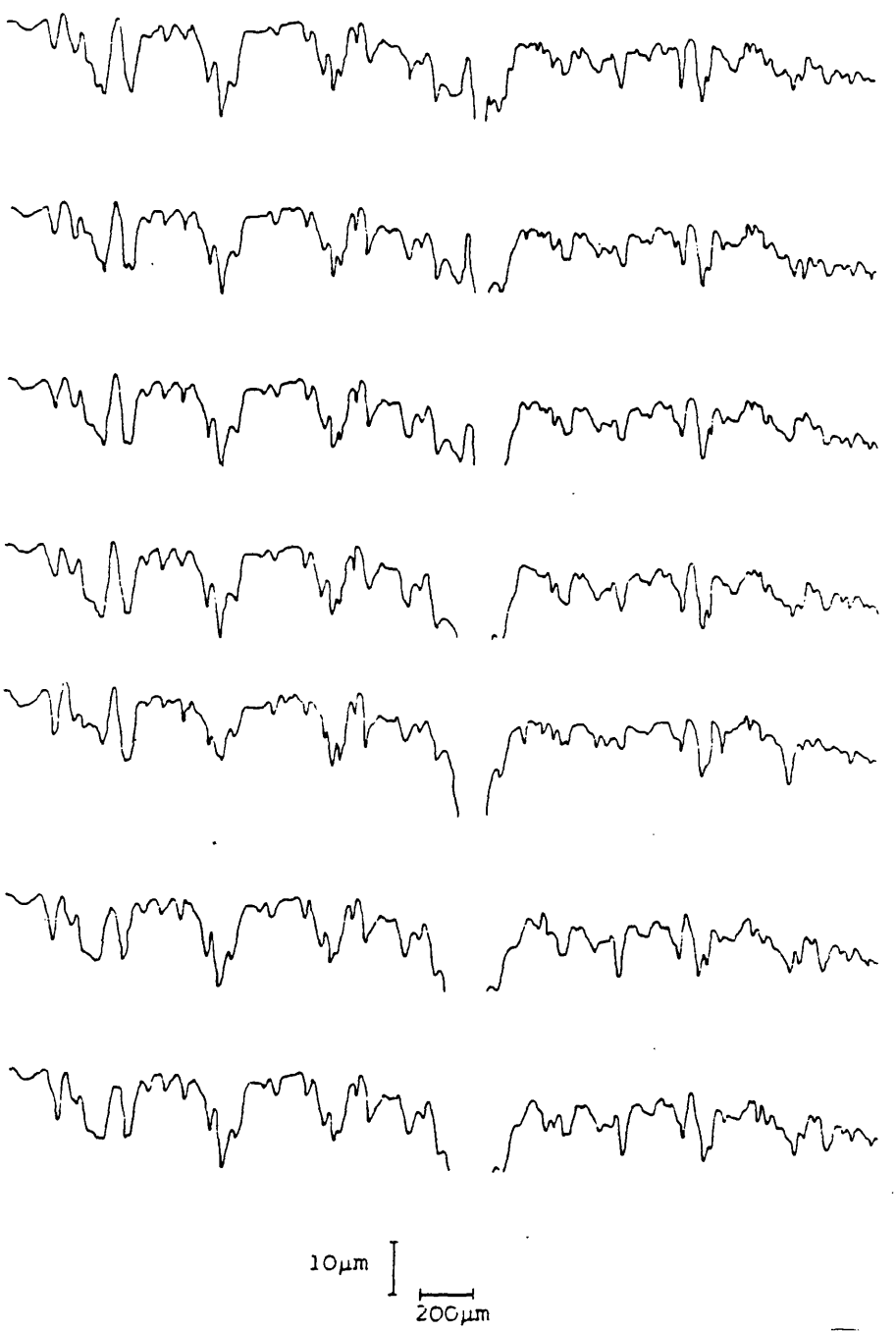

Figure 7.16 Surface roughness profile of roughened mild steel, using a nylon skid, showing seven consecutive relocations.

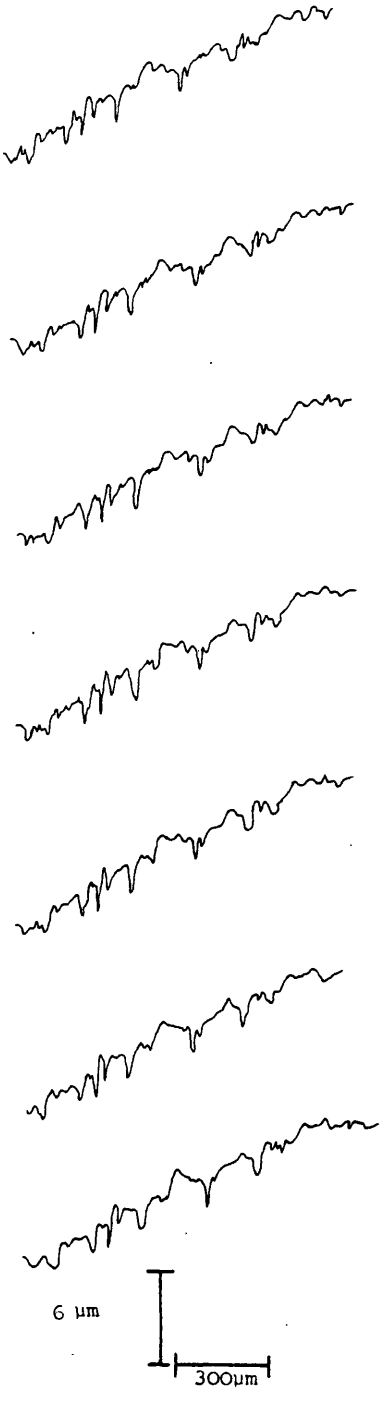

35 ml min^{-1} under the conditions described in Section 4.3.1.3. Rotation of the tablet and relocation stage on the model coating system for 10 minutes did not affect the surface roughness trace (Figure 7.17), confirming that the tablet and stage were firmly stuck together. At intervals during the build-up of the coating, the relocation stage was removed and the surface profile recorded (Figure 7.18). The thickness of the applied films was estimated from the measurement of films stripped from glass plates adjacent to the relocation stage on the coating belt.

7.3 Results and Discussion

Figure 7.18 shows the changes in surface topography which occurred as the coating increased in thickness up to 40 μm. Minor irregularities were rapidly obliterated and the major peaks and valleys became more rounded. However, even at a film thickness of 40 μm it was the presence of large irregularities in the core which determined the surface roughness. This obvious reduction in asperity was accompanied by R_a decreasing from 2.80 to 1.80 μm (five determinations, standard deviation zero)

Examination of the surface profiles may also indicate the physical state of the coating solution when it reached the tablet surface. A 'wet' freely mobile solution would be expected to run off the peaks and fill the valleys, whilst Figure 7.18 indicates a more even coverage of both peaks and valleys. This suggested that under the chosen coating conditions the solution

Figure 7.17. Surface roughness traces of two 25.4 mm diameter lactose-microcrystalline cellulose tablets, using a nylon skid, showing the effect of 10 minutes rotation on the model coating system.

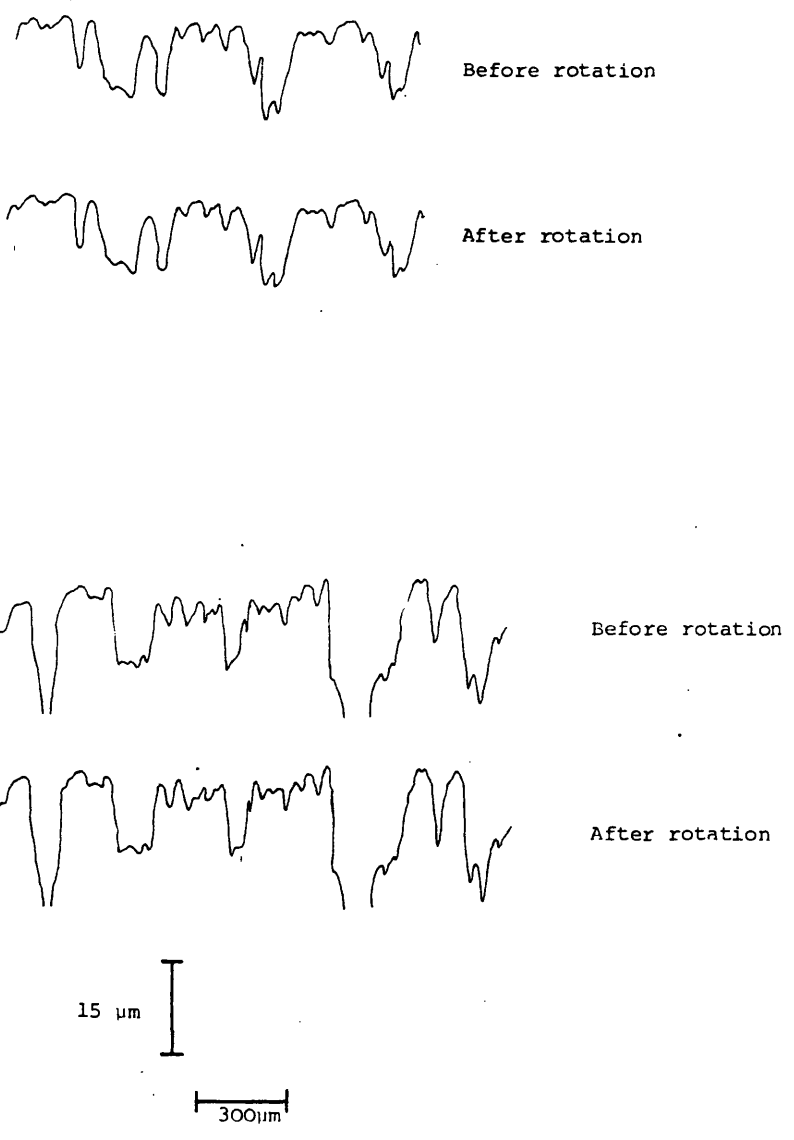

Figure 7.18 Surface roughness traces of a 25.4 mm diameter lactose-microcrystalline cellulose tablet during the build-up of a film coating 40 μm thick.

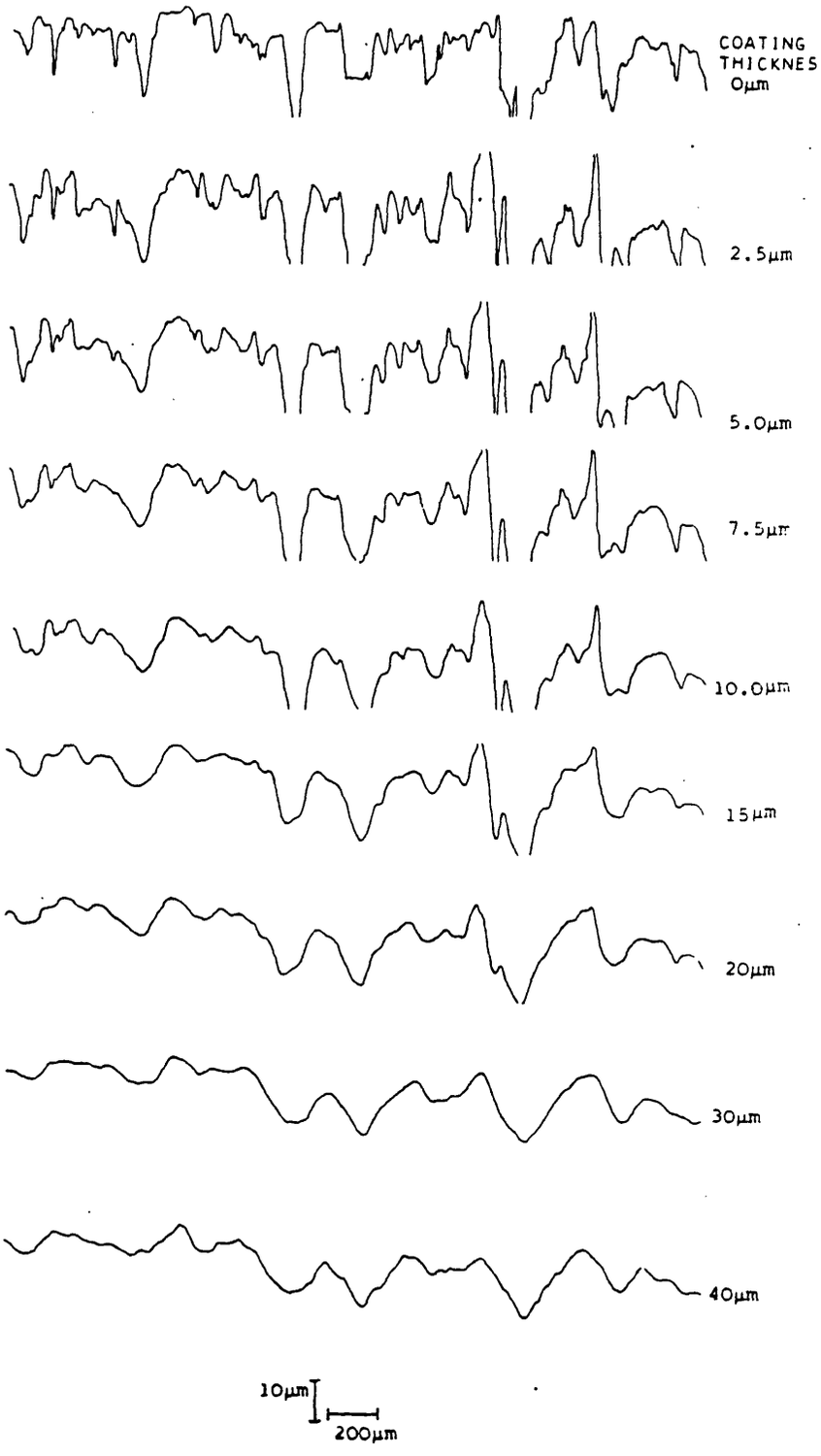

reaching the tablet surface was in a fairly 'dry' viscous state, with little chance to spread selectively into certain regions of the surface profile.

Precise quantification of these changes during the build-up of a film coating can be obtained by analysis techniques such as cumulative peak height distributions, peak and valley distributions, slope curvature distributions and power spectra[272]. However their calculation requires the conversion of the analogue output from the Talysurf to a digital signal, with subsequent data processing by mainframe or micro computer. Furthermore, to ensure the digitizing of the signal always starts and finishes at the same points, proximity switches would need to be fitted to the gearbox,underneath the pick-up arm, to overcome the mechanical backlash in the resetting system.

Such developments were beyond the scope of this project, but the work described has demonstrated the applicability of the relocation technique in discerning the changes in tablet asperity during the build-up of a film coating.

RESULTS AND DISCUSSION

8. THE PROPERTIES OF COATING SOLUTIONS

8.1 Results and Discussion

8.1.1 Viscosity Measurements

a) Dilute Solution Viscometry

Figure 8.1 shows the Huggins' plots of reduced specific viscosity versus concentration for the three samples of HPMC and one of HPC, at 20°C in distilled water (see Section 3.3a). The plots were linear with correlation coefficients greater than 0.9960 ($r_{tab}P=0.01$) = 0.959) (Table 8.1). Table 8.2 gives the values for each polymer of the viscosity of a 2% w/v solution, the Huggins' constant (k_H) , intrinsic viscosity($[\eta]$) and peak molecular weights.

The Huggins' constants of 0.97 and 0.77 for Pharmacoat 606 and Methocel E5 Premium respectively, indicated a rod-like polymer configuration whilst Pharmacoat 603 existed as random coils (k_H = 0.58)[247]. A value of 2.18 for Klucel L.F. indicated a solid sphere configuration, probably due to poor solvation of the polymer.

The viscosities of 2% w/v aqueous solutions conformed with the manufacturers specifications for the three types of HPMC and the peak molecular weights, calculated from these values using a relationship published by Rowe[209], (equation 8.1 and Table 8.2) agreed closely with the data presented in the literature[209]. Rowe[209] has also published values for the constants k_m and α of the Mark-Houwink equation (equation 3.9 and Table 8.2),

Figure 8.1 Huggins' plots of reduced specific viscosity versus concentration for aqueous solutions of coating polymers at 20°C

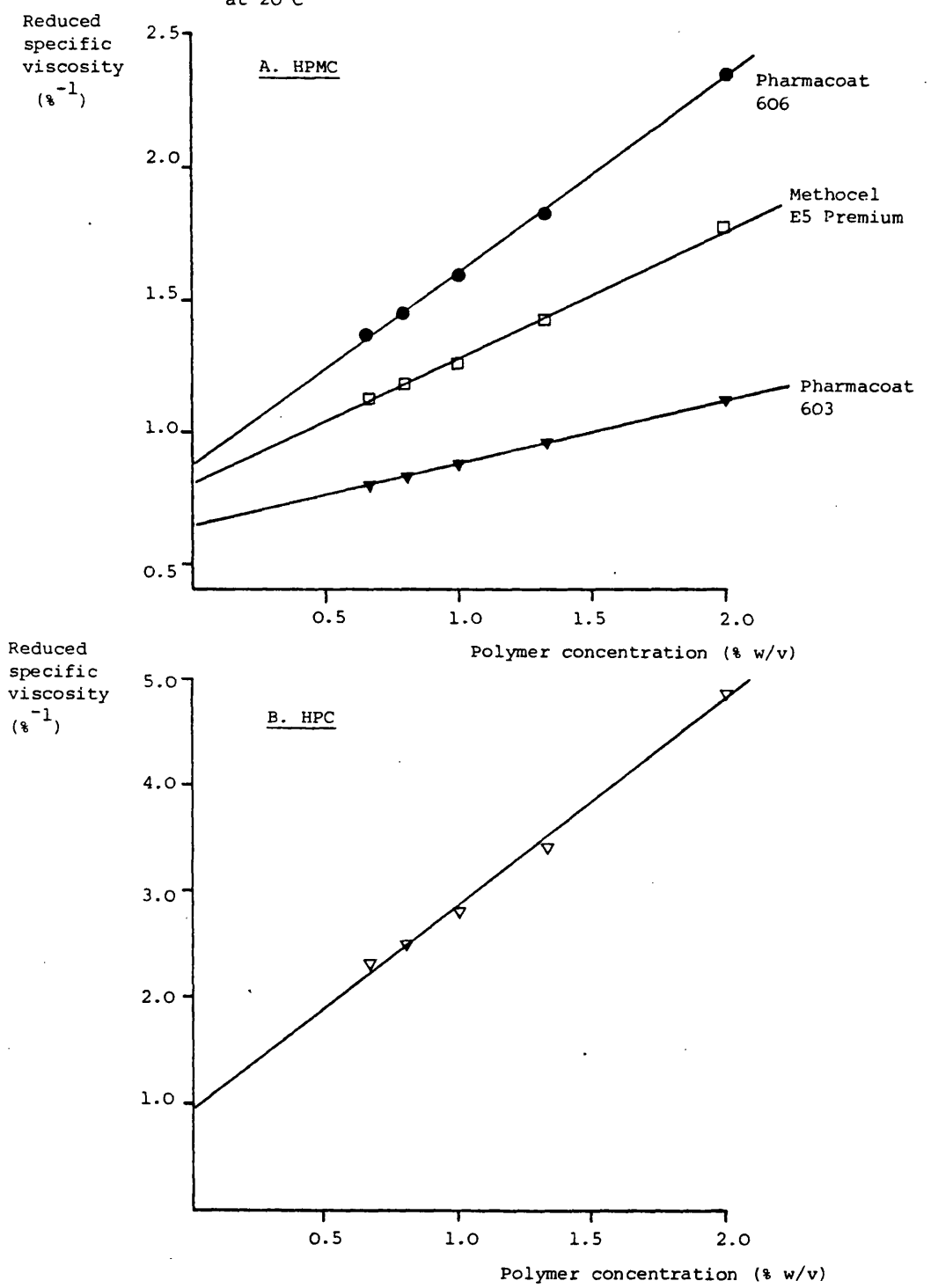

Table 8.1 Least squares regression data for the Huggins' plots of reduced specific viscosity versus concentration for aqueous film coating polymers at 20°C in distilled water

Polymer	Slope ($\%^{-2}$)	S.D. Slope	Relative S.D. Slope (%)	Intercept ($\%^{-1}$)	S.D. Intercept	Correlation Coefficient
Pharmacoat 606	0.7308	0.0240	3.29	0.8680	0.0301	0.9984
Pharmacoat 603	0.2348	0.0080	3.41	0.6380	0.0100	0.9983
Methocel E 5 Premium	0.4814	0.0171	3.55	0.7902	0.0214	0.9981
Klucel L.F.	1.9262	0.1001	5.20	0.9390	0.1255	0.9960

S.D. = Standard Deviation

Table 8.2 Huggins' constant, polymer configuration, viscosity and molecular weight data determined by aqueous dilute solution viscometry at 20°C of four film coating polymers

Polymer	Huggins' constant k	Probable Polymer Configuration	Viscosity of a 2% w/v aqueous solution (mPas)	Peak molecular weight determined from the viscosity of a 2%w/v aqueous solution (equation 8.1)	Intrinsic viscosity ($cc\ g^{-1}$)	Peak Molecular weight determined from the intrinsic viscosity (equation 8.2)
Pharmacoat 606	0.97	Rod-like	5.7	51,500	86.86	32,200
Pharmacoat 603	0.58	Random coils	3.2	39,700	63.80	24,300
Methocel E5 Premium	0.77	Rod-like	4.5	46,300	79.02	29,600
Klucel L.F.	2.18	Solid spheres	10.7	-	93.90	-

The peak molecular weights were calculated from the viscosity data, by reference to the relationship published by Rowe[209]:-

Equation 8.1 $M_p = k(\eta_{2\%})^n$ $k = 2.354 \times 10^4$, $n = 0.45$

Equation 8.2 $[\eta] = k_m M_p^{\alpha}$ $k_m = 9.94 \times 10^{-4}$, $\alpha = 1.096$

M_p = peak molecular weight

$[\eta]$ = intrinsic viscosity

$\eta_{2\%}$ = viscosity of a 2% w/v aqueous solution

by calculation[275] of the intrinsic viscosity from the viscosity of a 2% w/v polymer solution. However,using these values the peak molecular weights calculated from the intrinsic viscosity data obtained in this study were about 40% lower than those derived from the viscosities of the 2% w/v solutions and also those published by Rowe. The calculated molecular weights are greatly affected by small changes in the exponent α found in equation 8.2, but are relatively unaffected by variations in the exponent n of equation 8.1; a 4% error in the values of α and n altering the molecular weights by approximately 60% and 4% respectively. Since the scatter in the data presented by Rowe ($r = 0.847$, relative standard deviation of slope = 16.8%) could have introduced considerable errors into the assessment of α and n, the peak molecular weights determined from the viscosity of a 2% w/v solution using the latter, were considered to be more reliable than those calculated via equation 8.2. Furthermore, the calculation of intrinsic viscosities from single point viscosity measurements could have introduced additional errors into the molecular weights assessed by the Mark-Houwink relationship reported by Rowe[209].

The peak molecular weights for the three samples of HPMC were in the order Pharmacoat 606 > Methocel E5 Premium > Pharmacoat 603.

The molecular weight of the sample of HPC (Klucel L.F.) could not be calculated since the values of the Mark-Houwink constants were not readily available in the literature.

b) Continuous Shear Viscometry

Figure 8.2 shows typical rheograms measured using a cone and plate viscometer (see Section 3.3b). The rheograms were usually Newtonian with no hysteresis or yield points (Figure 8.2A), although highly concentrated solutions exhibited pseudoplastic behaviour, the extent of which increased with the polymer concentration (Figure 8.2B). Table 8.3 lists the values of Newtonian or apparent Newtonian viscosity and the index of non-Newtonian behaviour obtained with the four coating polymers; the latter two parameters being calculated from the Power Law (equation 3.10). The pseudoplastic nature of Klucel L.F. solutions was so great that the Power Plots became non linear for concentrations above 10% w/v, preventing assessment of the apparent Newtonian viscosity; an observation supported by the index of non-Newtonian behaviour decreasing rapidly with increasing polymer concentration.

Figure 8.3 indicates that plots of log Newtonian viscosity or apparent Newtonian viscosity versus polymer concentration were non-linear for the four coating polymers studied. Similar viscosity behaviour was reported by Pickard[106], although the extent of non-linearity in such plots was less than that observed in this study since the polymer concentrations investigated were lower. To allow adequate atomization of a coating solution, it is generally accepted that the viscosity should not exceed approximately 150 mPas[106,254]. This viscosity corresponds to polymer concentrations of 15% w/v, 9.5% w/v, 8.5% w/v and 5.5% w/v respectively for Pharmacoat 603, Methocel E5 Premium,

Figure 8.2 Typical rheograms for continuous shear cone and plate viscometry, at 29°C, of aqueous polymer solutions (sweep time 120s).

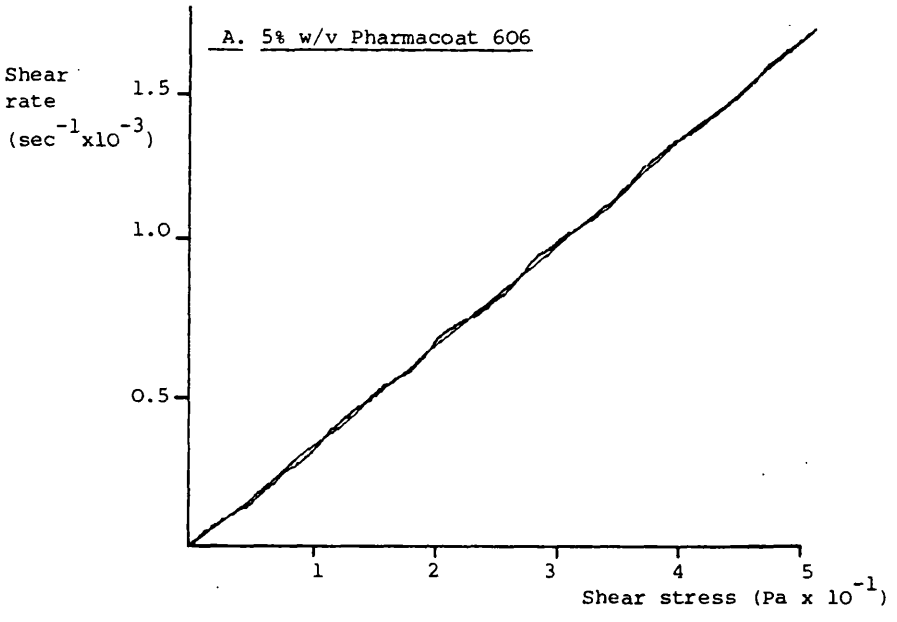

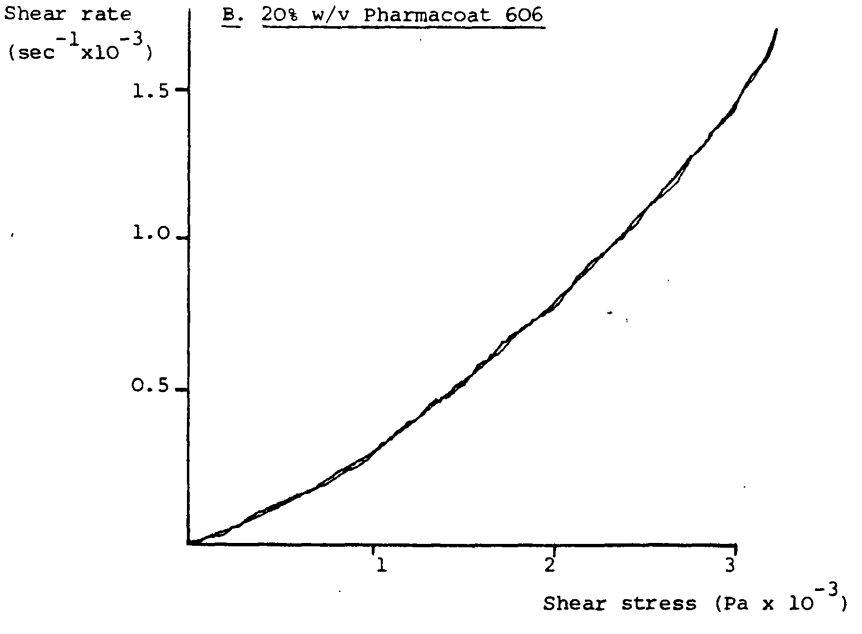

Table 8.3 Continuous shear viscosity data at 29°C for aqueous polymer solutions of concentration 0.25 to 20% w/v (minimum of 3 replicates at each concentration) (* Apparent Newtonian viscosity obtained from a power plot)

	PHARMACOAT 606		PHARMACOAT 603		METHOCEL E5 PREMIUM		KLUCEL L.F.	
Polymer Concentration (% w/v)	Newtonian viscosity (S.D.) (mPas)	Index of Non-Newtonian Behaviour (S.D.)	Newtonian viscosity (S.D) (mPas)	Index of Non-Newtonian Behaviour (S.D.)	Newtonian viscosity (S.D.) (mPas)	Index of Non-Newtonian Behaviour (S.D.)	Newtonian viscosity (S.D.) (mPas)	Index of Non-Newtonian Behaviour (S.D.)
0.25	1.18 (0.06)	1.00			1.24 (0.02)	1.00	1.41 (0.07)	1.00
0.5	1.68 (0.06)	1.00			1.44 (0.13)	1.00	1.77 (0.07)	1.00
1.0	2.65 (0.02)	1.00			2.07 (0.05)	1.00	3.62 (0.11)	1.00
2.0	5.05 (0.08)	1.00	3.06 (0.07)	1.00	4.18 (0.08)	1.00	9.87 (0.13)	1.00
3.0	10.20 (0.30)	1.00			7.43 (0.18)	1.00	19.29 (0.45)	1.00
4.0	18.34 (0.34)	1.00			14.16 (0.20)	1.00	44.8* (9.3)	0.94 (0.03)
5.0	30.15 (0.06)	1.00	10.23 (0.26)	1.00	21.68 (0.06)	1.00	97.9* (0.7)	0.96 (0.01)
7.5	87.0 (2.1)	1.00			60.4 (1.0)	1.00	459.0* (41.5)	0.89 (0.02)
10.0	239.1 (2.5)	1.00	58.0 (1.5)	1.00	152.5 (1.7)	1.00	3730* (1686)	0.72 (0.07)
15.0	1546* (158)	0.90 (0.01)			979* (119)	0.81 (0.01)	Power plot	
20.0	8879* (873)	0.80 (0.02)	305.6 (9.4)	1.00	4684* (569)	0.79 (0.02)	Non-Linear	

Figure 8.3 Continuous shear viscosity at 29°C versus concentration for aqueous solutions of four film coating polymers

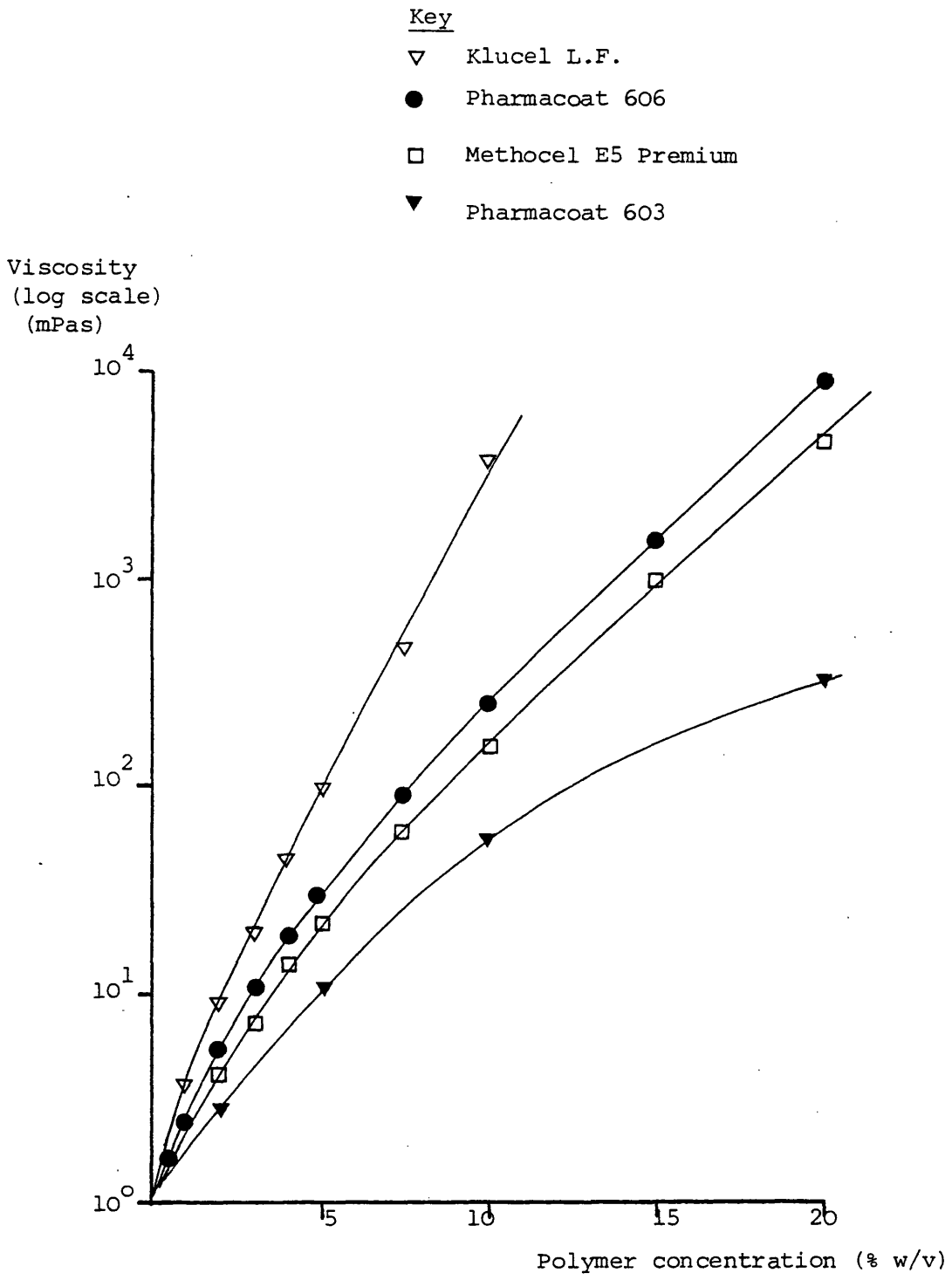

Pharmacoat 606 and Klucel L.F. Thus the lower molecular weight polymers represent an advantage in terms of the maximum possible polymer loading of the coating suspension, although they have been shown to produce films with inferior mechanical properties[106,168,186,210]

c) Creep Rheometry

Creep curves were obtained at 29°C with 20% w/v aqueous solutions of the coating polymers, as described in Section 3.2c. Figure 8.4 shows typical creep curves for HPMC and HPC and the creep parameters determined according to equation 3.15 are listed in Table 8.4. The Klucel L.F. solution was atypical in that time dependent rheological behaviour was totally absent, resulting in a linear creep curve. This suggested an absence of polymer-polymer interactions which would produce retardation of the flow.

The results obtained with HPMC solutions were very erratic (Table 8.4) despite standardization of the technique by which the sample was placed on the instrument, the time interval before testing (5 minutes) and the testing conditions. The reason for this irreproducibility was unclear; it may have been associated with evaporation of the solvent and subsequent gelation of the polymer at the edges of the cone, although use of a vapour hood did not improve the situation. Despite these variations, it was clear that concentrated HPMC solutions exhibited little elastic behaviour and the retardation times associated with the viscoelastic component were short.

Figure 8.4 Typical creep curves at 29°C for 20% w/v aqueous solutions of film coating polymers using a cone and plate creep rheometer.

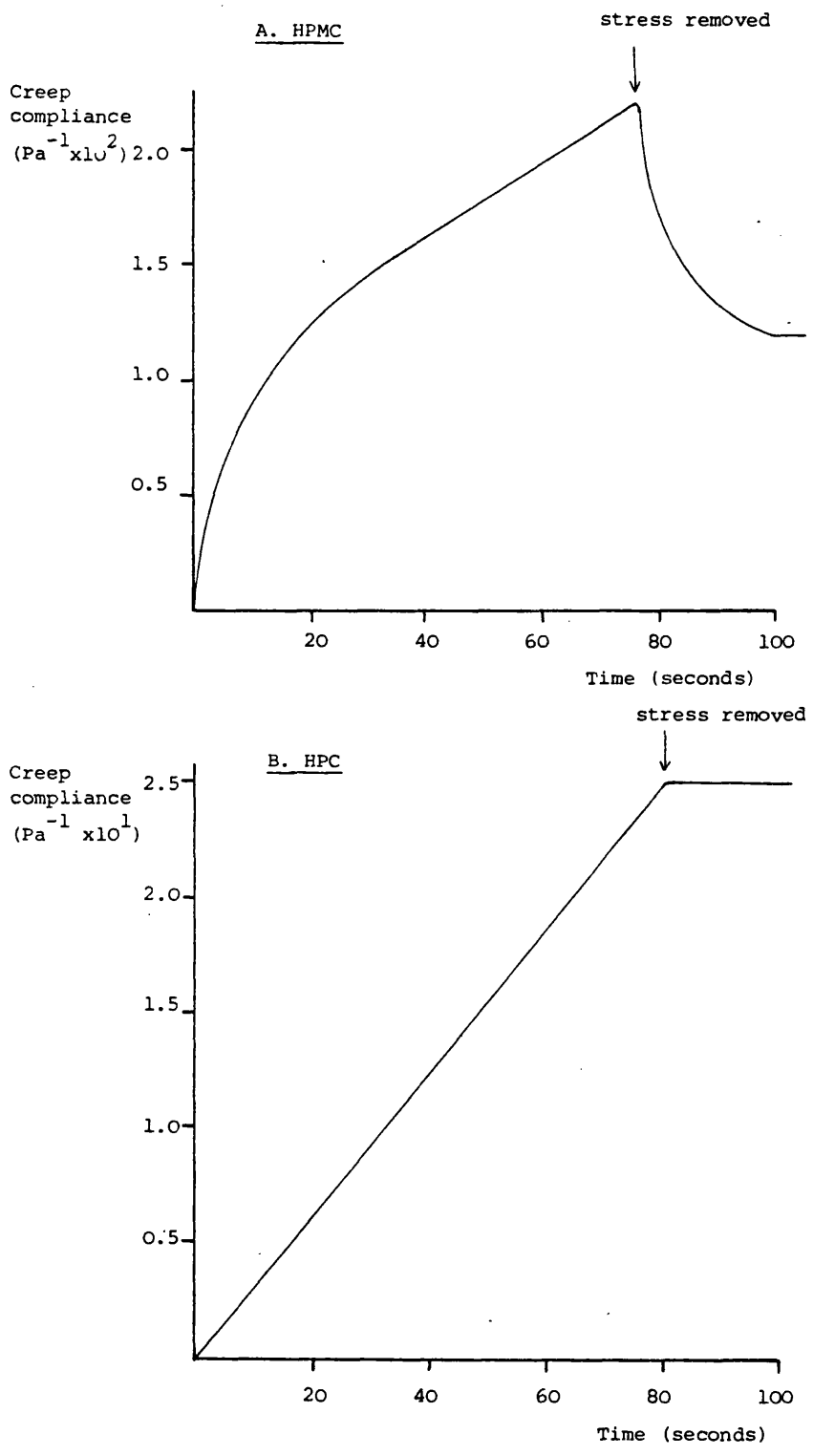

Table 8.4 Mean creep parameters at 29°C for 20% w/v aqueous solutions of film coating polymers, using a cone and plate creep rheometer.

(Figures in brackets are standard deviations)

	Pharmacoat 606	Pharmacoat 603	Methocel E5 Premium	Klucel L.F.
Instantaneous compliance J_o ($Pa^{-1} \times 10^6$)	7.8 (13.5)	0.005 (0.005)	769 (1088)	-
Retarded compliance J_1, ($Pa^{-1} \times 10^3$)	5.5 (3.4)	16.0 (4.7)	34.5 (13.3)	-
Retarded compliance J_2 ($Pa^{-1} \times 10^3$)	2.6 (0.7)	9.1 (2.4)	5.0 (7.1)	-
Newtonian viscosity η_o (Pas x 10^{-2})	111.0 (32.0)	21.6 (4.7)	26.5 (32.9)	2.5 (0.5)
Retarded viscosity η_1 (Pas x 10^{-2})	23.3 (11.2)	7.5 (0.7)	4.4 (3.9)	-
Retarded viscosity η_2 (Pas x 10^{-2})	3.0 (1.8)	0.8 (0.1)	84.2 (119.1)	-
Retardation time τ_1 (seconds)	10.3 (3.6)	11.8 (2.4)	13.4 (6.8)	-
Retardation time τ_2 (seconds)	0.7 (0.3)	0.8 (0.3)	0.9 (1.2)	-

Summation of the individual components of viscosity and compliance, obtained for each sample of HPMC, gave the data in Table 8.5. The summed viscosities of the solutions were in the order Pharmacoat 606 > Methocel E5 Premium > Pharmacoat 603; the same rank order as found by capillary (Table 8.2) and continuous shear (Table 8.3) viscometry. The total compliance value for Methocel E5 Premium was five times greater than that for Pharmacoat 606; an unforeseen discovery since the polymers had similar specifications (Section 2.2), molecular weights (Table 8.2) and viscosities (Tables 8.2 to 8.4). Although the large standard deviations observed about these values make detailed conclusions impossible, such differences in the total compliance may be reflected in the mechanical properties of films prepared from these polymers.

Table 8.5 The total compliance and viscosity data, at 29°C, for 20% w/v aqueous solutions of HPMC, using a cone and plate creep rheometer

	Pharmacoat 606	Pharmacoat 603	Methocel E5 Premium
Total compliance $\sum_{o}^{2} J$ ($Pa^{-1} \times 10^{3}$)	8.1 (4.1)	25.0 (2.3)	40.3 (7.2)
Total viscosity $\sum_{o}^{2}$ ($Pas \times 10^{-2}$)	137.3 (38.2)	29.9 (5.5)	115 (31.6)

8.1.2 Thermal Properties

a. Clouding Behaviour

The increase in turbidity or clouding of aqueous solutions of film coating polymers as the temperature was raised was investigated using the techniques described in Section 3.4a. The results presented in Figure 8.5 show that as the polymer concentration was increased the temperature at which clouding began, decreased by up to 15°C and the initial rate of rise in absorbance with temperature was slightly reduced. Observation of the 0.25% w/v solutions indicated that clouding was due to precipitation of the polymer rather than coacervation; HPC (Klucel L.F.) was precipitated as fine particles which remained suspended whilst all three HPMC grades produced swollen flocs which sedimented as the temperature was raised, leading to the observed fall in absorbance at 450 nm.

Figure 8.6 shows the data replotted to allow direct comparison of the clouding behaviour of the four polymers. Klucel L.F. solutions clouded over the range 35 to 45°C, as expected from the manufacturer's data which indicated that HPC was insoluble in water above 40 to 45°C. HPMC solutions clouded in the range 40 to 65°C, corresponding with manufacturer's data that HPMC was insoluble in water above 60°C. Thus the clouding behaviour was a reflection of the inverse temperature-solubility relationship exhibited by these substituted cellulose derivatives and the earlier clouding of the more concentrated solutions was to be expected as polymer dehydration commences prior to precipitation.

Figure 8.5 Increase in absorbance at 450 nm versus temperature, for aqueous solutions of film coating polymers.

Key ▲ 20% w/v □ 1% w/v
▽ 10% w/v ○ 0.25% w/v
● 5% w/v

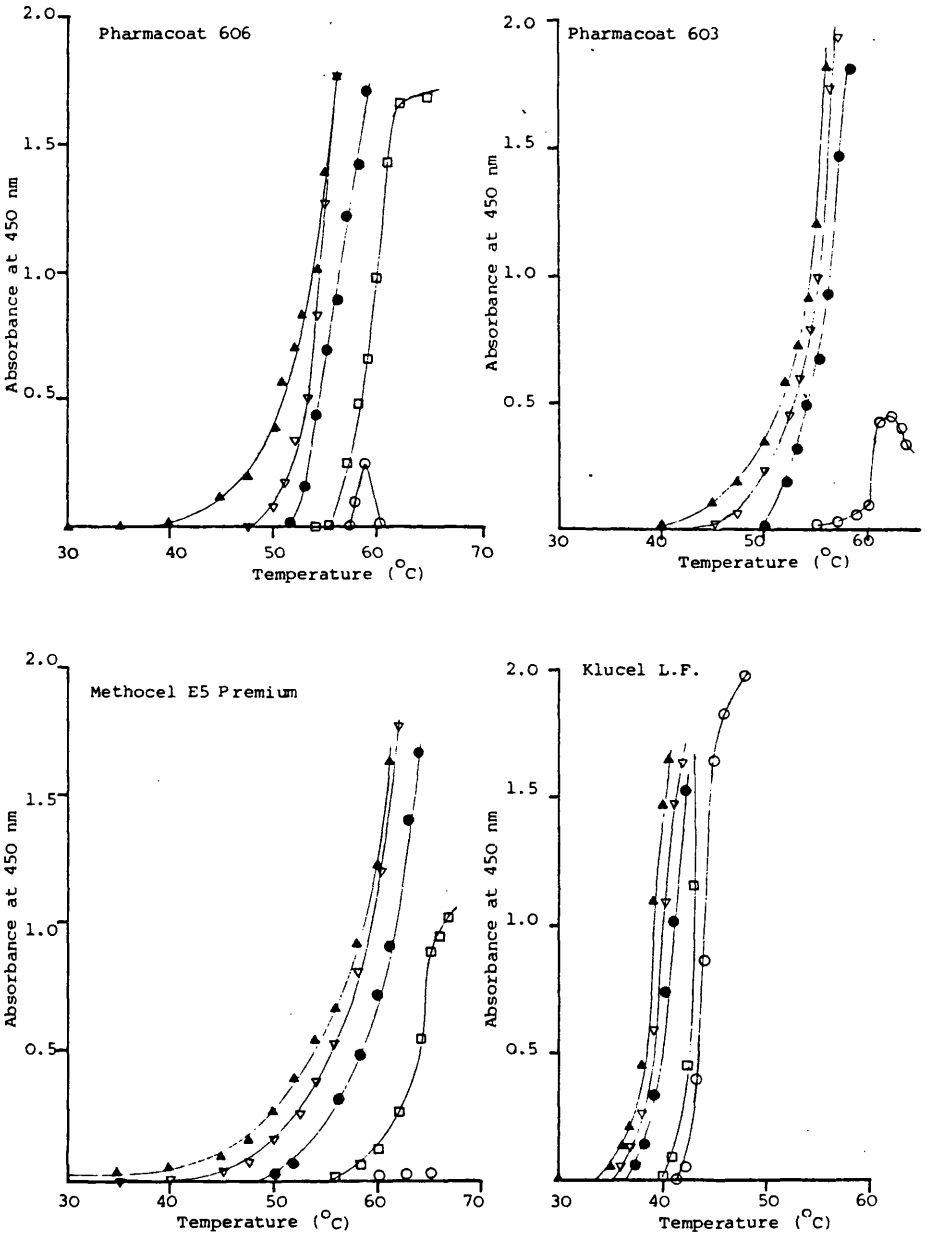

Figure 8.6 The increase in absorbance at 450 nm versus temperature, for aqueous solutions of film coating polymers

Key ● Pharmacoat 606 □ Methocel E5 Premium
▼ Pharmacoat 603 ▽ Klucel L.F.

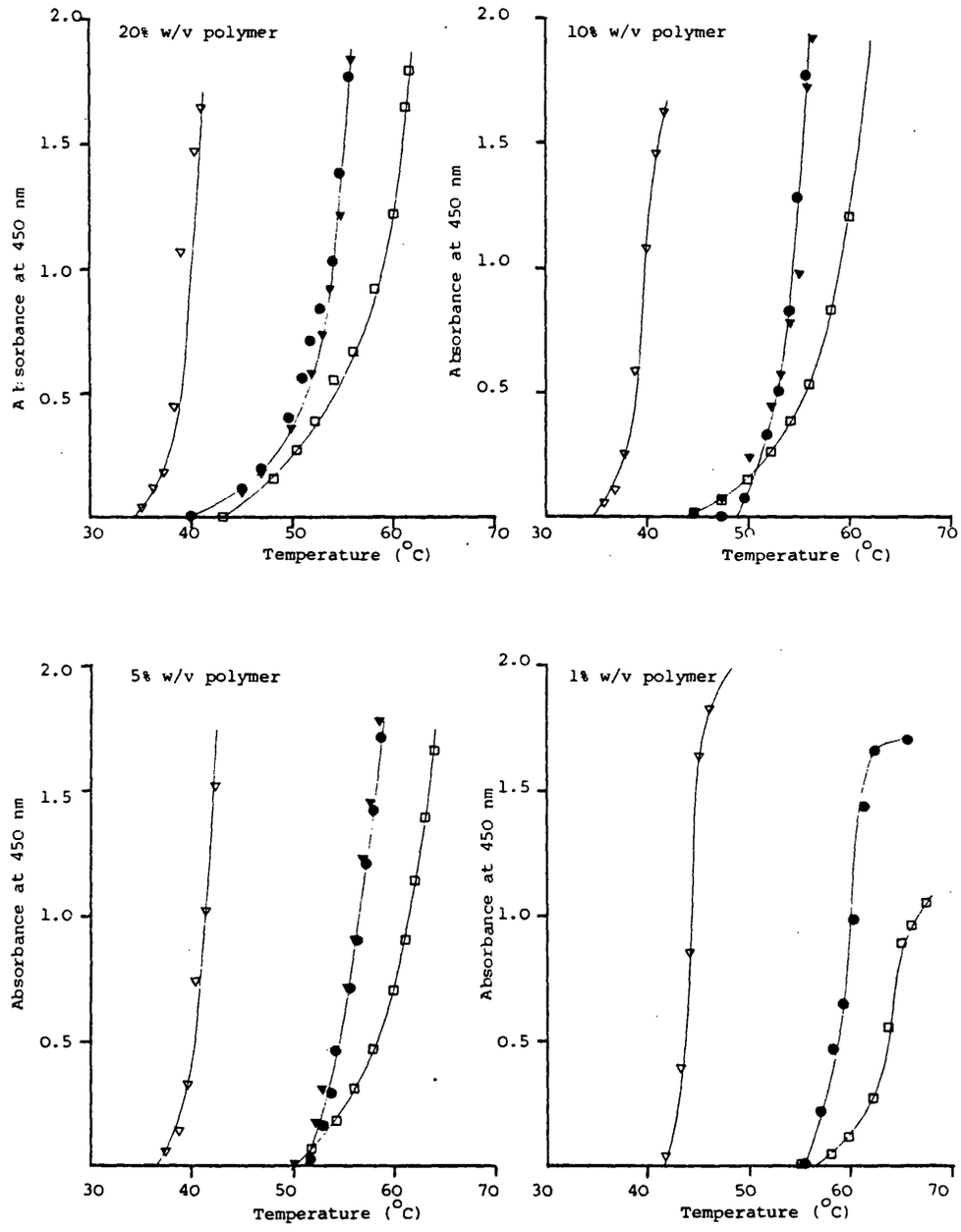

The temperature at which clouding began was similar for all three types of HPMC and the complete curves for Pharmacoat 606 and 603 were superimposable. However, the initial slope of the absorbance-temperature curve for Methocel E5 Premium was considerably lower, resulting in a 5°C higher temperature, for a given absorbance, at higher absorbances. Such differences are discussed further in section 8.2 but may have arisen as a consequence of differing polymer molecular weights, molecular weight distributions, substituent ratios or impurity profiles.

Figure 8.7 indicates that neither sodium chloride (a known impurity of HPMC) nor propylene glycol (a commonly used plasticizer), at the concentration levels evaluated, had a significant effect on the clouding behaviour of Pharmacoat 606 and Methocel E5 Premium.

b) Thermal Gelation

The point at which the viscosity of the polymer solutions changed rapidly with increasing temperature was investigated using the techniques described in Section 3.4b. To facilitate such measurements a Brookfield viscometer was used, although the viscosity data obtained, at constant shear rate, was not directly comparable with that measured by capillary, continuous shear or creep methods, since the shear geometry is ill-defined and hence the shear rate in the Brookfield instrument is difficult to resolve.

Figure 8.7 The effect of additives on the increase in absorbance at 450 nm versus temperature, for aqueous solutions of film coating polymers

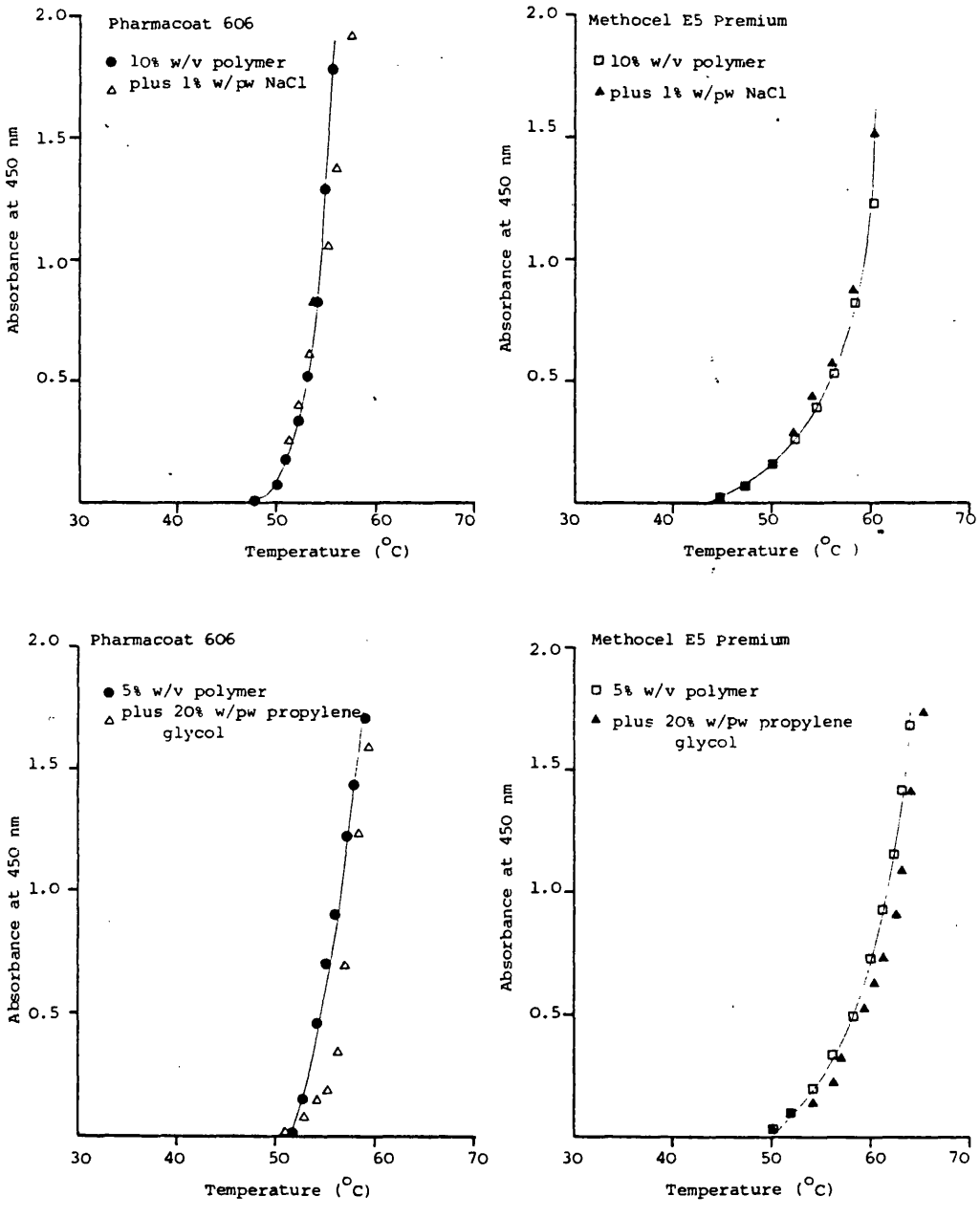

The viscosity-temperature profile of HPC (Klucel L.F.) was distinct from those of HPMC solutions in that a thermal gelation point was not observed (Figure 8.8). The solution viscosity decreased steadily with increasing temperature until complete precipitation of the polymer at 45°C rapidly changed the system from a viscous solution to a mobile suspension of under 200 mPas viscosity.

The temperature at which thermal gelation began was similar for all three samples of HPMC, although the subsequent rise in viscosity was faster for Methocel E5 Premium (Figure 8.9). As the polymer concentration increased the gelation temperature decreased slightly but the effect, approximately a 2°C fall for a 10% w/v rise in concentration, was small in comparison with a polymer such as methyl cellulose where a 2% w/v rise in concentration can decrease the gelation temperature by 10°C[276]. Increases in temperature after gelation rapidly increased the viscosity and at lower concentrations an inflexion in the curve was observed, corresponding to the appearance of a high degree of thixotropy. The viscosity at which thixotropy developed varied from 1 Pas to 80 Pas (Figure 8.8), depending upon the nature and concentration of the polymer, indicating that this behaviour may have been related to a change in gel structure rather than an artifact introduced by the viscometer. Once thixotropy had developed, further increases in temperature increased the time dependent nature of the behaviour until a gel was produced which exhibited a yield point beyond the range of the viscometer, which, when overcome, led to the breakdown of gel structure and a massive fall

Figure 8.8 The effect of temperature on the viscosity of aqueous solutions of four film coating polymers

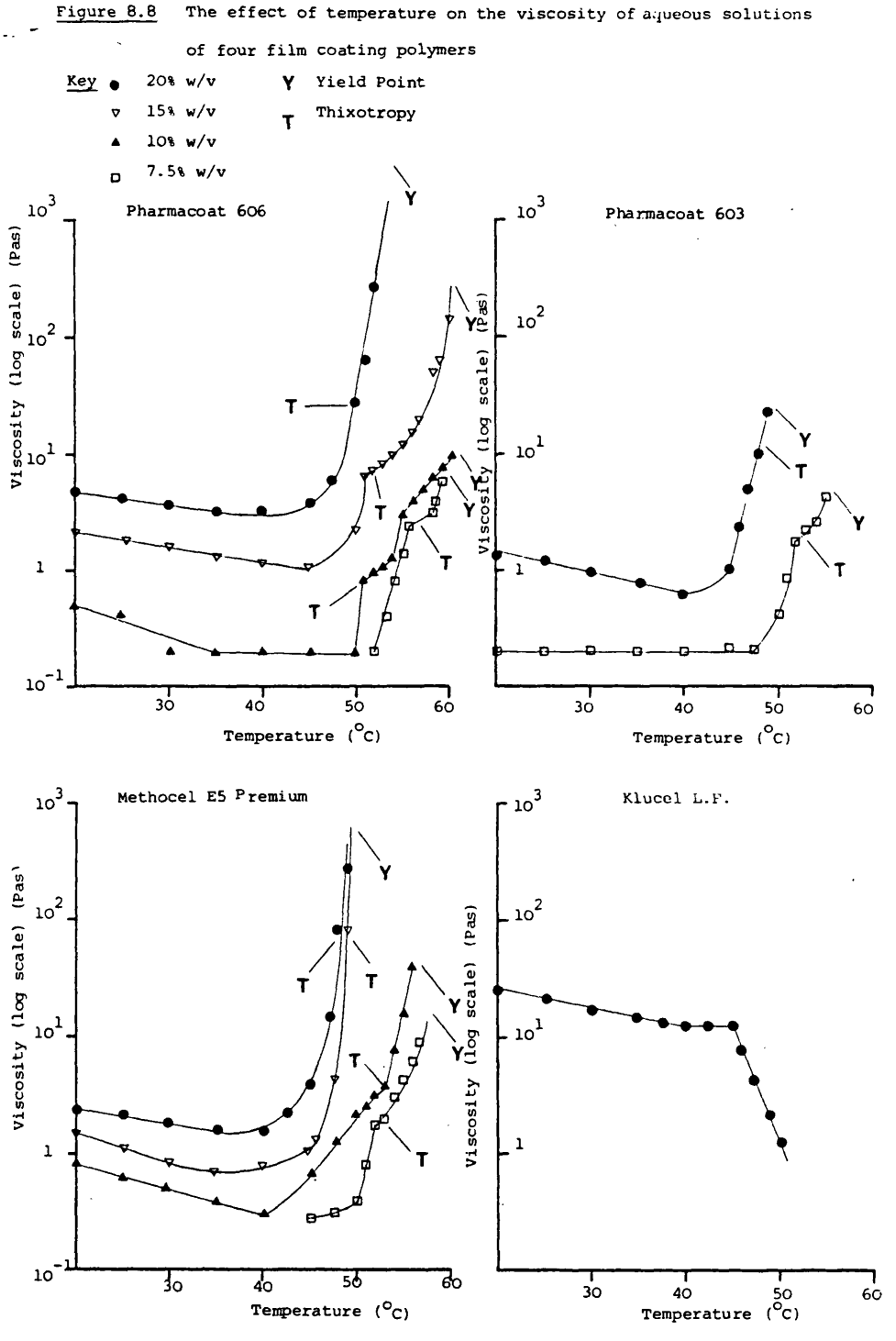

Figure 8.9 The effect of temperature on the viscosity of aqueous solutions of four film coating polymers.

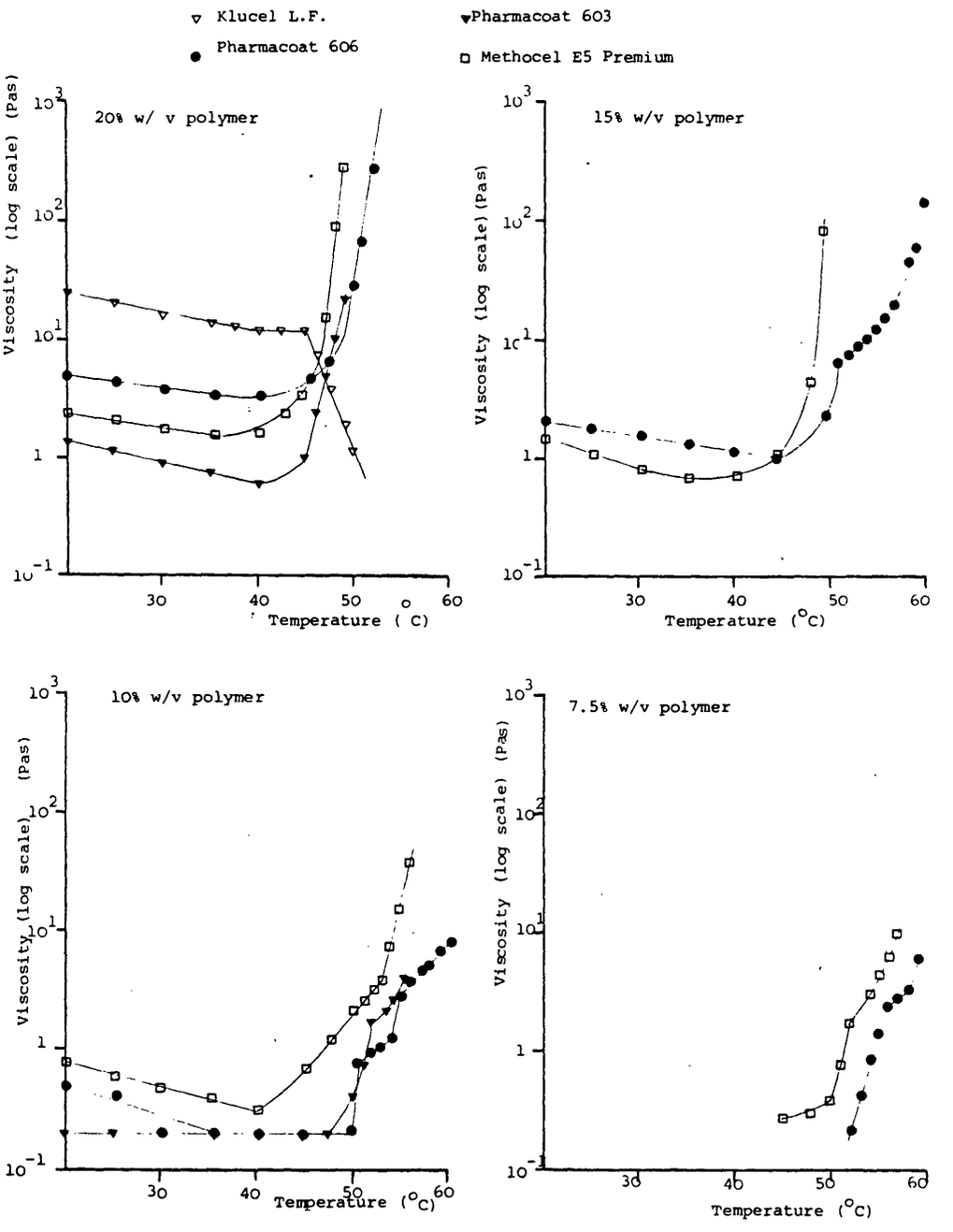

in viscosity to below 200 cps.

The variation of viscosity with temperature can be described by an Arrhenius relationship:-

$$\eta = A\, e^{\frac{E_a}{RT}} \qquad \text{...(equation 8.3)}$$

η is viscosity

A is a constant

E_a is the activation energy for viscous flow

R is the gas constant (8.314 $Jmol^{-1}k^{-1}$)

T is the absolute temperature

Plots of log viscosity versus the reciprocal of absolute temperature were prepared for the 20% w/v solutions of each polymer (Figure 8.10) and the linear sections, before and after gelation, subjected to least squares regression analysis (Table 8.6) enabling the activation energies for viscous flow to be calculated from the slopes. The activation energies for viscous flow before gelation were in the normal range for polymer solutions[247]; the values obtained for Pharmacoat 606 and Methocel E5 Premium not being significantly different. The slopes of the Arrhenius plots obtained after thermal gelation were not significantly different for the three types of HPMC, although the values were negative. Since activation energies cannot be negative, other thermal effects such as gelation, must have become dominant in the effect of temperature on the viscosity of aqueous HPMC solutions.

Figure 8.10 Arrhenius plots of log viscosity versus reciprocal of absolute temperature for 20% w/v aqueous solutions of four film coating polymers

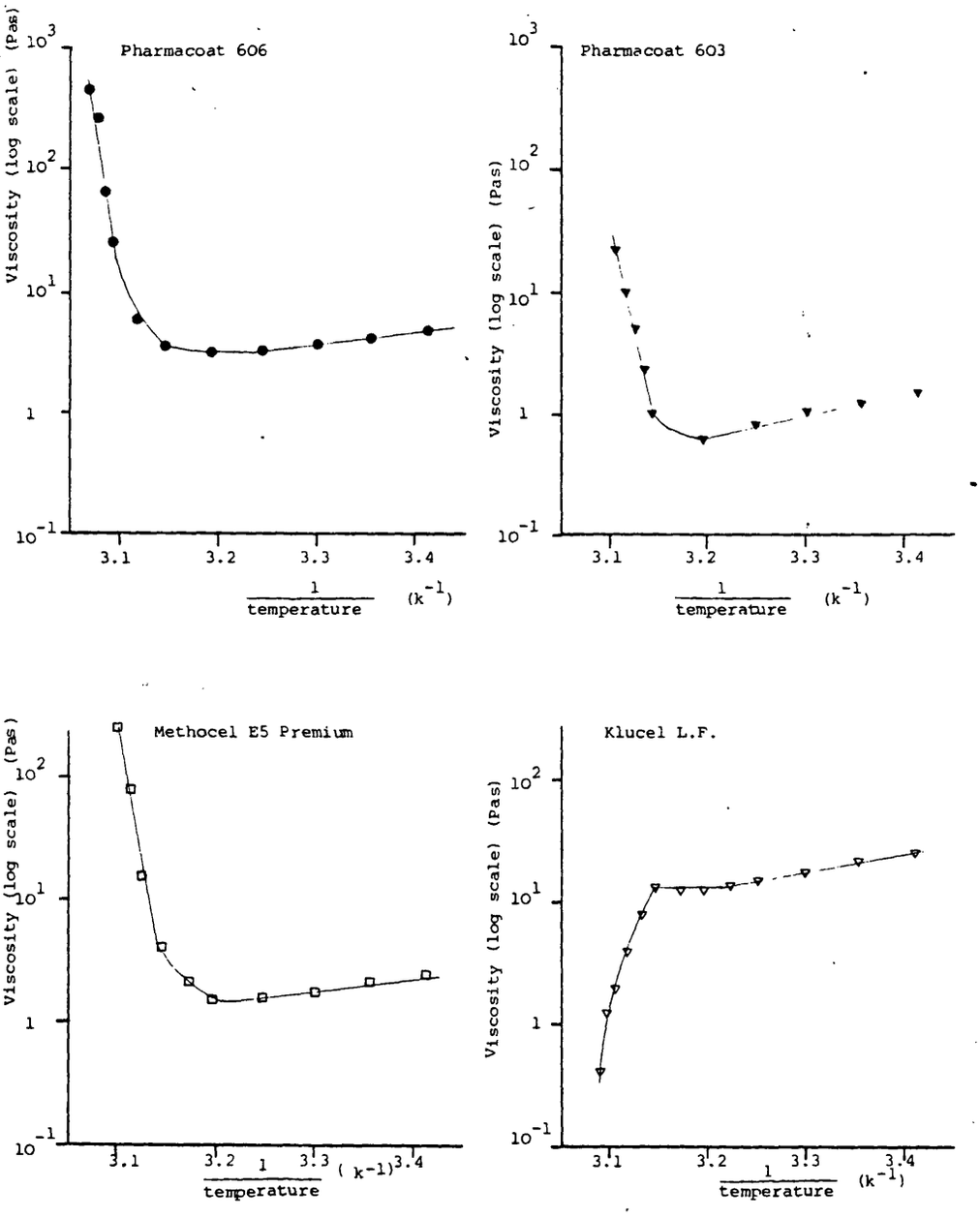

Table 8.6 Slopes of the Arrhenius plots before and after thermal gelation and the activation energies for viscous flow, for aqueous solutions of film coating polymers

Polymer	Concentration (% w/v)	Gelation State	Slope of Arrhenius plot ($PaK \times 10^{-3}$)	(S.D.)	Activation energy for viscous flow ($KJ\ mole^{-1}$)	(S.D.)	$t_{calculated}$	t_{tab} P=0.05
Pharmacoat 606	20 (1)	Before	1.10	(0.13)	21.1	(2.4)	1,3 2.99	2.57
	20 (2)	After	-44.56	(5.83)	-		1,5 0.68	2.78
							2,4 1.96	2.57
Pharmacoat 603	20 (3)	Before	1.67	(0.14)	32.0	(2.7)	2,6 0.31	2.78
	20 (4)	After	-33.08	(0.65)	-		1,7 2.81	2.45
Methocel E5 Premium	20 (5)	Before	1.21	(0.08)	23.1	(1.6)	3,7 0.72	2.36
	20 (6)	After	-47.43	(7.36)	-		5,7 2.72	2.45
Klucell L.F.	20 (7)	Before	1.55	(0.09)	29.6	(1.8)		

Figure 8.11 shows the effects of sodium chloride and propylene glycol on the thermal gelation of Pharmacoat 606 and Methocel E5 Premium. Sodium chloride lowered the thermal gelation temperature of both polymers by 2.5°C and increased the rate at which the viscosity rose with further increases in temperature. Propylene glycol had little effect, although the gelation temperature of the Methocel E5 Premium solution may have risen 1 - 2°C.

Thermal gelation has been explained[276] by postulating that the polymer chains are hydrated by sheaths of water molecules, so increasing the polymer bulk, preventing polymer-polymer interactions and thus allowing the chains to slide over one another to produce a smooth pouring viscous liquid. As the temperature is raised, the viscosity initially decreases as the hydrodynamic volume of the polymer is reduced by the outer layer of water molecules breaking away as their energy increases. When enough water molecules have been driven off, the polymer-water interactions no longer dominate, allowing polymer-polymer interactions to lock the chains together and produce a gel. Further increases in temperature drive off more water molecules leading to a change in gel structure.

The inability of Klucel L.F. to form thermal gels may thus be related to its hydration state since the data in Tables 8.2 and 8.4 indicated that in aqueous solution its molecules existed in a spherical configuration, which implies there is relatively little interaction between the polymer chains. Consequently dehydration of the molecules, by increasing the temperature, could not result in gel formation by an interlocking of the polymer chains.

Figure 8.11 The effects of additives on the increase in viscosity of aqueous solutions of film coating polymers, with increasing temperature

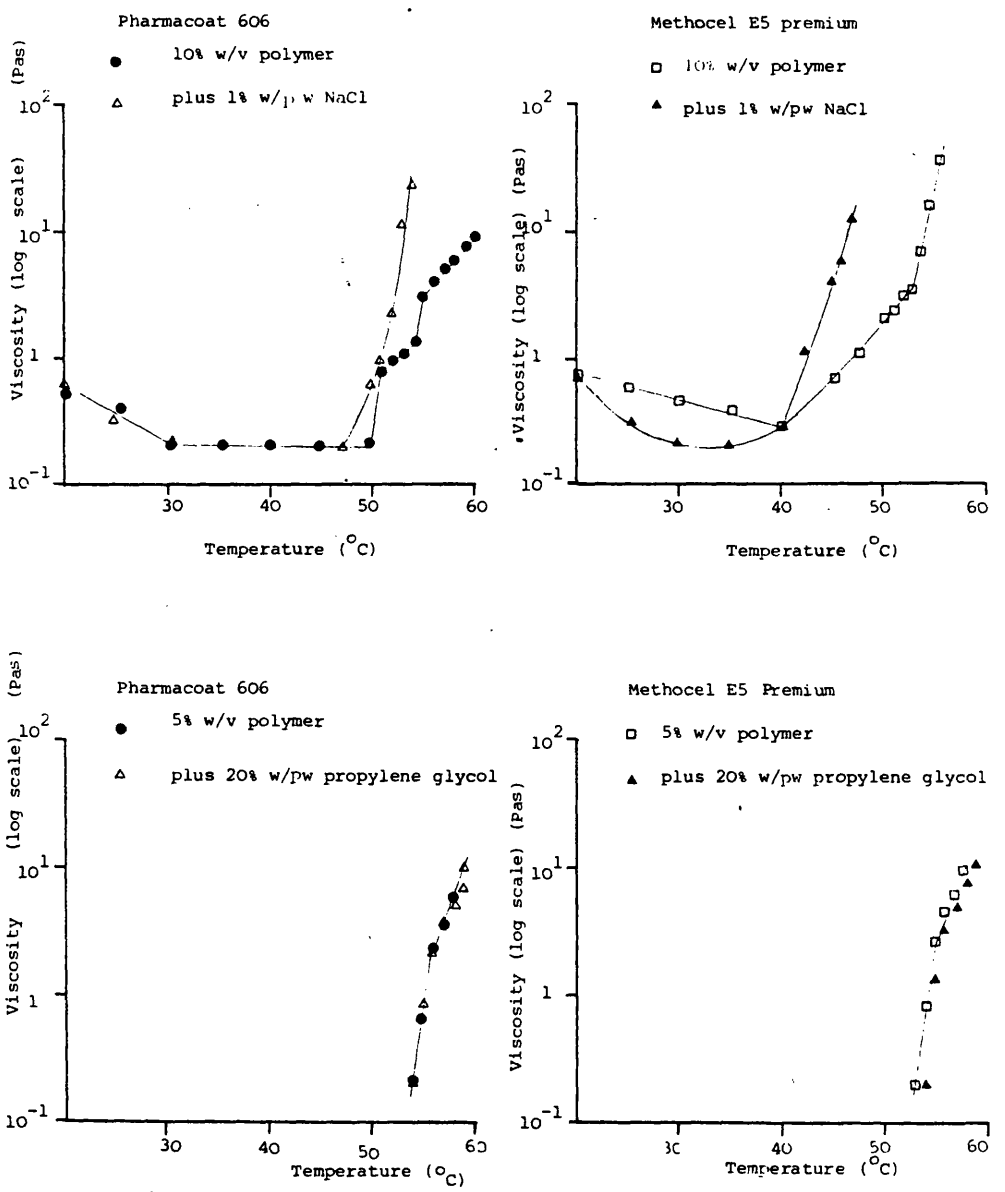

From the above postulates, it also follows that HPMC solutions of higher concentration would gel at lower temperatures, since the increased number and proximity of polymer chains allows the initial polymer-polymer interactions to become significant earlier. The change in gel structure at increased temperatures, caused by further dehydration of the polymer chains, could explain the inflexion observed in the graphs of log viscosity versus temperature (Figure 8.8). The point at which such a change occurred would be dependent upon the number of water molecules available to hydrate the polymer chains, which would be governed by the temperature and concentration of the solution rather than its viscosity.

The decrease in gelation temperature caused by sodium chloride can be explained by a decrease in polymer hydration arising from the hydration of added sodium and chloride ions. The marginal increase in thermal gelation temperature caused by the addition of propylene glycol can be attributed to its action as a plasticizer decreasing polymer-polymer interactions and so delaying the point at which the chains locked together.

The difference in gelation behaviour between Pharmacoat 606 and Methocel E5 Premium cannot be explained in terms of polymer molecular weight, since the former material, having a higher peak molecular weight, would be expected to gel at a lower rather than higher temperature. Possible sources of this difference include:

i. Different impurity profiles, especially the presence of inorganic ions such as sodium chloride

ii. Different molecular weight distributions

iii. Different number and ratio of substituents attached to the anhydroglucose ring (within the manufacturers limits), since these were known to govern the specific thermal gelation temperature.

c. Temperatures attained in the 24" Accela-Cota

The data obtained from measurement of the temperatures in the spray zone, during a coating run in the 24" Accela-Cota, are presented in Table 8.7. Despite an inlet air temperature of 90°C, that in the spray cone never exceeded 55°C and was further reduced as the liquid feed rate was increased.

Figures 8.12 and 8.13 depict respectively the variation in temperature in the spray cone with distance from the spray nozzle (up to 200 mm, the gun to bed distance) and spray rate (0 to 141 g min^{-1}). The cooling effect of the compressed air was minimal, as seen from the temperature-distance curve at a spray rate of zero g min^{-1}. As the liquid feed rate was increased, evaporation of the water rapidly reduced the temperatures attained in the spray zone, until a plateau was reached at approximately 30 g min^{-1} when no part of the spray exceeded 30°C. At low spray rates, the rise in temperature of the spray, with distance from the nozzle was attributed to a reduction in evaporative cooling caused by either extensive spray drying of the coating solution or by thermal gelation raising the viscosity. This

Table 8.7 The effect of spray rate and distance from the nozzle on the temperatures attained in the spray zone during a coating run in the 24" Accela-Cota

Spray Rate ($g min^{-1}$)	Temperature (^{o}C) at distances from 2050/120 nozzle (mm)						Coating comments
	10	25	50	100	200	Exhaust plenum	
0	47.9	49.8	52.2	54.4	52.5	51.8	
7	35.8	43.5	48.1	49.8	53.0	52.2	'orange-peel' coating due to spray drying
11	19.8	41.1	45.5	50.8	51.0	50.3	
20	18.8	23.7	34.8	42.6	43.0	51.3	
32	18.4	21.0	24.7	25.1	28.5	46.8	
46	17.9	20.3	23.0	23.7	26.5	42.6	Tendency to pick
63	18.1	21.3	23.7	23.7	24.9	42.0	Tablets overwet and sticking together
141	17.3	18.8	20.8	25.1	26.1	28.0	

Figure 8.12 The effect of distance from a 2050/120 spray nozzle on the temperatures attained in the spray zone, during coating runs at different liquid feed rates, in the 24" Accela-Cota.

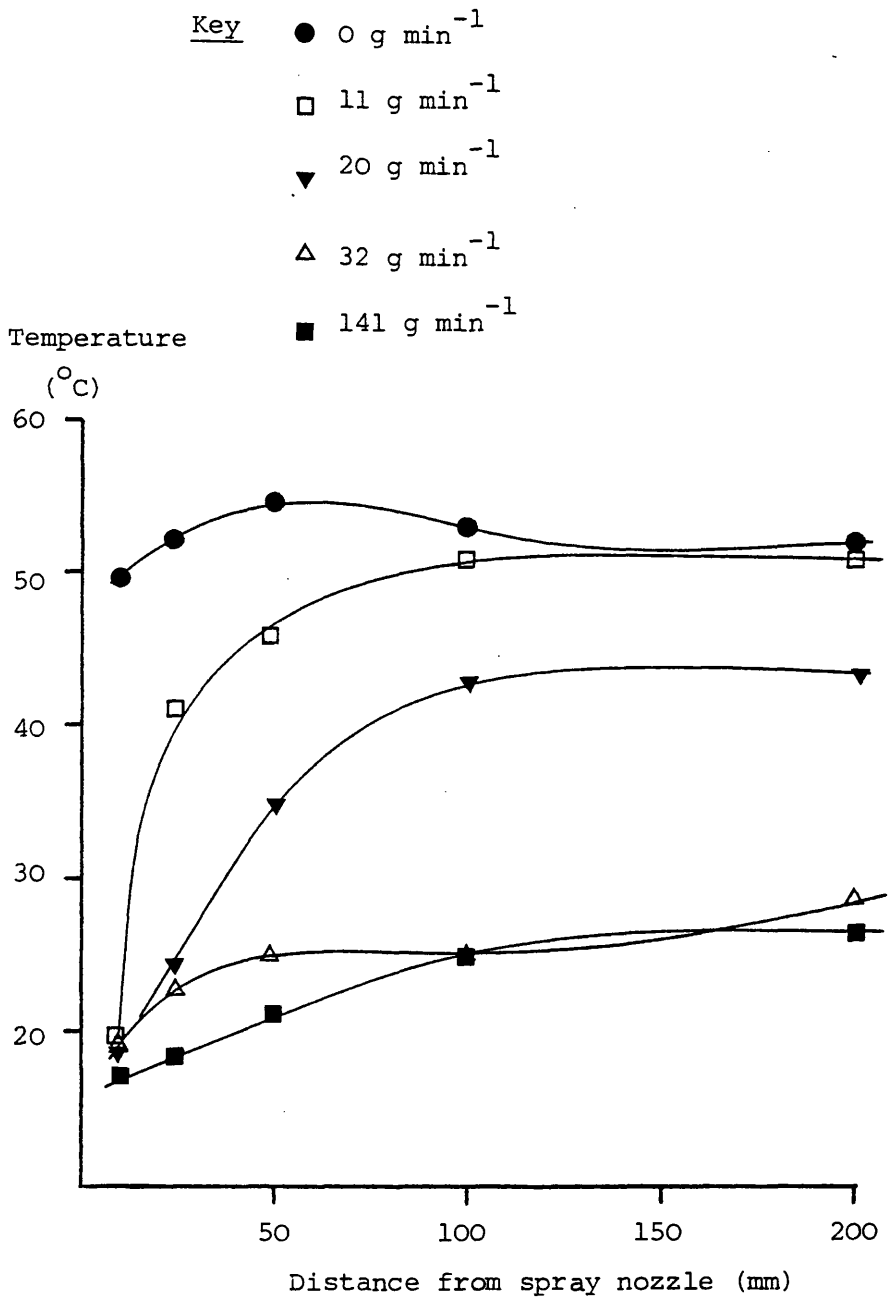

Figure 8.13 The effect of liquid feed rate on the temperatures attained at various distances from a 2050/120 spray nozzle during a coating run in the 24" Accela-Cota.

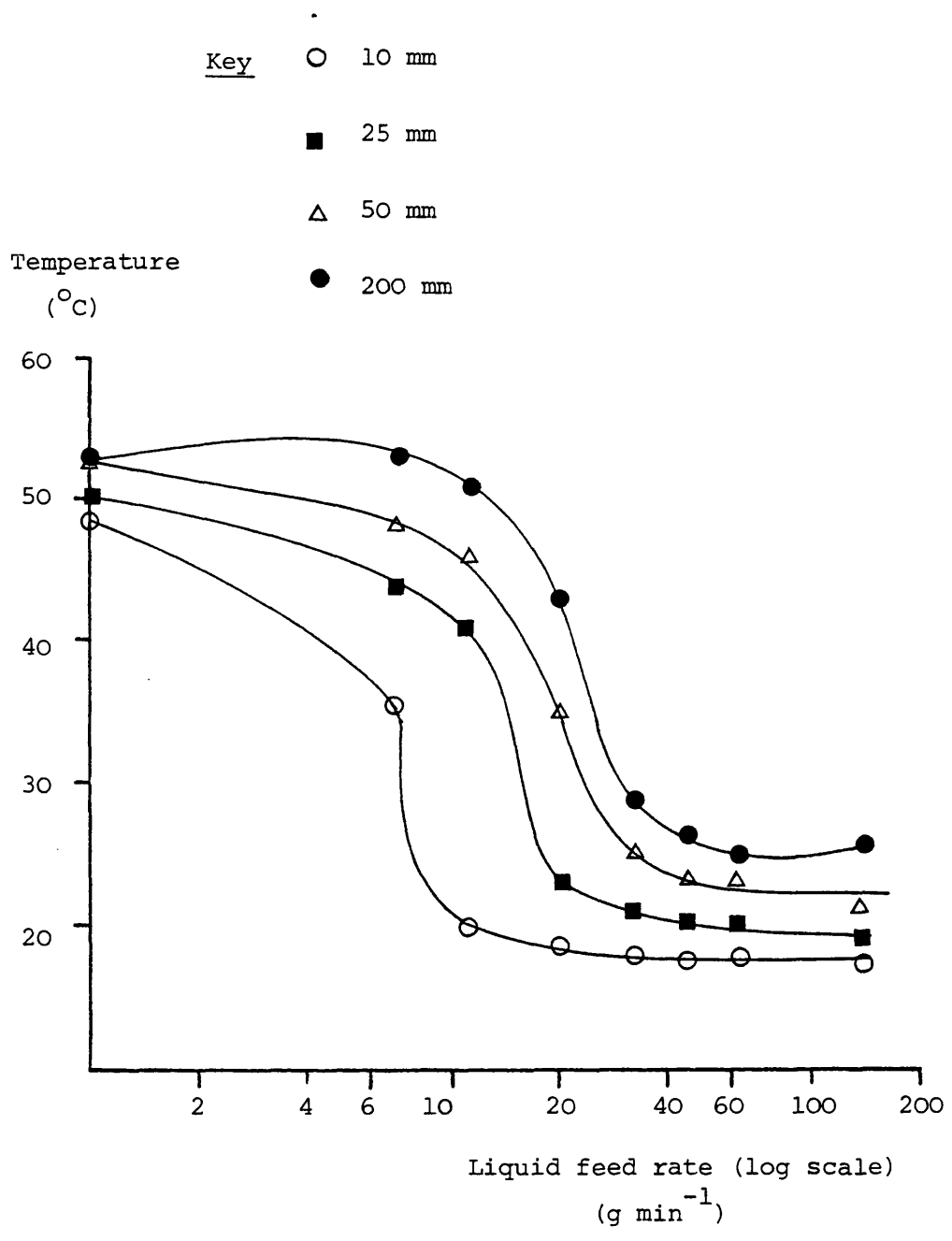

was confirmed by a rough 'orange-peel' coating being deposited on the tablets. At spray rates above 11 g min^{-1} evaporative cooling was present throughout the spray cone, allowing partial but not complete spray drying of the solution. Thus a smooth coating was deposited on the tablets until, at liquid feed rates of 46 g min^{-1} and above, the tablets began to stick together due to overwetting.

Therefore, at liquid feed rates in excess of 25 g min^{-1}, the temperature of the spray did not exceed 35°C and the coating solution would be deposited on the tablets as a solution rather than a thermal gel or spray dried particles.

8.2 Conclusions

The results demonstrated that in aqueous solution Klucel L.F. molecules probably exist in a tightly coiled spherical configuration with few polymer-polymer interactions. This structure is consistent with the absence of time dependent viscoelastic behaviour and may also be responsible for its complete precipitation from solution, rather than thermal gelation, at temperatures in excess of 35 to 45°C.

The viscosity, clouding and gelation properties of the three types of HPMC were similar, although solutions of Methocel E5 Premium clouded at slightly higher temperatures and the viscosity rise subsequent to thermal gelation was more rapid. These differences were most likely to have resulted from a slight

variation, within the manufacturer's specification, of the number and ratio of substituents attached to the anhydroglucose ring, since the presence of impurities such as sodium chloride had little effect on the clouding behaviour. These differences could also have been responsible for the discrepancy between the summed creep compliance values observed for Pharmacoat 606 and Methocel E5 Premium. Although slight hazing of the solutions always preceded the thermal gelation temperature (40 - 50°C), clouding did not become very marked until gelation was complete (50 - 60°C). This supported the theory that thermal gelation was due to dehydration of the polymer chains, since precipitation of the polymer and hence clouding of the solution was a continuation of this process.

At spray rates above 25 g min^{-1} thermal gelation and/or precipitation of the polymer during the coating process were unlikely to occur, since the temperature in the spray zone did not exceed 35°C. Furthermore, the clouding and gelation changes which were observed took up to one hour to develop fully (see Section 3.4), whilst a coating solution was atomized, spread on the tablets and dried very rapidly. Thus even if the necessary temperatures were attained, there may have been insufficient time available for these phenomena to arise. However, the possibility still existed that thermal gelation of HPMC solutions played a role in the transition from sol to gel during drying of the coating material on the tablets, since concentration of the solution, due to evaporation of the solvent, would have lowered the thermal gelation temperature at the same time as the temperature rose due to the reduction in evaporative cooling.

9. THE PROPERTIES OF POLYMER FILMS.

9.1 Results and Discussion

9.1.1. Reproducibility of Film Properties

The data presented in Table 9.1 shows the reproducibility of the measured oxygen transfer rate across a single 17 μm thick HPMC film reseated in the permeability cell on four successive days. The intercept of each Barrer plot lies within $\pm$ two standard deviations of zero and a Bartlett test confirmed that the variations are not significant . The mean transfer rate had a coefficient of variation of 5.7% and a Bartlett test showed the individual rates to be significantly different even at the 1% level. Nevertheless this level of reproducibility was considered satisfactory in view of the errors which could have occurred on repeatedly handling the film to install and remove it from the cell. Despite careful handling it is possible that finger grease and Apiezon grease from the sealing surfaces of the cell may have been transferred to the test area of the film. Thickness changes due to stretching of the film could not be detected, although the accuracy of determination (0.5 μm) could have resulted in a 3% error for this 17 μm thick film.

The oxygen transfer rate was measured (2, 3 or 4 determinations) for 13 HPMC films of thickness 17 to 55 μm, obtained from a single coating run. Bartlett or 't' tests showed that the measured transfer rates for each film were not usually significantly different at the 5% level. Consequently the mean oxygen transfer rate and oxygen permeability coefficients were calculated and are listed in Table 9.2.

Table 9.1 Replicate data, after re-seating the film on four successive days, for the oxygen transfer rate across a 17 μm thick Pharmacoat 606 film, sprayed on to a glass substrate at a rate of 25 ml min^{-1} on the model system.

Number of points on line	Oxygen transfer rate (ppm sec^{-1})	S.D. Slope	Relative S.D. Slope (%)	Intercept (ppm)	S.D. Intercept	Correlation Coefficient
5	0.1700	0.0028	1.67	8.74	21.70	0.9996
5	0.1855	0.0040	2.17	37.57	30.78	0.9993
5	0.1887	0.0058	3.07	-71.01	51.76	0.9989
5	0.1692	0.0041	2.42	80.81	54.43	0.9993

Mean transfer rate 0.1784 ppm sec^{-1} Mean intercept 14.03 ppm

S.D. 0.0102 S.D. 63.96

C.V. 5.71%

$\chi^2_{transfer}$ = 16.78 $\chi^2_{intercept}$ = 6.95

S.D. = Standard Deviation χ^2_{tab} (P=0.05) = 7.82

C.V. = Coefficient of Variation χ^2_{tab} (P=0.01) = 11.34

Table 9.2 The mean oxygen permeability coefficients for HPMC films prepared from a single coating run by spraying a 5% w/v aqueous solution of Pharmacoat 606 on to glass at a rate of 25 ml min^{-1}

Film Thickness (μm)	Number of determinations on each film	Mean rate of oxygen transfer (S.D.) ($ppm\ s^{-1}$)	Oxygen permeability coefficient ($m^2 s^{-1} \times 10^{13}$) Mean	S.D.	C.V. %	Mean (S.D)
17.0	4	0.1785 (0.0101)	8.686	0.497	5.72	
17.5	4	0.1432 (0.0076)	7.177	0.381	5.31	
29.5	2	0.0938 (0.0036)	7.925	0.305	3.85	
29.5	2	0.0985 (0.0000)	8.323	0.000	0	
30.0	2	0.0938 (0.0048)	8.059	0.041	0.51	8.284
40.0	2	0.0961 (0.0016)	11.006	0.182	1.65	(1.071)
40.0	2	0.0689 (0.0018)	7.894	0.202	2.56	C.V. 12.92%
42.0	2	0.0752 (0.0037)	9.050	0.441	4.87	
50.0	2	0.0642 (0.0013)	9.187	0.181	1.97	
51.0	3	0.0462 (0.0016)	6.749	0.230	3.41	
51.0	3	0.0538 (0.0024)	7.864	0.343	4.36	
53.0	2	0.0548 (0.0008)	8.321	0.123	1.48	
55.0	3	0.0473 (0.0009)	7.454	0.142	1.91	

S.D. = Standard Deviation C.V. = Coefficient of Variation

The presence of pinholes, identified by a very rapid increase in receptor oxygen concentration (e.g. 55 ppm sec^{-1} compared to 0.15 ppm sec^{-1} for an intact film), caused several films which had been installed in the cell to be discarded. Pinholes were more prevalent in thin films (< 25 μm) and re-sealing of the film, with addition of a silicone rubber washer (21 mm o.d., 15 mm i.d., 25 μm thick)did not reduce the rapid rise in receptor oxygen concentration, confirming that leakage around the film seating was not occurring.

The variation in permeability between the thirteen films was considerably greater than that for repeat determinations on the same film. An analysis of variance gave the data in Table 9.3 and an F test confirmed that the permeability of the films were significantly different at the 5% level ($F=10.15 > F_{12,20}(0.05) = 2.28$). Examination of the data presented in Table

Table 9.3 Analysis of variance data for the oxygen permeability coefficients for 13 HPMC films prepared from a single coating run by spraying a 5% w/v aqueous solution of Pharmacoat 606 on to glass at a rate of 25 ml min^{-1}

	Sum of Squares	Degrees of Freedom	Variance	F
Between groups	32.88	12	2.74	$\frac{2.74}{0.27} = 10.15$
Within groups	5.35	20	0.27	
Total	38.23	32		
$F = 10.15 > F_{12,20}(0.05) = 2.28$				

9.2 and Figure 9.1 did not indicate a visible trend between the film thickness and the variations in oxygen permeability coefficients. Equation 6.5 shows that the transmission rate should be inversely proportional to the film thickness and a plot of reciprocal rate versus film thickness will be linear, with a slope directly related to the permeability coefficient. Figure 9.2 shows that this plot was linear ($r = 0.939$) with a slope of 3.68×10^{-5} s ppm^{-1} μm^{-1} (relative standard deviation 11.03%) and intercept within $\pm$ two standard deviations of zero (-0.67 ± 1.66). The permeability coefficient, calculated from this slope was 7.8×10^{-13} m^{2}s^{-1} compared to a mean figure of 8.3×10^{-13} m^{2}s^{-1} obtained from the data in Table 9.2. Equation 6.5 also shows that a plot of log rate versus log thickness should have a slope of -1. Figure 9.3 shows that this plot was linear ($r = 0.955$) with a slope of -0.989 (relative standard deviation 9.4%); thus the permeability coefficients were independent of film thickness. Therefore these plots demonstrate that oxygen transfer through HPMC films follows Fickian diffusion.

The mean oxygen permeability coefficient for HPMC films, sprayed on to glass at a rate of 25 ml min^{-1}, was 8.28×10^{-13} m^{2}s^{-1}, with a coefficient of variation of 12.9% (Table 9.2). Although the films had been prepared on the same coating run, this reproducibility was considered satisfactory since slight variations in the surface of each substrate and subsequent small differences in film removal and handling may have affected the film properties. Therefore during subsequent experiments the

Figure 9.1 The variation in oxygen permeability coefficients for HPMC films prepared from a single coating run by spraying a 5% w/v aqueous solution of Pharmacoat 606 on to glass at a rate of 25 ml min^{-1} (showing standard deviation bars).

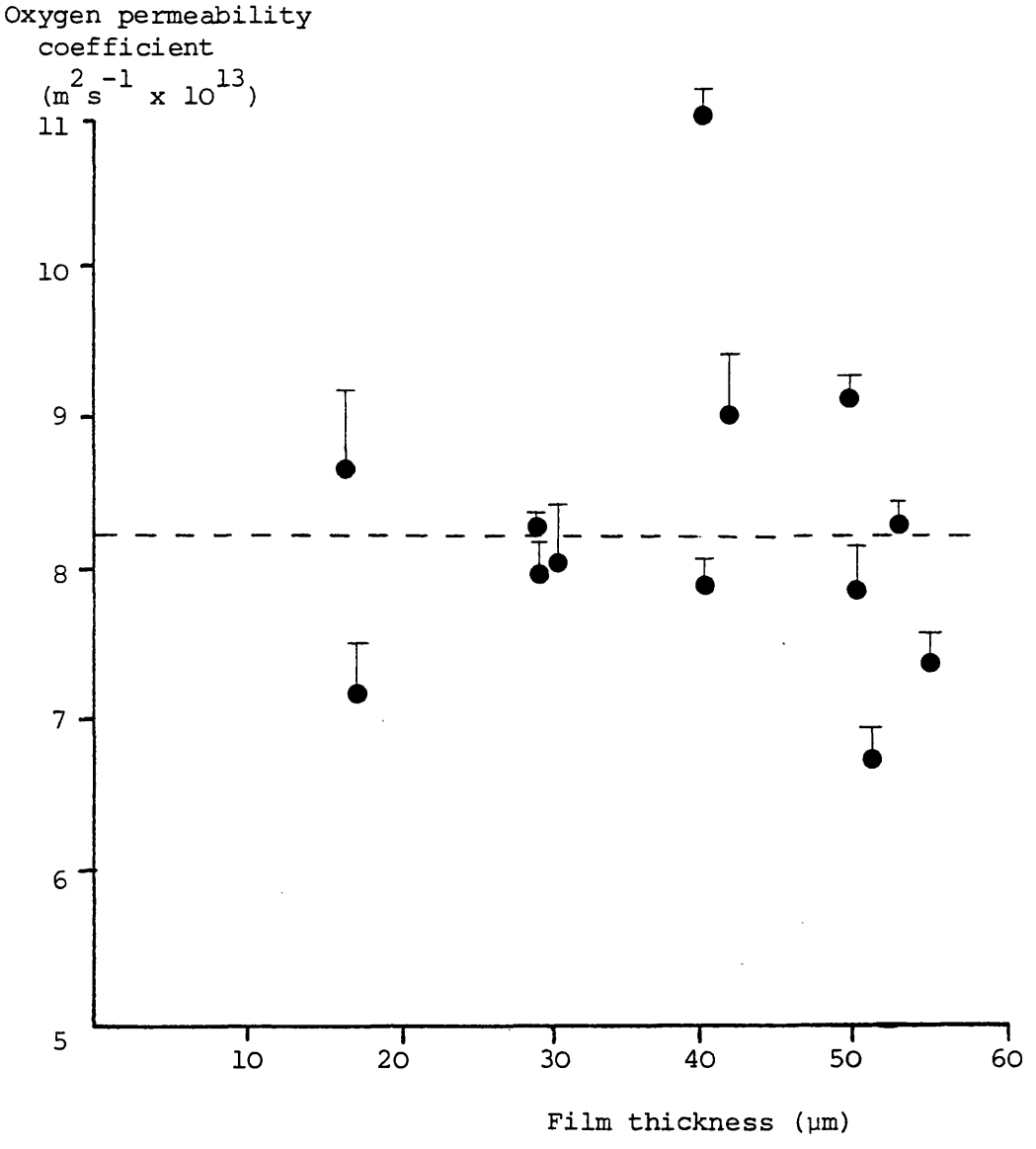

Figure 9.2 Reciprocal rate of oxygen transfer versus film thickness for HPMC films prepared from a single coating run by spraying a 5% w/v aqueous solution of Pharmacoat 606 on to glass at a rate of 25 ml min^{-1}.

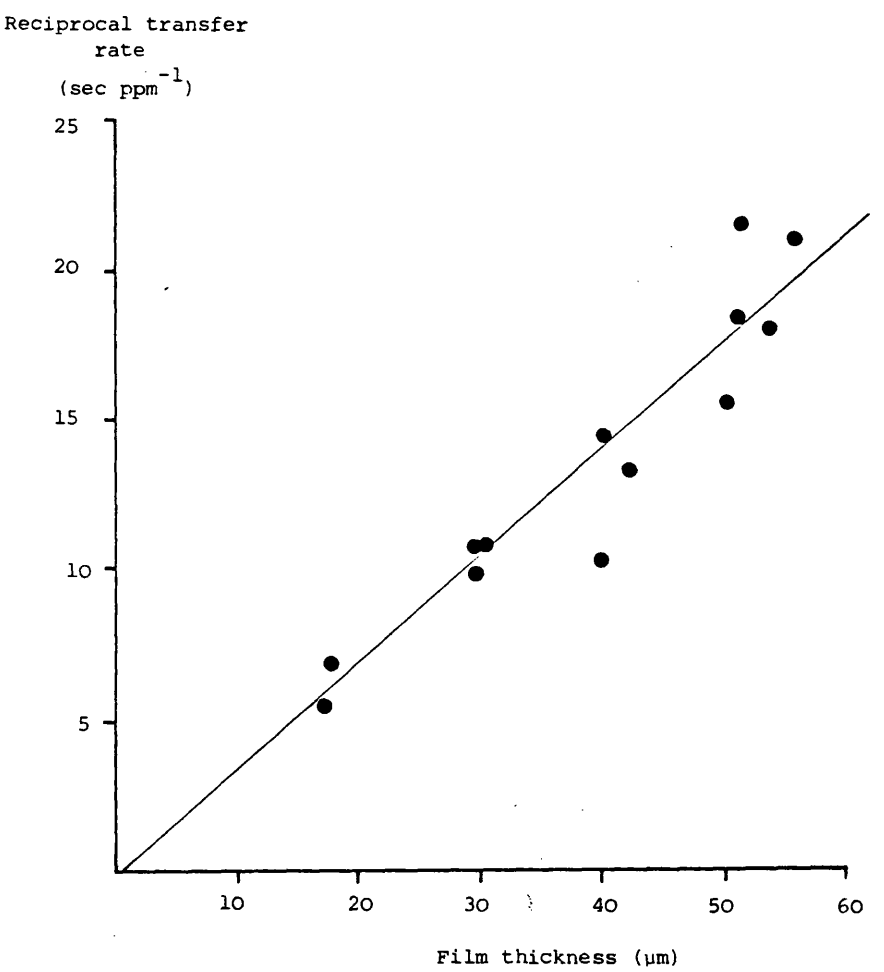

Figure 9.3 The effect of film thickness on the oxygen transfer rate across HPMC films prepared by spraying a 5% w/v solution of Pharmacoat 606 on to glass at a rate of 25 ml min^{-1}

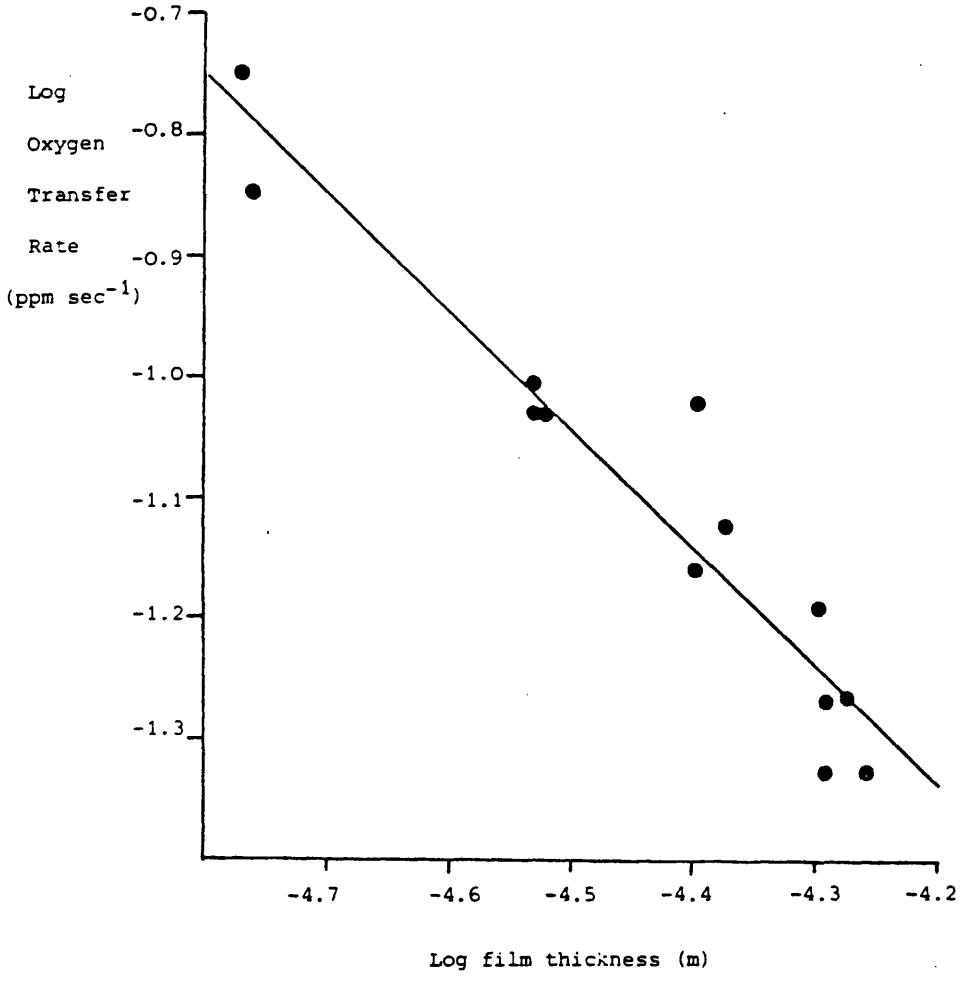

Regression data		
	Slope	-0.9886
	S.D. slope	0.0929
	Rel.S.D. Slope	9.40%
	Intercept	-5.491
	S.D. intercept	0.413
	Correlation coefficient	0.9547

rate of oxygen transmission was measured in duplicate for each of several nominally identical films.

For all the films tested, the intercept of the Barrer plots lay within two standard deviations of zero or were negative. However, even for thick films (55 μm) the intercept on the time axis (t) was too small (always under 5 minutes) to allow the diffusion coefficient to be accurately determined by the lag time method using equation 1.5 under the condition that when $C_2^s \rightarrow 0$ $D = \frac{L^2}{6t}$, since the value of t is assumed to be large in the derivation of the Barrer equation[269] (equation 1.5).

Table 9.2 indicates that the variation in thickness of films removed at intervals from the model coating system became greater with increasing film thickness. This was attributed to slight inequalities in the model system which became increasingly significant at the long coating times (120 minutes) necessary to produce thick films, when using a spray rate of 25 ml min^{-1}. Since the model system was designed to allow coating solution to reach the substrate for one revolution of the timing belt every 25 seconds (Section 4.3.1.3e), slight errors in these settings may have allowed some substrates occasionally to either miss being coated, or to receive an extra quantity of coating solution. In addition, the uneven nature of the spray pattern (Section 4.3.1.2c) would affect the amount of coating deposited on each substrate unless they were positioned identically within the spray cone.

The mechanical properties of films of different thickness, prepared on one coating run, are listed in Table 9.4. The reproducibility of the measurements at any one thickness was similar to that described in Table 6.19 for films sprayed on to various substrates and cast on to glass. Analysis of variance demonstrated that with the exception of the elastic modulus, the values of these properties increased significantly with increasing film thickness (Table 9.4 and Figure 9.4). Such an effect was expected for the elongation at failure and work of failure, but unforeseen for tensile strength, work of failure per unit area and work of failure per unit volume, where the film thickness is a parameter used in their calculation.These variations may have been due to different opportunities for stress relaxation (see also section 6.3) during testing for films of different thickness, since the elastic modulus, calculated from the initial slope of the stress-strain curve,was not significantly affected by film thickness. Consequently the mechanical properties of films prepared with different techniques, substrates and formulations could only be compared for films of similar thickness.

Table 9.5 shows the oxygen permeabilities of HPMC films prepared by three identical coating runs. For each replicate coating run, the permeabilities of three films thickness 25 to 30 μm and three films 45 to 55 μm were measured and compared with all the data presented in Table 9.2 (13 films) and with three films of each of the above thickness groups from this

Table 9.4 The effect of film thickness on the mechanical properties of HPMC films (4 replicates) prepared by spraying a 5% w/v solution of Pharmacoat 606 on to glass plates, at a rate of 25 ml min^{-1}.

Film Thickness (μm)	Ultimate tensile strength ($Pa \times 10^{-7}$)	C.V.	Elongation at failure (%)	C.V.	Elastic Modulus ($Pa \times 10^{-9}$)	C.V.	Work done in failure per unit film ($J \times 10^{3}$)	C.V.	Work done in failure per unit cross-sectional area ($Jm^{-2} \times 10^{-3}$)	C.V.	Work done in failure per unit volume ($Jm^{-3} \times 10^{-6}$)	C.V.
50	6.617 (0.567)	8.56	9.332 (0.877)	9.40	3.806 (0.094)	2.46	6.247 (1.053)	16.86	24.260 (4.213)	16.86	4.997 (0.843)	16.86
40	6.206 (0.722)	11.64	6.997 (3.391)	48.46	3.840 (0.648)	16.87	2.904 (1.501)	51.69	14.519 (7.504)	51.69	2.904 (1.501)	51.69
30	5.005 (0.629)	12.57	4.338 (1.645)	37.93	3.646 (0.394	10.80	1.532 (0.724)	47.23	10.213 (4.823)	47.23	2.043 (0.965)	47.23
17	3.761 (0.044)	1.16	2.443 (0.139)	5.68	3.525 (0.035)	0.99	0.258 (0.000)	0	3.029 (0.000)	0	0.606 (0.000)	0
Mean	5.397×10^{7} Pa		5.778%		3.704×10^{9} Pa		2.735×10^{-3} J		13.005×10^{3} Jm^{-2}		2.638×10^{6} Jm^{-3}	
Standard deviation	1.288×10^{7}		3.017		0.146×10^{9}		2.578×10^{-3}		8.875×10^{3}		1.837×10^{6}	
Coefficient of variation	22.86%		52.22%		3.95%		94.28%		68.24%		69.62%	
Between groups variance	5.92		35.71		0.05		29.50		314.61		0.61	
Within groups variance	0.32		3.11		0.21		0.96		22.66		1.83	
F_{calc}	18.50		11.48		0.24		30.73		13.88		14.58	
$F_{3,11}^{(0.05)}$	3.59		3.59		3.59		3.59		3.59		3.59	

Figure 9.4 The effect of film thickness on the mechanical properties of HPMC films prepared by spraying a 5% w/v solution of Pharmacoat 606 on to glass plates, at a rate of 25 ml min^{-1}.

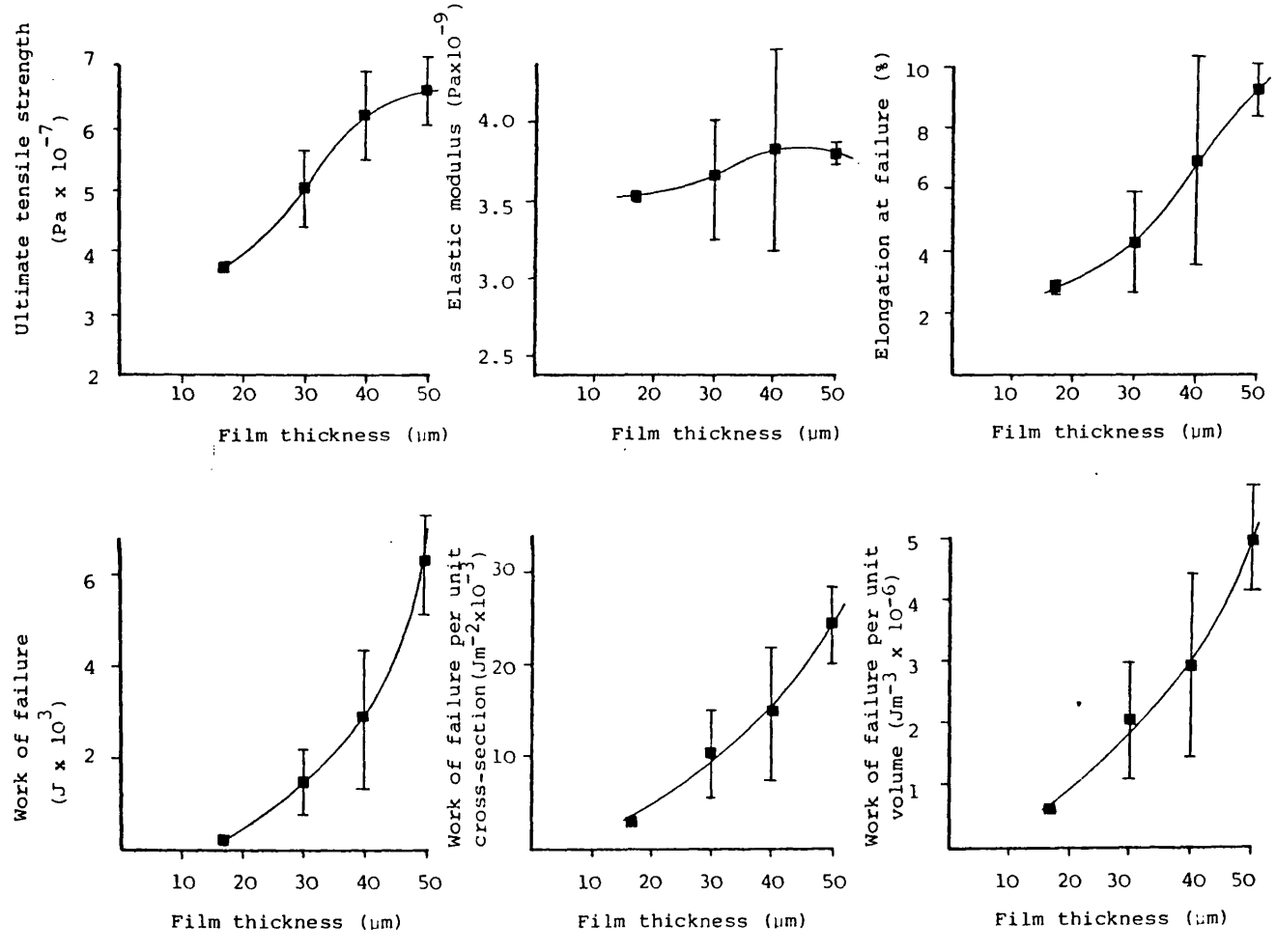

Table 9.5 The mean oxygen permeability coefficients of HPMC films (thickness 17 to 60 μm) prepared by spraying solutions containing 5% w/v Pharmacoat 606 on to glass plates, at a rate of 25 ml min^{-1}, on three identical coating runs on the model system

Coating Run	Number of films tested	Mean oxygen permeability coefficient ($m^2 s^{-1} \times 10^{13}$)	Standard Deviation ($\times 10^{13}$)	Coefficient of Variation (%)
1	13	8.28	1.07	12.9
	6	7.87	0.58	7.4
2	6	7.92	0.77	9.8
3	6	7.60	0.66	8.7

Coating runs 1_{13}, 2 and 3	Coating runs 1_6, 2 and 3
Grand mean = 7.94×10^{-13}	Grand mean = 7.80×10^{-13}
Standard Deviation = 0.34×10^{-13}	Standard Deviation = 0.17×10^{-13}
Coefficient of Variation = 4.3%	Coefficient of Variation = 2.2%

original coating run. The mean permeability coefficients were similar and analysis of variance for six films from each coating run demonstrated that the within group variance was larger than the between group variance; an F test confirming that the permeability of films from each coating run were not significantly different (Table 9.6).

Table 9.7 shows that the mechanical properties of HPMC films, thickness 40 μm, produced by three identical coating runs were not significantly different at the 5% level.

Thus different batches of film coatings prepared under identical conditions on the model system had similar oxygen transport and mechanical properties, allowing the influence of other variables to be studied.

The oxygen permeability data generated in this work could not be satisfactorily compared with that of other workers[110,140] since the details of the test conditions were inadequate to allow conversion of the data to S.I. units ($m^2 s^{-1}$). Furthermore, differences in the test methods and film materials would have made such comparisons of little value.

The mechanical properties of the films used in this study are in reasonable agreement with data published in the literature for HPMC films, allowing for differences in film preparation and testing conditions. The ultimate tensile strength of 35 to

Table 9.6 Analysis of variance data for the oxygen permeability coefficients of HPMC films prepared by spraying solutions containing 5% w/v Pharmacoat 606 on to glass, on three identical coating runs on the model system.

	Sum of Squares	Degrees of Freedom	Variance	F
Between groups	0.35	2	0.18	
Within groups	6.43	15	0.43	$\frac{0.18}{0.43} = 0.42$
Total	6.78	17		
$F = 0.42 < F_{2, 15}\ (0.05) = 3.68$				

65 MPa compares with values of 55 MPa, 45 MPa and 35 MPa found respectively by Abdul-Razzak[277], Pickard[106] and Porter[105], although the values reported by Hawes[102] were ten times less. The elastic modulus values of 2,000 MPa and 1,800 MPa reported by Pickard[106] and Abdul-Razzak[277] respectively, were somewhat lower than that found here (approximately 3650 MPa). The percentage elongation (approximately 6%) was similar to that found by Abdul-Razzak[277] (8.6%). The reproducibility of the published tensile properties (5 to 15%) was better than that observed in this study (5 - 50%), probably due to the larger test area used by these workers.

Table 9.7 The mean mechanical properties of five films (thickness 40 μm) from each of three identical coating runs on the model system, using a coating solution containing 5% w/v Pharmacoat 606.

Coating Run	Ultimate Tensile Strength ($Pa \times 10^{-7}$)	Elongation at break (%)	Elastic modulus ($Pax10^{-9}$)	Work of failure ($Jx10^{3}$)	Work of failure per unit cross-sectional area ($Jm^{-2} \times 10^{-3}$)	Work of failure per unit volume ($Jm^{-3} \times 10^{-6}$)
1	6.21 (0.72)	6.99 (3.39)	3.84 (0.65)	2.90 (1.50)	14.52 (7.50)	2.90 (1.50)
2	5.46 (0.60)	5.85 (2.27)	3.92 (0.34)	2.61 (1.35)	13.36 (6.93)	2.67 (1.39)
3	4.84 (0.45)	6.18 (1.74)	3.44 (0.16)	2.51 (0.98)	12.55 (4.91)	2.51 (0.98)
Mean	$5.503x10^{7}$ Pa	6.34%	$3.733x10^{9}$ Pa	$2.673x10^{-3}$ J	$13.477x10^{3}$ Jm^{-2}	$2.693x10^{6}$ Jm^{3}
Standard Deviation	$0.686x10^{7}$	0.587	$0.257x10^{9}$	0.203×10^{-3}	$0.990x10^{3}$	0.196×10^{6}
Coefficient of variation	12.47%	9.25 %	6.89%	7.59%	7.35%	7.28%
Between groups variance	1.79	1.38	0.35	0.16	3.63	0.15
Within group variance	1.33	5.51	0.14	1.61	41.41	1.65
F	1.34	0.25	2.50	0.10	0.09	0.09
$F_{2,12}(0.05)$	3.89	3.89	3.84	3.89	3.89	3.89

9.1.2 The effects of preparation technique, substrate and titanium dioxide content

a). Oxygen Permeability

The mean oxygen permeability coefficients of HPMC films containing titanium dioxide, prepared by casting on to glass and spraying on to glass, calcium phosphate/lactose and lactose/Avicel substrates, are listed in Table 9.8 and presented graphically in Figure 9.5. The titanium dioxide concentration in the dry film was calculated and expressed as a percentage of the polymer weight (% w/pw) and as a percentage of the total volume of solids present (% v/v), the latter allowing comparison with data produced by other workers[105] and for fillers of widely different density.

The permeability coefficients of films sprayed on to glass at rates of 25 ml min^{-1} (Table 9.2 , 8.28×10^{-13} $m^2 s^{-1} \pm 1.1 \times 10^{-13}$) and 32 ml min^{-1} (Table 9.8, 7.90×10^{-13} $m^2 s^{-1} \pm 0.7 \times 10^{-13}$) were not significantly different ($t_{calc} = 0.56$, t_{tab} (0.05) = 2.14). Thus small variations in the spray rates, used in this study, did not affect the oxygen permeability of HPMC films sprayed on to glass.

The data presented in Figure 9.5 clearly shows that there were large differences in the size of the standard deviation bars associated with each point. The data in Table 9.2 demonstrated that for 13 films,produced from one spray run, the mean permeability coefficient had a coefficient of variation of 13% and consequently

Table 9.8 The mean oxygen permeability coefficients of HPMC films containing titanium dioxide, for each of three films prepared by casting on to glass and spraying on to glass and calcium phosphate/lactose substrates and each of two films sprayed on to lactose/Avicel substrates (thickness 25 to 40 μm).

Titanium dioxide concentration in dry film		OXYGEN PERMEABILITY COEFFICIENTS Cast on to Glass		Sprayed on to Glass		Calcium phosphate/lactose		Lactose/Avicel		Between groups variance	Within groups variance	F_{calc}	F_{tab} (0.05)	Least significant difference (0.05)	
(%w/pw)	(% v/v)	Mean ($m^2s^{-1}x10^{13}$) (S.D.$x10^{13}$)	C.V. (%)	Mean ($m^2s^{-1}x10^{13}$) (S.D.$x10^{13}$)	C.V. (%)	Mean ($m^2s^{-1}x10^{13}$) (S.D.$x10^{13}$)	C.V. (%)	Mean ($m^2s^{-1}x10^{13}$) (S.D.$x10^{13}$)	C.V. (%)					3 vs 3 films	3 vs 2 films
0	0	7.79 (0.83)	10.7	7.90 (0.73)	9.2	7.18 (0.02)	0.2	4.02 (0.42)	10.6	5.68	0.47	12.09	4.35	1.32	1.47
10	2.99	8.39 (0.87)	10.4	7.61 (0.73)	9.6	6.97 (0.33)	4.7	5.44 (0.00)	0.0	3.70	0.40	9.25	4.35	1.22	1.36
20	5.81	8.32 (0.14)	1.7	8.90 (0.49)	5.5	9.34 (0.34)	3.6	5.06 (0.85)	16.8	8.37	0.21	39.86	4.35	0.88	0.99
40	10.97	12.73 (2.49)	19.6	7.85 (0.42)	5.3	7.28 (0.12)	1.7	3.93 (0.40)	10.1	36.96	1.85	19.98	4.35	2.62	2.92
60	15.60	13.28 (0.44)	3.3	8.58 (0.74)	8.6	6.18 (1.05)	16.9	4.36 (0.77)	17.7	39.72	0.14	283.7	4.35	0.72	0.81
Mean (S.D.)		10.10 (2.67)		8.17 (0.55)		7.39 (1.17)		4.56 (0.67)							
Between groups variance		22.63		0.89		2.03		0.02							
Within groups variance		1.50		0.40		0.34		0.31							
F_{calc}		15.09		2.23		5.97		0.07							
F_{tab} (0.05)		3.48		3.48		3.48		5.19							
Least significant difference (.05)		2.23		1.15		1.06		1.43							

S.D. = Standard Deviation

C.V. = Coefficient of Variation

Figure 9.5 The effect of preparation technique, film substrate and titanium dioxide content, on the oxygen permeability coefficient of HPMC films (showing standard deviation bars).

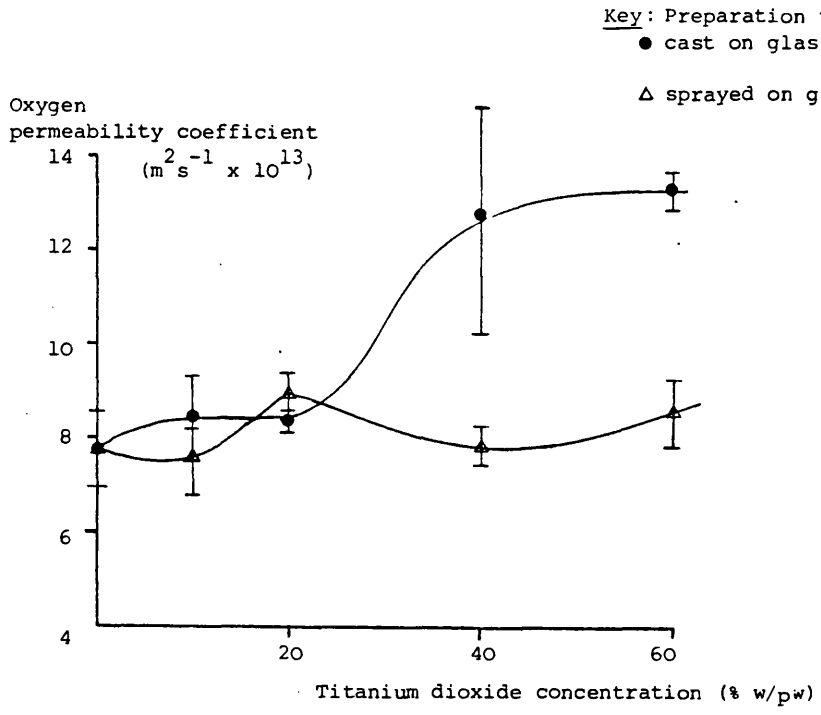

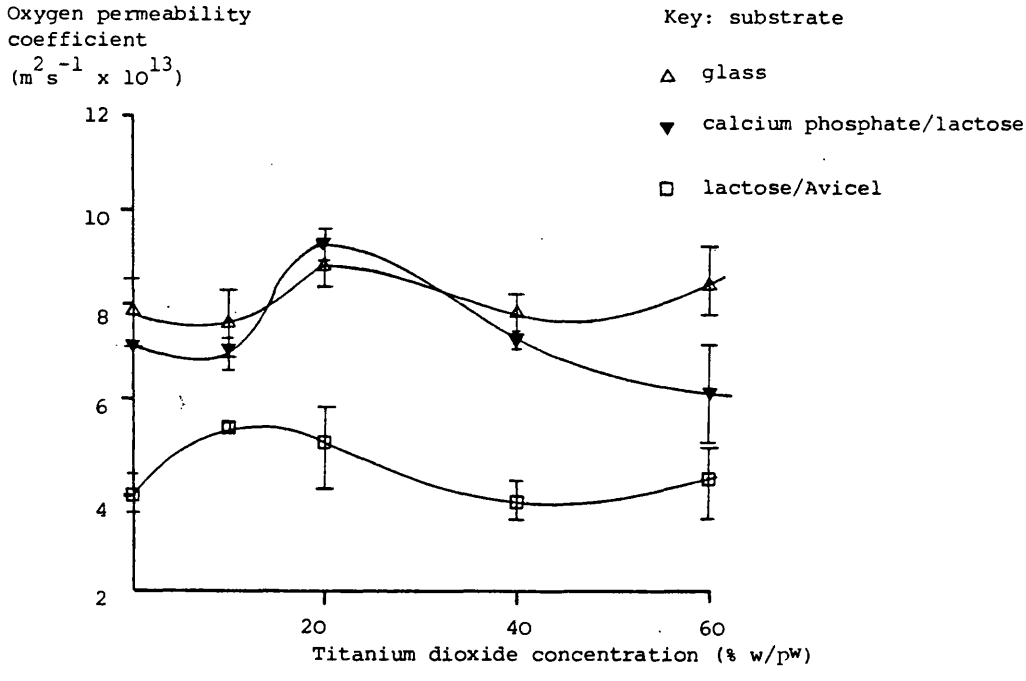

it may well be fortuitous that in some case the permeabilities of replicate films were identical, whilst others varied by 19%.

The titanium dioxide concentration did not materially affect the oxygen permeability of sprayed films, although analysis of variance and an F test indicated that the variation in permeability of films sprayed on to calcium phosphate/lactose substrates was significant at the 5% level, but not at the 1% level (Table 9.8). This difference may have arisen as a consequence of the small standard deviations associated with several of these permeability coefficients, in comparison to those obtained for the films sprayed on to glass and lactose/Avicel substrates.

The permeability of films sprayed on to lactose/Avicel compacts was half that of films sprayed onto other substrates. Visual comparison of the films suggested that more tablet core particles were adhering to the underside of those sprayed on to lactose/Avicel substrates, a finding confirmed by SEM of the underside of the films. Figure 9.6 shows the smooth particle-free lower surface of a film sprayed on to glass, in contrast to the rough surface of films sprayed on to calcium phosphate/lactose substrates (Figure 9.7) and lactose/Avicel substrates (Figure 9.8); the adhering particles being arrowed. Since the thickness of films sprayed on to tablet substrates was estimated from that of films sprayed on to glass, as described in Section 5.3, the observed reduction in permeability could not have been due to an error in the film thickness measurement caused by the

Figure 9.6 The underside of an HPMC film sprayed on to a glass substrate.

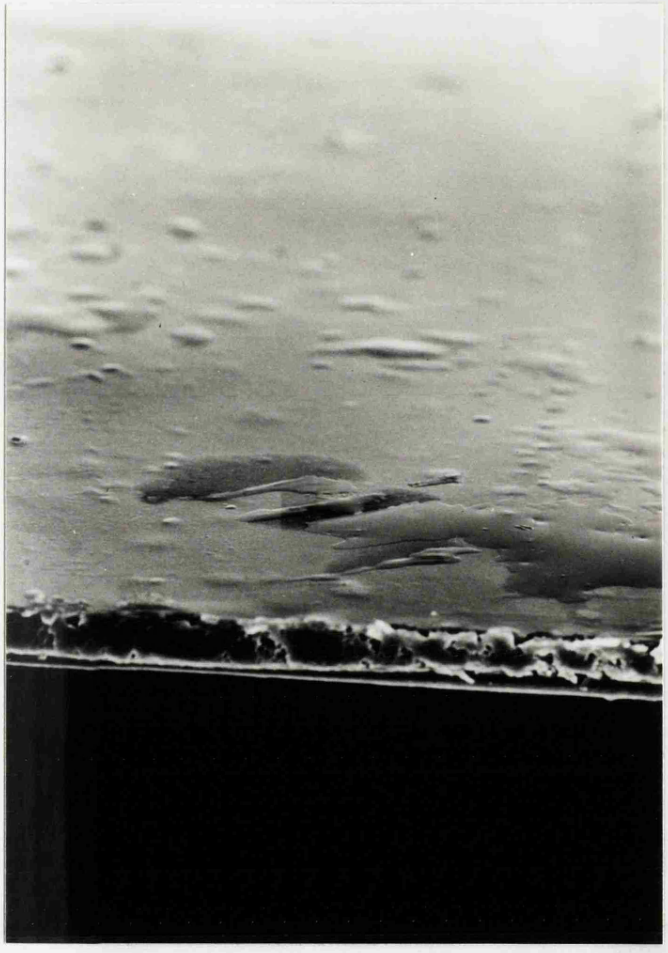

Figure 9.7 The underside of an HPMC film sprayed on to a calcium phosphate/lactose substrate showing the adhering substrate particles (arrowed).

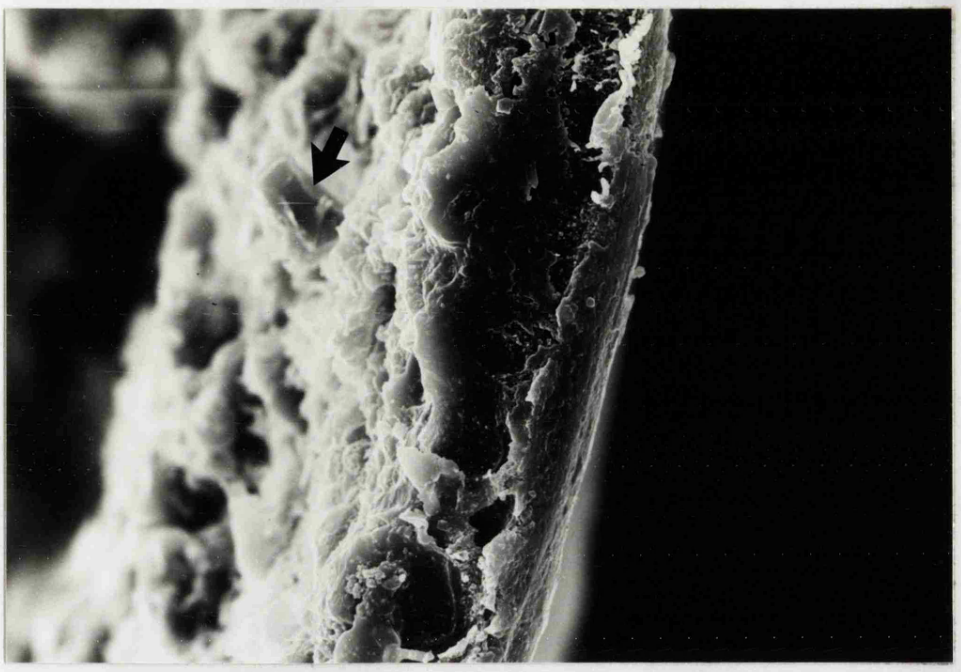

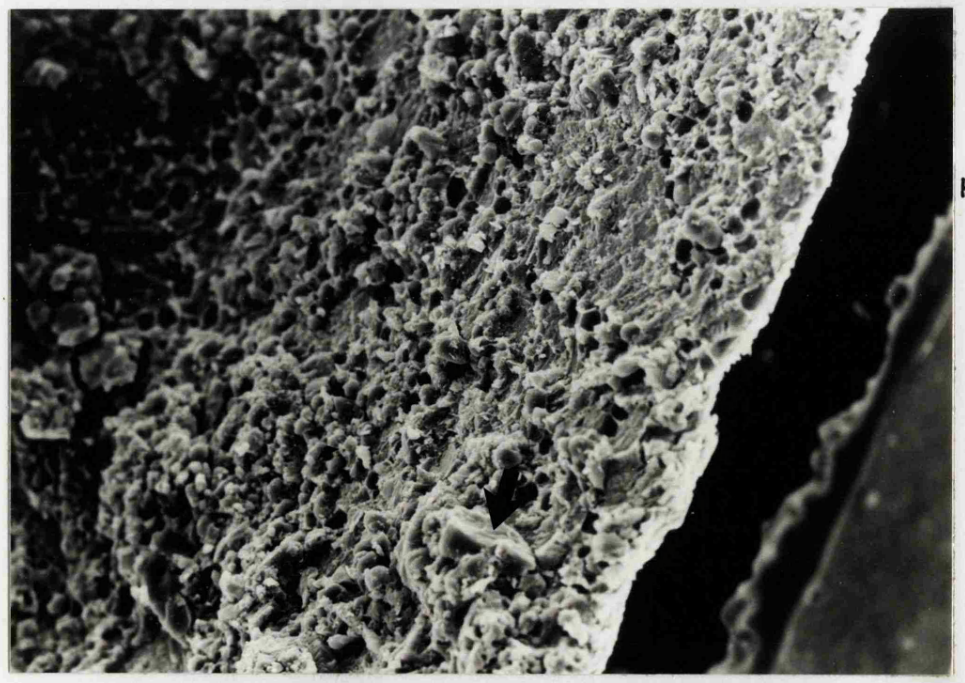

Figure 9.8 The underside of an HPMC film sprayed on to a lactose/Avicel substrate, showing the adhering substrate particles (arrowed).

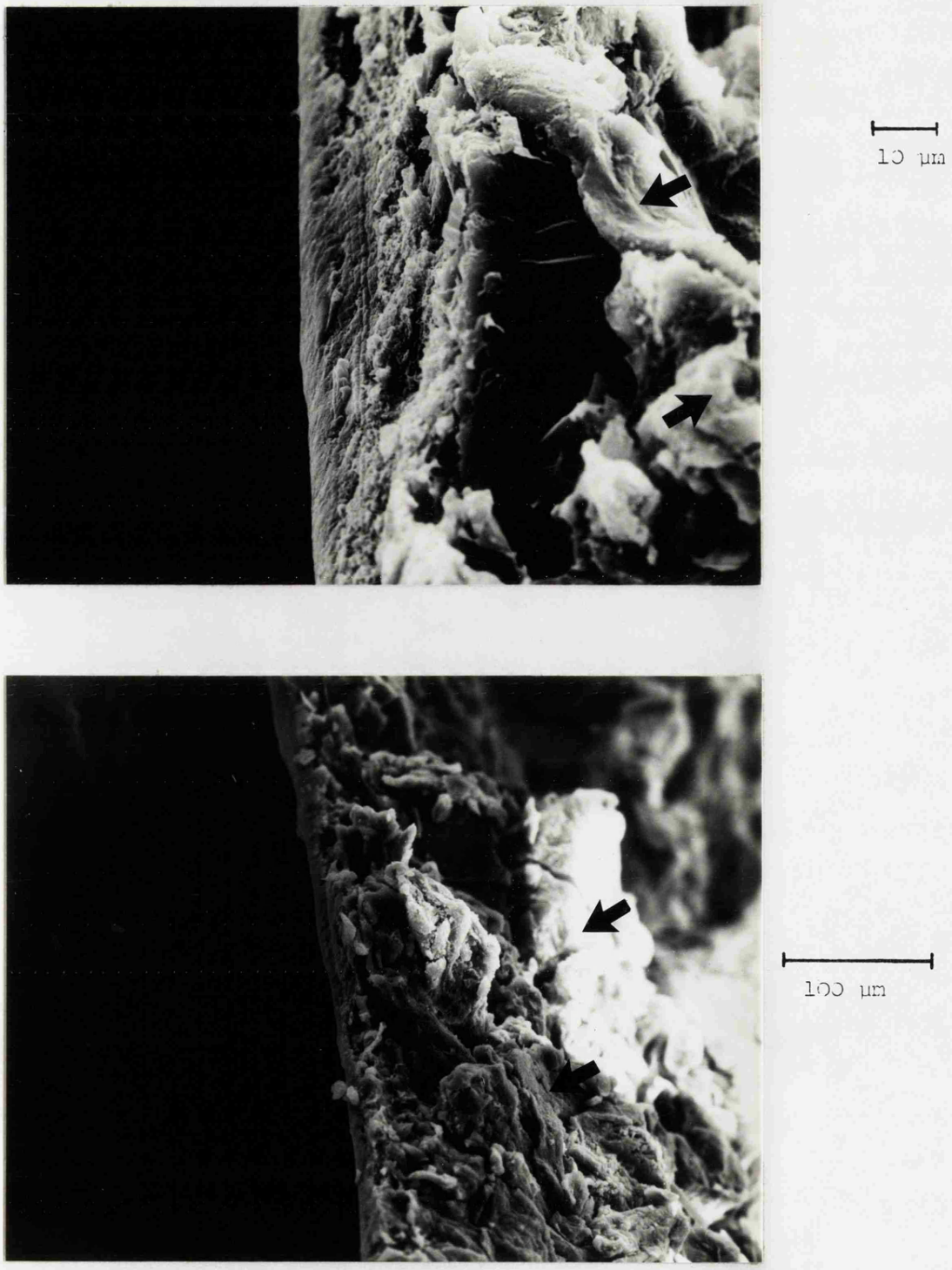

presence of tablet-core particles. The layer of adhering particles could therefore have acted as an additional barrier to the diffusion of oxygen across these films, thus reducing the measured permeability coefficient. The increased adherence of particles was unlikely to have occurred through a mechanical interlocking of the coating and substrate, since lactose/Avicel compacts had a similar surface roughness to calcium phosphate/lactose compacts (1.9 μm and 2.1 μm respectively, Table 4.3). A possible explanation was that the microcrystalline cellulose, present in the lactose/Avicel compacts, promoted adhesion between the film and substrate by hydrogen bonding[178].

An alternative hypothesis for this effect was that the polymer molecules orientated differently at the more hydrophilic lactose/Avicel surface, resulting in a film with a greater resistance to the permeation of oxygen. However, the films sprayed on to glass,which also has a hydrophilic surface, had a similar permeability to those sprayed on to calcium phosphate/lactose substrates, suggesting that such an effect was unlikely to be significant.

At high filler contents the oxygen permeability of cast films was 60% greater than that of films sprayed on to glass, probably due to sedimentation of filler as the casting solvent slowly evaporated. EDAX of the cross-section of films containing 20 and 60% w/pw titanium dioxide, cast or sprayed on to glass, gave the results shown in Figures 9.9 to 9.12. Point analyses

Figure 9.9 EDAX point analyses of a film containing 20% w/pw titanium dioxide sprayed on to a glass substrate

Point Number	Counts per minute titanium (cpm)
1	428
2	492
3	570
4	618
5	609
6	564
7	521
8	575

5 Replicate point analyses

Upper surface of film Mean = 480 cpm

Standard Deviation = 42

Coefficient of Variation = 8.8%

Lower surface of film Mean = 528 cpm

Standard Deviation = 42

Coefficient of Variation = 7.9%

$t_{calc} = 1.81$

t_{tab} (P=0.05) = 2.31

Figure 9.10 EDAX point analyses of a film containing 20% w/pw titanium dioxide cast on to a glass substrate

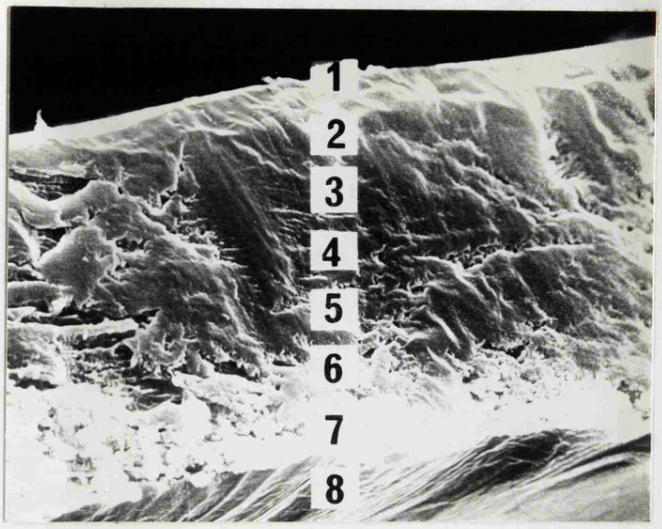

Point Number	Counts per minute titanium (cpm)
1	120
2	99
3	104
4	146
5	378
6	597
7	1088
8	1068

5 Replicate spot analyses

Upper surface of film

Mean = 92.1 cpm

Standard Deviation = 10.3

Coefficient of Variation = 11.1%

Lower surface of film

Mean = 1192 cpm

Standard Deivation = 30

Coefficient of Variation = 2.5%

t_{calc} = 77.53

t_{tab} (P=0.05) = 2.31

Figure 9.11 EDAX point analyses of a film containing 60% w/w titanium dioxide sprayed on to a glass substrate

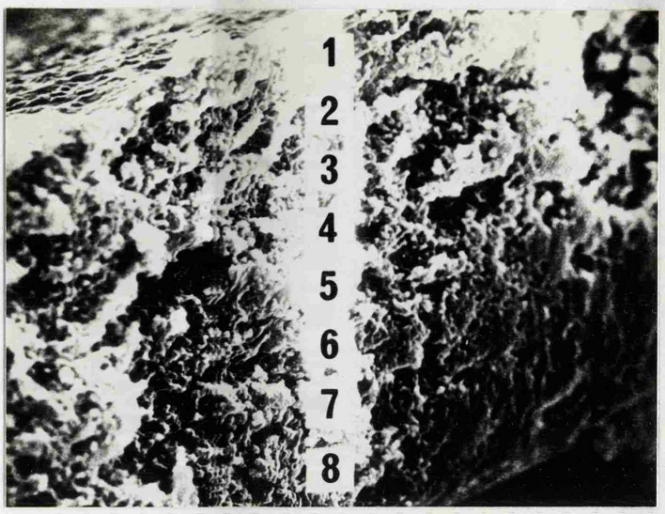

Point Number	Counts per minute titanium (cpm)
1	1667
2	1622
3	2308
4	2143
5	1818
6	1765
7	1622
8	1818

5 Replicate point analyses

Upper surface of film
- Mean = 1633 cpm
- Standard Deviation = 152
- Coefficient of Variation = 9.3%

Lower surface of film
- Mean = 1710 cpm
- Standard Deviation = 105
- Coefficient of Variation = 6.2%

$t_{calc} = 0.93$

$t_{tab}(P=0.05) = 2.31$

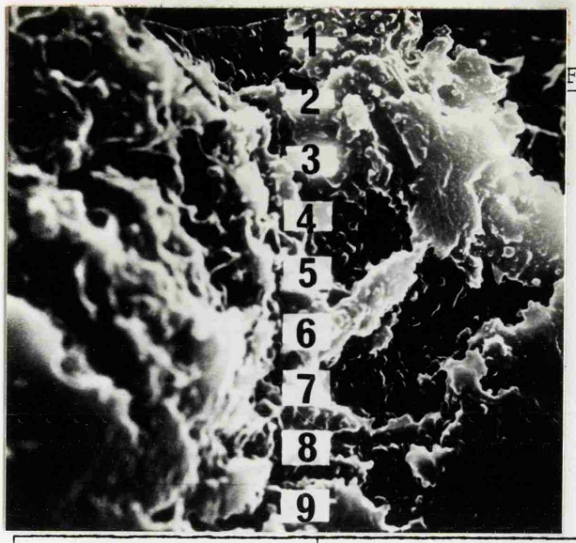

Figure 9.12 EDAX point analyses of a film containing 60% w/pw titanium dioxide cast on to a glass substrate

Point number	Counts per minute titanium (cpm)
1	1875
2	1875
3	3529
4	3750
5	5000
6	6000
7	6000
8	7500
9	6667

5 Replicate point analyses

Upper surface of film

Mean = 2206 cpm

Standard Deviation = 360

Coefficient of Variation = 16.3%

Lower surface of film

Mean = 6567 cpm

Standard Deviation = 619

Coefficient of Variation = 9.43%

$t_{calc} = 13.62$

$t_{tab}(P=0.05) = 2.31$

were carried out at intervals through the cross-section of each film (indicated by the centre of the squares) and five replicate analyses, on different areas of both upper and lower film surface, gave a mean titanium count per minute. The data is summarized in Table 9.9 and confirms that sedimentation of the filler occurred during casting; the difference in titanium counts per minute being significant only for the cast films. The slightly higher cpm in the middle and towards the underside of the sprayed films were probably artifacts due respectively to a mass effect and the lower side of the film being nearer the X-ray detector, since the sample could not be aligned completely perpendicular to the electron beam. These effects could only have been minimized by embedding the film in resin and cutting and polishing it to obtain a completely smooth surface in the desired orientation. However, as demonstrated in Figure 5.1, such a procedure may partially dissolve the film coating and the large differences observed between cast and sprayed films (Table 9.9) made an elaborate preparation technique superfluous.

The titanium dioxide content of the lower surface of the cast films was 10 times greater than that at the upper surface for the 20% w/pw concentration and 3 times greater at the 60% w/pw level. Since the oxygen permeability of cast and sprayed films were similar until between 30% w/pw and 40% w/pw titanium dioxide (Figure 9.5) it may be postulated that at lower filler concentrations despite sedimentation, there was still sufficient polymer to bind the particles together and produce a coherent film.

Table 9.9 Energy dispersive analysis of X-rays (EDAX) produced by film coatings containing titanium dioxide

Titanium Dioxide content (% w/pw)	20		60	
Film Preparation Technique	Cast on glass	Sprayed on glass	Cast on glass	Sprayed on glass
EDAX Peak for titanium	counts per minute	counts per minute	counts per minute	counts per minute
Upper surface	92	480	2206	1633
Lower surface	1192	528	6567	1710

Above 30 to 40% w/pw titanium dioxide there was insufficient polymer present to bind all the filler particles when they sediment to the lower surface of the film.

Increasing the titanium dioxide content has been shown to decrease and then increase the water vapour permeability of HPMC films[105,116]. This was explained in terms of the Chatfield theory[278], in which the filler particles act as a physical barrier to the diffusion of moisture, increasing the effective length of the diffusion pathway and reducing permeability by approximately 50 percent. Above a critical pigment volume concentration (CPVC) of between 5 and 15% v/v (20 to 60% w/pw) there was insufficient polymer to bind all the filler particles, creating voids and increasing permeability. Theoretically the Chatfield theory should be valid for all permeants, but the results shown in Table 9.8 and Figure 9.5

demonstrate this to be in error for the oxygen permeability of HPMC films.

An alternative mechanism for the initial reduction in permeability may be related to the plasticizing action of water vapour within the film. Kumins[156] has postulated that titanium dioxide was able to adsorb polymer chains and so restrict the possibilities for chain movement. Thus as the filler concentration increased it might be expected that the degree to which water vapour could plasticize the film would decrease, leading to a reduction in the observed water vapour permeability coefficient. However, the permeability of a non-plasticizing permeant, such as oxygen, would be relatively unaffected until there was insufficient polymer to hold the filler particles together, when it would rise sharply, as micro-voids were created. In this study,with the exception of cast films, the CPVC was not reached since the mechanical strength of films containing more than 60% w/pw titanium dioxide was too low to enable their installation in the permeability cell.

b) Water Vapour Permeability

The rate of water vapour transmission across HPMC films was too great to allow the accurate determination of the permeability coefficient using the mass spectrometry technique established for oxygen. The water vapour concentration in the receptor compartment of the permeability cell reached equilibrium with the donor gas relative humidity within one hour regardless

of the extent of saturation; 1% mass transfer therefore being exceeded within one minute. Although suitable corrections of the Barrer equation for significant mass transfer are available, the time necessary for the injection of a sample,obtained from a permeability cell remote from the mass spectrometer,would limit the number of points determined to a maximum of three (See Section 6.1.2.1). Modification of the permeability system to allow gas to be continuously leaked directly from the permeability cell to the mass spectrometer would overcome these problems and allow water vapour permeabilities to be determined by this method.

Figure 9.13 shows a typical plot of weight increase versus time for the transfer of water vapour across HPMC films containing 20% w/pw titanium dioxide, using the gravimetric technique described in Section 6.2. Least squares regression analysis for films cast on to glass, sprayed on to glass and sprayed on to calcium phosphate/lactose substrates gave the data listed in Table 9.10. The rate of transfer was linear and passed through the origin effectively within $\pm$ three standard deviations. The precision of these measurements was better than that obtained for oxygen, using the mass spectrometry technique, due to the former operating at a much higher concentration range ($2 - 3 \times 10^{-3}$ ml s^{-1} and $8 - 9 \times 10^{-6}$ ml s^{-1} of water vapour and oxygen respectively crossing the exposed area of film). The water vapour permeability coefficients were calculated from the transfer rates and are shown in Table 9.11. The data demonstrates that the permeability coefficients for water vapour (approximately 2×10^{-8} $m^2 s^{-1}$) were over four orders of

Figure 9.13 Typical plot of weight increase of a gravimetric permeability cell versus time, for the permeation of HPMC films by water vapour at 30°C and 75% relative humidity.

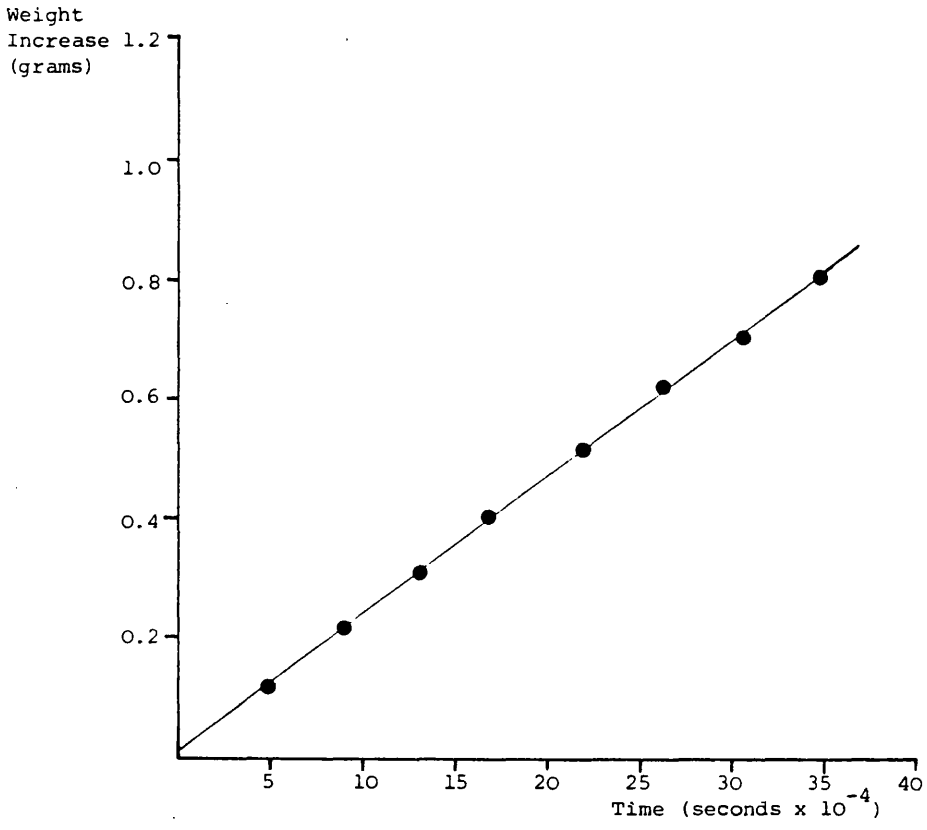

Table 9.10 The water vapour transmission rate across HPMC films (titanium dioxide content 20% w/pw) prepared from a solution containing 5% w/v Pharmacoat 606 and 1% w/v titanium dioxide by casting on to glass and spraying on to glass and calcium phosphate/lactose tablets at a rate of 32 ml min^{-1}

Preparation Technique	Substrate	Film Thickness (μm)	Rate of water vapour transmission ($gs^{-1} \times 10^{6}$)	Standard Deviation ($\times 10^{6}$)	Relative Standard Deviation (%)	Intercept ($g \times 10^{3}$)	Standard Deviation ($\times 10^{3}$)	Correlation Coefficient
Cast	Glass	30	2.147	0.014	0.67	8.695	3.003	0.9998
		31	2.024	0.010	0.50	6.512	2.127	0.9998
Sprayed	Glass	35	2.273	0.018	0.80	9.308	3.781	0.9998
		37	2.092	0.015	0.70	8.769	3.032	0.9998
	Tablet	36	1.935	0.024	1.23	4.502	4.869	0.9995
		36	1.837	0.030	1.62	8.993	6.128	0.9991

Table 9.11 The water vapour permeability coefficients, determined by a gravimetric technique, for HPMC films containing 20% w/w titanium dioxide, prepared by casting on to glass and spraying on to glass and calcium phosphate/ lactose substrates

Preparation Technique	Substrate	Water Vapour Permeability Coefficient ($m^2 s^{-1} \times 10^8$)		Mean ($m^2 s^{-1} \times 10^8$)	S.D. ($\times 10^8$)	C.V. (%)
Cast	Glass	1.844	(0.0120)	1.821	0.033	1.83
		1.797	(0.009)			
Sprayed	Glass	2.278	(0.018)	2.244	0.044	1.96
		2.216	(0.016)			
	Tablet	1.995	(0.025)	1.945	0.071	3.67
		1.894	(0.031)			

S.D. = Standard Deviation

C.V. = Coefficient of Variation

Between groups variance 0.0965 F = 35.09

Within groups variance 0.0037

$F_{2,3}(P=0.05) = 9.55$

Least significant difference $(P=0.05) = 0.19$

magnitude greater than those for oxygen (approximately 8×10^{-13} m^2 s^{-1}) confirming the rapid transfer of water vapour observed with the mass spectrometry technique. The magnitude of this difference also supports the concept of water vapour being a plasticizing permeant and oxygen a non-plasticizing permeant in HPMC films, as postulated in Section 9.1.2a.

Analysis of variance showed that the water vapour permeability of films cast on to glass was significantly lower than that for films sprayed on to glass (Table 9.11). This suggested that cast films were more coherent with greater polymer-polymer and polymer-pigment interactions, although the absence of this difference for the oxygen permeabilities, at the same filler content (Table 9.8), may indicate an alternative explanation in which the sedimented titanium dioxide in the cast films acted as a hydrophobic barrier to water but not oxygen.

The water vapour permeability coefficient was significantly lower for films sprayed on to calcium phosphate/lactose compacts than those sprayed on to a glass substrate (Table 9.11). The reason for this is unclear but may be associated with the presence of a small number of tablet-core particles adhering to the lower surface of films sprayed on to these compacts (Figure 9.7). As the oxygen permeabilities of similar films were not significantly different (Table 9.8) it is possible that the adhering particles altered the opportunities available for plasticization of the film by water, or acted as an additional barrier to the diffusion of water vapour, whilst the slower permeation of oxygen was limited solely by the film.

The value of approximately 2 x 10^{-8} $m^2 s^{-1}$ for the water vapour permeability of HPMC films containing 20% w/pw titanium dioxide is similar to those reported by Parker et al.[116] (3.8 x 10^{-8} $m^2 s^{-1}$), Hawes[102] (3.2 x 10^{-8} $m^2 s^{-1}$) and Porter[105] (4.2 x 10^{-8} $m^2 s^{-1}$).

c) Mechanical Properties

Figures 9.14 to 9.19 show the effects of preparation technique, substrate and titanium dioxide content on the mechanical properties of HPMC films. With the exception of the elastic modulus (Figure 9.16) the values of all the mechanical properties decreased with increasing titanium dioxide content. This probably resulted from filler particles reducing polymer-polymer interactions and thus creating disorder within the polymer matrix.

The decrease in the measured values of the mechanical properties was more marked for cast than sprayed films, possibly due to sedimentation of the filler during casting causing an uneven distribution of particles. Thus the adverse effects of titanium dioxide on the mechanical properties of HPMC films would be over estimated if cast films alone were used to evaluate prospective coating formulations.

It was difficult to evaluate the precise effects of the substrate on the properties of sprayed films due to the large variations about the mean value. However, general trends could be seen, most noticeably that of the elastic modulus being

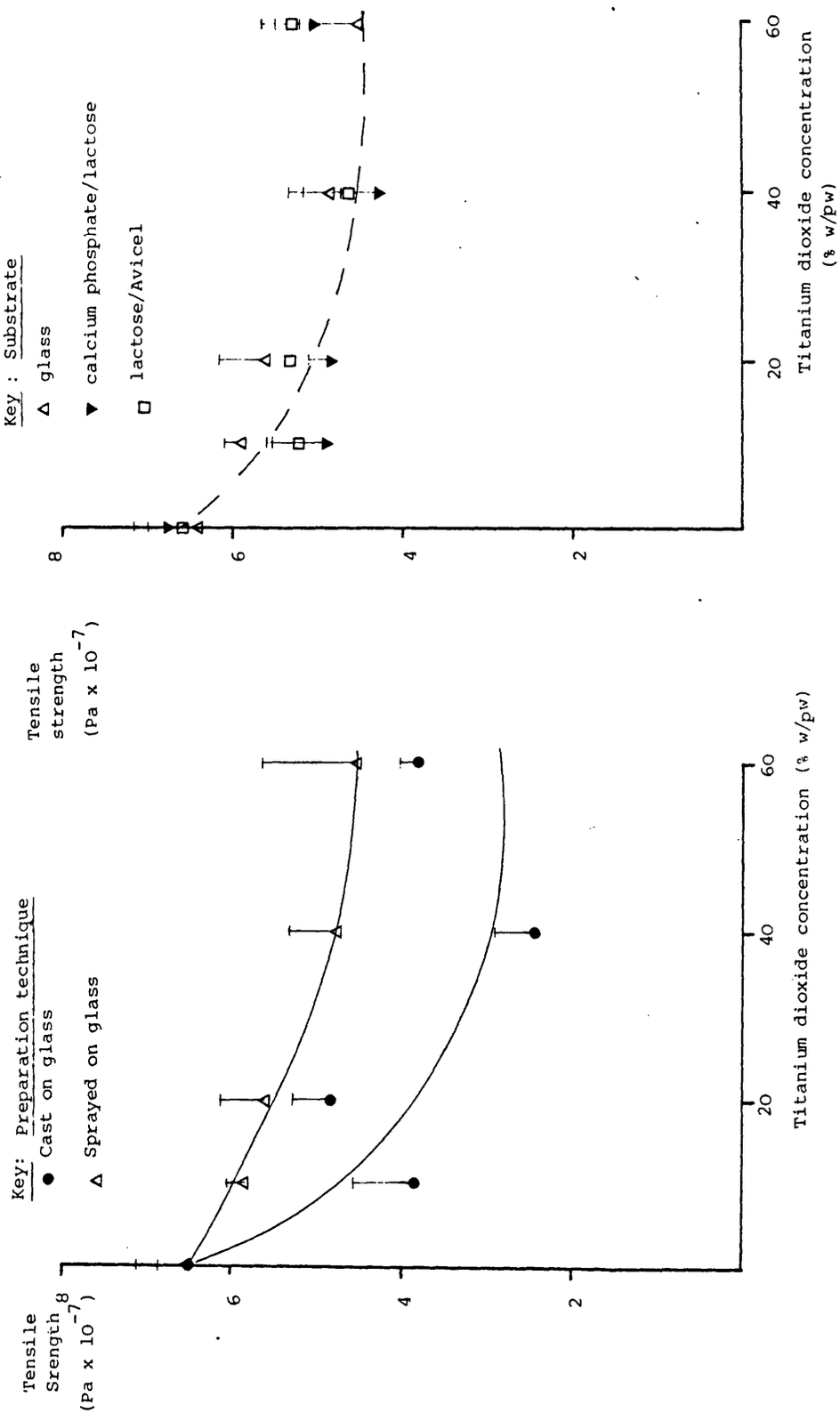

Figure 9.14 The effect of preparation technique, film substrate and titanium dioxide content on the ultimate tensile strength of HPMC films (showing standard deviation bars).

Figure 9.15 The effect of preparation technique, film substrate and titanium dioxide content on the elongation at failure of HPMC films (showing standard deviation bars).

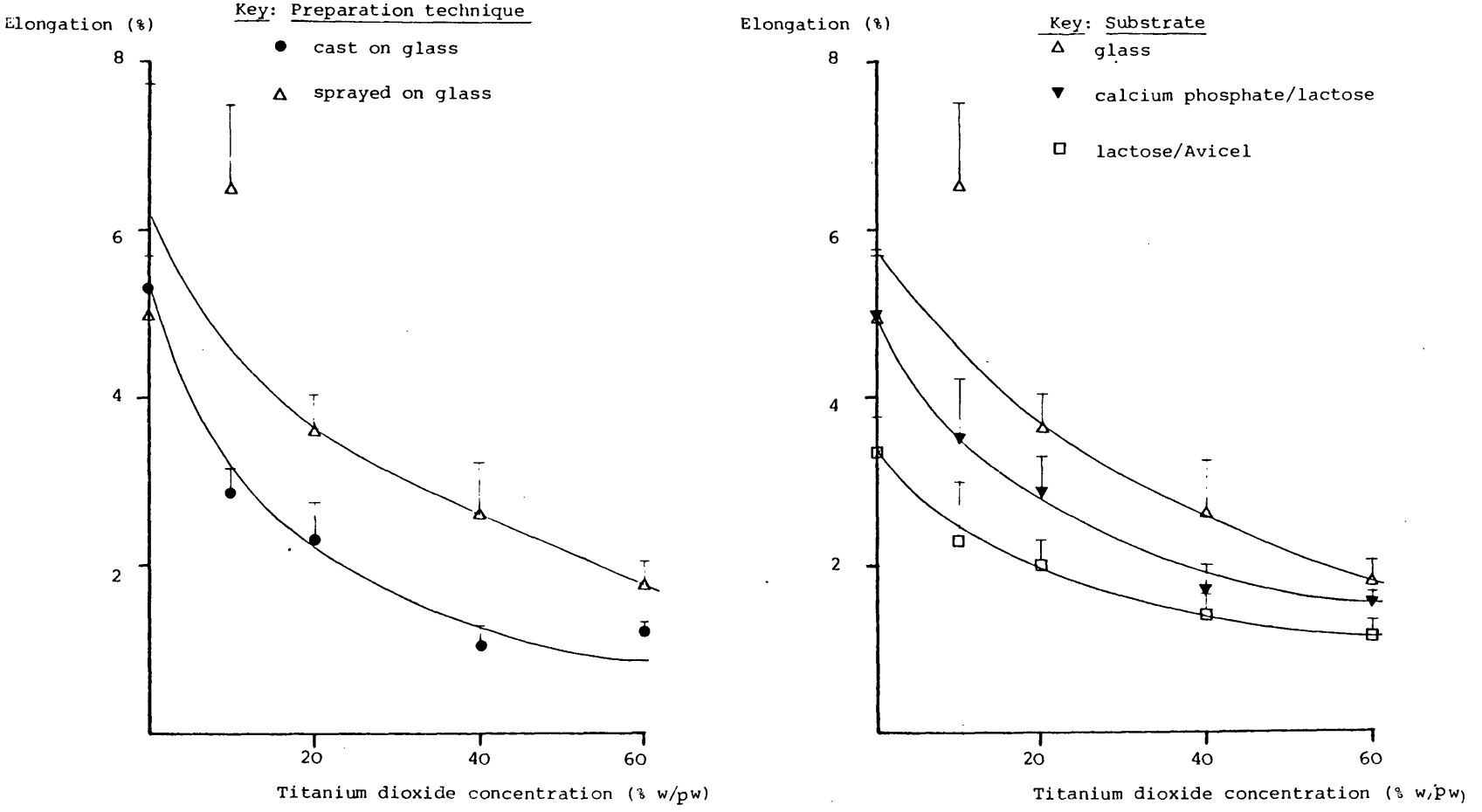

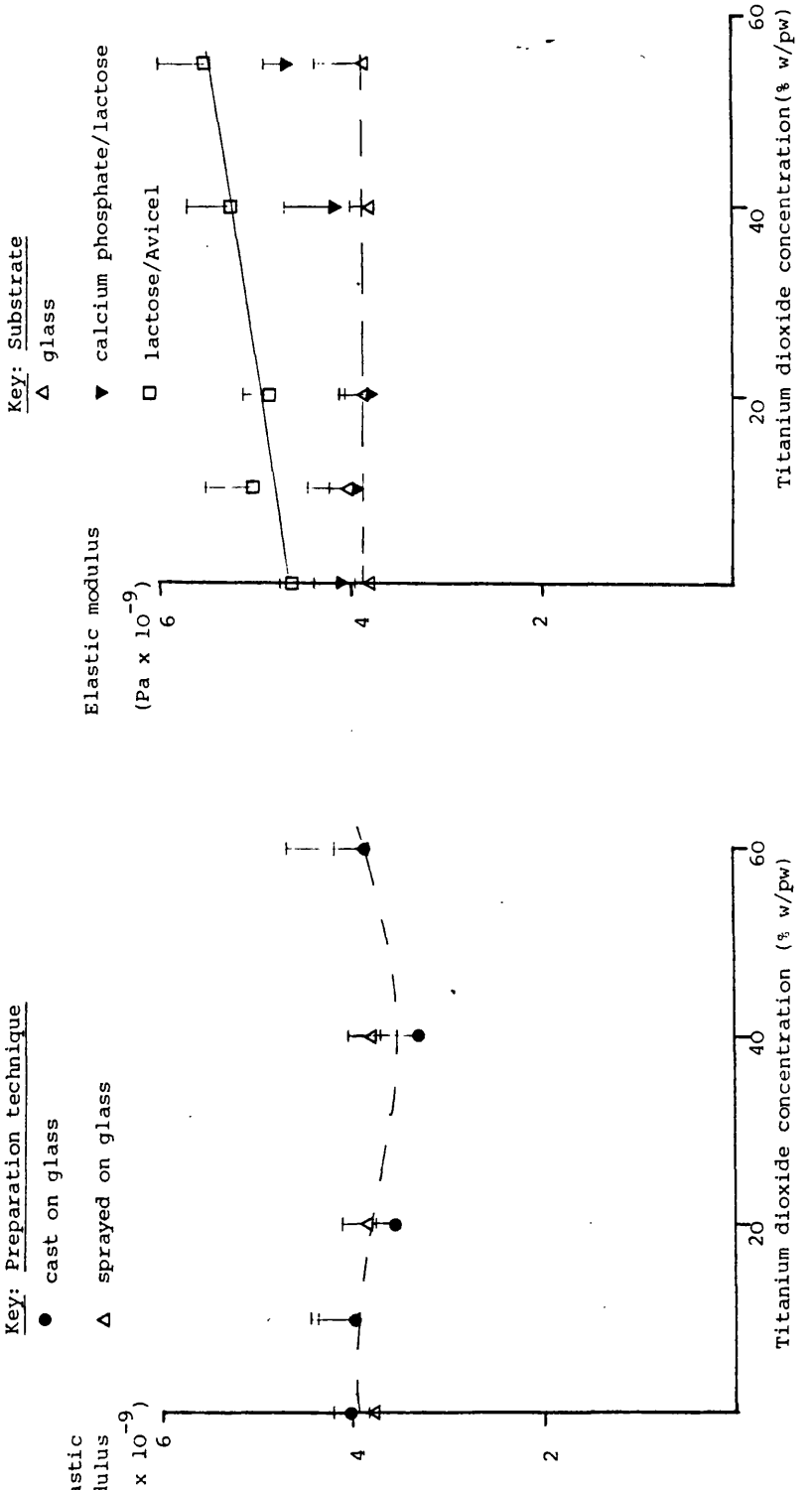

Figure 9.16 The effect of preparation technique, film substrate and titanium dioxide content, on the elastic modulus of HPMC films (showing standard deviation bars).

Figure 9.17 The effect of preparation technique, film substrate and titanium dioxide content on the work of failure of HPMC films (showing standard deviation bars).

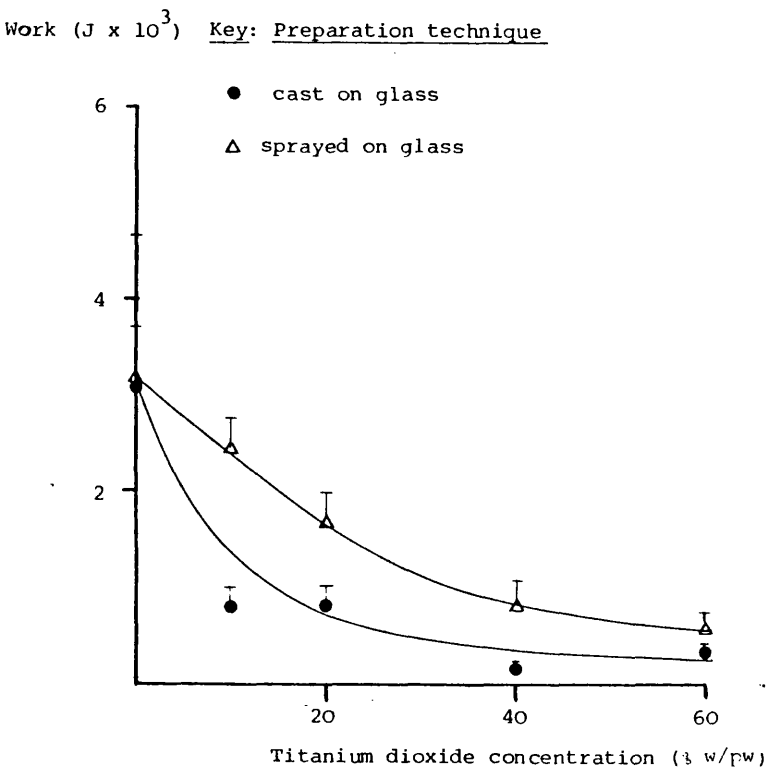

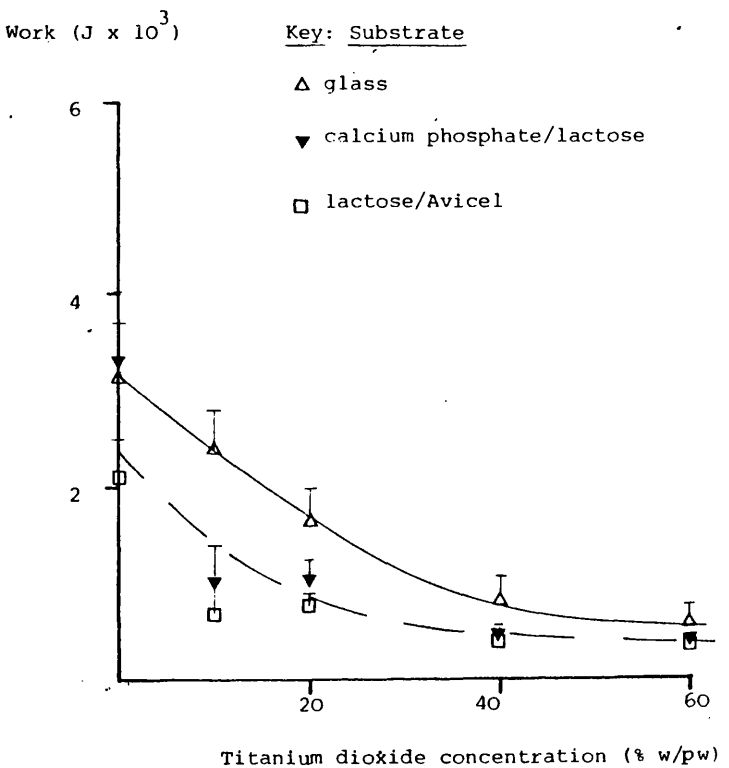

Figure 9.18 The effect of preparation technique, film substrate and titanium dioxide content, on the work of failure per unit cross sectional area of HPMC films (showing standard deviation bars).

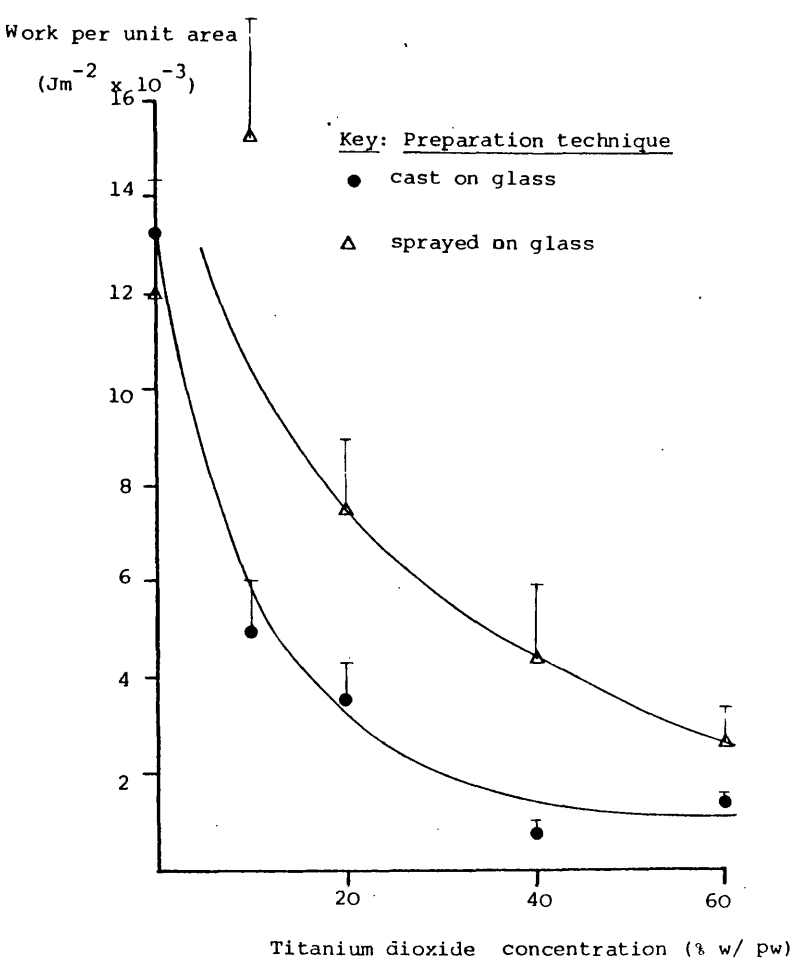

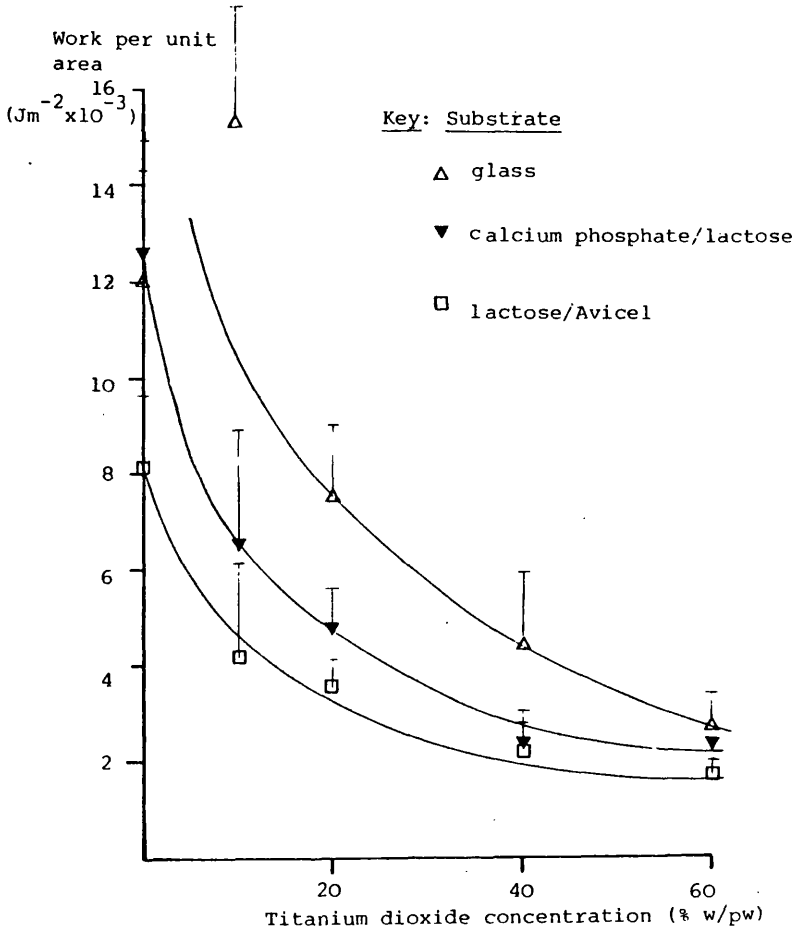

Figure 9.19 The effect of preparation technique, film substrate and titanium dioxide content on the work of failure per unit volume of HPMC films (showing standard deviation bars).

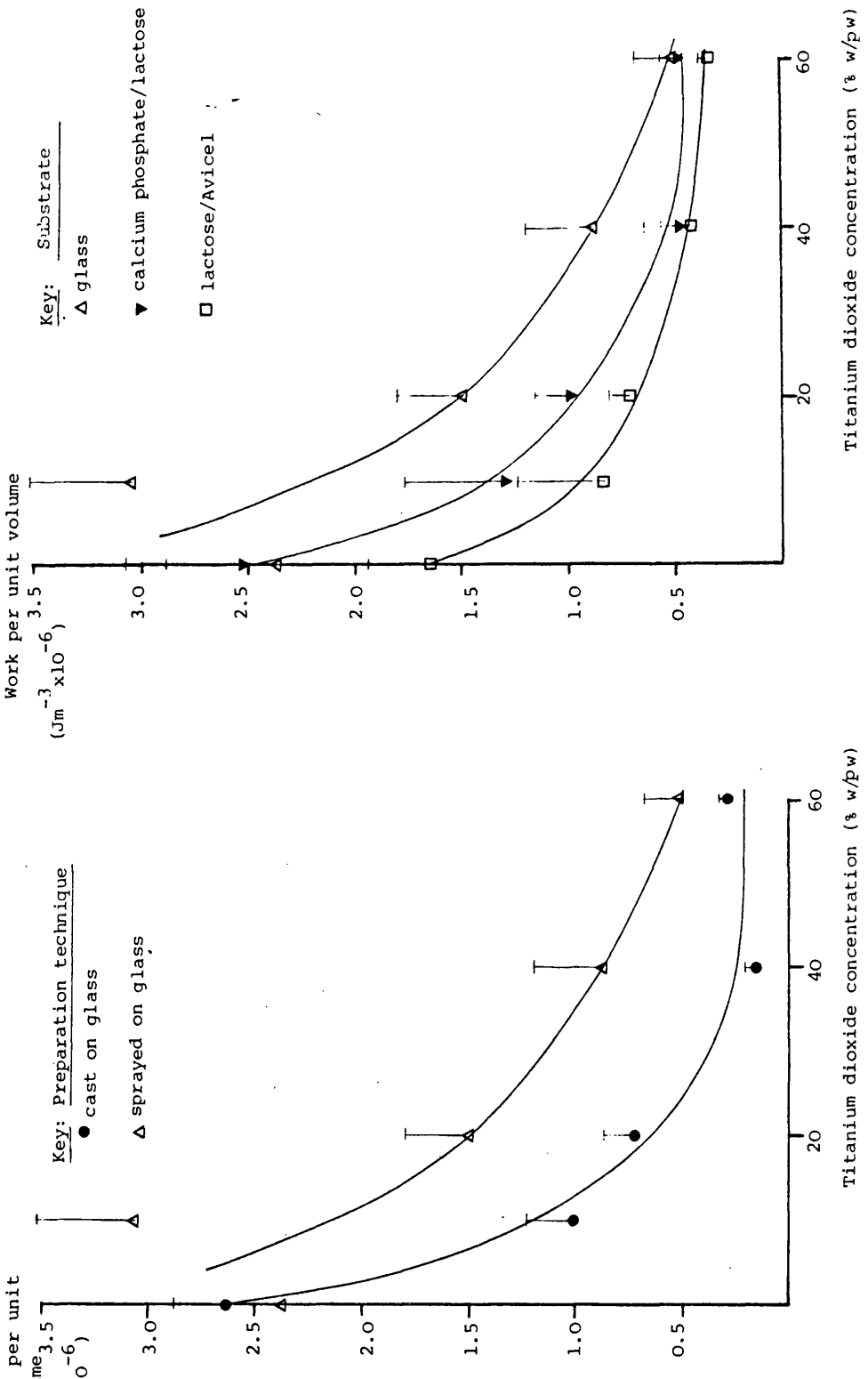

approximately 20% greater, at all titanium dioxide concentrations, for films sprayed on to a lactose/Avicel substrate. This phenomenon may have occurred as a result of the particles adhering to the underside of these films reducing the elongation at a given stress; a theory supported by the elongation at failure (Figure 9.15),work of failure per unit cross-sectional area (Figure 9.18) and work of failure per unit volume (Figure 9.19) being lower than for films sprayed on to other substrates.

Thus the superior mechanical properties of films containing titanium dioxide sprayed on to glass rather than cast on to glass can be attributed to sedimentation of the filler in the latter, whilst the variation between the different substrates for sprayed films was probably due to particles adhering to the underside of the film.

Other workers have also demonstrated that the mechanical properties of both cast[277] and sprayed[105] films decrease markedly with increasing titanium dioxide content, although Hawes[102] found the tensile strength was relatively unaffected by the titanium dioxide content. Numerical comparison of the reduction in film strength with increasing titanium dioxide content, observed by different workers,may be misleading since details of the filler particle size and shape are not stated in the literature.

9.1.3 The Effect of Water Vapour on the Oxygen Permeability of HPMC Films

Table 9.12 and Figure 9.20 show that water vapour had a similar effect on the oxygen permeability of both thin and thick HPMC films. At zero relative humidity these films had oxygen permeability coefficients in the same range as those presented in Table 9.2, further confirming the reproducibility of these measurements. The low equilibrium moisture content of HPMC at low relative humidities (Figure 2.1) caused a decrease in the oxygen permeability coefficient by either an antiplasticization effect[279] which enabled a closer packing of the polymer chains, or physically blocking the passage of oxygen into or through the polymer matrix. The greater quantity of water adsorbed/absorbed at high relative humidities led to gross plasticization of the film and an increased oxygen transfer rate.

A similar effect has been observed by Meyer *et al.*[141] for the permeation of nitrogen, oxygen and helium through Nylon 6 films at different relative humidities. This was also explained in terms of an initial antiplasticization effect allowing a closer packing of the polymer chains. At high relative humidities, gross plasticization by water vapour increased the permeability via an effect on the diffusion coefficient.

Table 9.12 The effect of donor gas relative humidity on the oxygen permeability coefficient of two films prepared by spraying a 5% w/v solution of Pharmacoat 606 on to glass plates, at a rate of 25 ml min^{-1}.

Donor Gas Relative Humidity (%)	OXYGEN PERMEABILITY COEFFICIENT					
	18 µm thick film			68 µm thick film		
	Mean ($m^2 s^{-1} \times 10^{13}$)	S.D. ($\times 10^{13}$)	C.V. (%)	Mean ($m^2 s^{-1} \times 10^{13}$)	S.D. ($\times 10^{13}$)	C.V. (%)
0	7.774	0.066	0.84	6.543	0.303	4.63
30	5.341	0.109	2.04	3.355	0.237	6.94
60	4.768	0.023	0.47	3.426	0.019	0.56
100	13.403	0.289	2.16	8.146	0.014	0.17

S.D. = Standard Deviation

C.V. = Coefficient of Variation

Figure 9.20 The effect of donor gas relative humidity on the oxygen permeability coefficient of two HPMC films prepared by spraying a 5% w/v solution of Pharmacoat 606 on to glass plates

Key
- ● 18 μm thick film
- ○ 68 μm thick film
- ▼ Equilibrium moisture content of Pharmacoat 606

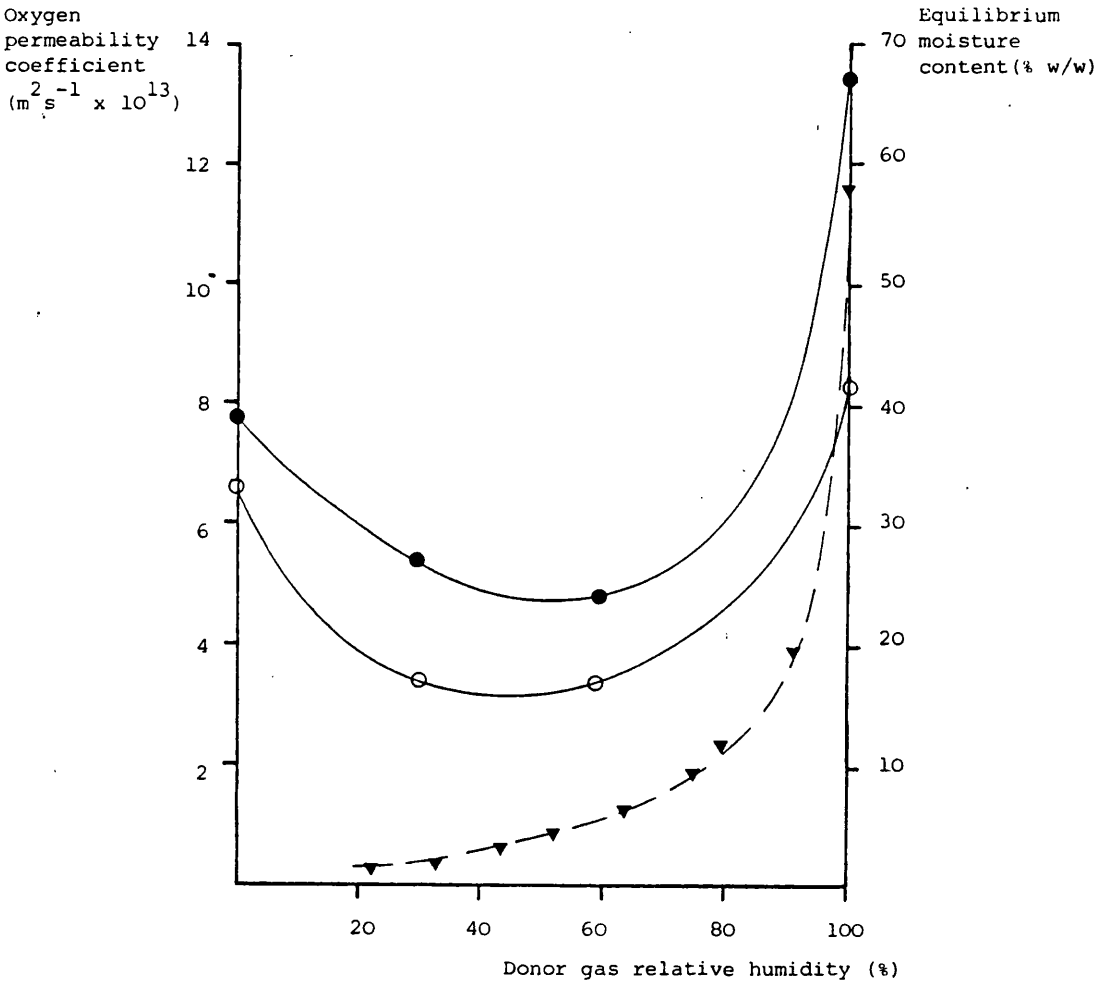

10 SUMMARY AND SUGGESTIONS FOR FURTHER WORK

10.1 Summary

The properties of some HPMC and HPC polymer solutions used in aqueous film coating were evaluated and compared with respect to their viscosity, clouding and thermal gelation behaviour (Section 8.1). Measurement of the temperature in the spray zone of a 24" Accela-Cota during a coating run, indicated that thermal changes of the coating solution were unlikely to occur if a spray rate in excess of 25 g min^{-1} was used (Section 8.1.2), although the possibility that thermal gelation of HPMC played a role in the transition from sol to gel on the tablet could not be ruled out (Section 8.2).

A new system for the preparation of aqueous film coatings under more realistic coating conditions was developed and evaluated. Although the deposition rate of coatings was four times greater on the model than in the Accela-Cota (Section 4.3.2.1), the water vapour permeabilities of HPMC films stripped from tablets coated on the model and in the Accela-Cota were not significantly different (Section 4.3.2.2). Time constraints prevented the development of techniques which would have enabled the mechanical properties of small areas of film, produced in the Accela-Cota, to be compared with those of films produced on the model system. To study the influence of preparation method on film properties, a film casting technique was developed (Section 4.2).

Methods for the removal of coatings from different substrates, the measurement of film thickness, SEM and EDAX of coatings were developed and evaluated; the latter being used to semi-quantitatively analyse the distribution of elements within the core and coating (Section 5). A mass spectrometric gas detection system was developed to enable the gas and vapour permeabilities of small areas of thin films to be determined; its accuracy was confirmed by showing good agreement between the experimental oxygen permeability coefficient for a sample of polyethylene sheeting and data obtained from the manufacturer and the literature (Section 6.1). A relocation technique for measuring the surface roughness of film coatings was developed and its application to the study of coating deposition demonstrated (Section 7). Existing test methods were modified to allow the evaluation of water vapour permeabilities, by a gravimetric technique (Section 6.2) and the mechanical properties of small pieces of film coating (Section 6.3).

The properties of film coatings were shown to vary depending upon the preparation technique, film substrate and property investigated (Section 9.1.2), thus justifying the development of a model system to produce film coatings.

The effect of titanium dioxide on the permeability and mechanical properties of HPMC films was studied in detail (Section 9.1.2). Increasing the filler content had little effect on the oxygen permeability of sprayed films, although the mechanical—

properties were progressively reduced until, above 60% w/pw filler, the films became too weak to handle. The absence of a reduction in oxygen permeability with increasing titanium dioxide content served to highlight the dangers of drawing conclusions from permeability data for a single permeant, such as water vapour, which can also plasticize the film. The effect of increasing donor gas relative humidity was to reduce then increase the oxygen permeability of unfilled HPMC films, indicating a slight plasticizing action, or physical blocking of the diffusion pathway at low moisture contents (Section 9.1.3).

10.2 Suggestions for Further Work

This study has enabled techniques for the production and testing of polymer film coatings to be developed and evaluated. However, several aspects of work require further investigation to improve the techniques developed and to establish a more integral knowledge of the aqueous film coating of tablets.

The volume change method by which the spray rate was measured on the model system was tedious to use and somewhat imprecise (Section 4.3.1.3c). A more accurate system could be developed in which the container of coating liquid is placed on a load transducer whose output is differentiated with respect to time, thus giving a direct read-out of flow rate in grams per unit time. The model coating system developed in this work could allow the effects of processing parameters including the dwell time, spray interval, atomizing air pressure and volume, inlet air temperature

and volume and exhaust capacity to be studied in detail. Although the mean spray interval (25 seconds) was used in the design of the system, it can be argued that the mode (2 - 3 seconds) or median (9 - 12 seconds) of the frequency versus interval distribution (Figures 4.12 and 4.13) should be used, since much of the film coating was built up by passages through the spray at short intervals. Additionally, a quantitative comparison of the wide range of coating conditions which are used industrially would help to isolate those which are essential for the successful aqueous film coating of tablets.

Further comparison of the properties of films produced on the model and in the Accela-Cota could be carried out with different coating formulations to ensure that information about coating variables, obtained using the model system, will be valid for tablet coating in the Accela-Cota. To facilitate this, additional techniques such as micro-indentation testing, adhesion testing, mercury porosimetry and differential thermal analysis could be evaluated for the analysis of film properties.

The relocation surface roughness technique showed the changes in roughness which occurred during deposition of a coating using the model system. However, the technique should be coupled with adequate computer analysis of the traces to allow the precise nature of these changes to be evaluated quantitatively for different formulations, processing conditions and film substrates.

The investigation of the properties of coating solutions revealed inadequacies in the data available for the determination of the molecular weight of HPMC and HPC samples. Further work could be carried out using aqueous gel permeation chromatography with fractionated HPMC and HPC standards, light scattering or osmotic pressure techniques to determine the true molecular weight and its distribution, for each polymer studied. The possibility that thermal gelation might affect film formation could be investigated further by measuring the rate of gelation at different polymer concentrations and temperatures, thus evaluating the time required for significant gelation to develop. At low spray rates the temperature in the spray cone near the tablet bed was not reduced by evaporative cooling, due to either spray drying or thermal gelation. To further establish which process is occurring samples of polymer solution taken from different regions in the spray cone and at different spray rates could be analysed for their water content.

The formulation parameters studied in this project were very limited and could be extended to include the effects of additives such as plasticizers, surface active agents, alternative polymers and fillers. In each case, the effect of water vapour on the oxygen permeability and mechanical properties should be investigated. The concentration and molecular weight of HPMC could be varied and the effect of combinations of hydrophilic polymers, such as HPMC and HPC, investigated. To reduce the water vapour permeability of the films, the effect of adding more hydrophobic polymers and other additives could be studied, including the use

of colloidal dispersions of ethyl cellulose and acrylic resins such as Aquacoat and Eudragit respectively. In view of the plasticizer loss reported by Pickard[106] any study involving the addition of plasticizers such as propylene glycol, polyethylene glycols, or glycerin would have to include analysis of the dry films for plasticizer content. The effects of alternative fillers and solid additives such as iron oxide and talc could be determined, although the results would have to be interpreted with caution due to differences in hydrophobicity, particle shape, particle size and aggregation behaviour.

Finally, the combination of formulation and processing variables studied could be subjected to mathematical analysis techniques designed to allow the rational optimization of aqueous film coating of tablets.

APPENDICES

APPENDIX I

Regression Data for the Daily Calibrations of the Mass Spectrometer

Calibration Date	Slope ($Pa\ ppm^{-1} \times 10^9$)	S.D. Slope ($\times 10^9$)	Rel.S.D. Slope (%)	Intercept ($Pa \times 10^7$)	S.D. Intercept ($\times 10^7$)	Correlation Coefficient	Calibration Range (ppm)
2.9.80	0.417	0.008	1.92	1.697	0.202	0.9987	216-5100
3.9.80	0.419	0.013	3.10	1.613	0.402	0.9981	540-5100
		Ionization Gauge Head Removed					
5.9.80	1.244	0.029	2.34	2.833	0.738	0.9981	216-5100
9.9.80	1.275	0.042	3.31	2.931	1.307	0.9978	540-5100
3.12.80	1.368	0.025	1.82	2.017	0.771	0.9993	540-5100
5.12.80	1.388	0.012	0.89	2.124	0.381	0.9998	540-5100
6.12.80	1.416	0.014	0.98	2.091	0.428	0.9998	540-5100
8.12.80	1.471	0.012	0.82	3.248	0.374	0.9999	540-5100
12.12.80	1.363	0.029	2.14	3.132	0.903	0.9991	540-5100
13.12.80	1.462	0.021	1.41	1.765	0.638	0.9996	540-5100
15.12.80	1.407	0.007	0.49	2.130	0.214	1.0000	540-5100
16.12.80	1.400	0.017	1.20	3.364	0.520	0.9997	540-5100
17.12.80	1.401	0.021	1.51	2.883	0.655	0.9995	540-5100
19.12.80	1.365	0.010	0.75	2.704	0.306	0.9999	540-5100
20.12.80	1.337	0.023	1.72	2.752	0.118	0.9994	55-1020
		System Rebaked					
2.1.81	1.042	0.015	1.49	2.453	0.079	0.9996	55-1020
3.1.81	1.086	0.023	2.08	2.595	0.125	0.9994	55-1020
5.1.81	1.035	0.014	1.38	2.819	0.079	0.9997	55-1020
7.1.81	1.178	0.017	1.46	2.843	0.095	0.9997	55-1020
8.1.81	1.050	0.013	1.23	2.745	0.103	0.9997	55-1530
10.1.81	1.049	0.016	1.52	2.688	0.091	0.9996	55-1020
13.1.81	1.039	0.016	1.54	2.485	0.087	0.9997	55-1020
14.1.81	1.014	0.010	1.00	2.289	0.088	0.9999	55-1530
16.1.81	0.806	0.002	0.20	2.036	0.014	1.0000	55-1530
		Mass Spectrometer Filament Replaced					
29.1.81	0.601	0.005	0.87	1.340	0.045	0.9999	55-1530

Calibration Date	Slope $^{-1}$ (Pa ppm $^{-1}$ x 10^{9})	S.D. Slope (x10^{9})	Rel. S.D. Slope (%)	Intercept (Pa x 10^{7})	S.D. Intercept (x 10^{7})	Correlation Coefficient	Calibration Range (ppm)
30.1.81	0.596	0.005	0.75	1.632	0.025	0.9999	55-1020
31.1.81	0.632	0.010	1.62	1.693	0.057	0.9996	55-1020
2.2.81	0.657	0.009	1.30	1.977	0.047	0.9998	55-1020
3.2.81	0.709	0.015	2.16	2.159	0.132	0.9993	55-1530
4.2.81	0.597	0.019	3.17	2.103	0.164	0.9985	55-1530
5.2.81	0.631	0.016	2.57	2.285	0.140	0.9990	55-1530
14.2.81	0.604	0.010	1.63	2.407	0.085	0.9996	55-1530
16.2.81	0.721	0.011	1.50	2.376	0.060	0.9997	55-1020
17.2.81	0.669	0.010	1.52	2.363	0.056	0.9997	55-1020
23.2.81	0.572	0.003	0.46	2.441	0.015	1.0000	55-1020
24.2.81	0.583	0.002	0.29	2.527	0.009	1.0000	55-1020
26.2.81	0.663	0.004	0.67	2.555	0.024	0.9999	55-1020
2.3.81	0.722	0.009	1.24	2.563	0.051	0.9998	55-1020
3.3.81	0.690	0.006	0.85	2.424	0.051	0.9999	55-1530
4.3.81	0.591	0.011	1.91	2.524	0.098	0.9995	55-1530
5.3.81	0.606	0.006	0.94	2.264	0.125	0.9998	55-4080
6.3.81	0.569	0.008	1.41	2.461	0.045	0.9997	55-1020
9.3.81	0.706	0.004	0.55	2.569	0.033	1.0000	55-1530
10.3.81	0.711	0.005	0.64	2.627	0.040	0.9999	55-1530
11.3.81	0.680	0.007	1.01	2.661	0.059	0.9999	55-1530
12.3.81	0.735	0.007	0.89	2.693	0.057	0.9999	55-1530
13.3.81	0.768	0.008	1.06	2.835	0.071	0.9998	55-1530
14.3.81	0.796	0.005	0.62	2.699	0.027	0.9999	55-1020
16.3.81	0.870	0.009	0.98	2.836	0.047	0.9999	55-1020
17.3.81	0.882	0.003	0.35	2.947	0.071	1.0000	55-4080
23.3.81	0.917	0.016	1.74	2.887	0.089	0.9995	55-1020
24.3.81	0.949	0.010	1.03	2.644	0.123	0.9998	55-2040
25.3.81	0.892	0.008	0.84	2.853	0.093	0.9999	55-2040
26.3.81	0.913	0.008	0.87	2.880	0.099	0.9999	55-2040
27.3.81	0.893	0.008	0.89	2.811	0.099	0.9999	55-2040

Calibration Date	Slope ($Pa\ ppm^{-1} \times 10^9$)	S.D. Slope ($\times 10^9$)	Rel. S.D. Slope (%)	Intercept ($Pa \times 10^7$)	S.D. Intercept ($\times 10^7$)	Correlation Coefficient	Calibration Range (ppm)
28.3.81	0.904	0.013	1.41	2.712	0.160	0.9997	55-2040
30.3.81	0.930	0.010	1.49	2.650	0.174	0.9997	55-2040
31.3.81	0.929	0.023	2.44	2.733	0.284	0.9991	55-2040
1.4.81	0.891	0.009	1.02	2.792	0.113	0.9999	55-2040
2.4.81	0.924	0.013	1.42	2.673	0.164	0.9997	55-2040
3.4.81	0.899	0.023	2.50	2.572	0.282	0.9991	55-2040
4.4.81	0.845	0.010	1.18	2.807	0.087	0.9998	55-1530
6.4.81	0.868	0.012	1.37	2.640	0.149	0.9997	55-2040
7.4.81	0.878	0.013	1.47	2.504	0.161	0.9997	55-2040
8.4.81	0.850	0.008	0.89	2.564	0.095	0.9999	55-2040
13.4.81	0.854	0.010	1.19	2.027	0.127	0.9998	55-2040
14.4.81	0.832	0.011	1.37	2.125	0.143	0.9997	55-2040
15.4.81	0.812	0.012	1.53	2.153	0.155	0.9997	55-2040
16.4.81	0.827	0.007	0.84	2.227	0.087	0.9999	55-2040
	Mass Spectrometer Filament Replaced						
23.4.81	0.164	0.002	1.32	0.866	0.027	0.9997	55-2040
24.4.81	0.211	0.004	2.02	1.098	0.053	0.9994	55-2040
24.4.81	0.242	0.003	1.13	1.144	0.034	0.9998	55-2040
25.4.81	0.272	0.004	1.40	1.204	0.048	0.9997	55-2040
27.4.81	0.667	0.014	2.11	2.148	0.176	0.9993	55-2040
28.4.81	0.586	0.014	2.44	2.087	0.124	0.9991	55-1530
29.4.81	0.533	0.010	1.79	2.160	0.120	0.9995	55-2040
30.4.81	0.574	0.016	2.70	2.177	0.195	0.9989	55-2040
31.4.81	0.513	0.017	3.31	2.445	0.205	0.9986	55-2040
2.5.81	0.555	0.011	1.91	2.404	0.133	0.9995	55-2040
4.5.81	0.594	0.015	2.51	2.320	0.187	0.9991	55-2040
5.5.81	0.598	0.011	1.81	2.337	0.135	0.9995	55-2040
6.5.81	0.592	0.008	1.35	2.399	0.100	0.9997	55-2040
8.5.81	0.671	0.010	1.47	2.832	0.123	0.9997	55-2040

Calibration Date	Slope ($Pa\ ppm^{-1} \times 10^9$)	S.D. Slope ($\times 10^9$)	Rel. S.D. Slope (%)	Intercept ($Pa \times 10^7$)	S.D. Intercept ($\times 10^7$)	Correlation Coefficient	Calibration Range (ppm)
9.5.81	0.657	0.014	2.13	2.825	0.176	0.9993	55-2040
11.5.81	0.691	0.013	1.92	2.636	0.166	0.9995	55-2040
12.5.81	0.681	0.021	3.05	2.851	0.287	0.9983	55-2040
14.5.81	0.679	0.011	1.68	2.881	0.143	0.9996	55-2040
15.5.81	0.694	0.018	2.62	2.580	0.228	0.9990	55-2040
16.5.81	0.717	0.010	1.45	2.651	0.130	0.9997	55-2040
17.5.81	0.722	0.016	2.20	2.648	0.199	0.9993	55-2040
19.5.81	0.719	0.009	1.18	2.769	0.107	0.9998	55-2040
20.5.81	0.747	0.022	2.91	2.652	0.272	0.9987	55-2040
21.5.81	0.725	0.006	0.78	2.787	0.071	0.9999	55-2040
22.5.81	0.728	0.018	2.51	2.831	0.228	0.9991	55-2040
23.5.81	0.724	0.011	1.52	3.013	0.138	0.9997	55-2040
26.5.81	0.788	0.012	1.51	2.945	0.149	0.9997	55-2040
27.5.81	0.796	0.014	1.76	3.293	0.176	0.9995	55-2040
28.5.81	0.814	0.004	0.53	3.001	0.053	1.0000	55-2040
30.5.81	0.891	0.014	1.54	3.117	0.172	0.9996	55-2040
31.5.81	0.934	0.008	0.84	3.035	0.098	0.9999	55-2040
1.6.81	0.985	0.019	1.94	2.888	0.240	0.9994	55-2040
2.6.81	0.946	0.012	1.22	2.940	0.145	0.9998	55-2040
3.6.81	0.987	0.013	1.36	2.867	0.168	0.9997	55-2040
4.6.81	0.987	0.007	0.68	2.828	0.084	0.9999	55-2040
5.6.81	0.994	0.011	1.09	2.905	0.136	0.9998	55-2040
8.6.81	1.049	0.008	0.80	3.036	0.105	0.9999	55-2040
15.6.81	1.147	0.016	1.41	3.351	0.202	0.9997	55-2040
16.6.81	1.035	0.010	0.99	3.348	0.128	0.9999	55-2040
17.6.81	1.141	0.019	1.68	3.177	0.240	0.9996	55-2040
18.6.81	1.233	0.014	1.12	3.184	0.173	0.9998	55-2040
19.6.81	1.177	0.010	0.88	3.492	0.129	0.9999	55-2040
20.6.81	1.277	0.020	1.55	3.277	0.248	0.9996	55-2040
23.6.81	1.404	0.020	1.43	3.593	0.250	0.9997	55-2040

APPENDIX II

Conversion of Manufacturers and Literature Values for Gas Permeability Coefficients to Strict S.I. Units and 30°C

AII.1 Literature Values

a. Temperature Conversion

The permeability coefficients for non plasticizing permeants are often related to temperature by the exponential relationship[270]

$$P = P_o \, e^{(-E_p/RT)}$$

P = Permeability Coefficient at quoted temperature

P_o = Permeability Coefficient at $\frac{1}{T} = 0$

E_p = Activation Energy For Permeation

R = Gas Constant

T = Temperature

Literature values for the oxygen permeability coefficient of polyethylene at 25°C can thus be recalculated for 30°C if the activation energy for permeation is stated.

The polymer handbook[270] quotes two different sets of data:

a) $P_{298} = 2.88 \times 10^{-10}$ cc cms^{-1} cm^{-2} cm Hg^{-1}

$E_p = 4.26 \times 10^{4}$ J mol^{-1}

$R = 8.3144$ J mol^{-1} k^{-1}

$T = 298$ k

Thus $2.88 \times 10^{-10} = P_o \, e^{-\frac{4.26 \times 10^4}{8.3144 . 298}}$

$P_o = 8.441 \times 10^{-3}$ cc cms^{-1} cm^{-2} cm Hg^{-1}

$$P_{303} = 8.441 \times 10^{-3} \; e^{\frac{-4.26 \times 10^4}{8.3144 \, . \, 303}}$$

$= 3.83 \times 10^{-10}$ cc cm s^{-1} cm^{-2} cm Hg^{-1}

b) $P_{298} = 2.72 \times 10^{-10}$ cc cm s^{-1} cm^{-2} cm Hg^{-1}

$E_p = 4.51 \times 10^{4}$ J mol^{-1}

Similarly to a)

$P_{303} = 3.67 \times 10^{-10}$ cc cm s^{-1} cm^{-2} cm Hg^{-1}

b. Conversion to S.I. Units

Permeability coefficients for gases, expressed in S.I. units, will have the following units. From equation 6.5.

$$P = \frac{d\,C_R}{dt} \cdot \frac{V_R \quad L}{A \quad C_D}$$

the preferred units of volume, area and length will be m^3, m^2 and m respectively. The concentration units of permeant in the donor and receptor compartments, will cancel out when expressed in the same units (eg ppm).

Thus $P = \frac{ppm \; m^3 \; m}{s \; m^2 \; ppm}$ $\qquad \underline{\underline{P = m^2 \; s^{-1}}}$

Literature values of gas permeability coefficients are commonly expressed in the units cc cm s^{-1} cm^{-2} cm Hg^{-1}, since conventional techniques measure the volume of gas transferring under a pressure difference, expressed in cm Hg. Thus to convert to S.I. units, the pressure difference across the film must be converted to concentration .

76 cm Hg will represent unit concentration. Thus 1 cm Hg = 1.315×10^{-2} m^3/m^3. Consequently:

$$\frac{\text{cc cm}}{\text{s cm}^2 \text{ cm Hg}} = \frac{\text{m}^3 \times 10^{-6} \quad \text{m} \times 10^{-2}}{\text{s m}^2 \times 10^{-4} \quad 1.3158 \times 10^{2} \frac{\text{m}^3}{\text{m}^3}}$$

$$\frac{\text{m}^3 \text{ m}}{\text{s m}^2} \times 7.6 \times 10^{-3}$$

Thus P values in cc cm s^{-1} cm^{-2} cm Hg^{-1} must be multiplied by 7.6×10^{-3} to obtain the coefficient in terms of m^2 s^{-1}

Thus a) $3.83 \times 10^{-10} \times 7.6 \times 10^{-3} = 2.91 \times 10^{-12}$ m^2 s^{-1}

b) $3.67 \times 10^{-10} \times 7.6 \times 10^{-3} = 2.79 \times 10^{-12}$ m^2 s^{-1}

Similarly, water vapour permeability coefficients are commonly expressed in the units g m s^{-1} m^{-2} cm Hg^{-1}, since the absolute weight (g) of water vapour transferring under a vapour pressure difference (cm Hg) is measured. Thus to obtain S.I. units, the vapour pressure gradient must be converted to the concentration gradient expressed in g m^{-3}.

From the Ideal Gas Law

$$PV = n\,RT$$

Thus

$$P = \frac{n}{V}\,RT$$

$$P = \frac{\text{vapour pressure}}{\text{total pressure}}$$

$\frac{n}{V}$ = Moles per litre water vapour

R = Gas Constant

T = Temperature

At 30°C

$$\frac{n}{V} = \frac{\Delta P}{76} \times \frac{1}{0.082 \times 303} \quad \text{mole litre}^{-1}$$

$$= \frac{\Delta P}{76} \times \frac{1}{0.082 \times 303} \times 18 \times 10^{3} \quad g\ m^{-3}$$

$$\frac{n}{V} = \Delta P\ 9.53 \quad g\ m^{-3}$$

Thus P values expressed in g m s^{-1} m^{-2} cm Hg^{-1} must be multiplied by 9.53 to obtain the coefficient in terms of m^2 s^{-1}

AII.2. Manufacturers Values

The manufacturer (BXL Plastics Ltd.) of the polyethylene resin used to produce the sheeting tested, stated the oxygen permeability coefficient as 5,000 cc m^{-2} day^{-1} $atmosphere^{-1}$ at 23°C for a 38 μm thick film. The value in S.I. units was calculated as follows:-

$$P \quad 5{,}000\ \frac{cm^3 \times 10^{-6} \cdot 3.8 \times 10^{-5}}{day \times 24 \times 60 \times 60 \cdot m^2 \cdot 1} = \frac{m^3\ m}{s\ m^2\ \frac{m^3}{m}} = \frac{m^2}{s}$$

$$P = 2.20 \times 10^{-12}\ m^2\ s^{-1} \text{ at } 23^{\circ}C.$$

The value for the activation energy of permeation was not available for this sample of polyethylene, so the permeability coefficient at 30°C was calculated from the mean literature activation energy.

$$P_{296} = P_o \, e^{-E_P/RT}$$

$$2.20 \times 10^{-12} = P_o \, e^{\frac{-43.85 \times 10^3}{8.3144 \times 296}}$$

$$P_o = 1.204 \times 10^{-4}$$

$$P_{303} = 3.32 \times 10^{-12} \; m^2 s^{-1}$$

APPENDIX III

Statistical Analyses

AIII.1 Least Squares Regression Analysis

When a linear relationship is assumed to exist between two variables it is usual to fit a straight line by a least squares regression analysis. The simplest statistical model for this assumes that the independent variable (x) is known without error of measurement and that the corresponding measured values of the dependent variable (y) are scattered normally from their true values. Hence each value of y_i of the dependent is normally distributed about the mean, with a variance σ^2.

The method of least squares obtains estimates of c and m in the equation $y = mx + c$ such that the sum of the squares of the deviations of the observations y_i from their mean is a minimum.

These values are:-

$$m = \frac{n \Sigma x_i y_i - \Sigma x_i \Sigma y_i}{n \Sigma x_i^2 - \left[\Sigma x_i\right]^2}$$

$$= \frac{\Sigma (x_i - \bar{x})(y_i - \bar{y})}{\Sigma (x_i - \bar{x})^2}$$

$$c = \frac{\Sigma y_i - m \Sigma x_i}{n}$$

$$= \bar{y} - m\bar{x}$$

n is the number of points on the line.

Variance of the slope (m)

This is termed s_m^2 and is given by the equation

$$s_m^2 = \frac{\sigma_e^2}{\Sigma(x_i-\bar{x})^2}$$

where σ_e^2 is the residual variance of the dependent variable y and may be obtained by dividing the residual sum of squares ΣD^2 by (n-2), where $\Sigma D^2 = \Sigma(y_i-\bar{y})^2 - \frac{\left[\Sigma(x_i-\bar{x})(y_i-\bar{y})\right]^2}{\Sigma(x_i-\bar{x})^2}$

Residual sum of squares. (n-2) degrees of freedom

Total sum of squares. (n-1) degrees of freedom

Sum of squares due to regression. 1 degree of freedom

$$= \Sigma(y_i - \bar{y})^2 - m^2\Sigma(x_i-\bar{x})^2$$

The denominator (n-2) shows that two degrees of freedom have been lost because both slope and intercept were estimated from the data. The standard deviation of the slope is given by the square root of the variance.

Variance of the intercept (c)

This is termed $s_c^2 = \frac{\Sigma x_i^2 \sigma_e^2}{n\Sigma(x_i-\bar{x})^2}$

where $\sigma_e^2 = \frac{\Sigma D^2}{(n-2)}$

The standard deviation of the intercept is given by the square root of the variance.

Correlation Coefficient (r)

The correlation coefficient is given by:

$$r = \frac{\Sigma (x_i - \bar{x})\ (y_i - \bar{y})}{\left[\Sigma (x_i - \bar{x})^2\ (y_i - \bar{y})^2\right]^{\frac{1}{2}}}$$

$$= \frac{\Sigma\ x_i y_i - \frac{\Sigma\ x_i \Sigma\ y_i}{n}}{\left[\left[\Sigma x_i^{\,2} - \frac{(\Sigma x_i)^2}{n}\right]\left[\Sigma y_i^{\,2} - \frac{(\Sigma y_i)^2}{n}\right]\right]^{\frac{1}{2}}}$$

If the calculated value of r is greater than the tabulated value, a significant linear relationship exists between x and y, although it must be emphasised that this test is somewhat insensitive.

The above computations were carried out using a Fortran program on a Honeywell Multics System Computer.

AIII.2 To Determine the Equality of Two Estimates of a Parameter (Student's t test)

The equality of estimates p_1 and p_2, with respective variances $s_1^{\,2}$ and $s_2^{\,2}$, of a parameter p is assessed as follows:-

$$t = \frac{p_1 - p_2}{(s_1^{\,2} + s_2^{\,2})^{\frac{1}{2}}}$$

The value of t is compared with tabulated values with $n_1 + n_2 - 4$ degrees of freedom, where n_1 and n_2 are the number of observations used in the estimation of p_1 and p_2 respectively. If the value of

t (t_{calc}) does not exceed the tabulated value (t_{tab}) at the 5 per cent (P = 0.05) probability level, the values are assumed to be indistinguishable at that level.

AIII.3 To Determine the Equality of More Than Two Estimates of a Parameter (Bartlett's Test)

The equality of more than two estimates of a parameter P is assessed as follows:-

$$B = \frac{\Sigma(P_i - \bar{P})^2}{\hat{\sigma}_2}$$

where $$\hat{\sigma}_2 = \frac{n_1\sigma_1^2 + n_2\sigma_2^2 + ... n_i\sigma_i^2}{n_1 + n_2 + ...n_i}$$

P_1, P_2....P_i are estimates of the parameter P having standard deviations σ_1, σ_2, ... σ_i respectively. n_1, n_2....n_i are the number of observations in making each estimate of P.

B will have a chi-squared (χ^2) distribution if the estimates of P come from a normal distribution and the calculated value of B may thus be compared with tabulated values of χ^2 having n-1 degrees of freedom, where n is the number of estimates of P.

If the calculated value exceeds the tabulated value at the 5% (P = 0.05) probability level, the estimates of P may be regarded as significantly different.

AIII.4 To Determine the Equality of Two Means of a Parameter (Student's t test)

The equality of means $\bar{x}_1$ and $\bar{x}_2$, with respective variances

s_1^2 and s_2^2, of a parameter is assessed as follows:-

$$t = \frac{\bar{x}_1 - \bar{x}_2}{s\left(\frac{1}{n_1} + \frac{1}{n_2}\right)^{\frac{1}{2}}}$$

where n_1 and n_2 are the number of observations used in the estimation of $\bar{x}_1$ and $\bar{x}_2$. s represents the total standard deviation given by:

$$s = \left[\frac{(n_1-1)s_1^2 + (n_2-1)s_2^2}{(n_1+n_2)-2}\right]^{\frac{1}{2}}$$

The value of 't' is compared with tabulated values with $n_1 + n_2 - 2$ degrees of freedom. If the value of t (t_{calc}) exceeds the tabulated value (t_{tab}) at the 5 per cent (P = 0.05) probability level, the means are considered to be significantly different at that level.

AIII.5 To Determine the Equality of More than Two Means of a Parameter (Analysis of Variance)

Where data is separated into a series of groups, each consisting of a number of observations or measurements, analysis of variance and an F test is used to establish if the variance between the groups is significantly greater than the variance within the groups. The following quantities are calculated from the data:-

A) Uncorrected sum of squares

$$= \sum_{i=1}^{k} \sum_{j=1}^{n} x_{ij}^2$$

where k is the number of groups, n is the number of observations in each group and x^2 is the square of the observation or measurement.

B) Mean sum of squares of group totals

$$= \sum_{i=1}^{k} \frac{\left(\sum_{j=1}^{n} x_{ij}\right)^2}{n_i}$$

C) Mean sum of squares of observations

$$= \frac{\left[\sum_{i=1}^{k} \sum_{j=1}^{n} x_{ij}\right]^2}{N}$$

where N is the total number of observations.

An analysis of variance table is now set up:

	Sum of Squares	Degrees of Freedom	Variance
Between groups	B-C	k-1	$\frac{B-C}{k-1} = s_2^2$
Within groups	A-B	N-k	$\frac{A-B}{N-k} = s_1^2$
Total	A-C	N-1	$\frac{A-C}{N-1}$

The ratio $\frac{s_2^2}{s_1^2}$ will come from an F distribution and if the groups are not significantly different this calculated value of F will be less than the tabulated value at P = 0.05 with k-1 and N-k degrees of freedom.

If the calculated value of F exceeds the tabulated value of F at the 5% level, the least significant difference(L.S.D.) between any pair of group means is given by:-

$$\text{L.S.D. } (0.05) = t_{N-k}(0.05).\ s_1.\ \left(\frac{1}{n_1} + \frac{1}{n_2}\right)^{\frac{1}{2}}$$

where $t_{N-k}(0.05)$ is the tabulated 2-tailed value in a student's 't' distribution, s_1 is the within groups standard deviation and n_1 and n_2 are the number of observations in groups 1 and 2 respectively.

BIBLIOGRAPHY

BIBLIOGRAPHY

1. Gross, H.M.; Endicott, C.J. Drug Cosmet. Ind., 86, 170, 1960.

2. Munzel, K. Pharm. Acta Helv., 38, 65-85, 129-146, 1963.

3. Pickard, J.F.; Rees, J.E. Mfg. Chem. Aerosol News, 45, 19-22, 1974.

4. Lehmann, K. Mfg. Chem. Aerosol News, 44 , 36, 1973.

5. Ellis, J.R.; Prillig, E.B.; Endicott, C.J. In: The theory and practice of industrial pharmacy (Lachman, L.; Lieberman , H.A., Kanig, T.L., ed.), Chapter 10, Philadelphia: Lea and Febiger, 1970.

6. Fishwick, K. Aqueous film coating. Presented at Interphex, April 1978.

7. Elliot, J.L. The Film Coating of Tablets. Presented at British Pharmaceutical Conference, Discussion Forum, September 1968.

8. Dow Chemical Company. Technical Information - Methocel cellulose ethers in aqueous systems for tablet coating.

9. Colorcon Ltd. Technical Information - M-1 type Opaspray and Methocel (HPMC) in aqueous cellulosic film coating.

10. Pickard, J.F.; Elworthy, P.H.; Sucker, H. J. Pharm. Pharmacol.,27, 6p, 1975.

11. Jackson, G.J., Film Coating of Solid Dosage Forms - Aqueous Systems. Presented to the Academy of Pharmaceutical Sciences, Industrial Pharmaceutical Section, Fifteenth Annual Eastern Regional Meeting, October 1975.

12. Hubberfield, D. Drug Cosmet. Ind., 117, 46-49, 139-141, 1975.

13. Hall, H.S.; Hinkes, T.M. Am. Chem. Soc. Div. Org. Coat. Plast. Chem. Pap., 33, 545-8, 1973.

14. Porter, S.C. Colorcon Ltd., Technical Information - Aqueous Film Coating .

15. Shin-etsu Chemical Industry Company. Technical Information - HPMC Tablet Coating In An Aqueous System.

16. Motoyama, S.; Tsujino, T. Drug Coating with an Aqueous Solution of Film Forming Substances. Jpn. Pat. 76,142, 522; through Chem. Abstr. 86, 177315h, 1977.

17. Colorcon Incorporated. Technical Information - Film Coating Technology.

18. Ahsan, S.S.; Blauy, S.M. Drug Standards, 26, 29-33, 1958.

19. Chaumeil, J.C.; Piton, Y.; Marchand, M.J. Ann. Pharm. Fr., 31, 375-84, 1973; Through Chem. Abstr., 80, 87470b, 1974.

20. El-Sayed, A.A.; Said, S.A.; Geneida, A.Sh. Mfg. Chem. Aerosol News, 49, 52-55, 1978.

21. Findlay, L.E. Progress in Tablet Film Coating Technology. Presented to the Annual Meeting of the Association of Faculties of Pharmacy of Canada, May 1975.

22. Fites, A.L.; Banker, G.S.; Smolem, V.F. J. Pharm. Sci., 59, 610-613, 1970.

23. Gans, E.H.; Chaukin, L. J. Am. Pharm. Assoc., 43, 483-485, 1954.

24. Tomasihi, L.; Goshkaryan, M.; Radeva, K.; Andonova, U. Pharmazie, 30, 779-782, 1975; through Chem. Abstr., 84, 111591x, 1976.

25. Laguna, O.; Luong, T.T.; Duchene, D.; Seiller, M. Sci. Tech. Pharm., 4, 91-99, 1975; through Chem. Abstr., 83, 168355g, 1975.

26. Lappas, L.C.; McKeehan, W. J. Pharm. Sci., 54, 176-181, 1965.

27. Lehmann, K. Mfg. Chem. Aerosol News, 44, 39-41, 1973.

28. Lehmann, K. Mfg. Chem. Aerosol News, 45, 48-50, 1974.

29. Miyawaki, G.M.; Patel, N.K.; Kostenbauder, H.B. J. Am. Pharm. Assoc., 48, 315-318, 1959.

30. Nessel, R.J.; De Kay, H.G.; Banker, G.S. J. Pharm. Sci., 53, 790-794, 1964.

31. Nessel, R.J.; De Kay, H.G.; Banker, G.S. J. Pharm. Sci., 53, 882-887, 1964.

32. Tuerck, P.A.; McVean, D.E. J. Pharm. Sci., 62, 1534-1537, 1973.

33. Pickard, J.F.; Rees, J.E. Mfg. Chem. Aerosol News, 47, 31, 1976.

34. Prickett, P.S.; Murray, H.L.; Mercer, N.H. J. Pharm. Sci., 50, 316-320, 1961.

35. Powell, D.R.; Banker, G.S. J. Pharm. Sci., 58, 1335-1340, 1969.

36. Prillig, E.B. J. Pharm. Sci., 58, 1245-1249, 1969.

37. Stempel, E. Drug. Cosmet. Ind., 98, 44-46, 118-123, 128, 1966.

38. Stempel, E. Drug. Cosmet. Ind., 98, 36-38, 139-142, 145-146, 148, 1966.

39. Utsumi, I.; Ida, T.; Takahashi, S.; Sugimoto, N. J. Pharm. Sci., 50, 592, 1961.

40. Wyandotte Chemicals Corporation. Technical Information - Pluronic Polyols.

41. Bayer, K. Über die Anwendung von Polymeren für Überzuge auf festen Arzneiformen. Ph.D. Thesis, Eidgenüssischen Technischen Hochschule, Zürich, 1970.

42. Roland, M.; Vemba, A.T. Labo-Pharma. Problèms et Techniques, 237, 935-947, 1974.

43. Abdel-Aziz, S.A.M.; Kassem, A.A.; Abou-Taleb, A.E.; Abdel-Hady, S.S. Pharm. Tech. Int., 4, 23-27, 1980.

44. Kassem, A.A.; Abdel-Aziz, S.A.M.; Abou-Taleb, A.E.; Abdel-Hady, S.S. Pharm. Tech. Int., 3, 71-75, 1979.

45. Kassem, A.A.; Abdel-Aziz, S.A.M.; Abou-Taleb, A.E.; Abdel-Hady, S.S. Pharm. Tech. Int.,3, 45-49, 1979.

46. Lehmann, K.; Dreher, D. Pharm. Tech. Int., 3, 33-35, 1979.

47. Tsukamato, H.; Nakagami, H. Coating Compositions. Jpn. Pat. 7984,020, 1979; through Chem. Abstr., 92, 47217r, 1980.

48. Kala, H.; Dittyen, M.; Moldenhauer, H.; Zessin, G. Pharmazie, 34, 755-765, 1979.

49. Fujio, S. Drug Coating. Jpn. Pat. 78133,625, 1978; through Chem. Abstr., 90, 109991h, 1979.

50. Bauer, K.H.; Osterwald, H. Pharm. Ind., 41, 1203-1207, 1979.

51. Onda, Y.; Muto, H.; Maruyama, K. Coating Materials for Solid Pharmaceuticals. Jpn. Pat. 7949,318, 1979; through Chem. Abstr., 91, 112453k, 1979.

52. Porter, S.C.; Ridgway, K. Expo.- Congr. Int. Technol. Pharm. 1st., 3, 75-85, 1977; through Chem. Abstr., 90, 76503v, 1979.

53. Sekikawa, F.; Harayama, M.; Araume, K. Coating Compositions for Tablets. Jpn. Pat. 79143,518, 1979; through Chem. Abstr., 92, 185917v, 1980.

54. Tonedachi, M.; Sekikawa, F.; Harayama, M. Drug Coating. Jpn. Pat. 78139,715, 1978; through Chem. Abstr., 90, 127562y, 1979.

55. Yoshida, K. Base Material for Film Coatings. Jpn. Pat., 7964,830, 1979; through Chem. Abstr., 91, 198938g, 1979.

56. Banker, G.S. Food and Pharmaceutical Coating Composition, Method of Preparation and Products So Coated. U.S. Pat. 7900,787, 1979.

57. Bauer, K.H.; Osterwald, H. Film-Coating a Particulate Solid Pharmaceutical and Emulsions for the Process. Ger. Pat. 2926,633, 1981.

58. Ceschel, G.C.; Gibellini, M. Farmaco. Ed. Prat., 35, 553-63, 1980; through Chem. Abstr., 94, 36276z, 1981.

59. Delporte, J.P. J. Pharm. Belg., 35, 417-426, 1980.

60. Gyozo, K.I.; Szentirmai, Z. Acta. Pharm. Hung., 50, 207-216, 1980; through Chem. Abstr., 94, 36266w, 1981.

61. Lippold, B.C.; Lippold, B.H., Sgoll, G.B. Pharm. Ind., 42, 745-752, 1980.

62. Osterwald, H.; Bauer, K.H. Acta Pharm. Technol., 26, 201-209, 1980.

63. Rhodes, A.; Leslie, S.T. Pharmaceutical Compositions in Solid Dosage Forms. Eur. Pat. Appl. 13,131, 1980; through Chem. Abstr., 93, 245475g, 1980.

64. Shimada, H.; Sugiyama, H.; Kimura, H. Ethyl Carboxyethyl Cellulose for Enteric Coating. Jpn. Pat. 8004,333, 1980 ; through Chem. Abstr., 93, 137987s, 1980.

65. Takeda Chemical Industries Ltd. Sustained Release Pharmaceuticals. Jpn. Pat. 80149,211, 1980.

66. Coletta, V.; Rubin, H. J. Pharm. Sci., 53, 953-955, 1964.

67. Shah, N.B.; Sheth, B.B. J. Pharm. Sci., 61, 412-415, 1972.

68. Donbrow, M.; Friedman, M. J. Pharm. Pharmacol., 26, 148-150, 1974.

69. Donbrow, M.; Friedman, M. J. Pharm. Pharmacol., 27, 633-646, 1975.

70. Donbrow, M.; Samuelov, Y. J. Pharm. Pharmacol., 32, 463-470, 1980.

71. Friedman,M.; Donbrow, M.; Samulov, Y. Drug Dev. Ind. Pharm., 5, 407-424, 1979.

72. Pickard, J.F.; Rees, J.E. Mfg. Chem. Aerosol News., 45, 42-45, 1974.

73. Porter, S.C. Pharm. Tech., 3, 55-59, 1979.

74. Lachman, L.; Cooper, J. J. Pharm. Sci., 52, 490-496, 1963.

75. Sutaria, R.H. Mfg. Chem. Aerosol News, 39, 37-42, 1968.

76. Manesty Machines Ltd. Technical Information - Accela-Cota Coating Unit.

77. Manesty Machines Ltd. Technical Information Newsletter 259G - Practical Aspects of Accela-Cota Usage, 1971.

78. Purdue Research Foundation. U.S. Pat. 316,037, 1972.

79. Daiichi, S. Jpn. Pat. 9020,316, 1972.

80. Tanabe Seiyaku Ltd. Brit. Pat. 1075,404, 1967.

81. American Home Products. U.S. Pat. 3900,583, 1971.

82. Steinberg, G. Ger. Pat. 2139,154, 1971.

83. Steinberg, G. Ger. Pat. 2323,853, 1973c.

84. Sandvikens Jernwerk. Dan. Pat. 2421,882, 1974.

85. Stellmach, B. U.S. Pat. 4118,522, 1978.

86. Vinter, H. Acta. Pharm. Sueica., 18, 104-105, 1981.

87. Mody, D.S.; Scott, M.W.; Lieberman, H.A. J. Pharm. Sci., 53, 949-952, 1964.

88. Biddle Sawyer and Co. Ltd. Mfg. Chem. Aerosol News, 36, 54, 1967.

89. Lindberg, N.O.; Jönsson, E. Acta. Pharm. Sueica, 9, 581-594, 1972.

90. Lantz, R.J.; Bailey, A.; Robinson, M.T. J. Pharm. Sci., 59, 1174-1177, 1970.

91. Heyd, A.; Kanig, J.L. J. Pharm. Sci., 59, 1171, 1970.

92. Anderson, W., Sakr, A. Mfg. Chem. Aerosol News, 36, 42-47, 1967.

93. Zatz, J.L.; Weiner, N.D.; Gibaldi, M. J. Pharm. Sci., 57, 1440-1442, 1968.

94. Zatz, J.L.; Knowles, B. J. Pharm. Sci., 59, 1188-1189, 1970.

95. Kanig, J.L.; Goodman, H. J. Pharm. Sci., 51, 77-83, 1962.

96. Banker, G.S.; Gore, A.Y.; Swarbrick, J. J. Pharm. Pharmacol., 18, 457-466, 1966.

97. Swarbrick, J.; Amann, A.H.; Lindstrom, R.E. J. Pharm. Sci., 61, 1645-1647, 1972.

98. Zaro, J.J. Jr. Experimental Methods for the Production and Evaluation of Free Polymeric Films and Simulated Coated

Dosage Forms. Ph.D. Thesis, Philadelphia College of Pharmacy and Science, 1973.

99. Banker, G.S.; Gore, A.Y.; Swarbrick, J. J. Pharm. Pharmacol., 18, 205s-211s, 1960.

100. Amann, A.H.; Lindstrom, R.E.; Swarbrick, J. J. Pharm. Sci., 63, 931-933, 1974.

101. Spitael, J.; Kinget, R. J. Pharm. Belg., 32, 569-577, 1977.

102. Hawes, M.R. The Effect of Some Commonly Used Excipients on the Physical Properties of Film Formers Used in the Aqueous Coating of Pharmaceutical Tablets. R.P. Scherer Award Paper, Presented to a Pharmaceutical Society Meeting, November 1978.

103. Allen, D.J.; De Marco, J.D.; Kwan, K.C. J. Pharm. Sci., 61, 106-110, 1972.

104. Gurney, R.; Mordier, D.; Buri, P. Pharm. Acta Helv., 51, 384-390, 1976.

105. Porter, S.C. Pharm. Tech., 4, 67-75, 1980.

106. Pickard, J.F. An Investigation of Selected Cellulose Ethers as Film Coatings for Pharmaceutical Tablets. Ph.D. Thesis, CNAA, 1979.

107. Porter, S.C. The Properties of Enteric Film Coating Polymers. Ph.D. Thesis, University of London, 1980.

108. Morgan, P.W. Ind. Eng. Chem., 45, 2296-2306, 1953.

109. Lefort des Ylouses, D.; Seiller, D.; Duchene, D. Pharm. Acta Helv., 52, 65-78, 1977.

110. Munden, B.J.; DeKay, H.G. ; Banker, G.S. J. Pharm. Sci., 53, 395-401, 1964.

111. Gibaldi, M.; Kanig, J.L.; Espiruitu, P. J. Pharm. Sci., 53, 1434, 1964.

112. Crawford, R.R.; Esmerian, O.K. J. Pharm. Sci., 60, 212-214, 1971.

113. Lachman, L.; Drublis, A. J. Pharm. Sci., 53, 639-643, 1964.

114. Rowe, R.C. J. Pharm. Pharmacol., 28, 310-311, 1976.

115. Kuriyama, T.; Nobutoki, M.; Nakanishi, M. J. Pharm. Sci., 59, 1341-1344, 1970.

116. Parker, J.W.; Peck, G.E.; Banker, G.S. J. Pharm. Sci., 63, 119-125, 1974.

117. Pickard, J.F.; Rees, J.E.; Elworthy, P.H. J. Pharm. Pharmacol., 24, 139p., 1972.

118. Lindberg, N.O. Acta Pharm. Sueica, 8, 541-548, 1971.

119. Patel, M.; Patel, J.M.; Lemberger, A.P. J. Pharm. Sci., 53, 286-296, 1964.

120. Sciarra, J.J.; Patel, S.P. J. Soc. Cosmet. Chem., 23, 605-615, 1972.

121. Abdel-Aziz, S.A.M.; Anderson, W.; Armstrong, P.A.M. J. Appl. Polym. Sci., 19, 1181-1192, 1975.

122. Okor, R.S.; Anderson, W. J. Pharm. Pharmacol., 30, 4p, 1978.

123. Okor, R.S.; Anderson, W. J. Pharm. Pharmacol., 30, 6p, 1978.

124. Zaro, J.J.; Smith, W.E. J. Pharm. Sci., 61, 814-815, 1972.

125. Kildsig, D.O.; Nedlich, R.L.; Banker, G.S. J. Pharm. Sci., 59, 1634-1637, 1970.

126. Spitael, J.; Kinget, R. Pharm. Acta Helv., 52, 47-50, 1977.

127. Gurny, R.; Guitard, P.; Buri, P. Acta Pharm. Technol., 23, 29-38, 1977; through Chem. Abstr., 86, 161241v, 1977.

128. Smith, H.; Murley, R.D. J. Oil. Col. Chem. Assoc., 56, 178-183, 1973.

129. Tattersall, R. Improvements in and Relating to Coatings. Brit. Pat. 1311, 932, 1973.

130. Stannett, V.; Yasuda, H. In:Testing of Polymers,Volume I (Schmitz, J.V., ed.) New York: Interscience, 1965.

131. Yasuda, H.; Stannett, V. J. Macromol. Sci. - Phys., B3, 589-610, 1969.

132. Derham, K.W. The Diffusion of Water Vapour Through Poly-(Methylmethacrylate) Films. Project Report for Degree in Chemistry, Bath University,CB122, 1971.

133. Stannett, V.; Williams, J.L. J. Polym. Sci. Part C, Polym. Symp.,10, 45-59, 1965.

134. Stannett, V.; Szwarc, M.; Bharyava, R.L.; Meyer, J.A.; Myers, A.W.; Rogers, C.E. Tappi Monograph Number 23, New York: Tappi, 1962.

135. Richards, R.W. The Permeability of Polymers to Gases, Vapours and Liquids. Explosives Research and Development Establishment , Report Number ERDE TR135, Ministry of Defence, 1974.

136. Lomax, M. Polymer Testing, 1, 105-147, 1980.

137. Lomax, M. Polymer Testing, 1, 211-242, 1980.

138. Woodruff, W.C.; Peck, G.E.; Banker, G.S. J. Pharm. Sci., 61, 1956, 1972.

139. Newns, A.C. J. Textile Inst., 41, T269-T308, 1950.

140. Hom, F.S., Veresh, S.A., Miskel, J.T. J. Pharm. Sci., 64, 851-857, 1975.

141. Meyer, J.A.; Rogers, C.; Stannett, V.; Szwarc, M. Tappi, 40, 142-146, 1957.

142. Brubaker, D.W.; Kammermeyer, K. Ind. Eng. Chem., 44, 1465-1478,1952.

143. Brubaker, D.W.; Kammermeyer, K. Ind. Eng. Chem., 45, 1148-1152, 1953.

144. Waack, R.; Alex, N.H.; Frisch, H.L.; Stannett, V.; Szwarc, M. Ind. Eng. Chem., 47, 2524-2527, 1955.

145. Stern, S.A.; Sen, S.K.; Rao, A.K. J. Macromol. Sci. - Phys., B10, 507-528, 1974.

146. Michaels, A.S.; Baddour, R.F.; Bixler, H.J.; Choo, C.Y. Ind. Eng. Chem. Process Design and Develop., 1, 14-25, 1962.

147. Higuchi, T.; Aguiar, A. J. Pharm. Sci., 48, 574-583, 1959.

148. James, R.J. Investigation of the Permeability of Poly (Methyl methacrylate) to Water Vapour. Project Report For Degree in Chemistry, Bath University, CB 105, 1970.

149. Eskilson, C.; Appelgren, C.; Bogentoft, C. Acta Pharm. Sueica, 13, 285-288, 1976.

150. Nowak, P. Kunstoffe, 34, 120-121, 1944; through Chem. Abstr., 40, 16935, 1946.

151. Verdin, A. In:Measurement of Oxygen - Proceedings of an Interdisciplinary Symposium Held at Odense University,

Denmark, 26 - 27th September 1974. (Degn, H.; Balslev, I.; Brook, R., eds.), pp. 248-259, New York: Elsevier, 1976.

152. Funke, W.; Zatloukal, H.; Hartfolder, B.; Flaig, R.P.; Flaig, R.D. Congr. Fatipec., 15, III287 - III297, 1980.

153. Nobbs, J. McK. In:Measurement of Oxygen-Proceedings of an Interdisciplinary Symposium Held at Odense University, Denmark, 26 - 27th September 1974. (Degn, H.; Balslev, I.; Brook, R., eds.), pp. 209-225, New York: Elsevier, 1976.

154. Gustov, V.F.; Chekalov, L.N.; Talakin, O.G.; Ivashchenko, D.A.; Duryaryan, S.G.; Novitshii, E. Membran. Tekhnol.-Nouoe, Napraulenie Nauke Tekh., 175-177, 1973. From Ref. Zh. Khim., Abstr. No. 185484, 1973;through Chem. Abstr., 83, 60052s, 1975.

155. Lugsgaard, J.S.; Petersen, L.C.; Degn, H. In:Measurement of Oxygen - Proceedings of an Interdisciplinary Symposium Held at Odense University, Denmark, 26 - 27th September, 1974. (Deng, H.; Balslev, I.; Brook, R., eds.) pp. 148-159, New York: Elsevier, 1976.

156. Kumins, C.A. J. Polym. Sci. Part C - Polym.Symp., 10, 1-9, 1965.

157. Yasuda, H.; Hirotso, T. J. Appl. Polym. Sci., 21, 105-112, 1972.

158. Swarbrick, J.; Amann, A.H. J. Pharm. Pharmacol., 20, 886-888, 1968.

159. Rubinstein, M.H.; Healy, J.N.C. J. Pharm. Pharmacol., 25, 168p. 1973.

160. Rudenko, B.M.; Muchnik, P.I.; Khadzhai, T.A. Lakokras. Mater. Ikh. Primen., 2, 42-43, 1972; through Chem. Abstr., 83, 61816f, 1975.

161. Aulton, M. Mfg. Chem. Aerosol News, 48, 28, 31, 32, 36, 1977.

162. Monk, C.J.H.; Wright, T.A. J.Oil Col. Chem. Assoc., 48, 520-528, 1965.

163. Ridgway, K.; Aulton, M.E.; Rosser, P.H. J. Pharm. Pharmacol., 22, 70s, 1970.

164. Morris, R.L.J. J. Oil Col. Chem. Assoc., 56, 555-565, 1973.

165. White, P.J.P., Aulton, M.E. J. Phys. E: Sci. Instrum., 13, 1980.

166. Rehacek, K. Plaste. Kautsch., 22, 442-447, 1975; through Chem. Abstr., 83, 117052y, 1975.

167. Lefort des Ylouses, D.; Prioux, P.; Duchene, D.; Seiller, M. Ann. Pharm. Fr., 31, 647-658, 1973.

168. Fell, J.T.; Rowe, R.C.; Newton, J.M. J. Pharm. Pharmacol., 31, 69-72, 1979.

169. Brewis, D.M. In:Polymer Science Volume 2, (Jenkins, A.D., ed.), pp. 933-958, Amsterdam; North Holland, 1972.

170. Sathyanaruyana, M.N.; Sampathkumaran, P.S.; Sivasamban, M.A. Packag. India, 8, 24-29, 1975.

171. Briscoe, B.J.; Tabor, D. Farad. Spec. Discuss. Chem. Soc., 2, 7-17, 1972.

172. Nadkarni, P.D.; Kildsig, D.O.; Kramer,P.A.; Banker, G.S. J. Pharm. Sci., 64, 1554-1557, 1975.

173. Wood, J.A.; Harder, S.W. Can. J. Pharm. Sci., 5, 18-23, 1970.

174. Rowe, R.C. J. Pharm. Pharmacol., 30, 343-346, 1978.

175. Fisher, D.G.; Rowe, R.C. J. Pharm. Pharmacol., 28, 886-889, 1976.

176. Starke, M.; Vohland, K.; Wroblowski, M. Plaste. Kautsch., 22, 779-800, 1975; through Chem. Abstr., 86, 91796d, 1977.

177. Rowe, R.C. J. Pharm. Pharmacol., 29, 58-59, 1977.

178. Rowe, R.C. J. Pharm. Pharmacol., 29, 723-726, 1977.

179. Rowe, R.C. J. Pharm. Pharmacol., 32, 214-125, 1980.

180. Jacobsson, R. Thin Solid Films, 34, 191-199, 1976.

181. Banker, G.S. J. Pharm. Sci., 55, 81-89, 1966.

182. Fung, R.M.; Parrott, E.L. J. Pharm. Sci., 69, 439-441, 1980.

183. McGill, W.J. J. Oil Col. Chem. Assoc., 60,121-126, 1977.

184. Jennings, C.W. In:Recent Advances in Adhesion, (Lee, L.H., ed.), pp. 469-483, New York: Gordon and Breech, 1973.

185. Ehrhardt, L.; Patt, L.; Schindler, L. Pharm. Ind., 35, 719-722, 1973.

186. Rowe, R.C. Pharm. Acta Helv., 51, 330-334, 1976.

187. Princen, L.H.; Baker, F.L.; Stolp, J.A. In:Applied Polymer Symposia 23, Scanning Electron Microscopy of Polymers and Coatings,II (Princen, L.H., ed.), pp. 27-34, New York: Wiley and Sons, 1974.

188. Labana, S.S.; Wheeler, M. In:Applied Polymer Symposia 23, Scanning Electron Microscopy of Polymers and Coatings, II

(Princen, L.H., ed.), pp. 61-72, New York: Wiley and Sons, 1974.

189. Cetnar, B.W.; Heitur, J.H. Tappi, 58, 91-95, 1975.

190. Bhatia, V.N.; Betts, A.L. J. Pharm. Sci., 53, 1104-1106, 1964.

191. British Standard 1134, The Assessment of Surface Texture, Parts I and II.London: British Standards Institute, 1972.

192. Rowe, R.C. J. Pharm. Pharmacol., 31, 473-474, 1979.

193. King, M.J.; Thomas, T.R. J. Coat. Technol., 50, 56-61, 1978.

194. Lines, R.W. Technical Information - Mercury Intrusion Porosimetry, Coulter Electronics Ltd.

195. Selkirk, A.B.; Ganderton, D. J. Pharm. Pharmacol., 22, 79s-85s, 1970.

196. Schwartz, J.B. J. Pharm. Sci., 63, 774-776, 1974.

197. Rowe, R.C.; Forse, S.F. J. Pharm. Pharmacol., 26, 61p, 1974.

198. Micromeritics Instrument Corporation. Technical Information - Helium-Air Pycnometer.

199. Coulter Electonics Ltd. Technical Information - Numinco Air-Displacement Porometer.

200. Kitazaki, Y.; Hatu, T. In:Recent Advances in Adhesion, (Lee, L.H., ed.), pp. 65-76, New York: Gordon and Breech, 1973.

201. Harder, S.A.; Zuck, D.A.; Wood, J.A. J. Pharm. Sci., 59, 1787-1792, 1970.

202. Ewane-Ebele, F.; Schreiber, H.P. J. Oil Col. Chem. Assoc., 60, 249-255, 1977.

203. Harder, S.W.; Zuck, D.A.; Wood, J.A. Can. J. Pharm. Sci., 6, 63-70, 1971.

204. Liao, W.C.; Zatz, J.L. J. Pharm. Sci., 68, 486-494, 1979.

205. Lee, W.M. Polym. Eng. Sci., 20, 65-69, 1980.

206. Kuenig, V.; Schuch, H. Kungststoffe, 67, 27-31, 1977; through Chem. Abstr., 86, 90765f, 1977.

207. Brantley, L.R.; Woodward, A.; Carpenter, G. Ind. Eng. Chem., 44, 2386, 1952.

208. Bullett, T.P. In:Recent Advances in Adhesion (Lee, L.H., ed.), pp. 210-212, New York:Gordon and Breech, 1973.

209. Rowe, R.C. J. Pharm. Pharmacol., 32, 116-119, 1980.

210. Rowe, R.C.; Forse, S.F. J. Pharm. Pharmacol., 32, 583-584, 1980.

211. Vakula, V.C.; Yun-tszui, K.; Vogutskii,S.S. J. Polym. Sci., 47, 544, 1966.

212. McLaren, A.D.; Seiler, C.J. J. Polym. Sci., 4, 63, 1949.

213. Rowe, R.C. J. Pharm. Pharmacol., 30, 669-672, 1978.

214. Abdel-Aziz, S.A.M.; Armstrong, P.A.M.; Anderson, W. J. Pharm. Pharmacol., 26, 131p. 1974.

215. Abdel-Aziz, S.A.M.; Anderson, W. J. Pharm. Pharmacol., 28, 801-805, 1976.

216. Kent, D.J.; Rowe, R.C. J. Pharm. Pharmacol., 30, 808-810, 1978.

217. Patt, L.; Hartmann, V Pharm. Ind., 38, 902-906, 1976; through Chem. Abstr., 86, 111134s, 1977.

218. List, P.H.; Laun, G. Pharm. Ind., 42, 399-401, 1980; through Chem. Abstr., 93, 137929z, 1980.

219. Pickard, J.F.; Elworthy, P.H.; Sucker, H. J. Pharm. Pharmacol., 28, 20p. 1976.

220. Tondachi, M.; Hoshi, N.; Sekiyawa, F. Drug Dev. Ind. Pharm., 3, 227-240, 1977.

221. Bayer, K.; Soliva, M.; Speiser, P. Pharm. Ind., 34, 677-682, 1972.

222. Lawrence, R.L.; McIntyre, B.B. Ind. Eng. Chem., 41, 689-694, 1949.

223. Entwistle, C.A.; Rowe, R.C. J. Pharm. Pharmacol, 30, 27p. 1978.

224. Entwistle, C.A.; Rowe, R.C. J. Pharm. Pharmacol., 31, 269-272, 1979.

225. Rowe, R.C. ; Forse, S.F. J. Pharm. Pharmacol., 33, 174-175, 1981.

226. Delporte, J.P. Pharm. Acta Helv., 45, 525-552, 1970.

227. Gurny, R. Pharm. Acta Helv., 51, 1-10, 1976.

228. Vemba, T.; Gillard, J.; Roland, M. Pharm. Acta Helv., 55, 65-71, 1980.

229. Gurny, R.; Buri, P.; Sucker, H.; Guitard, P.; Leuenberger, H. Pharm. Acta Helv., 52, 175-181, 1977.

230. Spitael, J.; Kinget, R. Pharm. Acta Helv., 52, 106-108, 1977.

231. Zorll, U. Acta Pharm. Technol., 25, 283-300, 1979.

232. Gorlovskii, I.A.; Garinova, G.N.; Zubkina, F.D.; Il'ingkh, A.V.; Kuznetsova, L.I. Lakokras. Mater. Ikh. Primen., 11, 19-21, 1981; through Chem. Abstr., 94, 123165f, 1981.

233. Hahn, F.J.; Steinhauer, S. J. Paint. Technol., 47, 54-56, 1975.

234. Rowe, R.C. J. Pharm. Pharmacol, 33, 1-4, 1981.

235. Cole, G.C.; May, G.; Wilde, J.S. J. Pharm. Pharmacol., 32, 91p,1980.

236. Gurny, R.; Buri, P.; Sucker, H.; Guitard, P.; Leuenberger, H. Pharm. Acta Helv., 52, 247-251, 1977.

237. Rowe, R.C. J. Pharm. Pharmacol., 32, 851, 1980.

238. Heyd, A. J. Pharm. Sci., 62, 818-820, 1973.

239. Stern, P.W. J. Pharm. Sci., 63, 1171-1173, 1974.

240. Binning, R.C.; Lee, R.J.; Jennings, J.F.; Martin, E.C. Ind. Eng. Chem., 53, 45-50, 1961.

241. Chaumeil, J.C.; Piton, Y. Ann. Pharm. Fr., 31, 691-704, 1973; through Chem. Abstr., 81, 68440w, 1974.

242. Rowe, R.C.; Forse, S.F. J. Pharm. Pharmacol., 32, 647-648, 1980.

243. Crank, J.; Park, G.S. Mathematics of Diffusion. London: Academic Press, 1968.

244. Hickman, M.J. Notes on Applied Science Number 4, Measurement of Humidity. London:HMSO,1970.

245. Lines, R.W.; Miller, B.V. Powder Technol, 24, 91-96, 1979.

246. Neale, P. Personal Communication.

247. Polymer Handbook, 2nd edn. ed. Brandrup, J.; Immergut, E.H., P. IV 136. New York:Wiley and Sons, 1975.

248. British Standard 188 The Measurement of Viscosity. London: British Standards Institute, 1957.

249. Lenk, R.S. Polymer Rheology. London: Applied Science, 1978.

250. Comshare Commander II Programme. Merck Sharp and Dohme Ltd.

251. Martin, A.N.; Swarbrick, J.; Cammarata, A. Physical Pharmacy, Chapter 19. Philadelphia: Lea and Febiger, 1969.

252. Carr, R.L. Chem. Eng., 72, 163-168, 1965.

253. Carr, R.L. Chem. Eng., 73, 69-72, 1965.

254. Cole, G. Personal Communication.

255. Rowe, R.C.; Forse, S.F. J. Pharm. Pharmacol., 33, 412, 1981.

256. Ashworth, A.J. Chem. Ind., 1432, 1972.

257. Wexler, A. Tappi, 44, 180A-191A, 1961.

258. Ayerst, G. Int. BioDeteriorative Bulletin, 1, 13-26, 1965.

259. Wilson, R.E. J. Ind. Eng. Chem., 13, 326-331, 1921.

260. Young, J.F. J. Appl. Chem., 17, 241-245, 1967.

261. Long, D. Personal Communication.

262. Laurenson, L. Vacuum, 30, 275-281, 1980.

263. V.G. Micromass Ltd. Technical Information - Publication 01-642, 1971.

264. Singleton, J.H. J. Chem. Phys., 45, 2819, 1966.

265. Davis, W.D. J. Vac. Sci. Technol., 5, 23, 1968.

266. Sharkey, A.G.; Schultz, J.L.; Friedel, R.A. Bur. Mines. Bull., 634, 57, 1967.

267. Festermacher, J.E. J. Vac. Sci. Technol., 8, 380, 1971.

268. Gasser, R.R.; Thwaites, R. Vacuum, 17, 265, 1967.

269. Bray, C.S. The Interaction of Benzocaine with PVC Formulations. M.Sc. Thesis, University of Bath, 1977.

270. Polymer Handbook. 2nd edn., ed. Brandrup , J.; Immergut, E.H.. pp. III229 - III240, New York:Wiley and Sons, 1975.

271. Grieve, D.J. Changes in Surface Topography During Wear. Ph.D. Thesis, University of Birmingham, 1970.

272. King, M.J.; Thomas, T.R. J. Coat. Tech., 50, 56-61, 1978.

273. Sayles, R.S.; Thomas, T.R. J. Phys. E: Sci. Instr., 9, 855-861, 1976.

274. Operating Instructions for Talysurf 3 Surface Measuring Instrument. Rank-Taylor- Hobson.

275. Rudin, A.; Wagner, R.A. J. Appl. Polym. Sci., 19, 3361-3367, 1975.

276. Methocel Cellulose Ether Products. Dow Handbook, Dow Chemical Company.

277. Abdul-Razzak, M.H. Mechanical Properties of Hydroxypropyl-methyl Cellulose Films Derived from Aqueous Systems. M. Phil. Thesis, C.N.A.A., 1980.

278. Chatfield, H.W. Science of Surface Coatings. pp. 452-454, New York: Van Nostrand, 1962.

279. Encyclopedia of Polymer Science and Technology. ed., Bikales, N.M., Volume 10, New York: Interscience, 1969.

280. Pickard, J.F. Personal Communication.